THE UNIVERSITY OF HULL

A Thesis submitted for the degree of Doctor of Philosophy

An investigation into the TRPV1-CGRP signalling pathway in vessel development and its role in zebrafish embryogenesis

at the University of Hull

Adam Arthur Bates MRes BSc (Hons)

MRes Medical Genetics Newcastle University
BSc (Hons) Biomedical Science University of Sunderland

June 2023

Declaration of Authorship

I hereby declare that this thesis and work herein are my own. All methodologies were approved by the University of Hull Ethics Committee and all procedures were performed in accordance with the unlicensed animal ethics approval reference no. U144B of Hull.

Contribution statement

I acknowledge the support provided from the aquarium staff at the University of Hull; Alan Smith and Sonia Jennings, for their help with breeding and maintaining Zebrafish stock during the SARS-Cov2 pandemic. I wish to thank undergraduate students Eleni Kammenou and Robert Griffin for their assistance in performing the LAMP reactions. The microarray data analysed in Chapter 2 are the property of Dr Leonid Nikitenko of the University of Hull and were analysed in this PhD as part of the Health GDP PhD cluster. The Bevacizumab used in Chapter 4 was kindly donated by Prof, Anthony Maraveyas. The thesis received revision and contribution from my primary supervisor Katharina Wollenberg Valero.

Conference Publications related to the thesis:

Poster presented at the Northern Vascular Biology forum, Bradford 2018:

Adrenomedullin and CGRP induce different transcriptional profiles and CLR expression patterns in primary human dermal lymphatic endothelial cells.

Adam Bates[1]*, Adam Moverley[1]*, Ewan Stephenson[1]*, Lydia Wharton[1]*, Edward Drydale[1]*, Shirin Hasan[1], Christine Blancher[2], Nischalan Pillay[3], Steve P. Watson[4], Chris Collins[1], Katharina Wollenberg Valero[1] and Leonid L. Nikitenko[1]

[1]School of Life Sciences, Faculty of Health Sciences, University of Hull, Kingston upon Hull, HU6 7RX, United Kingdom; [2]Wellcome Trust Centre for Human Genetics, Oxford, OX3 7BN, United Kingdom; [3]UCL Cancer Institute, London, WC1E 6DD, United Kingdom; [4]University of Birmingham, Birmingham, B15 2TT, United Kingdom. *Equal contribution. E-mail: l.nikitenko@hull.ac.uk

Oral presentation given at UK Lymphatics Science meeting, Birmingham 2019:

Neuropeptide CGRP affects primary human lymphatic endothelial cell biology

Adam Bates[1]*, Adam Moverley[1]*, Ewan Stephenson[1]*, Lydia Wharton[1]*, Edward Drydale[1]*, Shirin Hasan[1], Christine Blancher[2], Nischalan Pillay[3], Steve P. Watson[4], Chris Collins[1], Katharina Wollenberg Valero[1] and Leonid L. Nikitenko[1]

[1]School of Life Sciences, Faculty of Health Sciences, University of Hull, Kingston upon Hull, HU6 7RX, United Kingdom; [2]Wellcome Trust Centre for Human Genetics, Oxford, OX3 7BN, United Kingdom; [3]UCL Cancer Institute, London, WC1E 6DD, United Kingdom; [4]University of Birmingham, Birmingham, B15 2TT, United Kingdom. *Equal contribution. E-mail: l.nikitenko@hull.ac.uk

Abstract

TRPV1 is a non-selective cation channel which is activated through various different factors including, but not limited to, raised temperature and acidic pH. It has been linked in the past to endothelial cell proliferation in acidic conditions, but a direct link between TRPV1-CGRP signalling in endothelial cells in development has not been highlighted before. The main goal of this thesis is to explore the effects of manipulating TRPV1 on vessel formation.

The main three overarching hypotheses are that CGRP, which is released by TRPV1 activation will cause transcriptional changes in endothelial cells in culture, the knockdown of TRPV1 will cause transcriptional changes to a developing zebrafish embryo and that TRPV1 knockdown will have detrimental effects to a developing zebrafish embryo and its vascular system.

Chapter 2 analyses the effects of human dermal lymphatic endothelial cells (HDLECs) transcriptomic response to being stimulated by CGRP, a molecule which is released by TRPV1 activation. It was concluded that lymphatic endothelial cells were more prone to being stimulated than blood endothelial cells, and that a neuropeptide CGRP causes transcriptional changes to genes with functions relating to vessel development of HDLECs.

Results showed that CGRP induced changes to the expression of 144 genes, compared to 23 DEGs upon AM stimulation. The HDLECs experiments results were then explored in the in vivo model of a developing zebrafish embryo in the two subsequent chapters.

Chapter 3 explores the hypothesis that TRPV1 knockdown will have detrimental effects to the developing embryo, causing a change to the transcriptome. The embryo was injected with TRPV1 targeting morpholino in combination with the TRPV1 agonist 2-APB. Swim responses of MO injected embryos was half of the control upon response to heat stimuli

(0.52cm/sec compared to 1.02cm/sec). RNA-seq results show that the genes which are significantly differentially expressed upon TRPV1 knockdown have endothelial cell related functions and these results are supported through the use of antibody staining to identify the vessels in the developing embryo.

Chapter 4 investigates whether the changes to gene expression identified in the previous chapter are sustained when the embryo is exposed to different stressors, individually and in combination. Bevacuzimab was included to be a comparison of TRPV1 knockdown as it is known to affect the blood vessel development of zebrafish, by targeting the VEGFA pathway. Gene expression was measured using qLAMP and a novel analysis method in combination with developmental and survival rates of the embryo.

The results of the LAMP reactions showed that both bevacizumab injection and TRPV1 knockdown had a significant effect on the gene expression relating to vessel formation. When APB was used in combination with the knockdown, there was an even more significant change to overall gene expression ($p<0.0001$). Antibody staining also showed that TRPV1 is expressed in olfactory bulbs in the developing embryo which had been injected with bevacizumab.

These results show a novel in vivo link between TRPV1 and vessel development in zebrafish which may have implications in pathophysiological conditions such as cancer, hypertension and chronic pain as well as environmental conditions such as increasing heat.

Acknowledgments

I would like to thank both Dr Katharina Wollenberg-Valero and Dr Francisco Rivero for their supervision throughout this PhD and for giving me this opportunity. I would also like to take the time to thank my colleagues Dr Lauric Feugere, Dr Luana Mincarelli, Paula Tombs and Paulo Saldhana whose support was valuable throughout the PhD. I thank my colleagues in the ToL programme at the Sanger Institute for their support whilst writing this thesis. I thank the University of Hull for funding this research as a part of the Health GDP Cluster, investigating the role of endothelial cells in health and disease. I thank coffee for being my friend during writing sessions and stimulating my TRPV1 receptors. Lastly, I would like to state my gratitude to all my friends and family who supported me on this journey.

"With magic, you can turn a frog into a prince. With science, you can turn a frog into a PhD and you still have the frog you started with."

— Terry Pratchett

Contents

Table of Figures

Table of Tables

Table of abbreviations

Abbreviation	Definition
2-APB	2-Aminoethoxydiphenyl borate
aISV	arterial Intersegmental vessels
BEC	Blood Endothelial Cell
BEV	Bevacuzimab
DPF	Days Post Fertilisation
DRG	Dorsal Root Ganglion
E3	a media used for rearing zebrafish larvae
EC	Endothelial Cell
ECM	Extracellular matrix
EPC	Endothelial Precursor Cell
GO	Gene Ontology
HDLEC	Human Dermal Lymphatic Endotelial Cell
HUVEC	Human Umbilical Vein Endothelial Cell
ISLV	Intersegmental lymphatic vessels
KD	Knock Down
KEGG	Kyoto Encyclopedia of Genes and Genomes
LAMP	Loop-mediated isothermal Amplification
LEC	Lympatic Endothelial Cell
MDS	Multi-Dimensional Scaling
MO	Morpholino
NMDS	Non-metric MultiDimensional Scaling
OSN	Olfactory Sensory Neurons
PBS	Phosphate buffered saline
PCR	Polymerase Chain Reaction
PCV	posterior cardinal vein
qLAMP	quantitative Loop-mediated isothermal Amplification
qPCR	quantitative Polymerase Chain Reaction
TD	Thoracic Duct
TRP	Transient Receptor Potential
VEC	Vascular Endothelial Cell
vISV	venous Intersegmental vessels

Chapter 1: Introduction

1.1 Goal of the thesis and specific aims

The main aim of this thesis is to interrogate the TRPV1-CGRP signalling pathway in vessel development and investigate how alterations to this signalling pathway can cause phenotypic and molecular changes downstream.

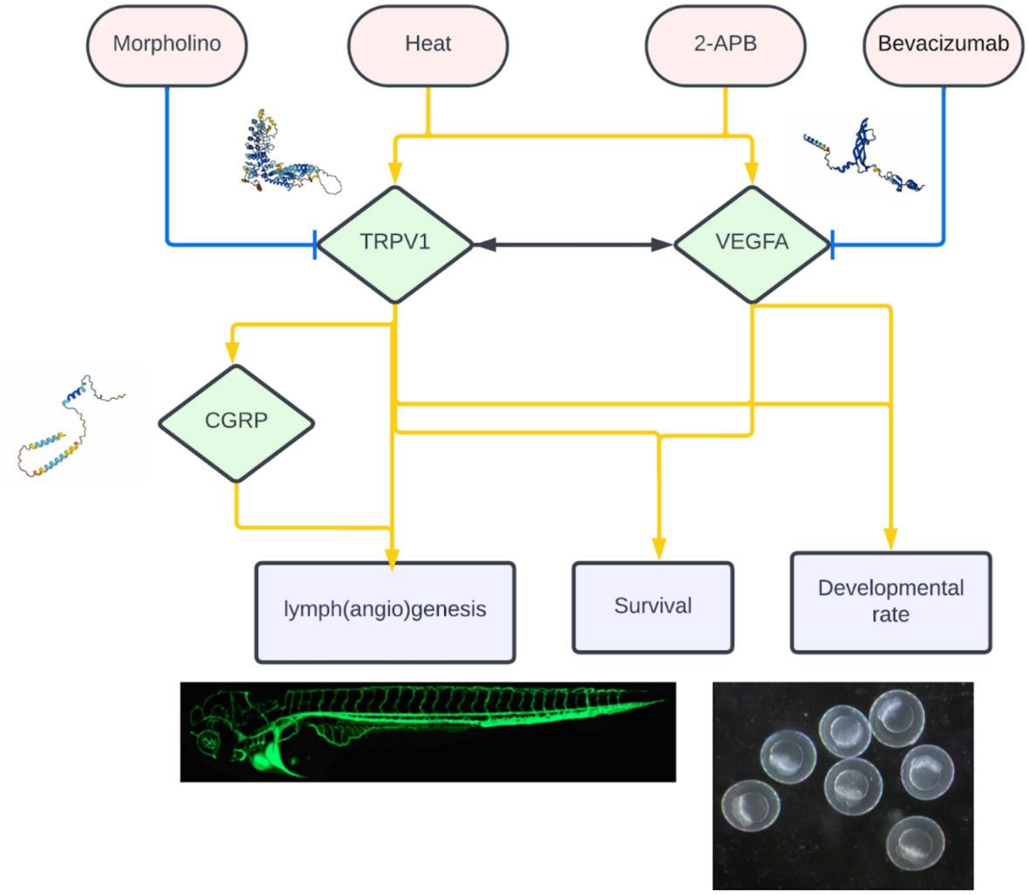

Figure 1.1. *A graphic outline of the molecular interactions which this thesis will investigate. The red boxes are the modifiers which will target two proteins thought to be important in vessel formation. These green diamonds are the key genes which are the focus of this thesis, and the purple boxes at the bottom represent the measured phenotypic changes. Yellow arrows represent positive modes of action, blue represent negative interactions and the black arrows between TRPV1 and VEGFA represent a link which is hypothesised but not yet proven.*

1.2 Evolution and structure of the TRP channels.

In order to adapt and evolve in response to changing environmental conditions, organisms change their phenotype, developing behavioural and morphological traits beneficial to survival in that environment (Keller & Seehausen, 2012). Sensing the environment and its changes are therefore vital to the survival and propagation of species. Disruption of somatosensory pathways which detect stimuli such as heat or pH, can have adverse effects on a species and can even be fatal, leaving some species to become threatened or extinct (Hoffmann & Sgrò, 2011; Naujokaitis-Lewis et al., 2021). The main thermosensors which have been described for the detection of environmental temperature changes are the Transient receptor potential (TRP) channels. These channels are tetrameric structures which contain six transmembrane domains (see Himmel & Cox, 2020). TRP channels contain different families of receptors, the most described members of these families are TRPV (TRP vanilloid) channels; TRPC (TRP canonical) channels; TRPM (TRP melastatin) channels and TRPA (TRP ankyrin) channels (Figure 1.2) (Himmel & Cox, 2020). TRPV channels are named due to their sensitivity to vanilloid compounds and were first described in humans in 1997 (Caterina et al., 1997), they have largely diversified over the years and have become sensors for multiple stimuli. TRPC channels were first described as ion channels in 1989 (Wang et al., 2020), where it was found to be essential in phototransduction in drosophilia, being predominantly expressed in photoreceptor cells (Montell & Rubin, 1989). TRPC play a key role in the phospholipase C transduction pathway (Wang et al, 2020). TRPM channels are non selective cation channels and are very similar in function to TRPV channels and can also detect changes in temperature (TRPM8 and TRPM3; Huang et al., 2020) and external stimuli but lack the ankyrin repeat domains that exist in vanilloid channels. TRPA channels are also polymodal ion channels, being able to detect hot and cold temperatures, as well as chemicals such as cannabinoids and cinnamaldehyde, they are named after their highly conserved ankyrin repeat domain (Himmel & Cox, 2020).The same TRP channels in different species can exhibit different properties, such as human and rodent TRPV1 being sensitive to capsaicin, although the bird and zebrafish forms of TRPV1 being insensitive to this irritant (Zheng, 2013;

Gau et al., 2013). The ThermoTRP channels are highly conserved across mammalian species and fishes, dating back as far as a common tetrapod ancestor (Saito & Shingai, 2006). They are sensitive to pH changes due to the protonation of a protonation site which exists either intra- or extracellularly depending on the function of the channell; the protonation occurs at the E600 site of the TRPV1 protein and mutations to this amino acid inhibited the responses of the channel to thermal activation (Zheng, 2013; Jordt et al., 2000). The least complex organism where TRPV1 has found to be expressed is on yeast (Myers et al., 2008). TRPV1 was shown to have heat activation properties across birds, amphibians, fish and mammals and single changes to the amino acid sequence can modify TRPV1's sensitivity to heat with some species even losing the ability to detect changes to heat at all, such is the case for the thirteen-lined ground squirrel (*Ictidomys tridecemlineatus)* (Laursen et al., 2016). The ankyrin repeat domain located near the N-terminus of the TRPV channels is highly conserved and is shown to bind ATP and calmodulin and this binding influences the sensitivity of the channel (Phelps et al., 2010). Whilst the sequence and structure of TRPV1 is highly conserved across vertebrates, with no variation in the akyrin repeat domain, there is variation in the tubulin binding structures within TRPV1 (TBS-1 and TBS-2), which may account for variability in channel function across species (Sardar et al., 2012). The S1 - S4 segment of the TRPV1 channels is the domain of the protein responsible for the themosensitive activation of the TRPV1, this region is also where the binding sites for chemical stimuli, such as capsaicin, as well as the activation through pH (Kim et al., 2020). The sensitivity of TRP channels has been shown to be much lower than that of classic voltage gated ion channels and this is thought to be due to the lack of charged amino acids in S4, which exist in other voltage gated channels (see Zheng, 2013). Upon the addition of increased temperature, capsaicin or other agonists, the ThermoTRP channels (TRPV1-3) become sensitised in the absence of a change in pH levels, even having the ability to open at resting membrane potential (Tominaga & Tominaga, 2005). Another agonist of the TRP channels is 2-Aminoethoxydiphenyl borate (2-APB). 2-APB is a synthetic compound which binds to this S1-S4 pocket in TRPV1 and causes the pocket to move towards the pore along with the S4-S5 linker and the TRP box, opening the channel (Zhao et al., 2021; Sun et al., 2022). There are TRP channels which also respond to the negative changes in temperature: TRPM8 activates when the temperature drops below 20°C in rats (McKemy et al., 2002). It is worth noting that TRP channels are not the only channels which respond to changes in external temperature, STIM1, an endoplasmic reticulum voltage sensor, can also be activated by noxious temperatures (Xiao et al., 2011).

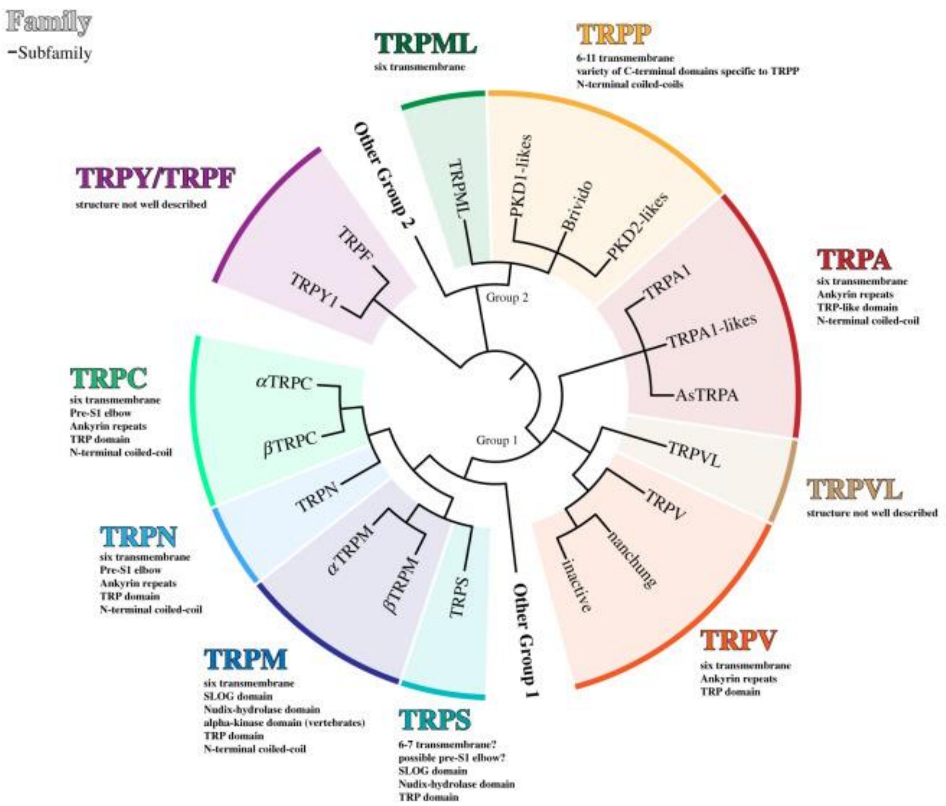

Figure 1.2. *The phylogenetic relationship of the different TRP families across all eukaryotes. Image from Himmel & Cox, 2020.*

1.3 TRPV1 structure and function.

Transient receptor potential cation channel subfamily V member 1 (TRPV1) is one of the more well characterised members of the TRP family of non-selective cation channels. The TRPV1 channels reside mostly on dorsal root ganglia (DRG) neurons where they aid in the detection of environmental changes through transmitting sensory information to the central nervous system (Tominaga & Tominaga, 2005), although have been shown to be expressed elsewhere. Fundamentally they are involved in the transport of cations across membranes in response to various stressors and external stimuli. This movement of cations across a membrane have been shown to be involved in various important cell processes such as cell migration (Waning et al., 2007), apoptosis and proliferation (Zhai et al., 2020). As all of these processes occur during embryonic development, the TRP channels are thought to play a large role in tissue maintenance and development (Ramsey et al, 2006). The protein itself, like all TRP channels, contains six transmembrane domains (S1-6) which have fourfold symmetry (Figure 1.3; Liao et al., 2013) of which the C and N terminus are located intracellularly. This structure has been shown to change in response to different agonists, two of these different structures have been shown, one formed in the presence of resiniferatoxin in combination with the double-knot toxin and the other structure was in the presence of capsaicin. Activation of the TRPV1 receptor in humans is known to cause the release of various sensory neuropeptides including calcitonin gene related peptide (CGRP) (Meng et al, 2009) and substance P (SP)(Gazzieri et al, 2007), both of which are involved in the sensations of pain and inflammation (Szallasi et al, 2006).

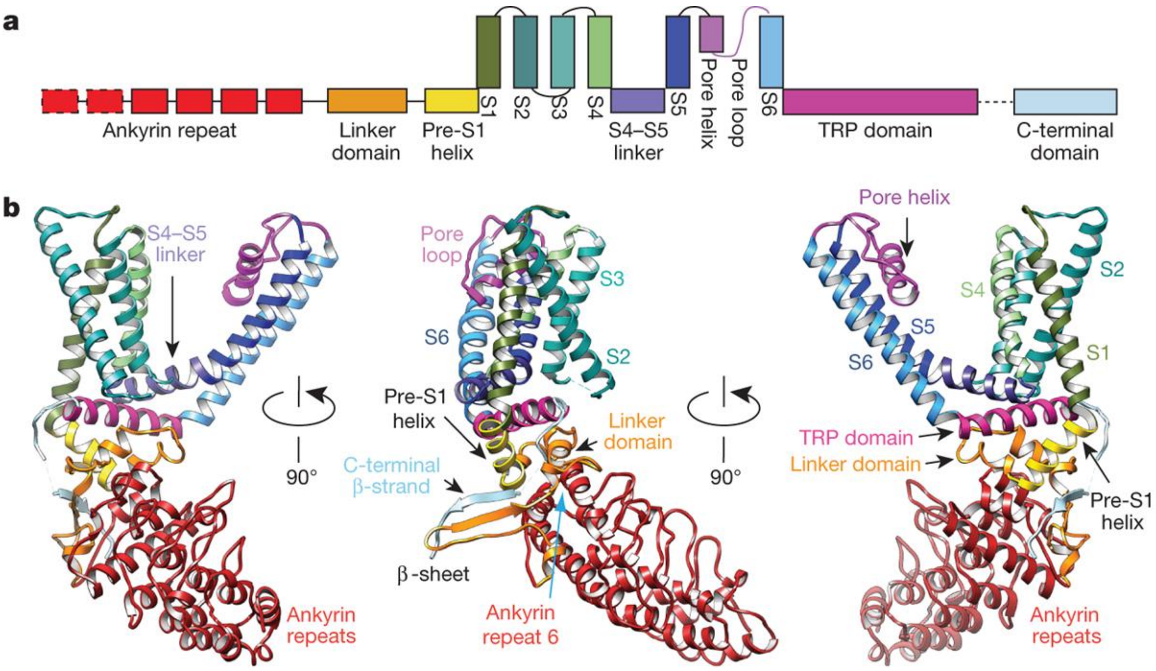

Figure 1.3. *Linear diagram depicting major structural domains in a TRPV1 subunit, colour coded to match ribbon diagrams. b, Ribbon diagrams showing three different angles of a TRPV1 monomer with the structural domains labelled. Image from Liao et al., 2013.*

1.4 TRPV1 and its role in vessel formation

In humans, administration of TRPV1 antagonists leads to increased body temperature, while TRPV1 agonists have the opposite effect, causing hypothermia (Gavva et al., 2008; Gavva, N, 2008). TRPV1 has also been implicated in lymphangiogenesis using an in vitro lymphatic endothelial cell model, specifically investigating the effects of acidosis on cancer metastasis to the lymphatic system. TRPV1 channels present on the endothelial cells themselves upregulated IL-8 expression, promoting lymphangiogenesis (Nakanishi et al., 2016). Endothelial cells in culture have shown a preference for migration towards an acidic environment compared to a neutral pH zone, suggesting a potential link between TRPV1 and cell migration (Paradise et al., 2013). The broader TRP channel family has direct involvement in angiogenesis, with the modulation of calcium (Ca^{2+}) uptake controlling the rate of the angiogenic process (Pla et al., 2013). In a mouse model, the introduction of a TRPV1 ligand resulted in upregulated angiogenesis in a matrigel plug, and this response was diminished in TRPV1 knockout mice. The study also revealed that TRPV1 activation is involved in simvastatin-induced Ca^{2+} influx in microvascular endothelial cells, leading to increased calcium-calmodulin dependent protein kinase II (CaMKII) signalling and the formation of the TRPV1-eNOS complex (Su et al., 2014). Importantly, this promotion of angiogenesis occurs independently of VEGF signalling pathways, where treatment of primary bovine endotelial cell cultures with a TRPV1 agonist, resiniferatoxin, didn't affect VEGF-induced Ca^{2+} signalling or tube formation, even upon inhibition. (Negri et al., 2020 ; O'Leary et al., 2019).

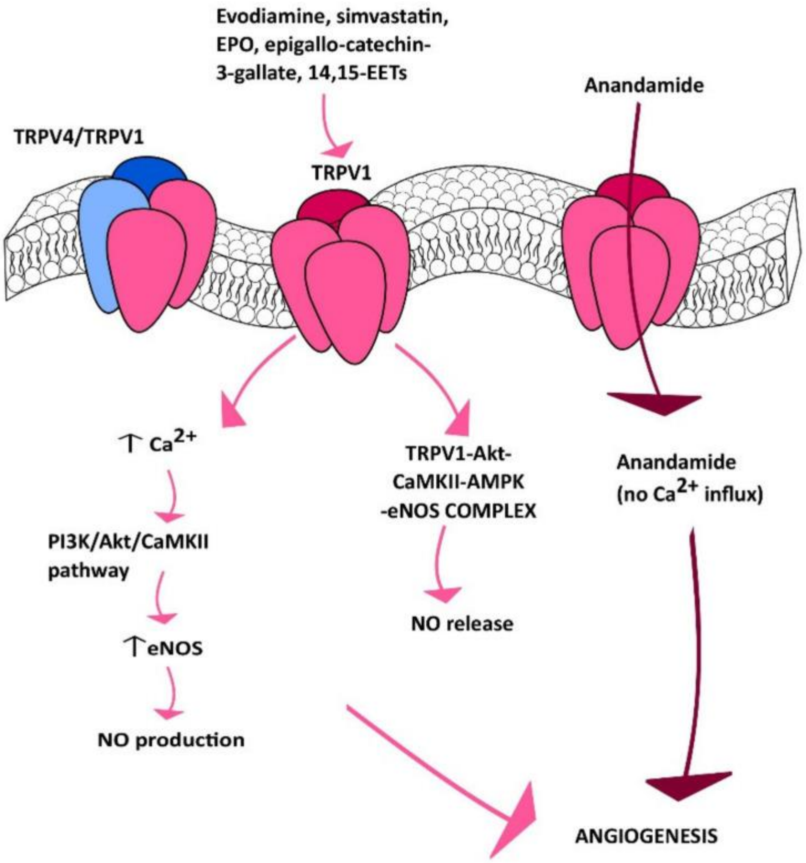

Figure 1.4. *Current understanding of the TRPV1 channel in angiogenesis. TRPV1 stimulates angiogenesis in response to evodiamine, simvastatin, EPO, epigallo-catechin-3-gallate, and 14,15-EETS in a Ca^{2+}-dependent manner. Image from Negri et al., 2020*

1.5 TRPV1 and its role in disease

TRPV1 has been associated with various diseases and conditions, including chronic cough (Groneberg et al., 2004), chronic pain (Kim et al., 2014) and cancer (Li et al., 2021). In chronic cough, the TRPV1 channels are expressed on the bronchi and bronchioles (Lee & Gu, 2009) and activation of these TRPV1 channels via external stimuli can lead to coughing and bronchoconstriction, or an increase in its expression can give rise to a chronic cough phenotype (Mitchell et al., 2005; Lee & Gu, 2009). The role of TRPV1 in neurological pain is caused by it becoming hypersensitive in response to agonists, causing an increase of inflammation in the nervous system and surrounding tissue which leads to pain (de Almeida et al., 2021). Treatment which targets TRPV1 in an effort to reduce the neurological pain of cancers in mouse models (de Almeida et al., 2021), found that expression of TRPV1 plays an essential role in the development of cancer-associated pain, and the loss of this channel can alleviate the pain. The parathyroid hormone related peptide (PTHrP) can also activate this pain pathway in cancers such as breast and prostate (Shepherd et al., 2018), through hypersensitisation of the TRPV1 channels in the surrounding neurons. In cancers, expression of TRPV1 showed a direct correlation with survival and metastasis rates, making TRPV1 an up-and-coming target for cancer drug treatment (Li et al, 2021).

1.6 Endothelial cells and Vessels

The interior lining of vessels throughout the entire cardiovascular system are composed of endothelial cells (ECs). ECs are a highly specific yet heterogeneous cell type which are known to line the interior of blood and lymphatic vessels. They arise from multipotent progenitor cells which exist in the mesoderm during embryogenesis. From the mesoderm, these stem cells begin to differentiate into angioblasts which then develop into endothelial cells that form the body’s first circulatory systems through a process known as vasculogenesis. Mature ECs reside in a quiescent state until required for angiogenesis, which is the development of blood vessels through sprouting from pre-existing ones (Wacker & Gerhardt, 2011). Blood endothelial cells (BECs) are endothelial cells which are in direct contact with the blood. BECs maintain the homeostasis of the circulatory system, protecting against physical forces such as shear stress and stretching. It has only recently been theorised that their plasma membranes play an important role in acting as a mechanosensor (Yamamoto & Ando, 2018). BECs have also been shown to respond to shear stress through hyperpolarization and an influx of extracellular Ca^{2+} which triggers a range of transcription factors in response (Ando & Yamamoto, 2013). Dysregulation of BECs has been shown to have the potential to cause and increase the risk of cardiovascular diseases such as hypertension and atherosclerosis. BECs are known to perform important homeostatic functions including maintaining blood flow, angiogenesis and also roles in the pathways of inflammation and clotting. ECs are morphologically heterogeneous and can form various different structures depending on their function. The morphology of ECs is controlled by a variety of transcription factors, such as

MEF2 and FOXO but there is still a need for a deeper understanding of the subject as most of this research has been performed on mice (Tsuji-Tamura & Ogawa, 2018). Depending on the function, the endothelium specialises to its required function, causing heterogeneity between different ECs. ECs can be continuous, discontinuous or fenestrated depending on the organ in which they reside and the function that they are required to perform. Fenestrated ECs are more often found in tissues that are used as a filter, such as the glomerulus in the kidney. Fenestrated ECs are also found in tissues which secrete hormones like the pancreas. Discontinuous ECs are located in sinusoidal beds, most prominently in those of the liver and the bone marrow, and are morphologically similar to fenestrated endothelium although have larger fenestrations and a poorly formed basement layer (Aird, 2012 ;Potente & Mäkinen, 2017). An example of these specialised barriers created by the differing structures can be observed in the blood brain barrier (BBB). The BBB is a highly selective barrier that is made up of continuous ECs with tight and adherens junctions with a low rate of movement of macromolecules across the cell membrane, known as transcytosis; this is aided by the pericytes residing on the vessel walls (Aird, 2012). This barrier is highly selective, in contrast to that of the glomeruli in the kidney which has a less selective, fenestrated EC barrier that allows for a rapid exchange of molecules and a large amount of transcytosis (Aird, 2012). Tissue specific ECs have been shown to aid the surrounding cells in the tissue, maintaining homeostasis and promoting growth and differentiation. An example of this, sinusoid ECs have been shown to supply hepatocytes with hepatocyte growth factor (HGF) which aids in the survival and expansion of the liver tissue (Crivellato et al., 2007). Each tissue-specific EC has its own expression pattern, and they also have varying rates of angiogenesis. ECs which reside in the heart were found to have the largest angiogenic potential, and also the highest rate of oxygen consumption when compared to ECs of the liver, lungs and kidneys during human embryogenesis (Marcu et al., 2018). Immature ECs that circulate in the blood are known as endothelial progenitor cells (EPCs). EPCs are theorised to be recruited during damage and angiogenesis to help the repair and expansion of the endothelium. In a mouse model, EPCs were found to not directly have a function relating directly to vascular repair and there is still debate as to how much involvement they have (Hagensen et al., 2011). In angiogenesis, EPCs aid in the production of new blood vessels through the secretion of paracrine factors that promote the proliferation of surrounding endothelium (Zhang et al., 2014).

1.7 Lymphatic system and lymphatic endothelium

The lymphatic system is composed of lymphatic vessels and lymphoid tissues. The lymphatic vessels are lined by ECs known as lymphatic endothelial cells (LECs). Unlike the development of the blood vessels, the exact development of the lymphatic system is one which has been under debate (Semo et al., 2016). The most widely accepted theory is that ECs bud out from the vein and differentiate into LEC progenitors, through lymphangiogenesis, the development of lymphatic vessels through sprouting from pre-existing vessels. This theory is the most accepted and has been validated through genetic experiments on mouse and zebrafish (Tammela & Alitalo, 2010). There is a second, less accepted theory that the vessels develop from progenitors in the mesenchyme, independent from the development of the cardiovascular system (Wong et al., 2018). The lymphatic system is important to body homeostasis as it is known to have roles in fluid homeostasis, the clearance of lipids from the blood, the immune response and inflammation. Much like the vascular endothelial cells (VECs) found in blood vessels, the LECs have also been shown to have organ specific morphology depending on the function that is required of them (Wong et al., 2018). Examples of this can be seen in the hepatic lymphatic system, where there is a complex superficial system of lymphatic vessels which are specialised to where they are found in the liver. This is required because the liver is a large producer of lymph and has important roles in the clearance of lipids from the body (Tanaka & Iwakiri, 2016).

1.8 CGRP signalling and CLR receptors.

The calcitonin related family of peptides is a collection of six hormones: two (alpha and beta) forms of calcitonin gene related peptide (gene *CALCA*, protein CGRP), adrenomedullin (gene

ADM, protein AM), intermedin (gene *ADM2*, protein AM2), amylin (gene *IAPP*, protein AMY) and calcitonin itself (gene *CALCA*, protein CT). All these hormones are known to bind to a common receptor known as the calcitonin receptor like-receptor (gene *CALCRL*, protein CLR, Wimalawansa et al, 1997). This receptor is a member of the seven-transmembrane G-protein coupled receptors (GPCR). CGRP release is mediated by TRPV1 but also serotonin receptors are known to control the release of CGRP (Durham & Vause, 2010). GPCRs are among the largest of membrane-bound molecules and control many important physiological functions, with 34% of small molecule drugs against a wide range of metabolic diseases from diabetes to cancer targeting them directly (Congreve et al, 2020). The binding affinity of the CLR receptor is dependent on the receptor-activity-modifying-proteins (RAMPs). These aid in guiding the receptor to the cell surface through terminal glycosylation, forming a heterodimer complex. The RAMP family contains three different proteins RAMP1, RAMP2 and RAMP3. AM binds to CLR with higher affinity when either the RAMP2-CLR or RAMP3-CLR heterodimer complex is formed; RAMP1-CLR is the complex with the highest affinity for CGRP (Figure 1.5) (Gibbons et al., 2007; Kuwasako, 2011; Hay et al, 2018). Despite higher affinity to these receptors, AM and CGRP are still able to bind to other CLR-RAMP complexes. CLR signalling is also a key factor in pathophysiology of cardiovascular diseases and vascular cancers, being highly expressed in Kaposi's sarcoma (Hagner et al, 2006) and renal cell carcinoma (Nikitenko et al, 2013).

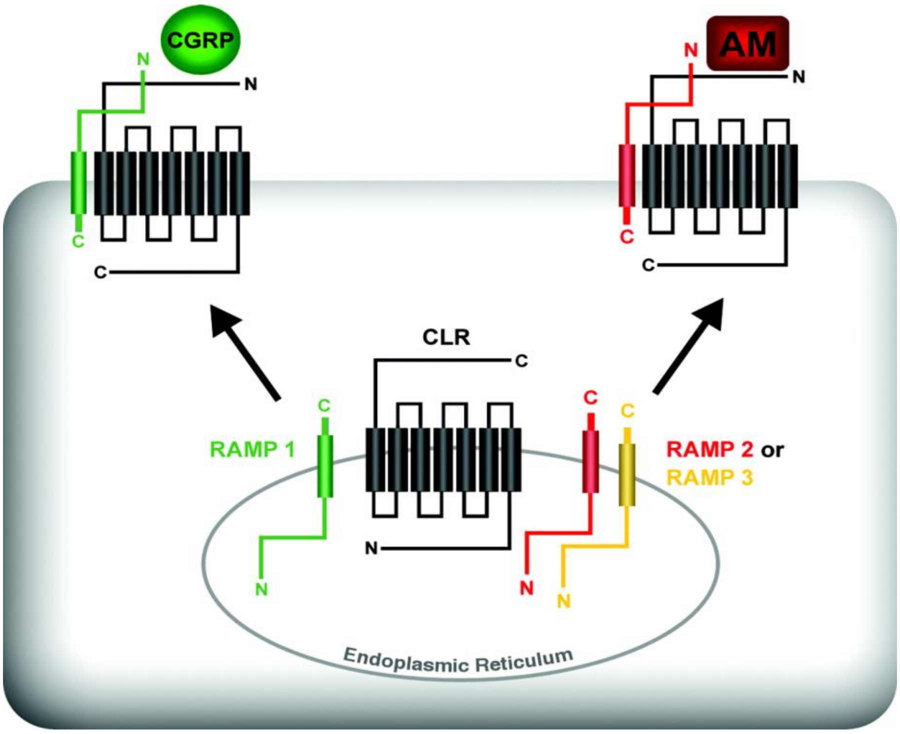

Figure 1.5. *The relationship between CLR and RAMPs. The CLR/RAMP1 heterodimer has an affinity for CGRP (green), where as the association of CLR with RAMP2 or RAMP3 has an affinity for binding AM. Image taken from* Gibbons et al., 2007.

Both AM and CGRP are well-studied hormones. AM is circulated in plasma, meaning it is in direct contact with the blood endothelium. In fact, it has been shown to be a multifunctional peptide relevant for endothelial cell function. AM is involved in angiogenesis (Ribatti et al, 2005), development (Garayoa et al, 2002), and is a potent vasodilator (Heaton et al, 1995). AM knockouts in mice cause embryonic lethality (Ando & Fujita, 2003); with endothelial cell-specific knockout mice showing reduced levels of angiogenesis, increased vessel permeability but less ischemia-induced brain damage (Ochoa-Callejero et al, 2016). AM expression is also, to a lesser extent, mediated through another GPCR, ACKR3 (also known as CXCR7), which is similar in structure to CLR and has been shown to scavenge AM and therefore regulate its function by acting as a decoy receptor (Klein et al, 2014). This plays an important role in mediating AM signalling in cardiac and lymphatic development (Klein et al, 2014).

CGRP is primarily a neuropeptide and exists in two forms, named αCGRP and βCGRP. While they have similar functions to AM, they are coded by two different genes that both reside on chromosome 11 and have 90% homology (Hu et al, 2016). The gene for αCGRP is the same as for CT (*CALCA*) and is transcribed through alternative splicing whereas βCGRP originates from the distinct *CALCB* gene. The peptide, in humans, is most abundant in sensory C and Aδ nerve fibres (Hu et al, 2016). CGRP is released by sensory neurons through the activation of the thermosensitive TRPV1 channel in response to various noxious stimuli, including low pH and chemicals such as capcaisin (Peng & Li, 2010). Levels of this peptide in the blood are linked to migraines, making CGRP a drug target (Russo, 2015). Similarly, to AM, CGRP is also a potent vasodilator (McCormack et al, 1989; Russell et al, 2014). Whilst both peptides bind to the same CLR receptor, they were hypothesised to desensitise the receptor through independent mechanisms (Nikitenko et al, 2006).

1.9 Erenumab as a CGRP focused drug treatment

A drug therapy of an anti-CGRP receptor humanised antibody, erenumab, being recently licenced in the EU and is available in scotland for the treatment of migraine (Edvinsson et al, 2017); the drug is currently undergoing approval by NICE to be used within the NHS and the rest of the UK. The treatment has, however, had variable responder rates with 50% response at 12 weeks and there being no significant reduction in monthly migraine attacks when compared to placebo after 12 weeks of treatment (Khan et al,2019). Side effects discovered in some of the clinical trials of erenumab have included injection site pain, nausea and infections (Khan et al,2019); all of which have the potential to be linked to the CGRP and TRPV1 signalling pathway. The sensory neuropeptides cause localised neurogenic inflammation, the disruption of which has been linked to various diseases such as migraine and also chronic diseases such as asthma (Cardell et al, 1994) and psoriasis (Saraceno et al, 2006). TRPV1 itself is increasingly becoming more of an interesting target for treatments, a recent study has shown that it is possible to target the various conformational changes of the channel, effectively inhibiting the signalling depending on the structure (Trkulja et al., 2021). This is a big breakthrough in treating chronic pain caused by the channel without causing any off-target effects by inhibiting healthy forms of the channel.

1.10 CLR Receptor and downstream binding of CGRP

CLR is a G protein-coupled receptor predominantly expressed in endothelial cells (Nikitenko et al., 2006). G protein-coupled receptors constitute the largest and most important group of cell membrane receptors. They function by detecting extracellular molecules, which trigger internal changes through transduction pathways. CLR is known to bind various ligands, including adrenomedullin (AM) (Hinson et al., 2000), calcitonin gene-related peptide (CGRP), adrenomedullin 2 (AM2; also known as intermedin, IMD) (Roh et al., 2004), and amylin (Muff et al., 1999). To reach the cell membrane, CLR forms a heterodimer with RAMPs. RAMPs are single-transmembrane domain proteins with a small intracellular C-terminal tail and a large N-terminal extracellular domain. Three RAMPs, namely RAMP1, RAMP2, and RAMP3, have been identified to form stable complexes with CLR. This heterodimeric complex is formed within the endoplasmic reticulum (ER) and remains stable throughout the receptor's lifecycle. Guidance by RAMP1 leads to CLR's specificity for CGRP, while transport by RAMP2 and RAMP3 confers high affinity to AM or AM2 (Parameswaran & Spielman, 2006). RAMP1 and RAMP3 can also form homodimers that reside inside the cell, primarily in the ER. Interestingly, RAMPs have been found to form complexes with various other G protein-coupled receptors, including parathyroid hormone receptors (PTH1R and PTH2R) (Christopoulos et al., 2003). Heterodimer complexes formed with other GPCRs perform similar functions to those formed with CLR, influencing post-translational modifications and ligand affinity of the receptors.

Knowledge Gap 1: There needs to be a greater understanding of CGRP signalling in the context of endothelial cell biology, studying the downstream effects on both a molecular and physiological level.

1.11 Endothelial cells and their roles in disease

ECs are important in maintaining the homeostasis of the circulatory system and are involved in a range of chronic diseases such as gestational diabetes mellitus (He & Wu, 2021), cancer (Yang et al., 2021) and inflammatory conditions such as rheumatoid arthritis (Totoson et al., 2014). Evidence has suggested that patients suffering from gestational diabetes have EC dysfunction which also makes them more susceptible to co-morbidities of the cardiovascular system for both the mother and the child (Cvitic et al., 2018). The dysfunction of ECs is caused by a reduction in angiogenesis being linked to a decrease in insulin sensitivity as insulin has been shown to have various protective effects on the vascular system (Vicent et al., 2003). Rheumatoid arthritis is a chronic disease caused by excessive inflammation within the joints. Patients with rheumatoid arthritis showed that they had an impaired ability to grow colonies of EPCs, which in turn increases the risk of cardiovascular disease. This is thought to be because of the inflammatory nature of the disease and the pro-inflammatory responses which are mediated in part by EPCs (Adawi et al., 2018).

1.11.2 Endothelial cells and Lymphedema

The disease which is directly linked to lymphatic endothelial cell dysfunction is lymphedema. Lymphedema is the accumulation of fluid in the tissues, caused by the abnormal draining of the lymphatic system. Abnormalities could arise sporadically, through genetics or syndromic disorders; cases such as this are known as primary lymphedema. Cases where the lymphedema is caused by surgery, cancer, infection or trauma are known as secondary lymphedema because the condition is secondary to the underlying cause (Rockson, 2021). On a molecular level, the contractility of the lymphatic vessels is diminished, which is believed to be caused by calcium signalling dysregulation, but exact molecular pathophysiology is still largely unknown(Azhar et al., 2020) . This disruption of calcium signalling has been thought to be caused by chronic inflammation and there is also evidence that VEGFC plays a role due to its roles in vessel leakiness, where mutations in either VEGFC or its receptor VEGFR3 can cause congenital regional or widespread lympodema (Rockson, 2021)

1.11.3 Endothelial cells and TRPV1 in Chronic Pain

Changes to TRPV1 expression were observed in chronic pain conditions, where the expression was increased by 167% after spinal cord injury (Brandt et al., 2012). Allelic variants of the channel can cause different sensitivities to pain, in a similar way that temperature sensitivity is modified, sometimes even causing the channel to desensitise in the absence of external stimuli (Brandt et al., 2012). TRPV1 is trafficked by VEGFR1, showing a direct role for VEGF in mediating the nociceptive pathway (Selvaraj et al, 2015). This mechanism found VEGF to have neuroprotective effects and that it actively protects against repeated desensitisation of TRPV1 (Hulse et al., 2014). Dysregulation of this nociceptive pathway has the potential to cause pain and may be the link between anti-cancer VEGFA targeted treatments and the pain associated with them.

1.11.4 Endothelial cells and TRPV1 in Cancer

Cancer is a term used to describe cells which are maintained in abnormal growth or dysregulation of the cell cycle. These cells can then go on to form a mass, known as a tumour. There are many theories about the origins of cancer, such as the two-hit hypothesis where two mutational events were required for carcinogenesis (Knudson, 1971). Although this theory is widely accepted and used as a foundation for many studies; recent studies in yeast have shown that haploinsufficiency of a tumour suppressor gene is enough to cause an organism to be genetically unstable and therefore have the potential to become cancerous (Coelho et al., 2019). As the tumour grows, it develops what is called a microenvironment, which is the interaction between the cancerous cells within the tumour and the surrounding environment, such as oxygen concentration (Michiels et al., 2016) and pH (Ji et al., 2019). This microenvironment is what is important for endothelial cells and their involvement in cancer as the cancerous cells have been shown to release the various forms of VEGF, thus promoting angiogenesis and lymphangiogenesis of the surrounding circulatory and lymphatic systems respectively (Catalano et al., 2013). Tumours rely on a constant supply of oxygen and nutrients to be able to proliferate, as well as harnessing vessels to metastasise to other areas of the body. The microenvironment in cancer may be enough to activate extracellular TRPV1 receptors expressed in proximity to the tumour. Although the involvement of TRPV1 in cancer and disease are still not fully understood as modulation of its activity can either increase or decrease the severity of the cancer (Li et al., 2021; Figure 1.5). Evidence shows that overexpression can decrease proliferation in pancreatic cancer (Huang et al, 2020) and skin carcinoma (Bode et al, 2009) and using capsaicin as an agonist in renal cell carcinoma cell lines and RT4 positive urothelial cancer cells inhibited proliferation (Liu et al, 2016 ;Amantini et al, 2009) whilst promoting proliferation and migration in oesophogeal squamous cell carcinoma (Huang et al, 2019). This is most likely dose and time dependent, as constant activation could lead to a pathological level of Ca^{2+} influx, causing apoptosis, whilst a smaller activation would increase growth and upregulate factors such as MAPK and cause the cancer to grow quicker. The effects are also different between differing cancer types, showing us that there is still much to learn about TRPV1s involvement in the disease (Li et al., 2021). As the tumour grows larger, they become more and more hypoxic, decreasing the intracellular pH and inducing the secretion of hypoxia inducible factors (HIF) in conjunction with proangiogenic factors to promote vessel growth and development (Pouysségur et al., 2006). Inhibiting the growth of vessels is important as the main cause of mortality in cancer is primary metastasis (Chaffer & Weinberg, 2011) which is influenced by the amount of lymphatic and blood vessels that are available to the tumour (Lee et al., 2017). Figure 1.6 displays a breakdown of the involvement of TRPV1 in cancer from a systematic review of the literature (Li et al., 2021) where all the stimulators and repressors of the TRPV1 signalling in cancer are documented in relation to the downstream biological function. The figure does well to show the complexity of the signalling axis, with capsaicin both upregulating and downregulating proliferation, migration and cell death; all of which are key developmental pathways.

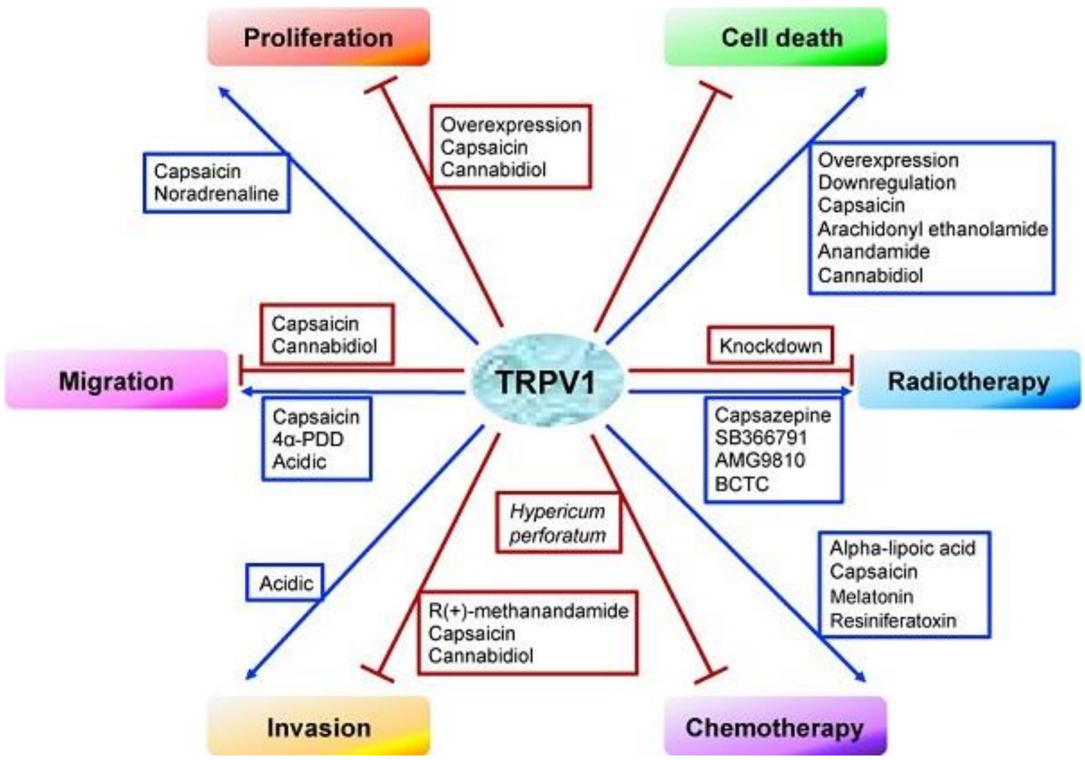

Figure 1.6. *The documented effects of TRPV1 on cancer related functions, blue arrows indicate a positive role and red lines denote a negative role of TRPV1. Image from Li et al., 2021.*

1.12 Zebrafish as a model

In vivo animal models are highly valuable for studying human diseases and conditions as they allow monitoring of disease progression over time, unlike in vitro cell models. However, it's crucial to acknowledge that animals are not humans, which can introduce translational issues when using in vivo models. When planning experiments involving in vivo modelling, these differences between the model organism and human disease must be carefully considered. The zebrafish embryo serves as a valuable model for studying vessel generation in vivo. Due to its closed circulatory system, the vasculogenesis processes during zebrafish embryo development exhibit strong similarities to other vertebrates (Gore et al., 2012). For angiogenic research, transgenic lines of zebrafish with GFP-tagged endothelial cell markers can be utilised, enabling observation of development using fluorescent microscopy and live imaging (Gore et al., 2012, Figure 1.7). Another advantage of using zebrafish for studying vascular development and disease, compared to other animal models, is their ability to survive up to four days without a functional cardiovascular system. This is attributed to their small size and their capability to passively diffuse oxygen during development (Gore et al., 2012). Such characteristics facilitate gene knockouts or knockdowns that may result in early embryonic lethality in higher order vertebrates, like mice. Additionally, zebrafish possess a lymphatic system that shares many similarities with lymphatic vessels found in other vertebrates. During the 2-4 days post-fertilization (dpf) stage, zebrafish embryos develop a colony of parachordal cells (PACs) along the midline, forming the basis of the lymphatic system (Padberg et al., 2017).

These cells originate from the posterior cardinal vein (PCV), and at around 2.5 dpf, they begin to migrate and generate the main lymphatic vessel; the thoracic duct (Nicenboim et al., 2015). Zebrafish lymphatics do display similar lymphatic markers as humans, expressing both prox1 and lyve-1. Although, prox1 exists in two forms in the zebrafish, named prox1a and prox1b. This is a result of the genome duplication event known to occur in teleost fishes (Deguchi et al., 2009). prox1a was shown to not be integral to lymphangiogenesis through targeted mutation but is expressed in lymphatic endothelial cells only (Impel et al., 2014). prox1b, however, is not exclusively expressed in lymphatic endothelium and therefore cannot be used as a marker for lymphatic analysis; it was also shown to not be integral to the development of the lymphatic system through a knockdown study (Tao et al., 2011).

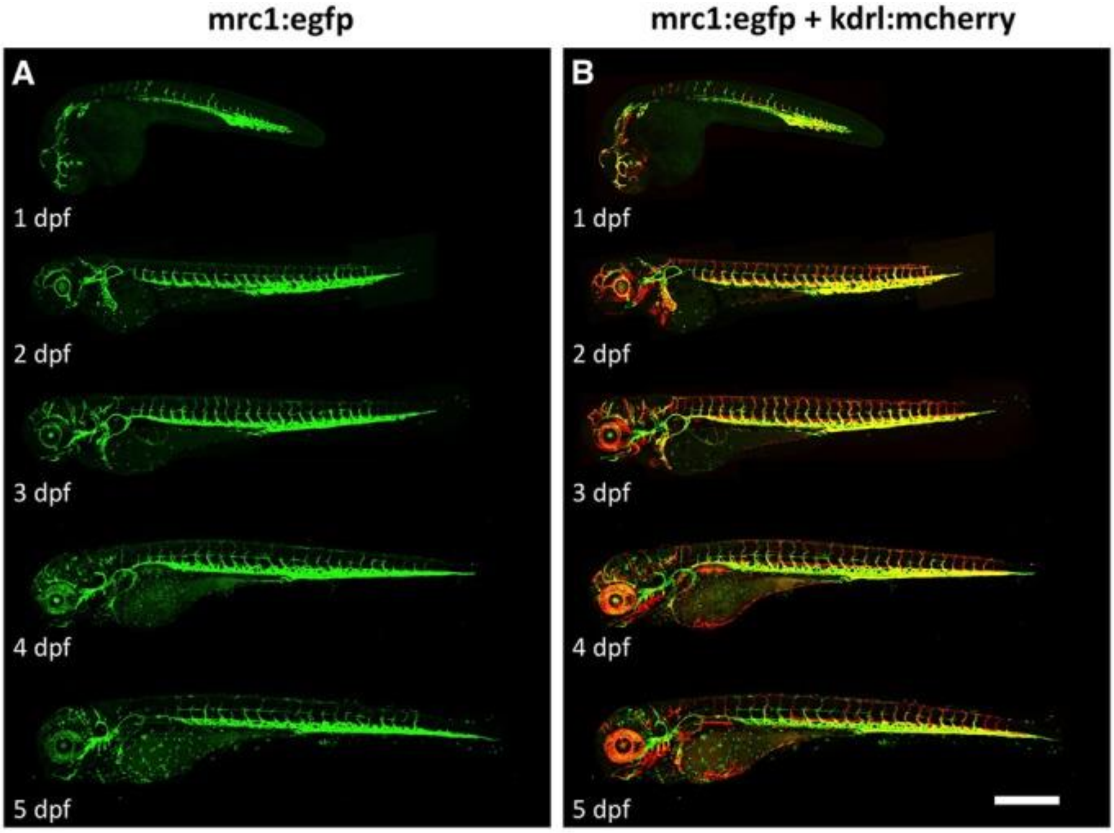

Figure 1.7. *Tg(mrc1a:egfp)y251 transgenic zebrafish express EGFP in veins and lymphatics. Images of mrc1:egfp green fluorescence (A), staining only the lymphatic cells and both mrc1:egfp green and kdrl:mcherry red fluorescence, staining both the lymphatic and blood vessels (B) in double transgenic Tg(mrc1a:egfp)y251, Tg(kdrl:mcherry)y171 embryos during development up until 5 dpf. Image from Jung et al., 2017*

1.13 Zebrafish TRPV1 expression and functions

Zebrafish express a single TRPV1/2 ortholog which has been derived from an evolutionary precursor of tetrapod TRPV1 and 2 (Saito et al, 2006). Throughout this thesis, zebrafish TRPV1/2 is referred to as TRPV1. It is expressed in the trigeminal ganglia, the lateral line, Rohon Beard neurons and the DRG, here it is expressed as early as 1 dpf, increasing over the course of development (Son & Ali, 2022). As development progresses, TRPV1 is expressed on the epithelial layer, as well as continuing to be expressed throughout the nervous system and different organs, including the heart, gills and ovaries (Figure 1.8; Graham et al., 2013) The channel, much like the mammalian TRPV1 is sensitive to acidic changes in pH, heat stress and 2-APB; however, it is not activated by capsaicin (Gau et al., 2013). Outside of development and thermosensitivity roles, TRPV1 was shown to be involved in sperm motility in zebrafish, where blocking the function decreased successful fertility rates (Chen et al., 2020). There is, however, little investigation to the pathways and transcriptional responses which are activated via the activation of TRPV1 in zebrafish.

Knowledge Gap 2: There is a need to understand these mechanisms in a greater depth to aid our understanding of these signalling pathways in vivo and what transcription responses are occurring at scale during development.

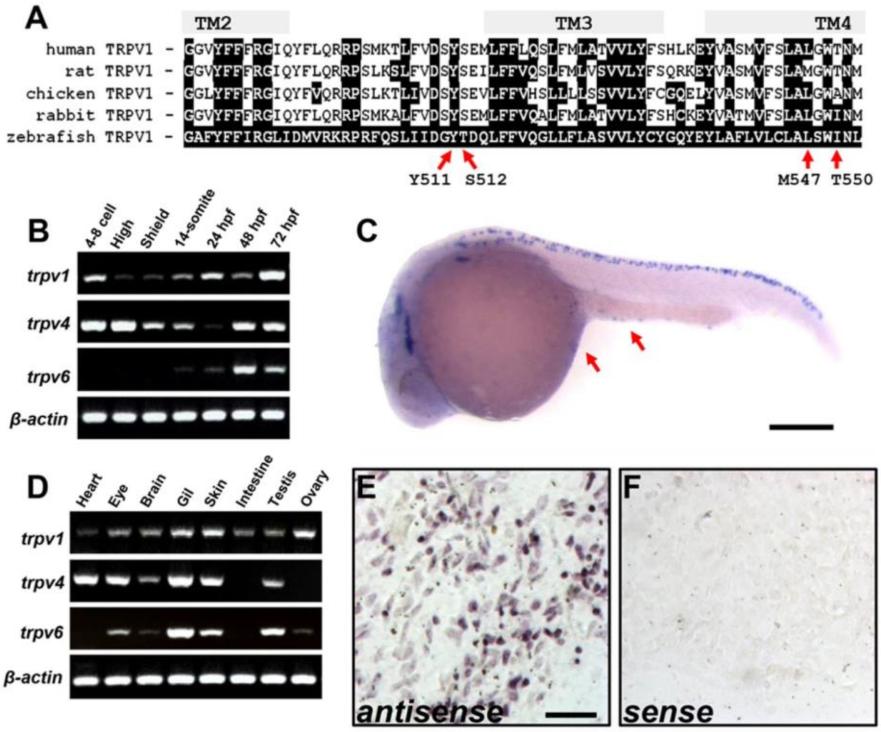

Figure 1.8. *The sequence of TRPV1 and its conservation across species, with red arrows pointing to the regions responsible for capsaicin sensitivity (A), Expression of TRPV in zebrafish identified by RT-PCR at different timepoints, where "high" refers to 3.3hpf and "shield" is 6hpf (B) and in different tissues (D). In-situ hybridization staining of TRPV1 in a 24hpf zebrafish embryo (C), as well as epidermal staning for TRPV1 using RNA probes (E&F). Image from Graham et al, 2013*

1.14 VEGF signalling

The principal regulators of developmental angiogenesis and lymphangiogenesis are known as the vascular endothelial cell growth factor (VEGF) group of molecules and their respective receptors (VEGFR) (Kliche & Waltenberger, 2001). On the whole, VEGFs have essential roles in vasculogenesis, angiogenesis and arteriogenesis with most functional VEGF signalling occurring through the VEGFR-2 receptor (Kliche & Waltenberger, 2001). In endothelial cells, VEGFA inhibits apoptosis by activating the Akt/PBK pathway (Ruan & Kazlauskas, 2012) and upregulates proliferation through the activation of ERK1/2 kinases and regulates various downstream transcription factors (Kliche & Waltenberger, 2001). The expression of VEGFA also increases the production of NO in endothelial cells, which is known to have downstream effects on vascular permeability as well as proliferation and angiogenesis (Vallance & Hingorani, 1999).

1.15 VEGF and disease

Haploinsufficiency of VEGFA in humans causes cardiovascular diseases such as tetralogy of fallot, anc complete loss of VEGFA is embryo lethal (Reuter et al., 2019). Other aberrations of VEGF signalling are implicated in multiple diseases such as pathologies of the eye (Witmer et al., 2003). The cornea relies on the absence of blood vessels for transparency, pathological ingrowth through aberrant signalling can block the cornea and therefore reduces visual activity. The cornea relies on no blood or lymphatic vessels crossing the limbus. VEGFA has also been shown to be expressed by not only endothelial cells but also by hypoxic tumour cells to increase viability and proliferation of the cancer and there is a direct link to the growth rate of the tumour and their ability to promote angiogenesis (Carmeliet, 2005). This link has caused VEGFA to become the most common target of anti-angiogenic treatment for cancer and is included in combination to most targeted therapies (Comunanza & Bussolino, 2017). Tumours rely on a constant supply of oxygen and nutrients to be able to proliferate. They also harness vessels for metastasis to other areas of the body. As the tumour grows larger, they become more and more hypoxic which decreases the intracellular pH, inducing the secretion of hypoxia inducible factors (HIF) and proangiogenic factors to promote vessel growth and development (Pouysségur et al., 2006). Among these factors, cancerous cells can release different forms of VEGF to promote angiogenesis and lymphangiogenesis of the surrounding cardiovascular vessels (Catalano et al., 2013). Because of this dysregulated secretion of proangiogenic factors, tumour vessel growth has been shown to be more chaotic than regular angiogenesis, lacking the uniformity and structure of normal vasculature (Warren, 1979), they are also leaky and less stable, caused by the overexpression of VEGFA (Ozawa et al., 2004). In humans, most solid tumours can exist in the body for months to years without their own blood supply but without a blood supply, are only able to grow to around 3mm in diameter (Carmeliet, 2005). Whilst there has been some promise using treatments which target pro-angiogenic factors and pathways such as MAPK (Huang et al., 2008) and VEGF (Kim et al., 1993), tumours have shown to grow a resistance to these treatments and there is a need to identify novel pathways that could provide alternate drug targets. One of the most common drug treatments for vascular forms of cancer is an anti-VEGFA antibody drug known as bevacizumab (brand name; Avastin). This drug blocks VEGFA signalling and prevents the formation of new blood vessels for the tumour. It is routinely used in cancers such as colorectal (Tol et al., 2009), renal (Yang, 2004) and breast (Kümler et al., 2014), among others (Garcia et al., 2020). Side effects of bevacizumab treatment are more commonly cardiovascular, with 23.6% of patients experiencing hypertension and 1.6-4% of patients suffering heart failure (Lewandowski & Szmit, 2016).

Knowledge Gap 3: There is a need for a greater understanding of whether TRPV1 signals through the same molecular pathways as VEGFA during development and if a stressed embryo during development can handle the loss of one of these two key proteins.

1.16. Thesis aims by chapter.

By identifying gaps in the knowledge, I have identified my specific objectives as being:

Chapter 2 will investigate the effects downstream of TRPV1, and to observe transcriptional responses of Human Dermal Lymphatic Endothelial cells (HDLECs) exposed to CGRP in vitro and will be focussed at addressing knowledge gap 1. This aims to provide a better understanding of which molecular pathways and genes are activated through the release of CGRP. **Chapter 3** investigates knowledge gap 2 and uses developing zebrafish embryos as a model and investigates the loss of TRPV1 during development and the phenotypic and transcriptional response. **Chapter 4** further elucidates these responses whilst addressing the third knowledge gap identified, by using a factorial design of TRPV1 stimulants in addition to bevacizumab and aims to investigate the changes in various cardiovascular related genes under different stressors, comparing against the VEGFA treatment.

In this thesis, I am aiming to tackle the knowledge gaps identified above in the following ways: Chapter 2 will tackle this aim by analysing microarray data from a HDLECs which have been stimulated by CGRP, to investigate the responses when the CALCRL receptor is activated via this neuropeptide. **Chapter 3**'s aim will be investigated using morpholino (MO) knockdown of TRPV1, and RNA-seq performed, as well as immunofluorescence staining to observe any phenotypic changes to the vessel structure and swim behaviour will also be recorded in order to document any behavioural changes in response to heat post knockdown. **Chapter 4** uses the same MO knockdown but also uses bevacizumab in order to draw a comparison between TRPV1 knockdown and VEGFA targeted inhibition.

The benefit of this research will further our understanding of TRPV1 signalling in stressed conditions and also what happens in the absence of this channel. This knowledge will have real world applications in diseases where TRPV1 is involved and situations where changes to the environmental niche can have detrimental effects to wild populations.

Chapter 2: Neuropeptides AM and CGRP upregulate CA2 but cause different downstream signalling in primary human lymphatic endothelial cells.

2.1 Abstract

Adrenomedullin (AM) and calcitonin gene related peptide (CGRP) are both a part of the calcitonin related family of peptides. They both bind to endothelial cells expressing CLR and have overlapping functions, including angiogenesis and vasodilation. Whilst they are similar, there is evidence that their downstream signalling pathways are different. This study aimed to investigate similarities and differences in CLR receptor activation in endothelial cells through these two common neuropeptides. Primary human dermal lymphatic endothelial cells (HDLECs) were stimulated for three hours with each ligand independently, gene expression was measured via microarray and fold change values were confirmed through qPCR. This study shows that both AM and CGRP were able to generate a transcriptional response in HDLEC cells, and that the CLR receptor was expressed in them. The functional enrichment analysis provided insight into the biological functions behind these genes, where it was discovered that the majority of those differentially expressed genes were involved in migration, proliferation and chemotaxis. Evidence shows that CGRP causes a larger transcriptional response in HDLECs, causing differential expression in 144 genes compared to 23 when stimulated by AM. Genes that were upregulated by both were involved in vasodilation and angiogenesis, with both peptides upregulating Carbonic Anhydrase 2. The remaining differentially expressed genes may perform biological functions unique to each peptide. This provides greater insight into the roles of the two signalling peptides in endothelial cell biology.

2.2 Introduction

While it is known that endothelial cells express the CLR receptor on their surface, little is known about the effects of stimulation with its different agonists on the transcriptome of the lymphatic endothelial cells. We planned to investigate these changes in vitro by stimulating lymphatic endothelial cells with the various ligands and then performing a microarray followed by a qPCR confirmation to identify potential novel lymphangiogenic pathways and mechanisms. In addition to this, the various RAMPs and CLR itself were knocked down in HDLEC cultures using siRNA to identify if there are any autocrine loops that would be disturbed upon the knockdown of the receptor.

CGRP is a well-known potent vasodilator (Brain et al, 1985; Tippins et al, 1986) and neurotransmitter (Kinoshita et al, 1993), which is part of a large group of molecules known as calcitonin agonists which includes amylin (AMY), adrenomedullin (ADM) and intermedin (also known as ADM2). There are two forms of CGRP in humans, αCGRP and βCGRP which are coded by separate genes on chromosome 11. αCGRP is the predominantly expressed and most studied form, being present in sensory neurons of the dorsal root ganglia as well as the trigeminal system and the vagal ganglia (Kumar et al., 2022). βCGRP is primarily expressed in the enteric nervous system (Mulderry et al, 1988). There is evidence of involvement of CGRP in the pathobiology of migraines, with the plasma concentration of CGRP being increased during the headache phase of a migraine attack or cluster headache (Doods et al, 2007).

R is an open-source software project that was developed in 1995. (R core team, 2017). While it has its benefits, R also has its disadvantages when developing and maintaining a pipeline. The main one is its reliance on packages and as it is possible that an established pipeline could be broken when R and its packages are updated. Within Bioconductor itself, there are over 1200 R packages for the analysis of various biological datasets. Limma is a widely used Bioconductor package that has been designed for the analysis of gene expression data generated by microarray or RNA-Seq (Smyth, 2005). It can successfully be used to analyse both two colour and single channel microarrays. At its core, the package uses linear modelling which takes the experimental design into account. It is a powerful tool in genome wide studies with the ability to compare many expression values in a given dataset, read data from various technologies and built in functions to process and normalise the data. The use of easily accessible, open-source packages such as limma is important in biological research as it allows anybody to recreate the analysis performed within a study.

Microarray technology generates such a large amount of data, meaning that the significance of differentially expressed genes could not be analysed with a standard t-test. To get around this, more stringent and powerful tests have been devised that will work with the larger datasets; the most notable and commonly used are the empirical Bayes (Smyth, 2004) and the TREAT (McCarthy & Smyth, 2009) tests. Empirical Bayes (eBayes) works similar to a t-test, calculating individual significance scores for each gene to define significance through the moderation of standard errors. The TREAT method uses the log fold change (logFC) to define the significance between conditions and is a more stringent method than eBayes.

The calcitonin related family of peptides comprises of six hormones: two (alpha and beta) forms of calcitonin gene related peptide (gene CALCA, protein CGRP), adrenomedullin (gene *ADM*, protein AM), intermedin (gene ADM2, protein AM2), amylin (gene IAPP, protein AMY) and calcitonin itself (gene CALCA, protein CT). These six hormones bind to a common GPCR, known as the calcitonin receptor like-receptor (gene CALCRL, protein CLR, Wimalawansa et al, 1997). The binding affinity of the CLR receptor is dependent on the receptor-activity-modifying-proteins (RAMPs). The RAMP family contains three different proteins; RAMP1, RAMP2 and RAMP3, each of which causes the CLR receptor to have a different binding affinity for each of the calcitonin related hormones through the formation of a heterodimer complex (Kuwasako, 2011). This heterodimer causes a conformational change in the binding site of the CLR receptor (Hay & Pioszak, 2016) RAMP2-CLR or RAMP3-CLR have a higher affinty for binding AM while RAMP1-CLR has the highest binding affinity for CGRP (Kuwasako, 2011; Hay et al, 2018). CLR signalling is also a key factor in pathophysiology of cardiovascular diseases and vascular cancers, being highly expressed in Kaposi's sarcoma (Hagner et al, 2006) and renal cell carcinoma (Nikitenko et al, 2013).

Both AM and CGRP are well-studied hormones. AM is circulated in plasma, meaning it is in direct contact with the blood endothelium. In fact, it has been shown to be a multifunctional peptide relevant for endothelial cell function. AM is involved in angiogenesis (Ribatti et al, 2005), development (Garayoa et al, 2002), and is a potent vasodilator (Heaton et al, 1995). AM knockouts in mice cause embryonic lethality (Ando & Fujita, 2003); with endothelial cell-specific knockout mice showing reduced levels of angiogenesis, increased vessel permeability but less ischemia-induced brain damage (Ochoa-Callejero et al, 2016). AM expression is also, to a lesser extent, mediated through another GPCR, ACKR3 (also known as CXCR7), which is similar in structure to CLR and has been shown to scavenge AM and therefore regulate its function by acting as a decoy receptor (Klein et al, 2014). This plays an important role in mediating AM signalling in cardiac and lymphatic development (Klein et al, 2014).

CGRP is primarily a neuropeptide and exists in two forms, named αCGRP and βCGRP. While they have similar functions to AM, they are coded by two different genes that both reside on chromosome 11 and have 90% homology (Hu et al, 2016). The gene for αCGRP is the same as for CT (CALCA) and is transcribed through alternative splicing whereas βCGRP originates from the distinct CALCB gene. The peptide, in humans, is most abundant in sensory C and Aδ nerve fibres (Hu et al, 2016). CGRP is released by the thermosensitive TRPV1 channel in response to various noxious stimuli, including low pH and chemicals such as capsaicin (Peng & Li, 2010). Levels of this peptide in the blood are linked to migraines, making CGRP a drug target (Russo, 2015). Similar to AM, CGRP is also a potent vasodilator (McCormack et al, 1989; Russel et al, 2014). Whilst both peptides bind to the same CLR receptor, they were hypothesised to desensitise the receptor through independent mechanisms (Nikitenko et al, 2006).

We hypothesise that AM and CGRP will induce different downstream signalling cascades, evident through differences in gene expression and the biological relevance of those genes in human dermal microvascular lymphatic endothelial cells.

2.3 Materials and Methods

2.3.1 CLR agnoism and Analysis

The data that was analysed as part of this project was collected through the stimulation of lymphatic endothelial cells with either adrenomedullin, amylin, CGRP or PBS for 4 hours at a concentration of 10^{-6}M. Stimulation was confirmed through the use of a western blot to show whether the MAPK pathway was activated. After 4 hours of stimulation in starved media with 1 x 10^{-6}M (or PBS for control), the RNA was extracted using a miRVANA RNA isolation kit (thermofisher), and cDNA was generated using a superscript II kit; both performed using manufacturer's protocol. The cDNA was then sent to collaborators at University College London (UCL) who performed a microarray using an illumina HT-12 V4 chipset and provided the raw data for this analysis.

To determine differentially expressed genes between AM stimulation and PBS control, and between CGRP stimulation and PBS control, the microarray data was pre-processed using the Illumina Beadchip proprietary software, which provides spot intensity values and p values for each spot to determine whether or not the fluorescence value is true or not for both the control and the experimental conditions.

This data was read into R (R core team, 2017) using the linear models for microarrays (limma) package (Smyth, 2005) within Bioconductor (Gentleman et al, 2004) where it was quantile -normalised and fit to a linear model, followed by empirical Bayesian transformation (Efron & Tibshirani, 2002). The p values were adjusted using the FDR adjustment set at 0.05, to control false discoveries (Benjamini & Hochberg, 1995).

The full code of the reading of the data with statistical transformation with respect to adrenomedullin stimulation compared to PBS control (as an example for the analysis performed for all conditions) is as follows:

```
Illumina.data = {setwd("wd")
```

```
library(limma)

x = read.ilmn(files = "P170490_SampleProbeProfile.txt", ctrlfiles =
"P170490_ControlProbeProfile.txt")

targets = readTargets("targets2.txt")

y = neqc(x)

eset = y[,c("LN-2", "LN-8","LN-14","LN-6","LN-12","LN-18")]

ct = factor(targets$Conditions)

design = model.matrix(~0+ct)

colnames(design) = levels(ct)

contrasts = makeContrasts(AM-PBS, levels = design)

fit = lmFit(eset, design)

fit2 = contrasts.fit(fit, contrasts)

fit3 = eBayes(fit2, trend= TRUE)
```

Where “wd” refers to the working directory in which the data is kept. Once the data is read and the empirical bayes transformation has taken place, the genes that had statistically significant p-values after false discovery rate correction (< 0.05) were selected using the R code. The code extracts the raw data expression values of these significant genes and creates a new matrix:

```
selected = p.adjust(fit3$p.value, method = "fdr") <0.05

esetsel = eset[selected,]

matrix = data.matrix(esetsel$E)
```

The results of this analysis were then plotted into heatmaps and volcano plots. For the generation of heat maps, heatmap2 from the package gplots was used (Warnes et al, 2015). For volcano plots, ggplot2 was used (Wickham, 2016)

2.3.2 Western Blot

For the analysis of MAPK, cells were lysed at 15 minutes with RIPA buffer and the protein was collected for western blot analysis. Lysate was separated on a 10% SDS-PAGE gel and then transferred to a polyvinylidene difluoride (PVDF) membrane using a standard wet transfer technique. Protein was quantified using ThermoFisher's Pierce™ BCA assay following manufacturer's instructions and 30ug of protein lysate was reduced using B-mercaptoethanol before being loaded onto a 10% SDS page gel and ran using electrophoresis. Wet transfer was used to transfer the protein to a PVDF membrane for blotting. 5% Milk in 0.1%TBS/T was used for both blocking and blotting.

Table 2.1. *A table outlining the primary antibodies used in the western blot for MAPK and CLR*

Target	Producer	Product number	Dilution
P44/42 MAPK	Cell signalling	#9101S	1:1000
Total MAPK	Cell signalling	#9102S	1:1000
ACTB	abcam	#ab6276	1:1000
GAPDH	Advanced immuno-chemical	#2-RGM2	1:1000
CLR	Nikitenko et al., 2006	LN-1436	1:1000

2.3.3 RNA isolation and qPCR

qPCR was performed on a selection of genes (BMP4, CA2, CXCR4, EDNRB, F2RL1, ITGA6, VCAM1 and PTMA) that were significantly either under- or overexpressed in the microarray.

Primary foreskin HDLECs were obtained from promocell™ and seeded in 6 well plates and 75,000 cells were seeded per well. These cells were then left to grow over two days for full confluence, with regular media changes (MV2 with growth factors, promocell™). The cells were stimulated with 1 x 10^{-6}M of either adrenomedullin or CGRP diluted in MV2 media without the growth factors as was performed for the original microarray. Each step was replicated in its entirety for both experiments to ensure comparability, including the same passage for the cells. The cells were stimulated for a period of 4 hours before lysis. RNA was isolated from these plates using the mirvana miRNA isolation kit (ThermoFisher™) using manufacturer's instructions for total RNA extraction from cell cultures.

For qPCR, taqman™ probes (ThermoFisher™) were used to avoid the complications known to occur with the use of SYBR green. The genes which were selected are shown in Table 2.3. Genes were chosen to have a coverage of both up and down regulated genes in each condition cDNA was generated using superscript II (Invitrogen™) and random nonamers (Invitrogen™) and the manufacturer's instructions. 140 ng of RNA was used per reaction, providing a final cDNA concentration of 7ng/uL assuming a 1:1 conversion of RNA to cDNA. The cDNA product was then diluted 1:3 to give a concentration of 1.75ng/uL and 5ul was used per qPCR reaction, meaning 8.75ng of cDNA was used per qPCR reaction.

Premade, catalogued Taqman probes (see appendix for product codes) were used for the qPCR (ThermoFisher™) in a step one real time thermocycler. cDNA was used, making this a two-step reaction so that quality could be checked at every stage. ΔΔCt calculations were performed for the qPCR using the geometric mean of the housekeeping reference genes to calculate control averages (Vandesompele et al, 2002). Log Fold change was calculated as $log_{10}(-2^{-\Delta\Delta Ct})$. Statistical outliers were removed if a value fell ± 1.5 x IQR (interquartile range), using Tukey's boxplot outlier method (Tukey, 1977).

2.3.4 Gene Ontology

Gene Ontology enrichment analysis was performed within CYTOSCAPE (Shannon et al, 2003) using the ClueGo app (Bindea et al, 2009) with the CluePedia plug-in (Bindea et al, 2013). ShinyGo (Ge et al., 2020) was used for enrichment of differentially expressed genes against the Jensen Lab DISEASES database (Pletscher-Frankild et al., 2015).

2.3.5 Graphing and statistics

All statistical coding was done in R (R core team, 2017) and the correlation graphs were produced using the ggplot2 package (Wickham, 2016). The heatmaps were created using the gplots package (Warnes et al, 2015).

2.4 Results

2.4.1 Microarray

The intensity analysis of the microarray results demonstrated uniformity across the conducted samples (Figure 2.1A). Utilizing a multidimensional scaling (MDS) plot (Figure 2.1), the microarray data was plotted to isolate two random groups of genes. This graph revealed clear differences between the experimental conditions, indicating distinct groupings resulting from AM and CGRP treatments. It effectively showed whether the same genes were up or down regulated across the conditions.

A)

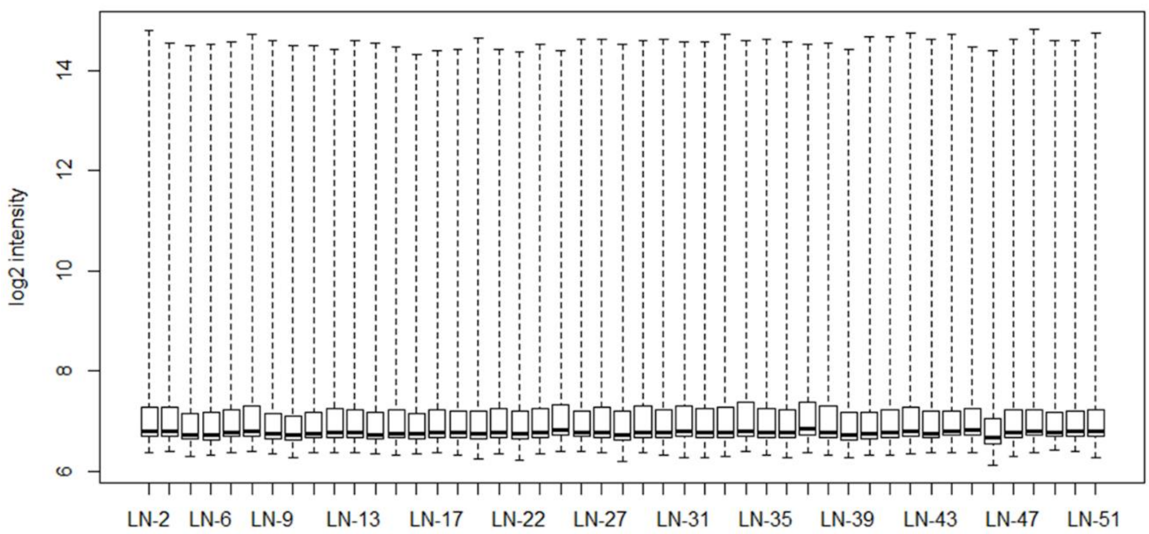

B)

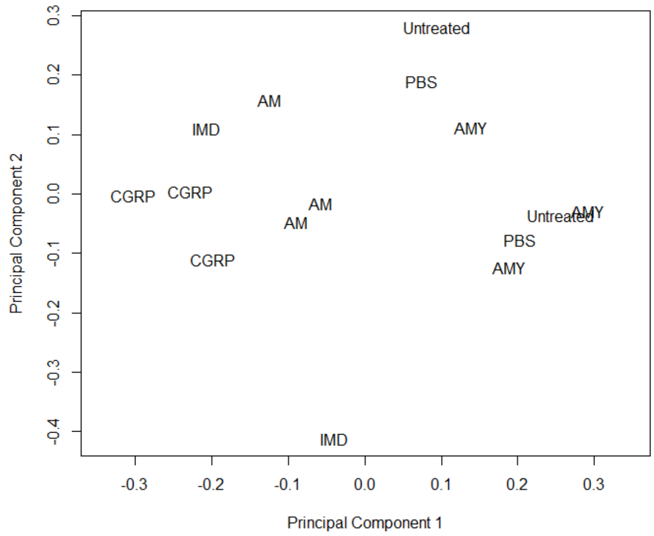

Figure 2.1. *A) boxplot showing the probe intensities across the microarray chips, each LN-X refers to a sample and log2 intensity refers to the fluorescence intensity of each probe. B) a multidimensional scaling plot (MDS) which uses two randomly chosen components (sets of genes) of the dataset to show the relatedness of the samples. AM = adrenomedullin; CGRP = calcitonin gene related peptide; IMD = intermedin; PBS = cells treated with PBS; Untreated = Untreated cells.*

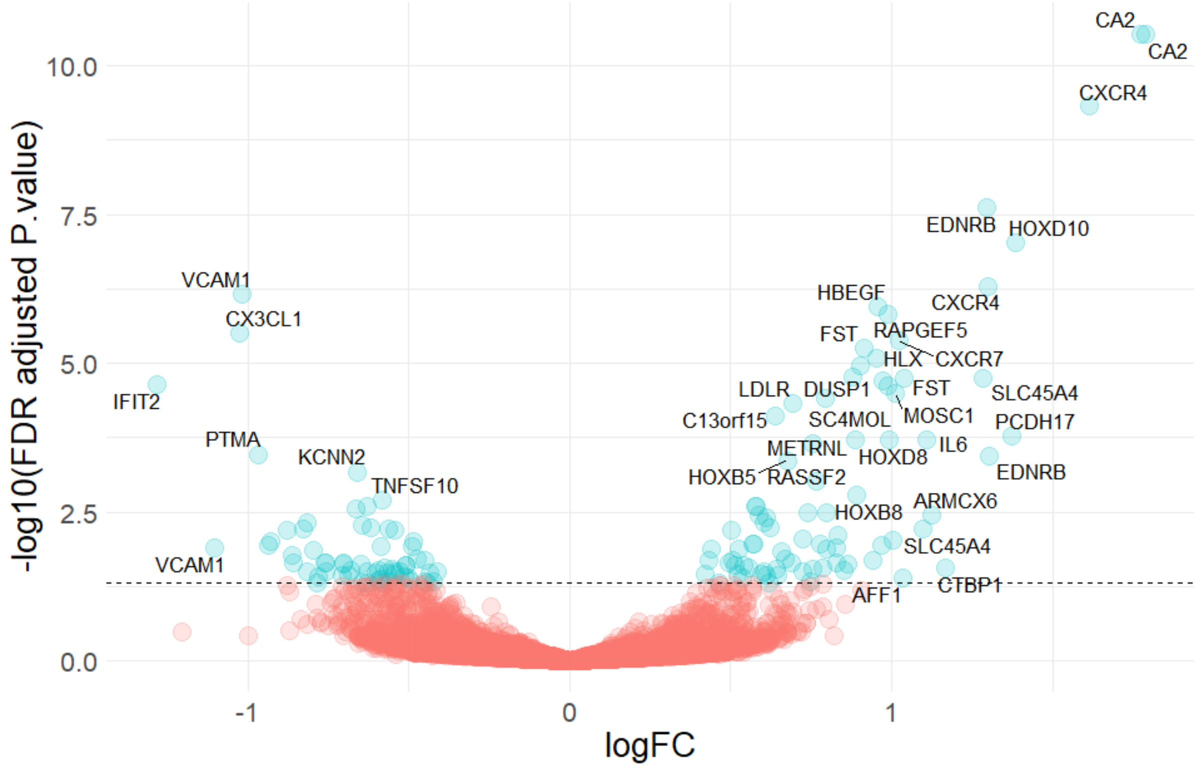

__Figure 2.2.__ Volcano plots showing the log fold changes and -log10 adjusted P-values of calcitonin gene related peptide treated HDLECs. Genes above the significance cut off are in blue and labelled, those that are considered non-significant are in red.

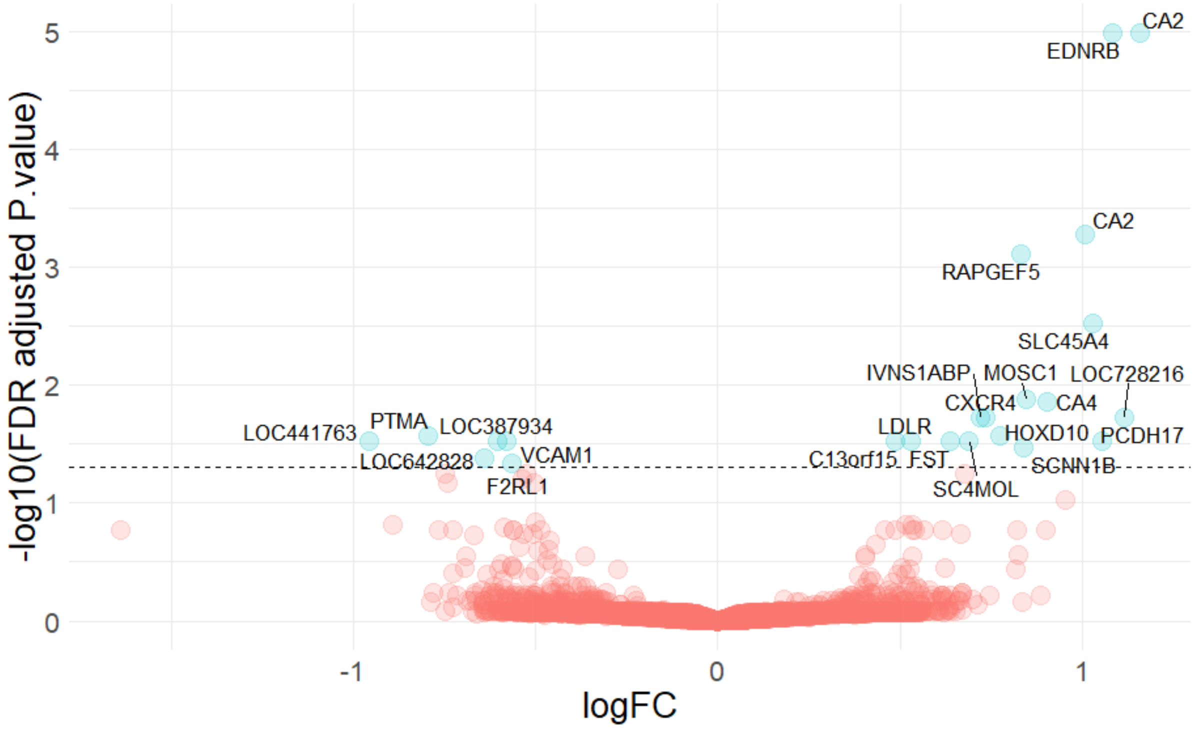

__Figure 2.3.__ Volcano plots showing the log fold changes and -log10 adjusted P-values of adrenomedullin treated HDLECs (B). Genes above the significance cut off are in blue and labelled, those that are considered non-significant are in red.

The volcano plots (Figures 2.2, 2.3) of the microarray analysis results using limma, comparing PBS against either CGRP stimulation (Figure 2.2) or AM stimulation (Figure 2.3) of HDLECs show differences not only on the numbers of genes differentially expressed but also the scale of this change in expression. Only 17 genes (Figure 2.5) were shared between the two conditions, whilst CGRP influenced the expression of 127 genes, almost 20-fold more genes than AM agonism, which only uniquely affected 6 genes. Of these genes, the numbers of up and down regulated was even in both conditions (Figure 2.5 and Table 2.1). Full lists of these genes are listed in Supplementary Tables 1.1 (CGRP) and 1.2 (AM). Two points for CA2 can be seen on both volcano plots (Figures 2.2 and 2.2), this is due to two probes being present for this gene, a practice which is not uncommon in microarray experiments although interestingly the two probes for CA2 in AM whilst both significant were quite different in terms of p.values, one of them being 1x10-5 and the other having a FDR-adjusted p.value of $5x10^{-4}$. This gene was the most significant in CGRP, with both probes having identical adjusted P. values of 3×10^{-11} (Supplementary Table 1.1). The results of the volcano plot also show the scale of these changes in expression, CA2 in CGRP expression was increased by a log fold change of 1.7, whilst the most significant probe for CA2 in AM only had a log fold change of 1.16. A similar pattern can be seen for the downregylated genes also, with VCAM1 being underexpresed in both conditions, with a log fold change of -1.017 in one probe and -0.75 in the other for CGRP, with FDR adjusted p. values of 4x10-5 and 7×10^{-7}, respectively. AM's expression of VCAM1 only had a log fold change of -0.5 with an FDR adjusted p.value of $8 \times 10^{-6.}$

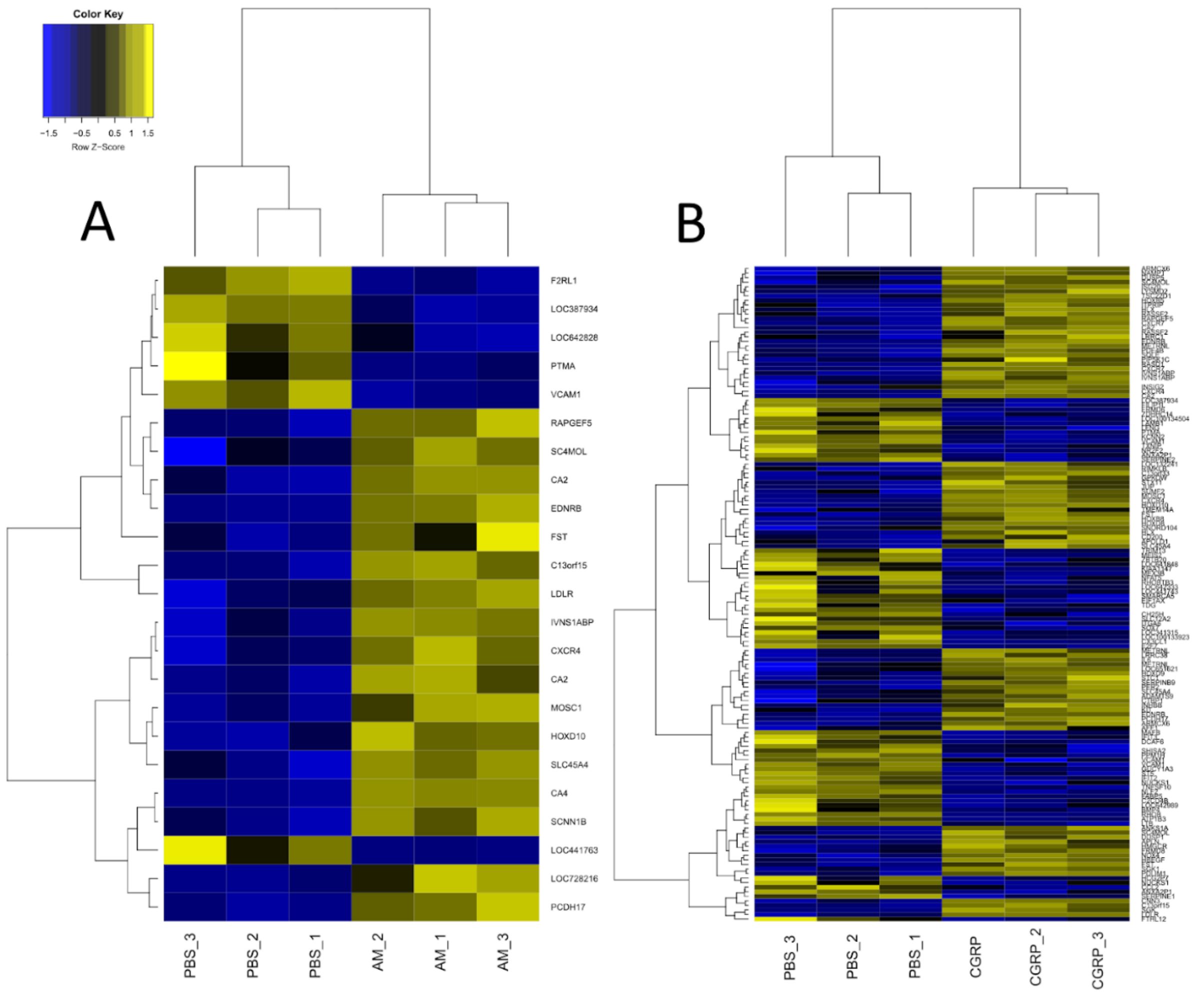

Figure 2.4. *A) A heat map showing the significantly differentially expressed genes between the PBS and the AM treatment groups. Blue is under expressed and yellow is overexpressed. The dendrograms represent the relatedness between the samples and the conditions. B) A heat map showing the significantly differentially expressed genes between the PBS and CGRP treatment groups. Blue is under expressed and yellow is overexpressed.*

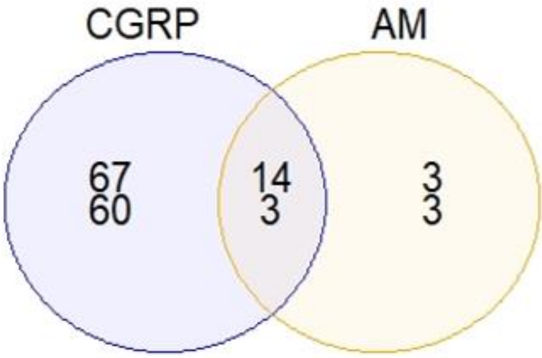

Figure 2.5. *A Venn diagram showing the relationship between the amount of significantly differentially expressed genes between the two conditions, the number on the top is overexpressed and the number on the bottom is under expressed.*

Table 2.2. *The list of shared genes between AM and CGRP stimulation in HDLECs*

Shared genes	
Upregulated	**Down regulated**
PCDH17	*PTMA*
MOSC1	*VCAM1*
LDLR	*LOC387934*
IVNS1ABP	
HOXD10	
EDNRB	
C13orf15	
CA2	
FST	
CXCR4	
RAPGEF5	
SC4MOL	
SLC45A4	

The results of the intermedin (IMD) agonism showed only 15 genes being differentially expressed (Figures 2.6 and 2.7), and only two out of three of the original samples passed the QC metrics to be run on the microarray. Intermedin stimulation was shown to influence some of the same genes shared by AM and CGPR, including FST, CA2, ENDRB, HOXD10, VCAM1 and LDLR, with again CA2 being the most significant.

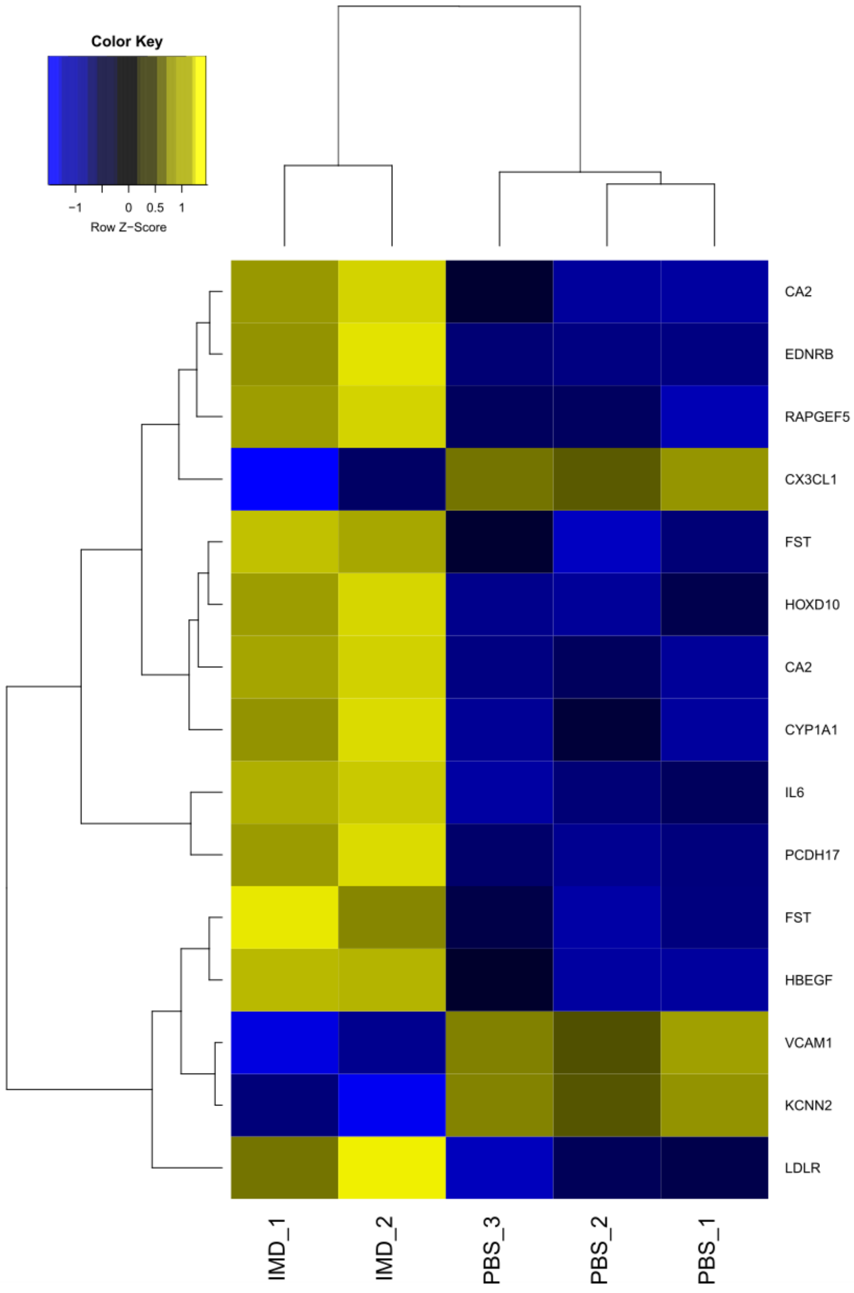

Figure 2.6. *A heatmap showing the differentially expressed genes upon HDLEC stimulation with intermedin compared to cells treated with PBS. Blue is under expressed and yellow is overexpressed. Dendrograms show the relatedness between the genes and the samples.*

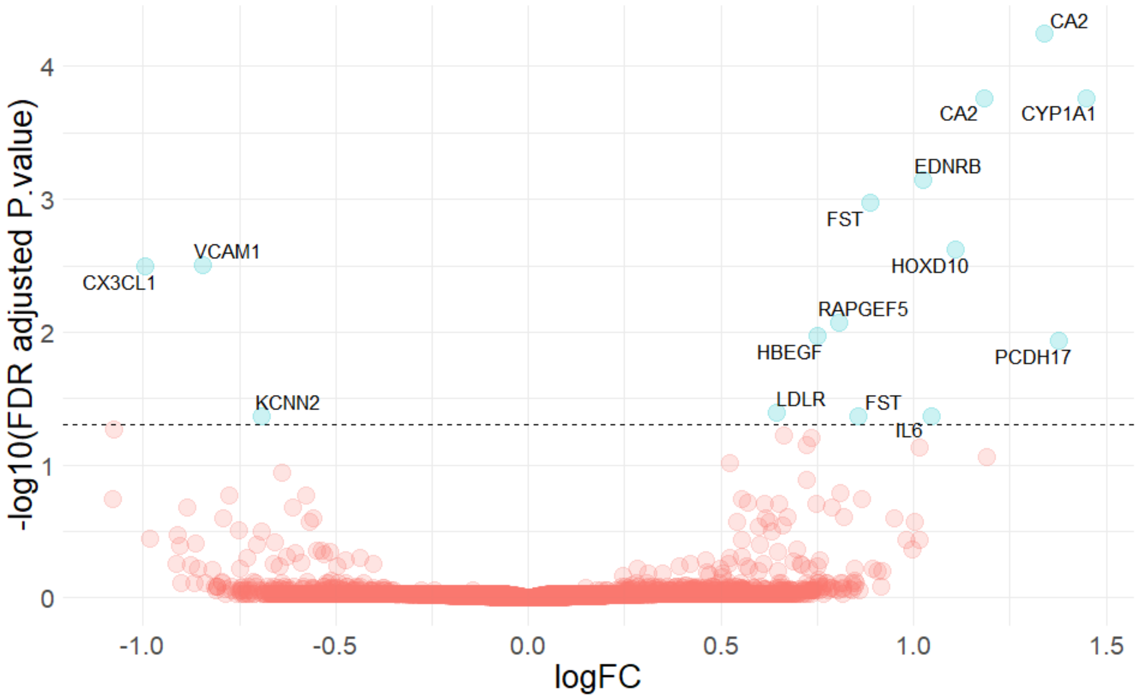

Figure 2.7. *A volcano plot showing the log fold change and the -log10 p. values, the genes that were significantly differentially expressed upon stimulation with intermedin are shown in blue with labels, those that are non-significant are in red.*

2.4.2 Western Blot

To confirm the microarray findings, an experiment which repeated the same conditions of the microarray treatment was performed and the RNA was extracted using the mirVana isolation kit. Before extracting RNA, the stimulation of the cells by the CALCRL ligand through the use of western blotting. Western blot was used to confirm the activation of the lymphatic endothelial cells upon stimulation of the growth factors prior to RNA extraction and the following microarray confirmation with qPCR. ACTB and GAPDH were used as loading controls.

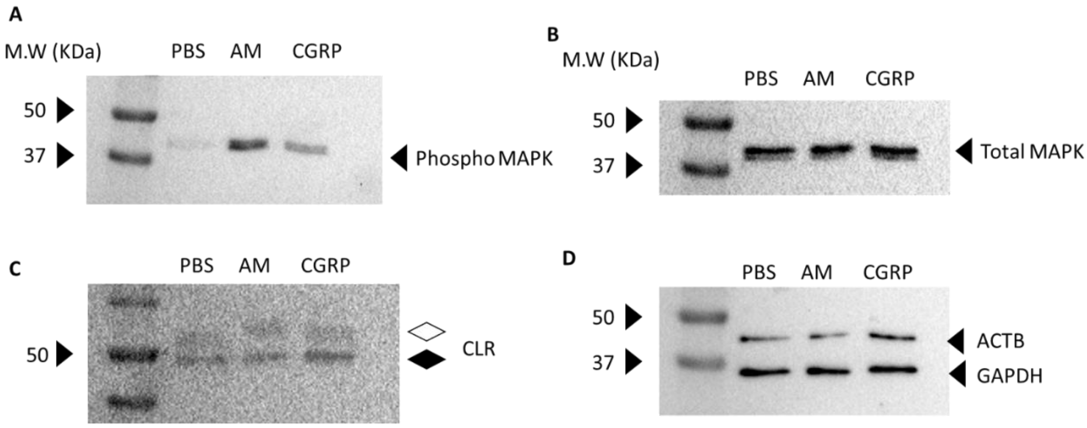

Figure 2.8. *Western blots showing that ligand stocks did stimulate MAPK in the studied endothelial cell population (A and B), whilst also showing that CLR is expressed in them (C). ACTB and GAPDH were used as loading controls (D). The black diamond in western blot (C) shows the core glycosylated form of the CLR receptor at ~50kDa, and white diamonds label the mature, fully glycosylated form at around ~55KDa. N=3*

The expression of phospho-MAPK was increased upon the addition of adrenomedullin and CGRP for 15 minutes post stimulation (Figure 2.8A). The expression of CLR also displays a motility shift, caused by translational modifications to the receptor, changing the size of the protein.

2.4.3 RNA Nanodrop Quantification

RNA was quantified using a nanodrop, which can also be used to assess purity. The 260/230 ratio from the nanodrop shows that the RNA extracted had remnants of phenol or guanidine thiocyanate from the kit used in the extraction, which may have affected the efficiency of the qPCR. The 260/280 ratios were 2 for all but two of the samples - PBS1 and PBS3, meaning that there was little protein contamination in the RNA samples (Table 2.3).

__Table 2.3.__ The nanodrop purity and concentrations of the RNA samples that were used in the qPCR experiment. Sample ID refers to the treatment that was performed to the HDLECs extracted, PBS being the control.

Sample ID	ng/ul	A260	A280	260/280	260/230
AM1	14.68	0.367	0.179	2	0.05
AM2	23.16	0.579	0.361	2	0.06
AM3	21.08	0.527	0.307	2	0.06
AM4	21	0.525	0.269	2	0.05
PBS1	43.64	1.091	0.829	1.32	0.11
PBS2	33.97	0.849	0.551	2	0.08
PBS3	23.94	0.599	0.408	1.47	0.08
PBS4	18.69	0.467	0.241	2	0.06
CGRP1	23.76	0.594	0.351	2	0.09
CGRP2	17.94	0.449	0.239	2	0.04
CGRP3	32.25	0.806	0.527	2	0.08
CGRP4	26.48	0.662	0.41	2	0.07

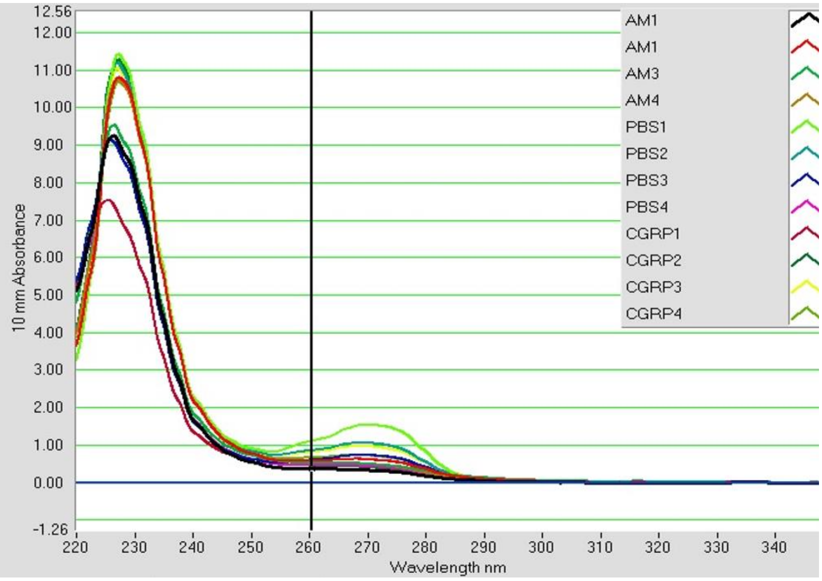

***Figure 2.9.** nanodrop curves for RNA extracted for the qPCR experiments.*

2.4.4 qPCR

qPCR standard curves were made to check both the efficiency of the taqman probes and the cDNA performance. The efficiency of the probes was 89.97% for ACTB and 97.39% for F2RL1 (Figure 2.10A). The products of the ACTB PCRs were also run on an agarose gel to observe specificity (shown in Figure 2.10C). When performing qPCR on the rest of the chosen genes (Table 2.4), they appeared to amplify much later than expected (Figure 2.11), with some genes amplifying as late as 30 cycles. Even though that these findings may be unreliable because of the late Ct, these results were kept in the analysis so as not to lose any data as these may be genes in which the expression was reduced so much that they would amplify much later than expected.

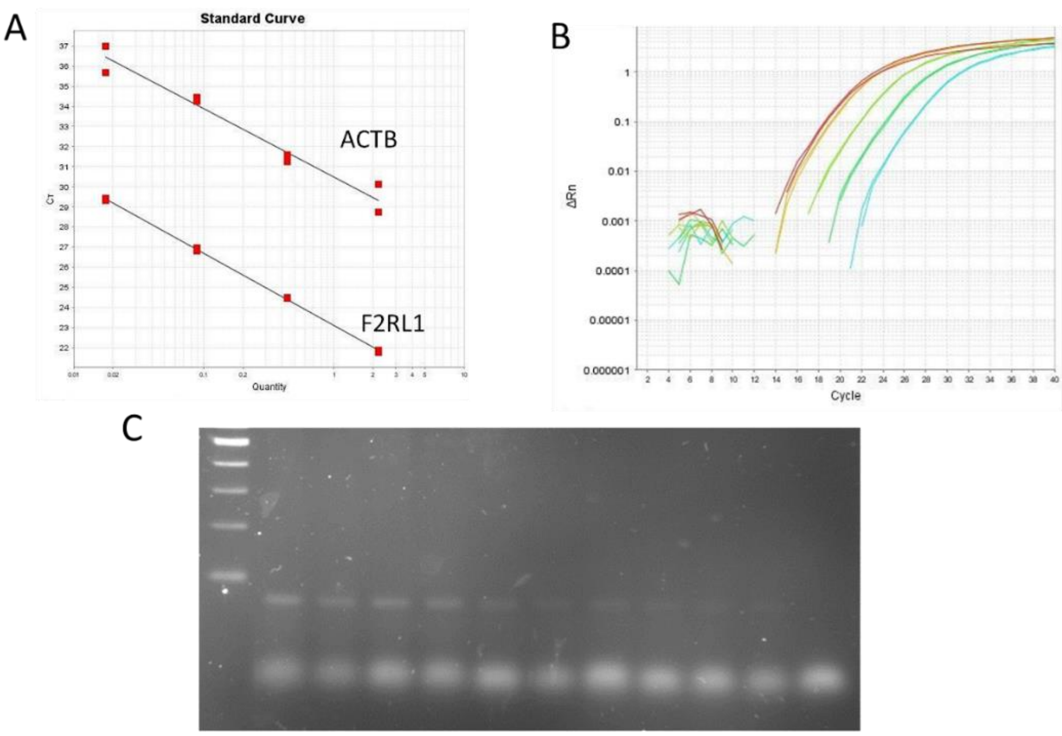

Figure 2.10. *A) The standard curves for F2RL1 (1) and ACTB (2), B) The amplification plot of the standard curve for ACTB. C) The ACTB standard curve visualised on a 2% agarose gel to check for product specificity, going from more concentrated (left) to less concentrated cDNA (right).*

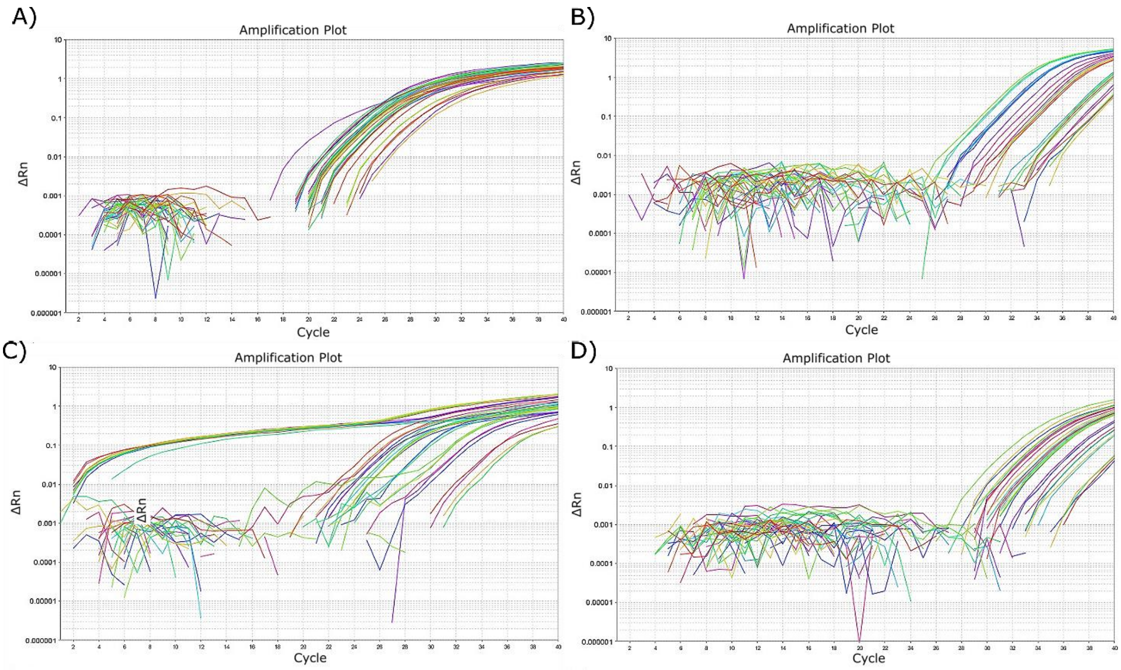

Figure 2.11. *Amplification plots for the genes E2RL7 (A), PTMA (B), ACTB (C) and LDLR (D)*

In Figure 2.11C, it is evident that some of the reactions amplified at a cycle earlier than expected and some of the negative controls did amplify in the ACTB plate. These wells were considered to be outliers and all repeated in a separate plate to improve their results. ACTB and B2M were chosen as housekeeping genes because of their robustness and stability in endothelial cells (Ju et al., 2018).

Table 2.4. *The list of genes that were selected for qPCR analysis from the microarray and their Taqman™ probe product code listed on Thermofisher. Housekeeping genes are highlighted in red.*

Gene	**Product Code**	**Gene**	**Product Code**
VCAM1	Hs01003372_m1	PTMA	Hs02339492_g1
ITGA6	Hs01041011_m1	BMP4	Hs01041266_m1
CA2	Hs00163869_m1	F2RL1	Hs00608346_m1
EDNRB	Hs00240747_m1	ACTB	Hs01060665_g1
CXCR4	Hs00607978_s1	B2M	Hs00187842_m1

Analysis of differential gene expression based on Microarray data revealed that 144 genes were differentially expressed when HDLECs were stimulated with CGRP (Figure 2.4B). In contrast, AM stimulation only caused 23 genes to be differentially expressed (Figure 2.4A). A total of 17 genes were shared between both conditions were chosen for qPCR validation of the results, of which 14 were upregulated with only 3 downregulated (Figure 2.5) in the microarray. The volcano plots in Figures 2.2 and 2.3 show that CA2 (coding for Carbonic Anhydrase 2) was the gene most significantly upregulated in both conditions. Quantitative PCR was performed on selected genes (BMP4, CA2, CXCR4, EDNRB, F2RL1, ITGA6, VCAM1 and PTMA) to replicate the experiment and verify the findings from the microarray. Figure 2.12 shows that (i) gene expression of qPCR data was calculated to have a lower mean log fold change when compared to the control, (ii) as well as larger inter-sample variance,and (iii) the measured mean log fold change was significantly correlated between the two methods (R^2= 0.8496, p = 0.0155 for the AM treatment; R^2= 0.7808, p = 0.0382 for the CGRP treatment) after the removal of outliers. The R^2 coefficients for both experimental conditions were within the limits reported in large-scale studies comparing the relative performance of Microarrays and qPCR (Wang et al, 2006).

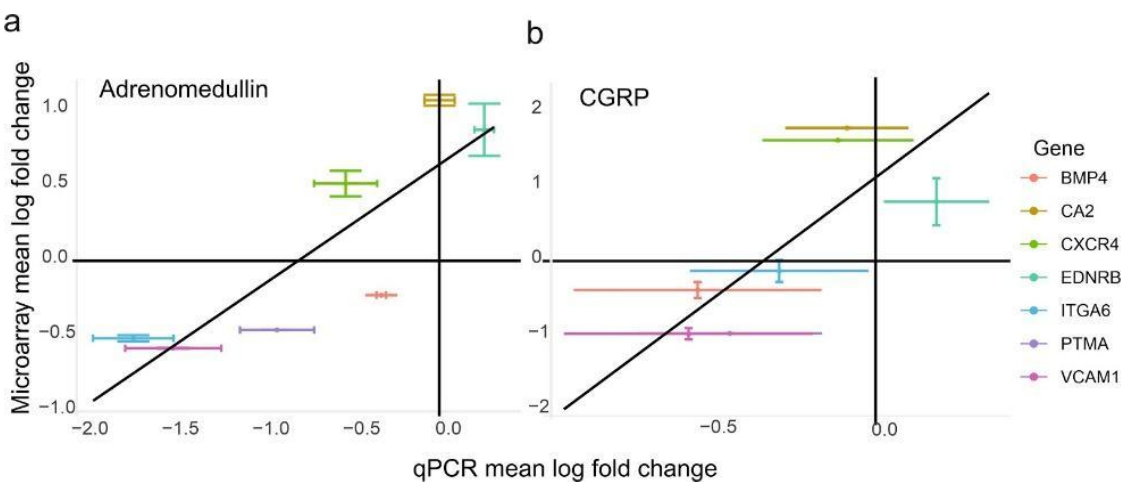

Figure 2.12. *Scatterplots showing the mean log fold changes of selected genes, calculated using the ΔΔCT method for qPCR data and the empirical Bayes method for microarray data.*

The error bars represent +/- standard error for qPCR on the x axis, and microarray on the y axis.

No functional enrichment was found within genes that were modulated by AM stimulation. In contrast, CGRP stimulation yielded 13 significantly enriched distinct functional groups (Figure 2.13); with the gene ontology (GO) biological process terms being actin-mediated cell contraction (GO:0070252); axis specification (GO:0009798); regulation of endothelial cell migration (GO:0010594); negative regulation of endothelial cell migration (GO:0010596); negative regulation of cell migration (GO:0030336); cell chemotaxis (GO:0060326); response to ionising radiation (GO:0010212); regulation of smooth muscle cell proliferation (GO:0048660); smooth muscle cell migration (GO:0014909); sterol biosynthetic process (GO:0016126); regulation of blood pressure (GO:0008217); transepithelial transport (GO:0070633) and peripheral nervous system neuron differentiation (GO:0048934).

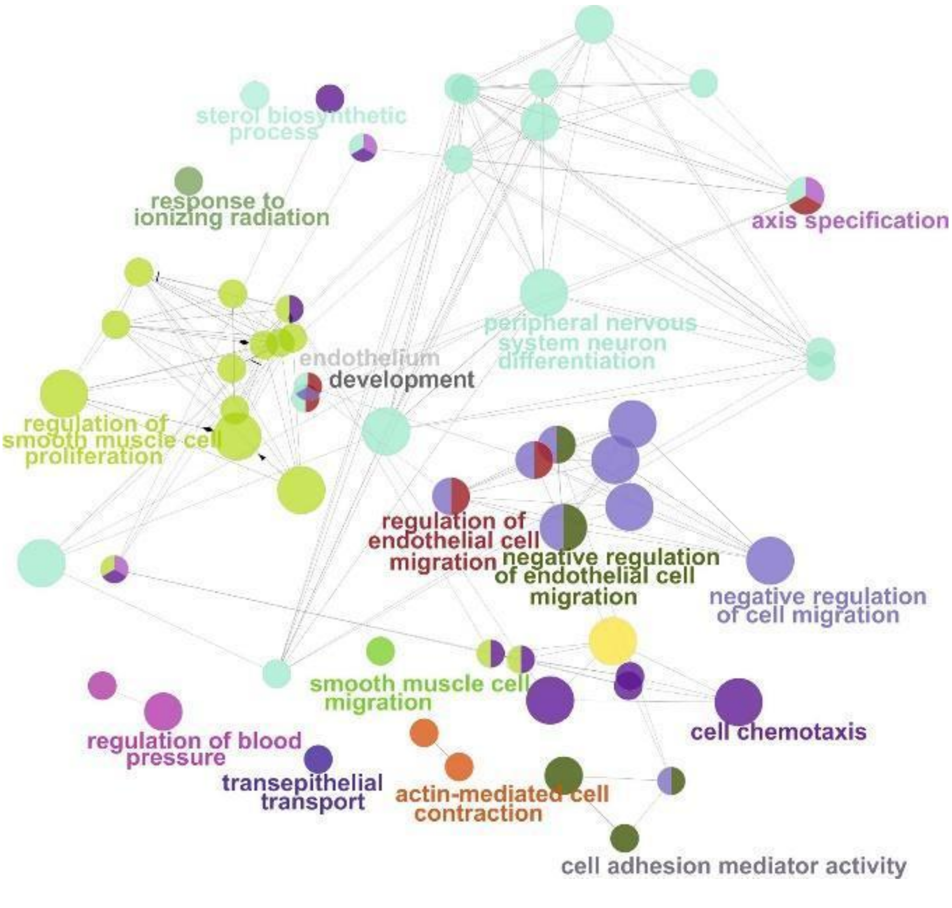

Figure 2.13. *Network diagram of enriched GO terms as result of three-hour CGRP treatment of HDLECs. Each node represents a gene ontology biological process term, with visualisation of dominant terms. The colours reflect the different biological process and the*

size of the node is how enriched that GO term was from the input list. Figure was generated using Cytoscape with the ClueGo add-on.

A shinyGO enrichment of the Jensen DISEASES database (Pletscher-Frankild et al., 2015) for the genes which were differentially expressed for the stimulation of CGRP, found that hypertension was the most significantly enriched disease (P.value$_{(FDR)}$ 7.7x10^{-6}), containing 11 genes from the genes significantly differentially expressed in the CGRP treatment. This was followed by fatty liver disease (P.value$_{(FDR)}$ 1.7x10^{-4}), which contained 6 genes; coronary artery disease (P.value$_{(FDR)}$ 1.7x10^{-4}), containing 8 genes and cerebrovascular disease (P.value$_{(FDR)}$ 2.5x10^{-4}) which was enriched from 8 genes also. The most enriched diseases from this geneset are displayed in Figure 1.14 (the full table of this enrichment analysis is available as Supplementary Table 1.4). There was some overlap between the genes in each of these enrichments, such as SERPINE1 and IL6 being present in all 4 of these diseases, although it is worth noting that both of these genes were specific to CGRP but were not present upon AM agonism. LDLR was present in the enrichments for fatty liver disease, coronary artery disease and cerebrovascular diseases, and this gene was shared by both AM and CGRP treatments. Of the genes which were enriched for hypertension, only EDNRB and VCAM1 were shared between the two experimental treatments.

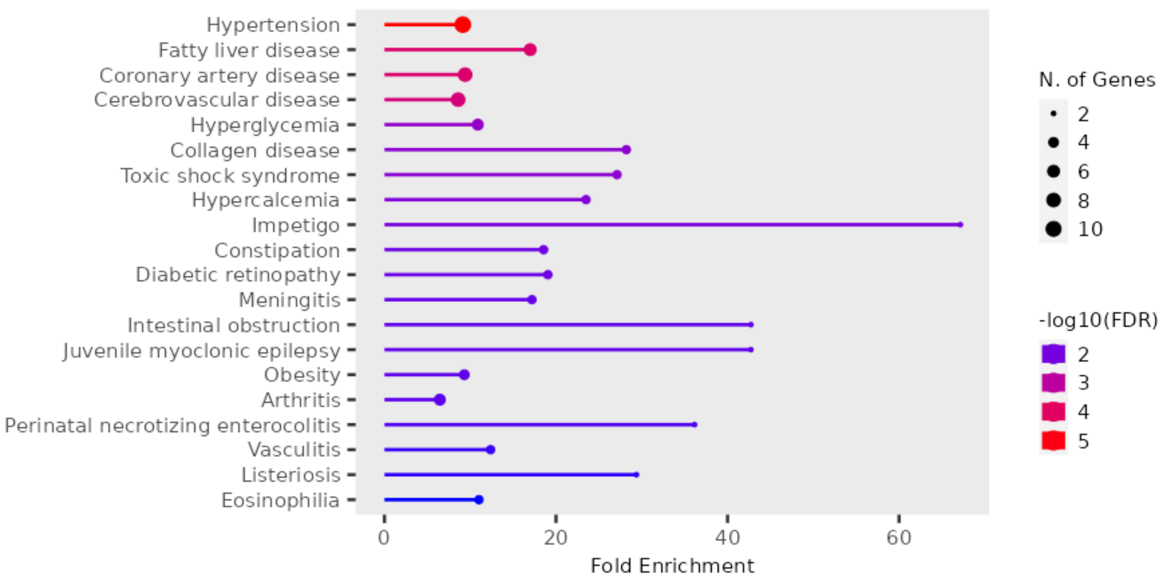

Figure 2.14. *Enrichment of the CGRP differentially expressed genes in the Jensen Disease database.*

2.5 Discussion

This study aimed to investigate similarities and differences in the downstream effects of CLR receptor activation in endothelial HDLEC cells through two common neuropeptides, AM and CGRP. Both of these have vasodilatory functions. CGRP-secreting perivascular sensory nerve fibres are known to spatially align with lymphatic vessels in the rat skin and secrete CGRP upon noxious stimulation (Yamada & Hoshino, 1996). AM is secreted by vascular endothelial cells themselves (Tomoda et al., 2001), stabilises the endothelial barrier in vivo (Dunworth et al., 2008), but also promotes sprouting angiogenesis in human umbilical vein endothelial cells (HUVECs, Kim et al., 2003) and tumour lymphangiogenesis (Karpinich et al., 2012). The results show that both AM and CGRP were able to stimulate the primary HDLEC cells used in the two independent replicates within this study, and that the CLR receptor was expressed in them. The results of the microarray were able to be replicated through an independently generated qPCR Experiment. The R^2 values observed between the qPCR and the microarray were within the limits of those published in a large-scale study comparing log fold changes of 900 genes though qPCR to that of Microarray platforms (Wang et al, 2006).

CGRP stimulation of primary HDLECs caused downstream transcriptional changes of five times more genes than AM stimulation. This supports the previously published finding that AM causes the *CLR*-receptor to internalise whereas CGRP does not, suggesting different mechanisms of action (Nikitenko et al, 2006). These two neuropeptide molecules were therefore hypothesised to have different downstream pathways with overlap to some degree. Klein et al (2014), performed AM stimulation of HDLECs at a 100-fold lower AM concentration, but identified a different transcriptional response compared to our study, with ACKR3 (CXCR7) being significantly upregulated after 1, 4, and 24 hours. This decoy receptor mediates AM expression and could mean that AM is binding to the ACKR3 receptor rather than to CLR in their study, indicating that the mechanism of response to AM might be concentration dependent. qPCR was performed in this chapter, and this technique can easily become inaccurate due to things like pipetteing error and bad primer design; these limitations were overcome through the use of taqman™ probes, which are validated to detect your target gene and also use a probe based approach rather than a dye such as SYBR green which could be more prone to problems such as pipetting errors. qPCR does have the advantage of being a cheap and quick method to indentify changes in gene expression, making it a suitable technique to validate the result of a microarray as it has been used in this chapter.

Despite the differences in magnitude of transcriptional changes, based on the functions of genes found to be differentially expressed here, both neuropeptides could induce similar physiological effects as some differentially expressed genes were shared between the two conditions.

The gene most highly upregulated in both conditions was CA2 (Carbonic Anhydrase 2). CA2 is a high activity isozyme that is involved in maintaining pH homeostasis in many tissues, including endothelial cells (Sly & Hu, 1995; Sun et al., 1999) and has a wide range of global physiological functions (Hassan et al, 2013). CA2 release by CGRP stimulation has already been documented to occur in the gills of oysters (Cudennec et al, 2006), where human CGRP increased activity of all CA enzymes in a dose dependent manner and contributed to mineralisation. CGRP-mediated release of CA2 was also documented in the trout (Najib et al, 1994), where it was shown that stimulation using human CGRP increased the levels of carbonic anhydrase activity as high as 5-fold the basal level. In contrast, this result was not obtained by stimulation with AMY (Najib et al, 1994). CA2 is not expressed in normal vessel endothelium, but overexpressed in the tumour vessel, for example in malignant melanoma and other cancers (Yoshiura et al, 2005). CA2 supports tumour blood endothelial cell survival under lactic acidosis in the tumour microenvironment (Annan et al., 2019).

Another gene which was upregulated in both conditions is CXCR4 which codes for the C-X-C chemokine receptor type 4 and regulates endothelial cell proliferation and migration in vivo and in vitro (Molino et al., 2000). This GPCR has been used as a prognostic marker in a wide variety of cancers (Yusen et al, 2018; Smith et al, 2004; Schrander et al, 2002), and higher levels of CXCR4 in biopsies correlated with higher levels of metastasis, vascularization and tumour growth through multiple mechanisms (see Mortezaee, 2020; Darash-Yahana et al, 2004). Endothelin receptor B (EDNRB) was also significantly upregulated in both experimental conditions. Endothelins bind to EDNRB and trigger the release of intracellular Ca^{2+}. This Ca^{2+} release upregulates the production of nitric oxide (NO) by the Ca^{2+}/calmodulin-dependent synthase in endothelial cells and ultimately induces vasodilation (Hirata et al, 1993). Endothelial EDNRB stimulates COX-2, increasing prostacyclin and inducing relaxation of smooth muscle through cAMP signalling, inducing vasodilation through a NOS independent pathway (Mazzuca & Khalil, 2012). Inhibition of EDNRB signalling in normal human microvascular endothelial cells reduces the melanogenesis and the pigmentation of normal human melanocytes in co-culture models (Regazzetti et al 2015). Nonsynonymous mutations of this receptor have been strongly linked with melanoma risk (Soufir et al, 2002) and secondary site metastasis of malignant melanoma (Demunter et al, 2001). Although the inhibition has increased apoptosis in melanoma, it also led to increased angiogenesis (Lahav et al 2004), which could be due to its signalling pathway promoting the expression of HiF-1a and VEGF (Spinella et al, 2007).

Low density lipoprotein receptor (LDLR) is also upregulated in both AM and CGRP treatments. It is a vital receptor for endothelial cells and attenuates their ability to uptake LDL cholesterol. LDL has been extensively studied for its direct association with cardiovascular disorders (Go & Mani, 2012). In addition to this, however, LDLR has links to tumour growth, with LDLR deficient mice having suppressed tumour growth, and also dampens the antiangiogenic effects of microparticles derived from apoptotic T-lymphocytes (LMPs) (Yang et al, 2010)

Vascular cell adhesion molecule 1 (VCAM1) was downregulated in both experimental conditions. Expression of VCAM1 is mediated through various cytokines, including NfKb and its main functions are in the activation and recruitment of white blood cells (Shu et al, 1993). In endothelial cells, its expression is required for lymphocyte migration to sites of inflammation across endothelial cell monolayers through a NADPH oxidase dependent production of reactive oxygen species, in both cell lines and primary cultures (Matheny et al, 2000). In atherosclerosis, the expression of VCAM1 is elevated (Ley & Huo, 2001). Abnormal levels of VCAM1 in breast cancer have been linked to metastasis to the lung (Chen et al, 2011) and bone (Lu et al, 2011), and correlates to progression and survival in colorectal cancers (Alexiou et al, 2001; Maurer et al, 1998). VCAM1 was also one of the genes present in the enrichments for cardiovascular related diseases hypertension, coronary artery disease and cerebrovascular disease in the enrichment of CGRP associated genes. Whilst this is not surprising given the above evidence, it is interesting to note that this was a significantly differentially expressed gene in both AM and CGRP treatments and highlights the potential overlap of these two signalling peptides on the same disease pathways. Only two genes were significantly altered in both conditions and enriched across the same disease pathways, the other one being LDLR; the function of which is also described earlier in this discussion. These results show that whilst there is some overlap between adrenomedullin and CGRP's downstream mechanisms, CGRP may be the more important player in pathobiology and developmental biology.

Beyond these single genes, the functional enrichment analysis supported the conclusion that many differentially expressed genes in response to CGRP treatment were involved in migration, proliferation and chemotaxis. CGRP responsive genes were enriched in 13 groups of biological functions. The most relevant term was regulation of endothelial cell migration. Migration of endothelial cells is an essential part of angiogenesis. One gene which is present in all of these functional groups is *ADAMTS9*, a gene which has been shown to be a tumour suppressor gene in gastric cancer by inhibiting the mTOR pathway (Du et al, 2012) but also inhibits angiogenesis in oesophageal and nasopharyngeal carcinoma, preventing the tumour from growing (Lo et al, 2010). Interestingly, the gene was upregulated in the CGRP conditions. In accordance with CGRP being a known vasodilator, regulation of blood pressure was an enriched GO. This group contained CXCR4, EDNRB and LDLR; all of which were upregulated by both AM and CGRP. This implies that these genes could explain the physiological similar functions of both peptides.

Enrichment of the Jensen DISEASES database for the genes which were differentially expressed upon CGRP agonism found hypertension to be the most significantly enriched disease. Hypertension is described as having an increase in systolic blood pressure, which could be caused through primary (such as genetics) or secondary sources (such as obesity) (Staessen et al., 2003). CGRP was first described for its ability to cause vasodilation (Tippins, 1986), and so it is not a particularly surprising finding that CGRP stimulated HDLECs did differentially express genes relating to hypertension. It was interesting, however, to find that only two of these genes were shared with the AM treatment; a signalling peptide which has also been shown in the past to have an inhibitory effect on blood pressure (Kato et al., 2006). These findings possibly allude to these two CLR agonists having different mechanisms of action for a common physiological function - the regulation of blood pressure. One of the genes which was specific to CGRP and was present across hypertension, fatty liver disease, coronary artery disease and cerebrovascular diseases was SERPINE1. This gene codes for the serpin family E protein member 1 and is sometimes called plasminogen activator inhibitor-1 (or PAI-1). SERPINE1/PAI-1 is involved in many physiological pathways and processes, including cell adhesion (Loskutoff et al., 1999), inflammation (Morrow et al., 2021) and most relevantly, angiogenesis, where it interacts directly with VEGFR-2 (Wu et al., 2015). In angiogenesis, SERPINE1/PAI-1 was found to positively correlate to angiogenesis rates in angiosarcomas, where it increased the expressions of pro-angiogenic factors (Ohuchi et al., 2023), although treatment of developing chicken eggs with therapeutic concentrations showed PAI-1 to be an inhibitor of angiogenesis in the chorioallantoic membrane, and the through two distinct mechanisms (Stefansson et al., 2001). The deviation from the effects of SERPINE1 in this experiment from previous studies show that there is still more to be understood regarding SERPINE1, but it nonetheless ascribes this gene to important regulatory functions for angiogenic pathways.

2.6 Conclusions

In conclusion, the results here provide evidence of pronounced transcriptional differences in HDLECs in response to two neuropeptide hormones - CGRP and AM, which both bind to the same CLR receptor. Both hormones upregulated the expression of the pH maintenance isozyme CA2. Whilst these peptides induce similar physiological effects, this experiment has provided a set of candidate markers to further study differences in their downstream effects. This information will also aid in identifying alternative therapy targets for lymphatic metastasis or possible side effects of already existing drugs.

Chapter 3: Investigating the role of TRPV1 knock-down in developing zebrafish with a focus on vessel formation.

3.1 Abstract

In **Chapter 2** I showed that CGRP caused transcriptional reprogramming of lymphatic endothelial cells. This neuropeptide is released via the activation of the TRPV1 channel and therefore paved the way to the novel hypothesis that this channel would be important for development and responding to stress in an in vivo model. Whilst it is known that TRPV1 activation mediates a range of signalling molecules which are involved in cell migration and proliferation, the channel has been previously shown to be directly responsible for the migration of lymphatic endothelial cells when activated through acidosis. However, there is a need for interrogating this mechanism through an in vivo model of development such that its importance in the early stages of life can be observed. Zebrafish were chosen as a model for this chapter due to their availability, ease of genetic manipulation and the ability to observe their embryonic development. The main goal of this chapter was to observe in vivo changes in lymphangiogenesis when modulating the TRPV1 channel. I aimed to knockdown TRPV1 using a morpholino to observe the effects of decreased expression of the channel. The knockdown of TRPV1 caused changes to the transcriptome of the developing zebrafish embryo, affecting pathways involved in proline metabolism, ECM receptor interaction, blood vessel branching and angiogenesis. Additionally, the knockdown was related to a range of zebrafish disease phenotypes. The data presented here provides evidence that TRPV1 is involved in vessel development pathways and that modulation of this expression could have implications in pathophysiological conditions.

3.2 Introduction

Transient receptor potential vanilloid type 1 (TRPV1) is a non-selective cation channel which resides on the cell surface. It has six transmembrane domains with a pore forming a hydrophobic section between the last two domains (Tominaga & Tominaga, 2005). The channel is mostly present throughout the peripheral nervous system, residing on sensory neurons, where it is used to detect temperature changes (Gunthorpe & Szallasi, 2008). There is evidence that the channel forms heterodimers with other TRP channels, causing their activation thresholds to change (Fischer et al., 2014). The TRPV1 channel in particular is activated through thermal and chemical stimuli, as this affects the protonation state of the channel, allowing it to be in either a closed or open formation (Tominaga & Tominaga, 2005). While it is known that temperature and capsaicin are key players in this conformational change, pH is also known to affect the threshold of the temperature due to the number of free protons in the surrounding matrix, and if the pH is low enough, can even cause the channel to be activated at ambient temperatures (Dhaka et al., 2009).

Whilst TRPV1 is one of the most studied TRP channels, there is little known about its role in developmental biology. It is known that TRPV1 is expressed as early as 1 dpf in the trigeminal ganglion, and the lateral line and its expression increases over the initial three days of development (Gau et al., 2013; Son & Ali, 2022). TRPV1 has also been shown to be involved in the motility of zebrafish sperm, implying that this channel could be important even prior to fertilisation of the embryo (Chen et al., 2020). In their study, Chen et al. (2020) also states the difficulty of identifying homozygous TRPV1-/- zebrafish, as the proportion of homozygous mutant adults was much lower than expected according to Mendel's law - speculating at the essentiality of TRPV1 in development due to this implied high lethality.

In the course of its activation, TRPV1 causes neurons to release a range of other signalling molecules, which are known to be involved in migration (Waning et al., 2007) and proliferation (Zhai et al., 2020); two important functions that are key to embryogenesis. The overall aim of this chapter is to investigate the consequence of TRPV1 modulation on the complete transcriptome of the developing zebrafish embryo.

This chapter will expand on the knowledge gained from the previous chapter, which showed a link between lymphangiogenesis and the excretion of the neurotransmitter peptide CGRP in an *in vitro* model using human dermal lymphatic endothelial cells. This signalling molecule is released in response to TRPV1 activation (Meng et al., 2009). CGRP excretion activates the calcitonin-like-receptors expressed on the endothelial cells, causing a variety of downstream transcriptional responses related to proliferation and endothelial cell migration (see **Chapter 2**). In this chapter and, in following, **Chapter 4** aims to investigate whether the TRPV1 channel upstream of CGRP affects lymphangiogenesis in an in vivo model, the developing zebrafish. The findings presented here will increase our understanding of the importance of this channel during development with an emphasis on the vascular development.

In order to address this knowledge gap of TRPV1 involvement in lymphangiogenesis, in this chapter, the TRPV1 channel will be knocked down (KD) using a previously published morpholino (Gau et al., 2013). Morpholinos (MOs) are modified oligonucleotides which are designed to block either translation or transcription of mRNA, by binding to specific regions on the gene. MOs are chemically synthesised and bind to complementary mRNA targets and prevent their translation; the method is not dissimilar to that of silencing RNA (siRNA) or small hairpin RNA (shRNA). The main difference between a morpholino and a siRNA is that morpholinos have been made to be non-ionic through the addition of an altered backbone which also makes them resistant to nucleases (Summerton & Weller, 1997); the neutral charge has also been proposed to interact less with cellular proteins and therefore removing non-specific phenotypic changes (Corey & Abrams, 2001). Since their development, MOs have been developed to be able to have fluorescent tags and are more complex, adding fluorophores with quenchers that cause the excitation to only occur when the target mRNA has been bound to the MO (Moulton, 2006). The MO used in this study was used previously in a paper published by Gau et al (2013), designed to bind to the intron 13- exon 13 boundary preventing splicing and translation of the mRNA. In their paper, the authors show that TRPV1 is a sensor of environmental heat in zebrafish and that the TRPV1 channels in trigeminal neurons are responsible for the heat-induced locomotion of zebrafish larvae. The paper also provides evidence that capsaicin does not activate zebrafish TRPV1 channels (Gau et al., 2013).

First, zebrafish larvae will be exposed to temperature stress followed by a swimming assay to show the efficiency of the knockdown, using a method outlined in the paper which first used the TRPV1 morpholino for knockdown. Knockdown embryos will then be RNA-sequenced in order to observe transcriptomic responses to TRPV1-knockdown. In addition, antibody staining will also be performed to investigate a change in the expression of both TRPV1 and PROX1 at the protein level of the developing embryo. PROX1 (Prospero Homeobox 1) is a lymphatic endothelial marker which will be used to visualize lymphatic development. In humans, it is a single-copy gene, but zebrafish have two copies of the gene - PROX1a and PROX1b. Both paralogs of this gene are involved in the lymphatic development of the zebrafish (van Impel et al., 2014), although it has been shown that the PROX1b gene is not essential for lymphatic development in the zebrafish and may not be as reliable as PROX1a in identifying the lymphatic endothelial cells (Tao et al., 2011). Here, larvae treated with the TRPV1-MO, or the scrambled control-MO will be assessed for both TRPV1 and PROX1 immunofluorescence to visualise vessel development. The PROX1 antibody used here is polyclonal and may detect both variants of the PROX1 protein simultaneously.

The expression levels of TRPV1 in vivo are not well known and may be low in the absence of receptor stimulation; 2-aminoethoxydiphenyl borate (2-APB) was first discovered for being a inhibitor of inositol trisphosphate receptors (Maruyama et al., 1997) but was later shown to inhibit of many other biologically significant channels, including ca2-ATPase pumps (Bilmen et al., 2002) and the mitochondrial permeability transition pore (Chinopoulos et al., 2003). Capsaicin, a common agonist of TRPV1 (Waning et al., 2007), has previously been shown to not activate the TRPV1 channel in zebrafish (Gau et al., 2013), and so the compound 2-Aminoethoxydiphenyl borate (2-APB) was chosen as a TRPV1 agonist. Previous studies have shown that 2-APB can activate the zebrafish channel in patch clamp experiments at concentrations as low as 200nM (Gau et al, 2013), and this was the concentration that was used throughout the study as it was shown to not cause any side effects during development

(Gau et al., 2013). 2-APB is now generally seen as an inhibitor of ion channels, although HEK (Human Embryonic Kidney) cells and *Xenopus* oocytes expressing the TRPV1 channel were shown to be activated by 2-APB and a similar activation was found in TRP channels V2 and V3, whilst an inhibitory effect was observed in the TRPC and TRPM channels (Hu et al., 2004). Hu and colleagues state that there is a similar hierarchy between the sensitivity to heat and the sensitivity to 2-APB in the TRPV channels, proposing that they activate the channels via a similar mechanism (Hu et al., 2004).

In summary, 2-APB likely activates TRPV1 (and possibly other TRP channels) and will be used here to activate the channel in conjunction with MO-treatments.

There are three hypotheses to be tested in this chapter:

1. TRPV1 knockdown will lessen swimming activity of 4dpf zebrafish larvae exposed to heat stimulus.
2. In 2-APB stimulated embryos, TRPV1 knockdown will cause a significant change to the zebrafish transcriptome during development, compared to scrambled morpholino-injected embryos.
3. TRPV1 knockdown will cause less of the channel to be expressed in developing zebrafish and this reduction in calcium signalling will consequently reduce vessel formation, which can be observed through PROX1 staining, compared to 2-APB only treated controls.

In summary, this chapter will investigate the effects of TRPV1 knockdown on the behaviour, vessel development and transcriptional responses in developing zebrafish.

3.3 Materials & Methods

3.3.1 Zebrafish husbandry, ethics and embryo collection

Adult AB strain zebrafish were kept in 28°C heated tanks in the aquarium of the University of Hull on a closed recirculating water system. They were fed twice daily on a varied diet of dried food, bloodworm and Copepods. All experiments were approved by the Ethics committee of the University of Hull (FEC_2019_194 Amendment 1). Embryos were collected using plastic collection trays filled with marbles and topped with artificial plants to stimulate reproduction. Trays were placed in the tank overnight and collected the following morning. The eggs were then transferred from the tray to a secondary container through the use of a plastic Pasteur pipette. During this step, efforts were taken to remove any dead or unfertilised embryos as well as any dirt and debris that were present in the collecting tray. Once collected, the embryos were bleached in 0.004% (v/v) bleach diluted in E3 media to remove any bacteria or parasites. They were washed with this bleach solution 3 times for 5 minutes each. After the bleaching they were placed in E3 supplemented with 0.0002% (v/v) methylene blue to prevent fungal growth. Fertilised eggs were selected for experimentation and transferred to fresh E3 medium that did not contain methylene blue. Eggs were collected at or before 1 cell stage before injection. The age of the egg is critical to the effectiveness of the MO.

3.3.2 Experimental design

Seven treatments were performed which were (1) scrambled MO injected, incubated with 2-APB (referred to as SCR or scrambled); (2) TRPV1 knockdown MO incubated with 2-APB (referred to as KD or knockdown); 3) SCR without 2-APB for the swim test in normal temperature (NormSCR); 4) SCR without 2-APB with acute exposure to high temperatures (35°C) to induce swim behaviour (HotSCR); 5) KD without 2-APB for the swim test in normal temperature (NormKD); 6) KD without 2-APB with acute exposure to high temperatures (35°C) to induce swim behaviour (HotKD). Lastly, 7) the control condition (CTRL) where the embryo normally developed in E3 medium (Westerfield, 1995) with nothing injected and no 2-APB being supplied, which was used as a reference transcriptome. More details are given in the following paragraphs.

Three endpoints were measured, (i) transcriptome-based expression through RNA sequencing, where the embryos were injected with either the TRPV1 KD morpholino or the scrambled morpholino and left to grow in 2-APB supplemented E3 media until 1dpf. In the other two endpoints, (ii) swimming behaviour of the larvae after developing up to 4dpf in normal E3 media and temperature and (iii) immunofluorescent staining of TRPV1 and PROX1 proteins in the larva, the zebrafish developed up until 4dpf in E3 media which was not supplemented with 2-APB and at normal temperatures (28°C). 2-APB supplementation was always at the concentration of 200nM throughout all experiments.

Table 3.1. *Experimental design for this chapter*

		Stimuli		
Morpholino		**Heat**	**2-APB**	**None**
	TRPV1	HotKD	KD	NormKD
	SCR	HotSCR	SCR	NormSCR
	None			CTRL

3.3.3 Generation of MO-knockdown embryos

Crystallised MOs (MOs, Gene Tools LLC, Oregon, USA) were resuspended in molecular grade water to a concentration of 300nM as per the product sheet. This was done for both a custom MO with the sequence 5'-GTCACCAAAGCTGCCGTGTAAAAAA-3' and the scrambled, control MO. This MO targets the TRPV1 exon-13 boundary, a part of the gene that is integral for TRPV1s pore formation (Gau et al, 2013). The scrambled MO was used as a control as it should not affect gene expression, but accounts for the process of injection and healing from injection-related injury. The MOs were suspended to a concentration of 1mM as per manufacturer's instructions. The MO was diluted further to 0.5mM prior to injection, in a solution containing molecular grade water and phenol red to a working concentration of 0.05% (w/v) phenol red. Phenol red is used as an indicator when injecting. 1ng of MO was injected into each embryo using a MPPI-3 (ASI™) pressure injector (Figure 3.1). After injection, the embryos were incubated in a bench top incubator at 28 degrees in petri dishes containing either E3 media or E3 media that had been supplemented with 2-APB. All embryos used in the RNA-seq were supplemented with 2-APB. For the MO injections, a mix of both prefabricated and needles that were generated in house were used. Needles generated in house were pulled using a Stutter p-87 pipette puller and 1mm O.D borosilicate glass capillaries (wpi; #1B100-4) with the settings – 450 heat, 120 pull, 80 velocity and 150 time. Premade needles were also purchased from WPI (#TIP10LT).

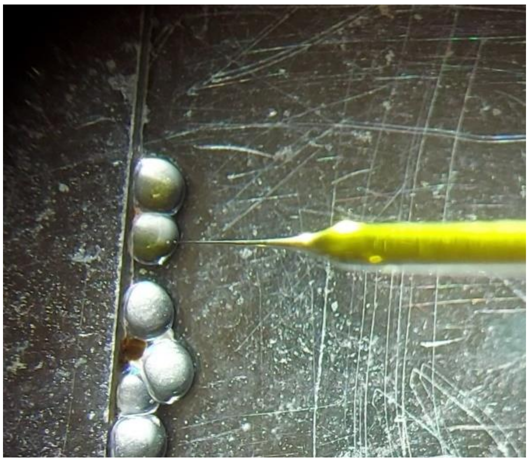

***Figure 3.1**. Images depicting the injection of an embryo (left), and some embryos that have grown to 1 dpf after having been injected with the TRPV1 knockdown MO (right).*

3.3.4 Behavioural assay

First, a behavioural assay was performed to show the effectiveness of the MO-knockdown, similar to the one that was performed in (Gau et al., 2013). Gau et al. (2013) heated E3 media on hot plates to different temperatures and recorded the zebrafish larvae responses to the heat through the distance that was swam. 4dpf KD and SCR larvae were exposed for 15 seconds to either normal temperature (28°C) or 35°C in a six-well plate (both in E3 medium). Movement of the larvae was recorded on video and analysed using kinovea® (a non-profit, open-source motion analysis software; available from www.kinovea.org), for each 20 embryos per condition. The x and y coordinates were exported as a .csv from the video analysis software and then converted into euclidean distances for statistical analysis. The distance (cm) travelled by the larvae was calculated as the overall difference between these x and y coordinates at each point. These data were then all divided by 15 in order to give a distance per time measurement, cm per second. Statistical analysis was done by performing a

Kruskal-Wallis test on the overall dataset which was followed up by a Wilcoxon ranked sum test on the experimental pairs (Hot KD vs Hot SCR; Normal KD vs Normal SCR, and their residuals).

3.3.5 RNA extraction and sequencing

Embryos which had been injected with either the TRPV1 MO or the scrambled MO were incubated at 27°C in 2-APB for 24 hours (11:00AM-11:00AM). The embryos were injected prior to one cell stage but were around 1-2 cell stages once they had been injected and sorted for incubation. After the 24-hour time period, the embryos were flash frozen, and their RNA was extracted using the Trizol protocol as described below. Pools of 20-25 embryos were used per extract and pooled into larger 1.5mL microcentrifuge tubes. As much media as possible was removed from the 1.5mL tube and the tube was flash frozen at -80°C. Each sample tube underwent manual mechanical disruption in 200µL of Trizol (ThermoFisher) using a plastic pestle until the tissue fully disrupted. Subsequently, more Trizol was added to have a final total volume of 500µL. Homogenates were centrifuged at 10,000g for 15 seconds to pellet both lipids and insoluble tissue to the bottom of the tube. Homogenates were then transferred to a new tube, leaving behind the insoluble material. 300µL of chloroform was added per 500µL of Trizol solution and followed by incubation at room temperature for 5 minutes. After the incubation, the tube was centrifuged at 12,000g for 15 minutes to separate the phases. The clear aqueous phase which contains the RNA was removed and placed in a fresh microcentrifuge tube. 100µL of room temperature isopropanol was added to the collected aqueous phase to precipitate the RNA before incubation for 10 minutes at room temperature. After 10 minutes the samples were centrifuged at 20,000g for 5 minutes to pellet the RNA. Supernatant was removed and the pellet was air dried before undergoing two washes with 75% ethanol in a temperature-controlled centrifuge at 4°C. After the washes, the pellet was air dried again to remove any excess ethanol before being suspended in 100µL nuclease free water. Once resuspended, the RNA was treated using TURBO DNase (Thermo Fisher, #AM1907), using the manufacturer's protocol for routine treatment. This protocol involved adding the DNAse directly to the extracted RNA sample, followed by incubation at 37°C for 30 minutes.

After the incubation, DNase inactivation reagent was added (0.1 volumes), the sample was incubated at room temperature for 5 minutes and then centrifuged. The centrifuge pellets the DNAse, and the treated RNA was transferred to a new tube. RNA was cleaned post DNAse treatment using 3M sodium acetate. 0.1 volumes of sodium acetate were added to the sample, followed by 2.5 volumes of 100% ethanol. This mix was then incubated at -20°C for at least 1 hour before being centrifuged at 12,000g for 15 minutes to pellet the RNA. The pellet was washed 3 times with 75% ethanol in a 4°C centrifuge and air dried before being resuspended in 100µL nuclease free water. A ND-1000 nanodrop spectrophotometer was used to assess purity and quantity of each RNA sample. DNAse treatment and sodium acetate clean up were all performed on the same day as the isolation to prevent freeze-thaw degradation of the samples.

RNA which passed quality control were shipped to Edinburgh Genomics for sequencing. A third E3 control condition with no MO injected and 2-APB not supplied in the medium was also sequenced. Illumina sequencing was performed using a TruSeq Total Stranded RNA-Seq library prep kit, of which the RNA was normalised to have the same input concentration and was run on an Illumina NovaSeq 6000.

3.3.6 RNA-Seq analysis

All bioinformatics analyses were performed on the University of Hull’s HPC, VIPER (see Figure 3.2). The files were initially checked using *fastqc* for overrepresented and polyN sequences which were removed using *fastp* (Chen et al., 2018). The reads were aligned using STAR (Dobin et al, 2013) against the *Danio rerio* genome build GRCz11, which was obtained from NCBIs ftp server. STAR is a long-read aligner which has the highest accuracy of read calling (Dobin et al., 2013). The count outputs of STAR were then read into R (version 4.0.2), using the *DESeq2* package (Love et al., 2014). *DESeq2* was also used for the differential expression analysis of the data. All code for RNA sequencing analyses is available in the Supplementary (Supplementary Material Chapter 3, 1). The *dupRadar* package was used for the graphing of reads which may have been duplicated through the generation of the sequencing libraries or sequencing. Biological duplicates tend to have high expression with high number of duplicate reads and reads with a large % duplicate read but low expression would be technical duplicates. Biologically, the genes that are overexpressed would also account for a high % of duplicate reads. Gene Ontology term (GO) enrichment was performed using the web tool *ShinyGO* (Ge et al., 2020). LOWESS distribution of the data was checked using *limma*'s *voom* function (Smyth, 2004).

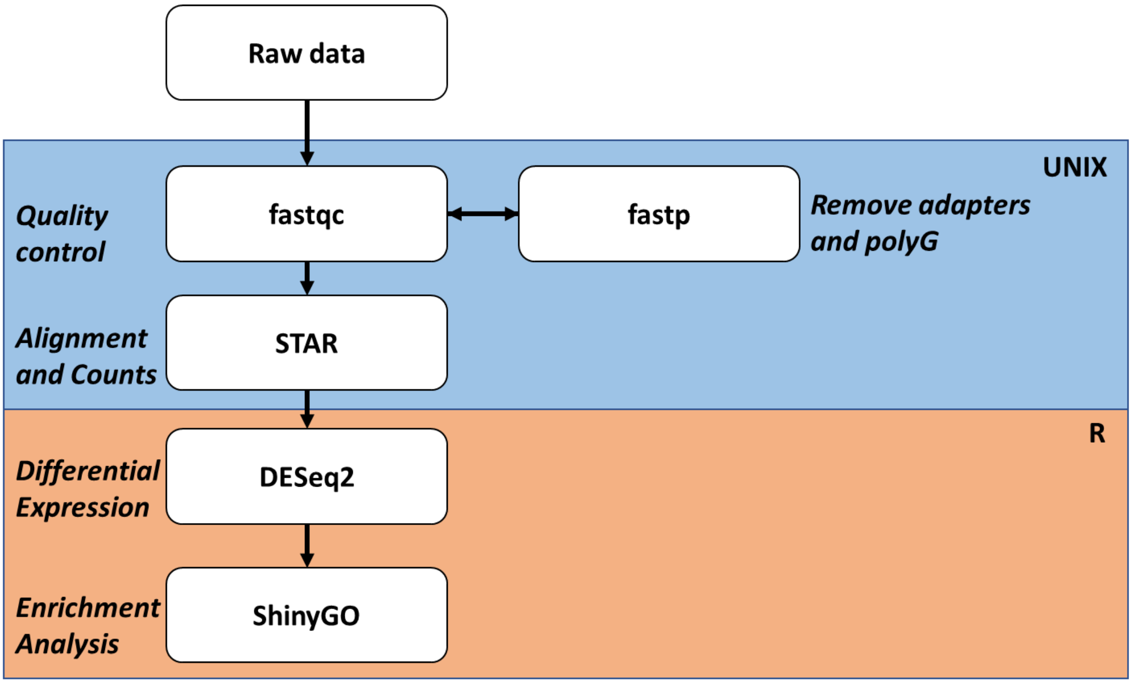

Figure 3.2 *Flowchart outlining the RNA seq pipeline used for the analysis.*

3.3.7 PTU treatment of zebrafish embryo lymphatic system

To prevent melanin formation in embryos stained for immunofluorescence, Phenylthiourea (PTU) was added to E3 media at a working concentration of 75µM while the embryo developed from the somite stage (10 hpf) up until 4 dpf (larva). This concentration was shown to be effective in previous studies whilst reducing the amount of side effects caused by the chemical exposure (Karlsson et al, 2001). This treatment was performed for all embryos that were imaged through fluorescence microscopy in order to reduce the amount of background. The treatment was successful in preventing melanin development in the embryo which showed no apparent side effects from this exposure (Figure 3.3).

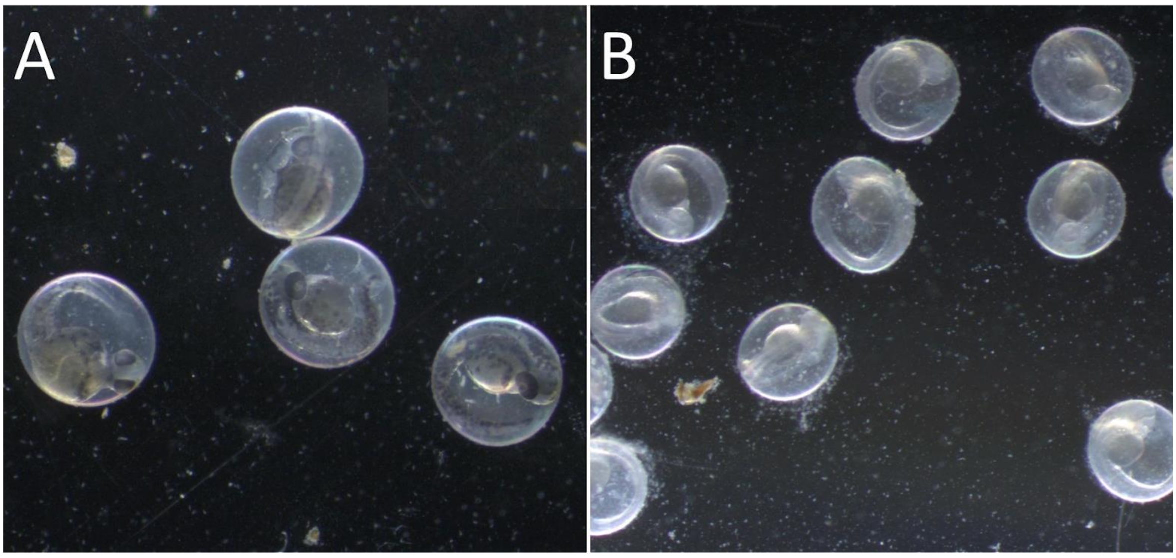

***Figure 3.3**: 4dpf embryos that have either been grown in normal E3 media (A) or E3 media supplemented with 75µM PTU (B) to prevent melanin formation.*

3.3.8 Western Blot to check performance of antibodies against zebrafish embryo lysate

Antibodies targeting zebrafish PROX1, TRPV1, ACTB and GAPDH were purchased from various suppliers (Table 3.1). GAPDH and ACTB were both monoclonal antibodies, while PROX1 and TRPV1 were polyclonal. Pools of 50 embryos from standard and hot conditions (27°C or 32°C incubation overnight until 3dpf) were lysed using RIPA buffer. Total protein was then quantified using a bicinchoninic acid (BCA) assay. For the Western Blotting, a 10% SDS page gel was used with 10ng of protein per lysate. HDLEC lysate was also used as a check for specificity of the antibodies. Samples were pre-treated using 7.5uL of 10% SDS, reducing the buffer containing 200mM of DTT and were then boiled at 100°C for 5 minutes. The gel was transferred to a PVDF membrane activated by immersion in methanol for 30 seconds. Transfers were performed using a standard wet transfer technique with sponges and filter paper within a transfer sandwich. This was performed at 4°C and was run at 60V for 3 hours. After transfer, the membrane was blocked in 0.05% TBS/T with 5% milk solution for 45 minutes, washed 4 times with 0.05% TBS/T, 5 minutes per wash and then incubated overnight with the desired primary antibody. After primary incubation, the membrane was washed 4 times in 0.05% TBS/T for 5 minutes per wash and then blocked in 0.05% TBS/T with 5% milk solution for 45 minutes – all at room temperature. Once blocking was finished, the membrane was incubated with the secondary antibody at its working dilution for 45 minutes at room temperature. After secondary incubation, membranes were washed 3 times in 0.05% TBS/T for 5 minutes each and the 4th wash was 30 minutes in PBS at room temperature. Blots were imaged using ECL solution. Loading controls were performed using the same method although these were incubated at room temperature for 45 minutes for both the primary and secondary antibodies rather than overnight at 4°C. For stripping, Thermo Fisher's Restore PLUS western blot stripping buffer (thermofisher, #46430) was used for 45 minutes at room temperature. Human dermal lymphatic endothelial cells (HDLEC) protein extract was also used to check the cross reactivity of the antibodies.

Table 3.2. *The antibodies used in this chapter and their dilutions.*

Primary Antibodies				
Target	**Supplier**	**Catalogue Number**	**IF**	**Western blot**
Prox-1	Merck Millipore	AB5475	1:500	1:1000
TRPV1	Osenses	OST00070G	1:500	1:1000
ACTB	Invitrogen	MA5-32540	1:500	1:1000
GAPDH	Invitrogen	MA5-31976	1:200	1:1000
Secondary Antibodies				
Alexa-Fluor 488 anti-rabbit	Invitrogen	A-21206	1:200	-
Goat anti-rabbit	ThermoFisher	31460	-	1:10,000

3.3.9 Immunofluorescence staining

The zebrafish embryos which were used in immunofluorescence staining were stored at 28°C and in E3 media once injected and left to develop until 4 dpf where they were dechorionated and then humanely sacrificed through flash freezing and fixed in a 4%(v/v) paraformaldehyde (PFA) solution for at least one hour at room temperature. After fixation, the embryos were stored in 100% methanol at -20°C for at least overnight as longer exposure was found to greatly reduce background fluorescence. The embryos were then rehydrated in increments of 25% methanol/TSBT (TBS with 0.1% Tween-20), from 75% to 25% MeOH and finally 100%

TBST for 5 minutes each. Once rehydrated, they were permeabilized in acetone for 20 minutes at -20°C. The embryos were then blocked in a solution of TBS, 0.5% (v/v) Triton, 1% (w/v) DMSO and 0.5% (w/v) BSA for one hour at room temperature. After blocking, primary incubation was performed using the same blocking solution with the antibody at 1:100 overnight at 4°C. The next day, the embryos were washed using TBST 4 times, 5 minutes per wash and then incubated with the secondary antibody for either 3 hours at room temperature; or overnight at 4°C using foil to keep samples in the dark. The Alexa-fluor secondary antibody was diluted in the same TBST/Triton/DMSO/BSA solution as used for blocking at a concentration of 1:1000. After three hours, the embryos were washed in TBST three times, mounted in 3% methyl cellulose and then imaged. Phalloidin was used in the secondary antibody solution as a counterstain at the same concentration. The stained embryos were imaged on a Zeiss LSM710 confocal microscope or an Olympus IX 71 inverted microscope.

3.4 Results

Behavioural Assay

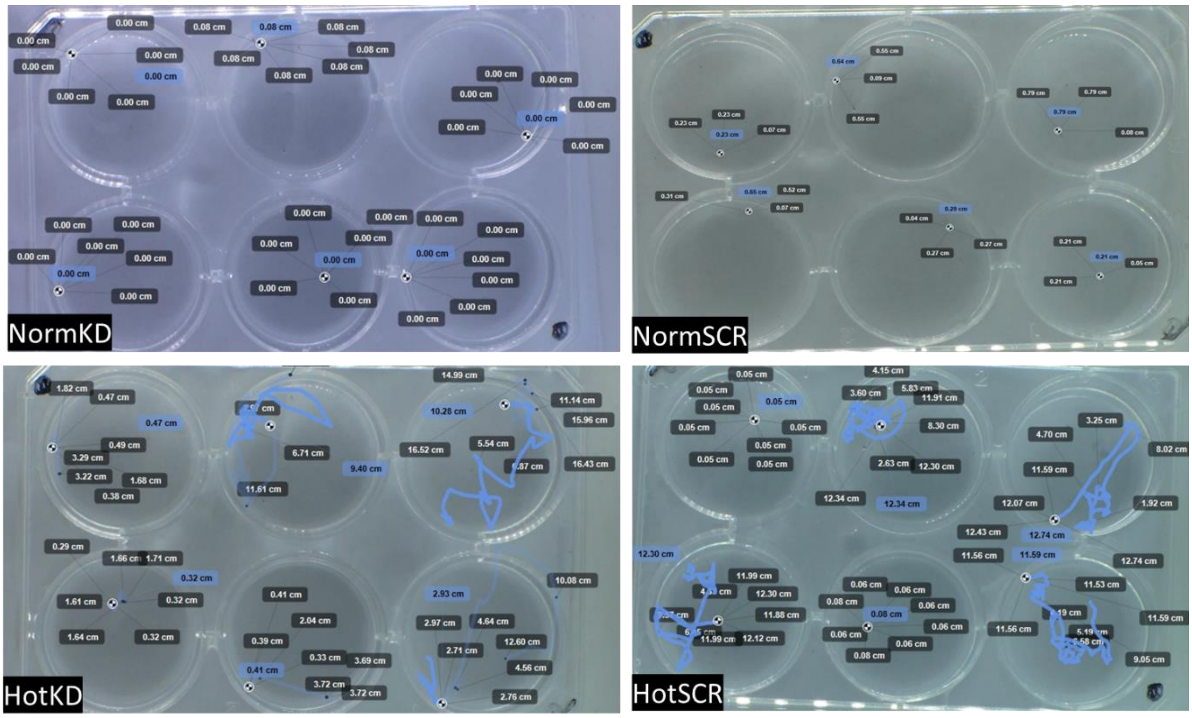

Figure 3.4. *Example results from swimming assays showing traces of the larvae's movement (blue lines) and the numbers are the distance travelled up until each checkpoint.*

The data generated from this behavioural assay was non-normal (Shapiro test; $w = 0.52782$, $p < 0.001$) and was still non-normal after log transformation (Shapiro test; $w = 0.90639$, $p < 0.001$). The means of the distance/time data showed that the heat-exposed larvae travelled more than those at regular temperature, with the Hot Scr condition having the highest mean out of all four groups (Figure 3.4). This can be clearly seen in Table 3.2 where the average of the Hot Scr condition is double that of the Hot KD, whilst the regular temperature-exposed larvae travelled a similar distance on average in the same 15 seconds. A Kruskal-Wallis test was performed on the log distance/time data, where it was found that the four conditions were significantly different ($\chi 2 = 40.508$, df = 3, $p < 0.001$, Figure 3.5). Following this with a Wilcoxon test between the matched conditions (Hot KD vs Hot Scr; Norm KD vs Norm Scr), it was found that there was a difference between the matched experimental groups with the activity of the Scr treatments being higher (Hot: $W = 141$, $p = 0.2637$; Norm: $W = 391$, $p = 0.1625$), however, both of these differences were non-significant.

Table 3.3: *the average distance per time (cm/sec) travelled for each of the experimental conditions for the behavioural assay. N = 20*

Condition	Average distance per time (cm/sec)
HotKD	0.52
HotScr	1.02
NormKD	0.075
NormScr	0.081

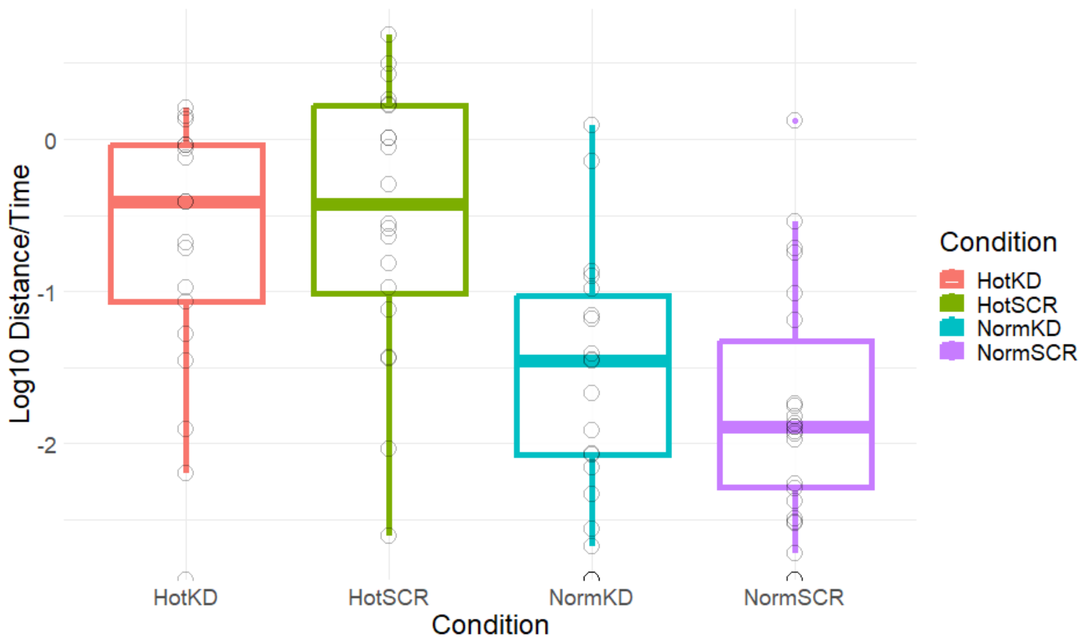

Figure 3.5 *A plot showing the log distance/time for the four conditions. The coloured points represent the means, and the bars are ± standard error. Raw data values are shown in grey circles. Distances were recorded in cm and time in seconds. N = 20*

In order to compare temperature-dependent variance in swimming behaviours across treatments, linear regression models were generated between each condition at the two different temperatures (HotScr relative to NormScr, and HotKD relative to NormKD). Residual values were extracted, which represent the variance in swimming response between each treatment's hot and normal temperature bioassays. Since residuals in a regression model always cluster around zero, they were squared to show differences in treatment variations between temperatures (Figure 3.6). A Wilcoxon test of the squared residuals was found to be significant (W = 1587, p = 0.03203), meaning the difference between the two treatment groups is significant with a higher variance in temperature-dependent swimming responses in the Scr than in the KD condition, which had lower variance in swimming responses.

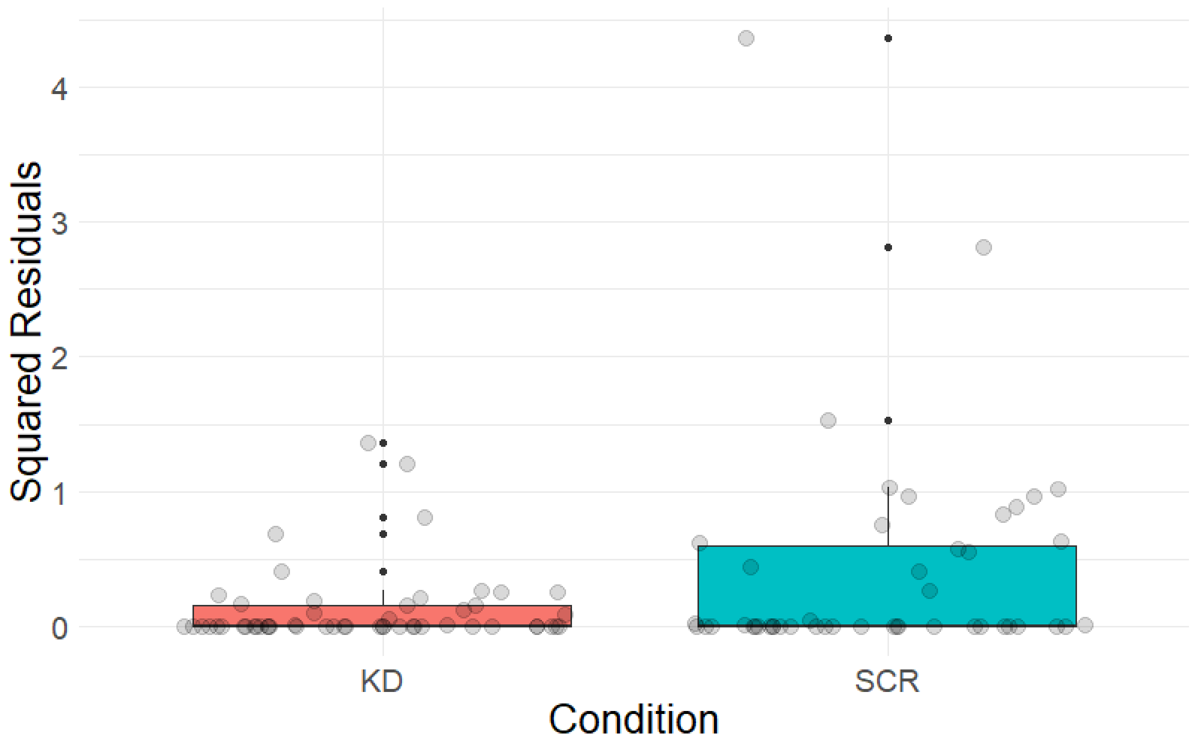

Figure 3.6. *Boxplot of the squared residuals between hot and normal temperature swim distances for the Knockdown (KD) and Scrambled (SCR) treatments showing higher variation in the SCR condition. N = 20*

The effects of 2-APB on the swim behaviour was not studied, as this experiment was performed to re-create the experiment performed by Gau et al (2013) to validate the efficacy of the Morpholino.

RNA isolation for RNA sequencing

The samples extracted for RNA-Seq were run on Agarose-gel Electrophoresis to assess the purity and the integrity of the RNA (for an example see Figure 3.7). Those that didn't meet the requirements were repeated until there were enough repeats for 3 Scr samples and 3 KD samples. The samples that were submitted are labelled in Figure 3.8, alongside their concentrations and nanodrop ratios. SCR1,3 & 5 had a range of concentrations, giving concentrations of 77.7, 28.8 and 28.0 ng/uL respectively. The KD conditions gave consistently higher concentrations, with samples 1,2 and 6 providing 33.3, 48.5 and 29.4 ng/uL of RNA (Table 3.4). The 260/280 ratios were either just below 2, or above 2, which shows that the samples had little contamination of proteins which would impact the sequencing reaction.

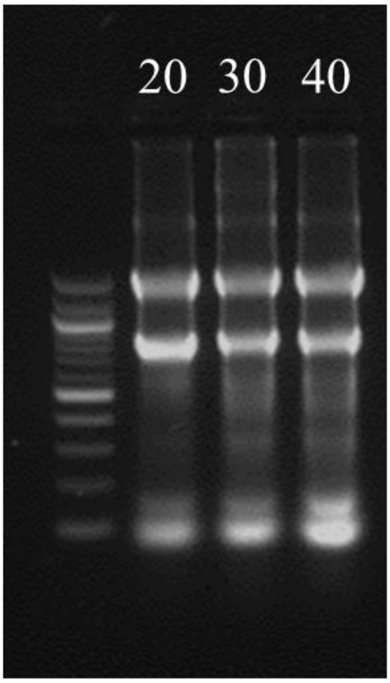

Figure 3.7. *An agarose gel showing the RNA extractions of 20, 30 and 40 embryos, where the number at the top of the lane denotes the number of embryos.*

Table 3.4. *The purity ratios and concentrations for the extracts of different numbers of embryos.*

Number of Embryos	Qubit Concentration (ng/µL)	Nanodrop Concentration (ng/µL)	260/280	230/280
20	339	374	1.95	0.84
30	387	464.1	1.92	1.61
40	450	524.4	1.95	1.62

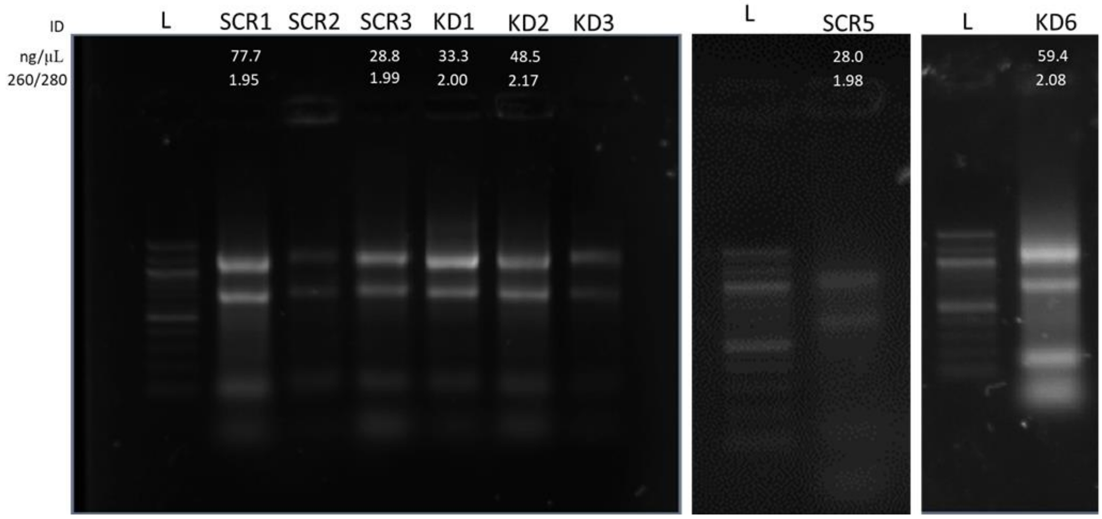

Figure 3.8. *Gel images of samples submitted to Edinburgh Genomics for sequencing. The concentration and 260/280 ratios were measured by nanodrop. KD refers to a knockdown sample; injected with the TRPV1 MO and Scr refers to a sample that was injected with the scrambled control MO with samples in both conditions stimulated with 2-APB. Each sample was a pool of 20-25 embryos.*

RNA Seq analysis

All the RNA samples that sequenced at Edinburgh Genomics fell within the guidelines of a 260/280 ratio of >1.9 and the concentration requirement of at least 20 ng/uL (Table 3.5).

Table 3.5. *A breakdown of the quality control (QC) results from Edinburgh Genomics for the submitted samples. The RIN for each sample was calculated using an Agilent Tapestation, including the number of sequenced reads.*

Sample	RIN	Concentration (ng/uL)	260/280	Total reads	Mapped	Properly paired
KD1	8.3	39.95	2	9.25E+07	9.25E+07	5.38E+07
KD2	6.8	31.7	2.17	6.41E+07	6.41E+07	3.74E+07
KD6	6.9	58	2.08	9.38E+07	9.38E+07	5.04E+07
SCR1	6.8	47.4	1.95	8.17E+07	8.17E+07	4.79E+07
SCR3	7.4	38.2	1.99	7.56E+07	7.56E+07	4.41E+07
SCR5	5.9	29.2	1.98	2.04E+08	2.04E+08	1.18E+08

However, the RNA integrity number (RIN) of four samples fell under Edinburgh Genomics' recommended value of >7. They were however, still sequenced at risk. Even with a lower RIN value, SCR5 still had a larger number of properly paired reads when compared to the other samples (Table 3.5). Initial *fastqc* analysis of the RNA sequencing reads showed the existence of overrepresented sequences, including both IlluminaTruSeq adapters and polyG strings that likely were artefacts from the sequencing method; the full list of adapters that were filtered is listed at the end alongside the code used in this study. The *fastqc* reports also indicated a large number of duplicated reads; however, Parekh et al., (2016) showed that deduplication can have a negative effect on differential expression analysis. These duplicated reads were therefore left in for analysis and not removed. Adapters and polyG sequences were removed using *fastp*. Then, reassessment using *fastqc* showed the removal of these sequences from the reads. The removal of these reads also improved the distribution of %GC content within the reads (Figure 3.9).

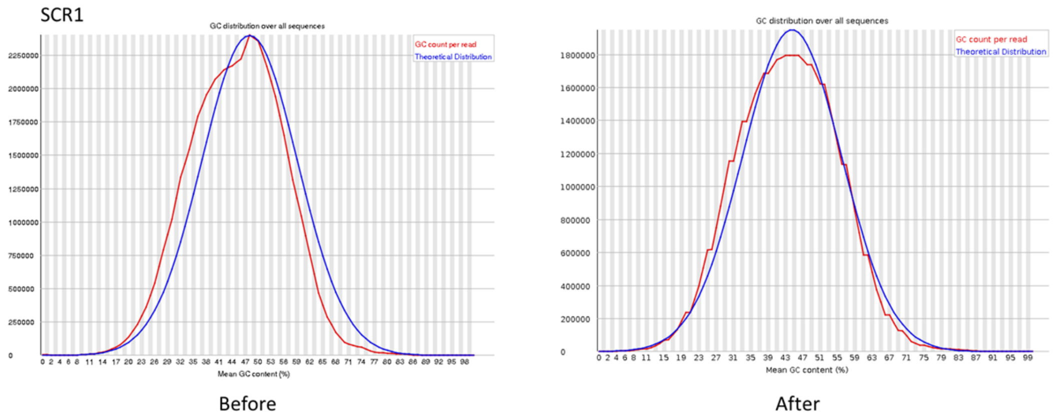

Figure 3.9. *The %GC content of the sample SCR before and after using the fastp package. The blue line is the expected GC% and the red line follows that of the sample.*

The multidimensional scaling (MDS) plot of counts per million in Figure 3.10 shows distinct grouping of the RNA-seq samples, with scrambled (SCR) being more proximal to control (CTRL), than the knockdown samples (KD) in three-dimensional space representing gene expression. The transcript counts per million for TRPV1 were extracted from the dataset, to further investigate the efficacy of the knockdown. A Shapiro-Wilks test on the counts per million showed that the data had a normal distribution (W = 0.96548, P.value = 0.8536) and t-tests between the conditions showed that there was no significant difference in number of TRPV1 transcripts (Table 3.6)

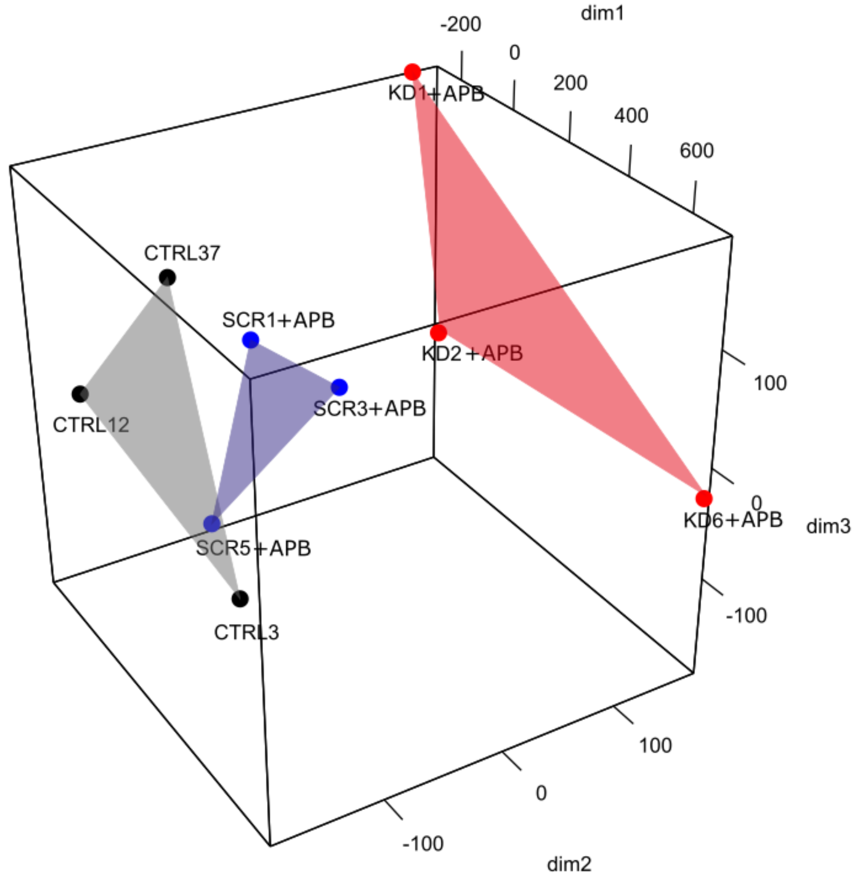

Figure 3.10. *A 3D MDS plot of the RNA-Seq samples, plotted using the limma function "plotMDS()" which uses two randomly selected sets of genes and the logFC of these genes as coordinates to show relatedness of gene expression between samples. The KD condition samples cluster to one side of the graph, away from the two control conditions CRTL and SCR, showing there is a clear difference between these RNA-seq datasets.*

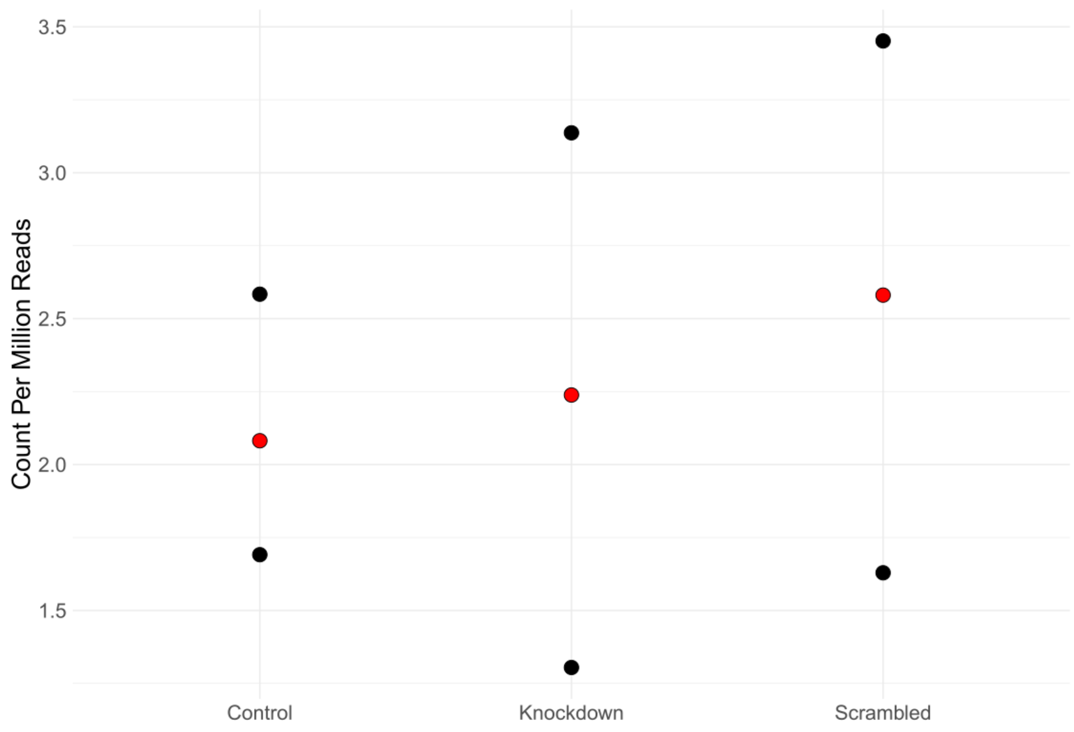

Figure 3.11. *the raw counts per million of TRPV1 per sample across the conditions with median values highlighted in red showing that there are differences between the medial counts, across the conditions. Note that TRPV1 in both knockdown and scrambled conditions were previously activated by 2-APB, but the control was not.*

Table 3.6. *Results of pairwise independent t-tests of the counts per million transcripts of TRPV1 between the three conditions.*

Conditions	t	df	p.value
KD – CTRL	0.183	2.903	0.867
KD – SCR	-0.439	3.999	0.684
CTRL – SCR	0.742	2.911	0.513

The read data showed a low number of technical duplicates, and also a low number of biological duplicates, with a low intercept of 0.06 (Figure 3.12A for the example of sample Scr1). The LOWESS trend (Figure 3.12B) shows that there is a low level of biological variation between the samples, which was expected since all the embryos researched were AB line zebrafish.

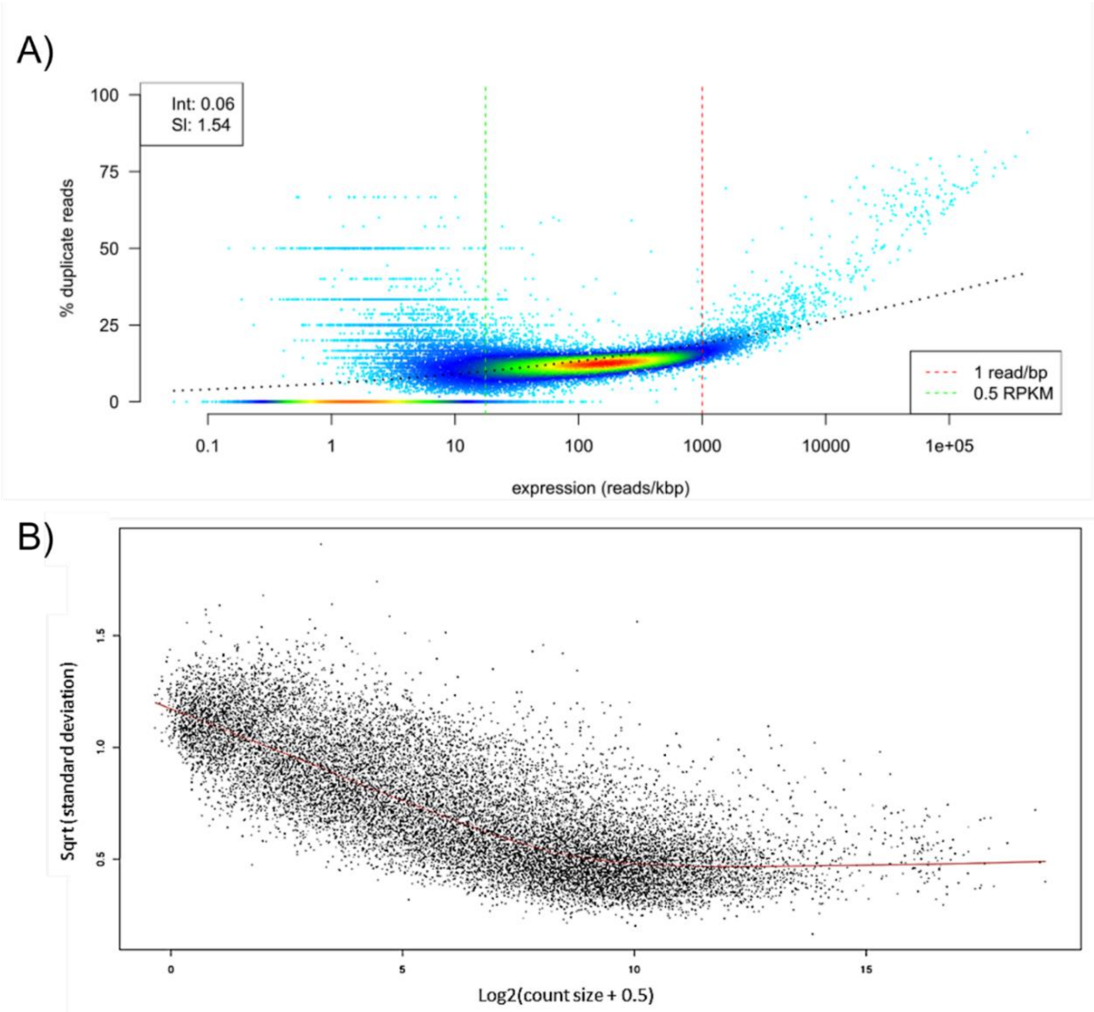

Figure 3.12. *Example plot displaying the duplicated reads from the SCR1 condition in relation to gene expression that were generated using the dupradar package (A) and a plot showing the relationship between the means and variances of the total RNA-Seq dataset (B). In graph (A), the intercept and the slope as listed in the top left of the graph. The colour of the plots indicates the density of the points that are located at that point, with red showing a high density in that area. In graph (B) each gene is represented as a dot, with a red line showing the LOWESS trend of the data. This graph was produced using limma's voom function.*

Differential expression analysis with DESeq2 resulted in a total of 55 differentially expressed genes between the scrambled and knockdown conditions (Table 3.7). Of the 55 genes, 49 had a positive fold change, meaning they were more expressed in the knockdown condition than the scrambled control. Only 6 genes had decreased expression in knockdown compared to scrambled control. FDR (False Discovery Rate, Benjamini & Yekutieli, 2005) correction removed all but 6 of the significant genes from the results. Therefore biological processes were interpreted additionally by using less strict P.value cut-off as raw p.value = <0.001

without any FDR correction for two reasons: i) the samples that were sequenced were pools of 20-25 embryos, which increases the confidence in the DEGs identified, and the effectiveness of the correction techniques being related to sample sizes (Shuken et al., 2021). ii) the experiment was to investigate the implications of modifying a single channel in the developing embryo, which is expected to lead to only a few downstream genes responding. This less conservative approach is becoming a common practice in single-pathway studies similar to this in which a non-adjusted p.value threshold is favoured when performing downstream analysis, such as GO terms (Tills et al, 2018). The largest positive fold change was observed in the si:ch211-106k21.5 predicted gene (ENSDARG00000086052). In fact, seven of the genes that were significant from the DESeq analysis were predicted genes, and had no formal annotation symbol, similar to si:ch211-106k21.5. The largest negative fold change was found in the gene EMAP like 5 (EML5; ENSDARG00000053517).

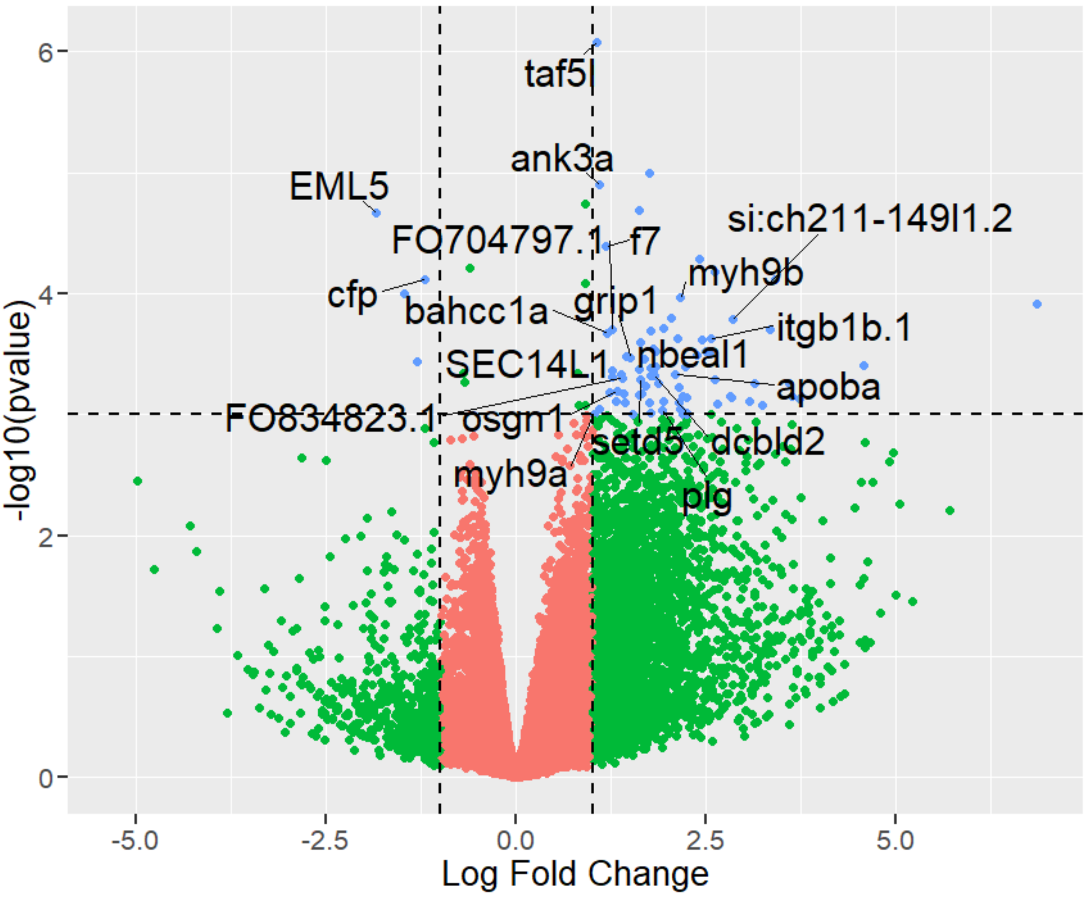

Figure 3.13. *Volcano plot created by plotting the log2FoldChange and the -log10(p.value) of the differential expression analysis performed by DESeq2. The horizontal dotted line denotes the cut off of raw p-value<0.001 and the vertical dotted lines represent log fold*

change greater than 1 or less than -1. Green points have either a significant p.value or a large fold change but not both and blue points have both a significant p.value and a large fold change. Red denotes those genes which are neither significant nor have a large fold change.

Table 3.7. *The differentially expressed genes that resulted from the DESeq analysis with raw p. values<0.001. The bold rows have FDR corrected p. values <0.05. Functions taken from zfin database*

Symbol	***ENSMBL ID***	***log_2FoldChange***	***Protein Function***
FO834823.1	ENSDARG00000112451	1.390881	CoA metabolism
grip1	ENSDARG00000015053	1.497657	Glutamine receptor
myh9b	ENSDARG00000001014	2.162825	Myosin cytoskeleton
bahcc1a	ENSDARG00000103739	1.201322	Transcription factor
nbeal1	ENSDARG00000099547	1.774253	Cholesterol metabolism
erbb3a	ENSDARG00000006202	0.813811	Tyrosine kinase
myh9a	ENSDARG00000063295	1.021383	Myosin cytoskeleton
SEC14L1	ENSDARG00000101792	1.378927	Lipid binding
setd5	ENSDARG00000078576	1.63493	Methyltransferase
arhgef25b	ENSDARG00000014465	0.804224	Nucleotide exchange factor
osgn1	ENSDARG00000052279	1.321206	RhoA regulation
itgb1b.1	ENSDARG00000053232	2.557567	Integrin binding
f7	ENSDARG00000034862	1.179066	Coagulation factor
si:ch211-149l1.2	ENSDARG00000079501	2.851756	Predicted microtubule binding
taf5l	**ENSDARG00000025808**	**1.055794**	**Transcription factor**
dcbld2	ENSDARG00000062177	1.814768	Neutrophilin-like
si:dkey-271j15.3	ENSDARG00000091627	-0.69132	Predicted gene
fmo5	**ENSDARG00000016357**	**0.912511**	**Flavin containing monoxygenase**
plg	ENSDARG00000023111	1.925121	Serine proteinase
cfp	ENSDARG00000094451	-1.20158	Immune response
ank3a	**ENSDARG00000061736**	**1.092601**	**Ankyrin**
apoba	ENSDARG00000042780	2.091241	Oxidative stress
eml5	**ENSDARG00000053517**	**-1.841**	**Microtubule binding**
FO704797.1	ENSDARG00000117244	1.253685	Predicted gene
unm_sa911	ENSDARG00000034063	2.242125	Predicted GTP binding activity
heatr5b	ENSDARG00000059116	1.802262	Endocytosis
xpo5	ENSDARG00000098868	2.115747	RNA binding
unc5b	ENSDARG00000033327	1.091597	Netrin receptor activity
sema3e	ENSDARG00000036571	1.706911	Neutrophilin binding
zgc:92040	ENSDARG00000021154	0.901384	Predicted proline metabolism
itga3b	**ENSDARG00000012824**	**1.607918**	**Integrin binding**
slc4a1b	ENSDARG00000024560	1.743491	Solute carrier

CABZ01071939.1	ENSDARG00000086326	1.830882	Predicted ankyrin binding
robo2	ENSDARG00000014891	1.307181	Axon guidance
anks1aa	ENSDARG00000062396	1.764255	Predicted ephrin binding
cdh26.1	ENSDARG00000078404	1.770388	Predicted cadherin binding
slc2a1a	ENSDARG00000001437	3.335311	Solute carrier
magi3	ENSDARG00000101869	1.441648	Cell signalling
hspg2	ENSDARG00000076564	1.798895	Predicted calcium binding
plxna1a	ENSDARG00000105452	1.259203	Predicted semaphorin receptor
rarga	ENSDARG00000034117	1.257128	Transcription factor
ppp1r14c	ENSDARG00000077341	-0.62005	Phosphotase
cdk5rap2	ENSDARG00000024219	1.683653	Predicted microtubule binding
shroom3	ENSDARG00000102180	1.423131	Predicted actin binding
comp	ENSDARG00000098431	-0.68737	Predicted calcium binding
flnb	ENSDARG00000098374	2.618669	Predicted actin binding
vezf1a	ENSDARG00000008247	2.544511	Predicted zinc finger
ca2	ENSDARG00000014488	3.633033	H+ transport
ppp4r1	ENSDARG00000101316	1.530762	Predicted phosphotase
tmprss9	ENSDARG00000029841	3.067407	Predicted proteolysis
he1.3	ENSDARG00000022670	2.137696	Predicted metalloendopeptidase
c3b.2	**ENSDARG00000001818**	**1.744421**	Complement component
c3b.1	ENSDARG00000093068	1.409819	Complement component
cp	ENSDARG00000010312	0.908809	Predicted ferroxidase
si:ch211-107e6.5	ENSDARG00000097573	-1.47422	Predicted membrane component

Enrichment analysis

The list of DEGs that were significant from the DESeq were analysed using the ShinyGO web tool. The molecular function GO term group that was most enriched in my dataset was proline dehydrogenase activity (GO:0004657), which contained one gene - zgc:92040; a predicted gene that is orthologous to human PRODH2. Cytoskeletal protein binding was the molecular function GO term that contained the most genes (GO:0008092) but was also the least enriched as a whole. In terms of cellular component GO terms, low-density lipoprotein particle (GO:0034362) was the most enriched in the dataset, but, similarly to molecular function, only contained 1 gene - APOBa, which is orthologous to the human APOB and was just short of being significant with an FDR adjusted P.value of 0.0862. This gene was also the only one present in the other lipoprotein related terms which were enriched, such as plasma lipoprotein particle and very low-density lipoprotein particle. The biological function enrichment GO term category contained anterior/posterior axon guidance (GO:0033564) with two genes, ROBO2 and UNC5b, with an adjusted enrichment P.value of 0.066. Angiogenesis (GO:0001525) was highlighted in this category, as well as morphogenesis of a branching structure (GO:0001763), however, these were also nonsignificant and only contained four and one genes respectively in their terms. Nitrogen metabolism (dre00910) was the most enriched in the KEGG term analysis, although it only contained one gene - carbonic anhydrase 2 (CA2), with an adjusted P.value of 0.106. CA2 was also found to be upregulated in **Chapter 2**, where the CGRP stimulated HDLECs gene expression was analysed. Two significant KEGG pathways resulted from this analysis, which were extracellular matrix (ECM)-receptor interaction (dre04512) and regulation of actin cytoskeleton (dre04810), these had FDR adjusted P.values of 0.00054 and 0.018 respectively.

The genes were also enriched for the ZFIN disease and phenotype databases, both available as options in the ShinyGO web tool. The most enriched disease within the differentially expressed genes was Autosomal dominant Alport syndrome, although this only contained both the a and b variants of the MYH9 gene. There were also some diseases related to the cardiovascular system within the enrichment including atherosclerosis, sickle cell anaemia and type 1 diabetes mellitus (Figure 3.15). These conditions all had significant enrichment p.values even after FDR correction and contained the genes C3b.1, C3b.2, F7, APOBa and CP (Supplementary Table 3.5).

ZFIN's phenotype database gives predicted phenotypic changes to the zebrafish by using evidence of previous studies. The differentially expressed genes from the RNA sequencing were aligned to a variety of predicted nervous system phenotypic changes such as axon midline disruption and abnormal olfactory receptor cells. In addition, there were changes relating to the vascular system such as abnormal glomerular base morphology, malformed intersegmental vessels and a collapsed dorsal aorta; all of these phenotypic changes had enrichment FDR p.values of <0.05 (Figure 3.15). These phenotypes were enriched by the genes MYH9a, UNC5b, SLC2A1a and HSPG2.

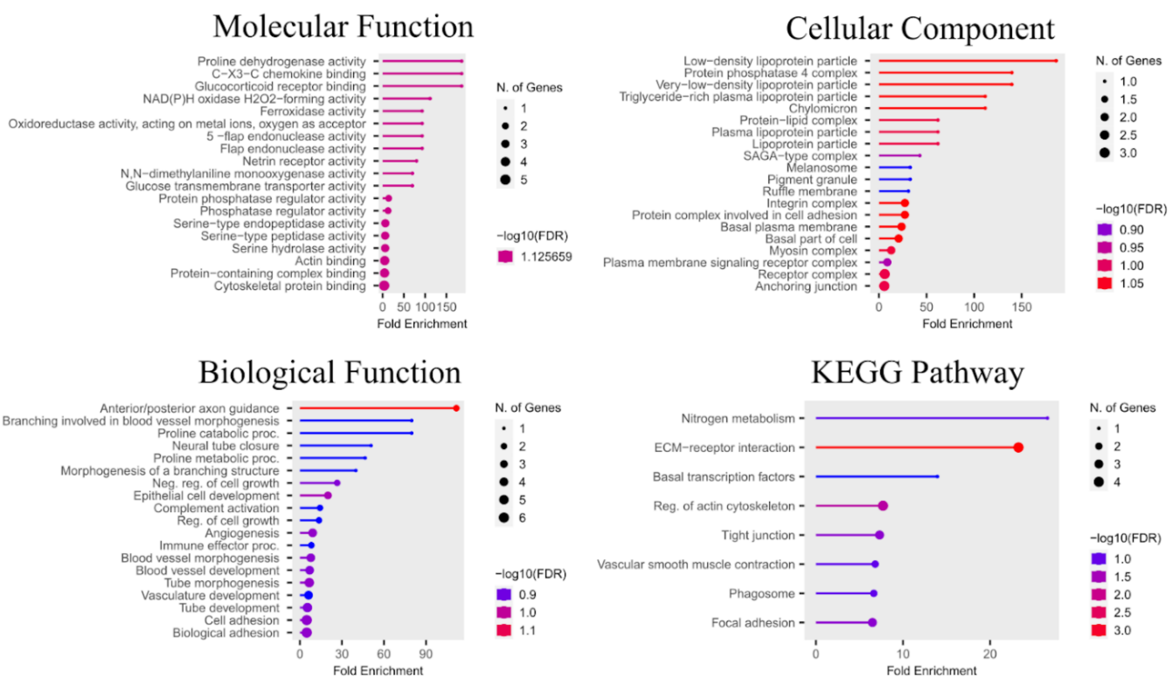

Figure 3.14. *The complete results from ShinyGO for the enrichment of the differentially expressed genes against the GO term categories and KEGG pathways. -log10FDR ≥1.3 is significant (p value $_{FDR}$ < 0.05)*

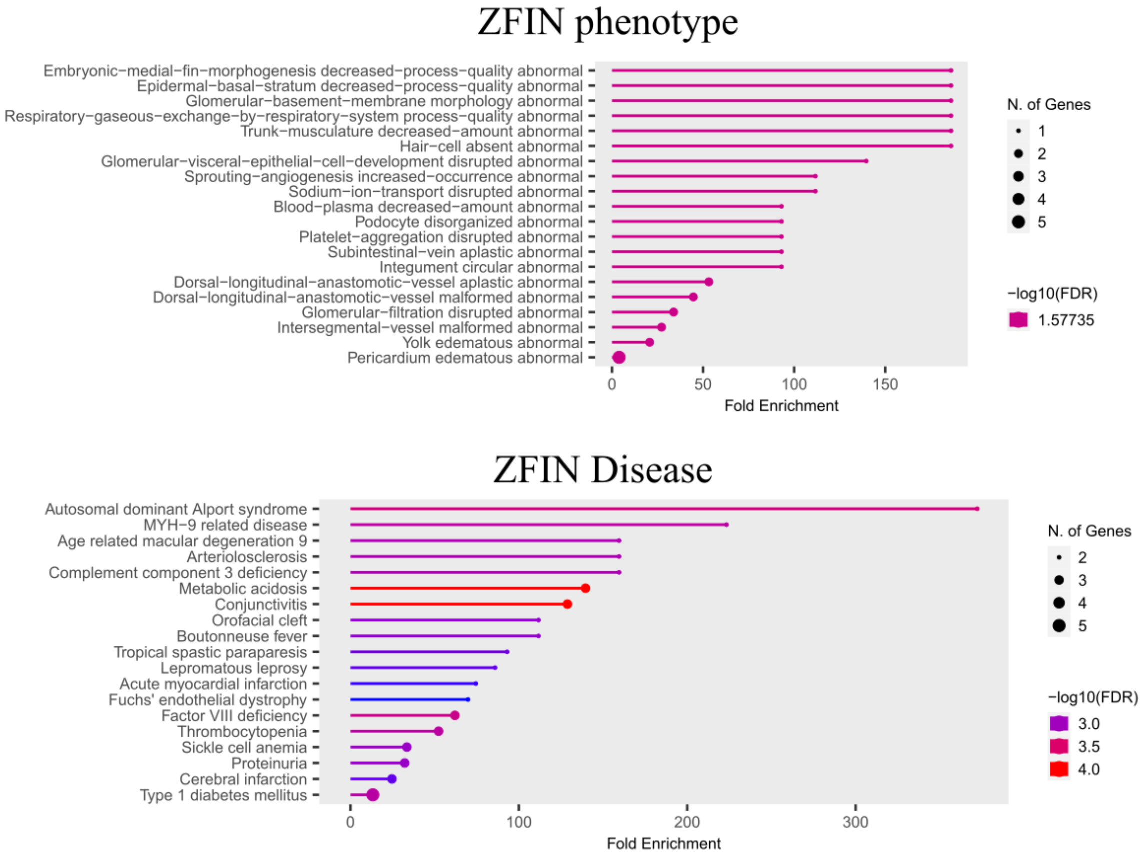

Figure 3.15. *The enrichment results from ShinyGO for the significantly differentially expressed genes against the ZFIN Phenotype and Disease databases. -log10FDR ≥1.3 is significant (p value $_{FDR}$ < 0.05)*

Western blot

To check the specificity of the TRPV1 and PROX1 immunofluoresence antibodies (Table 3.2), western blots were performed (Figure 3.16). The bound antibodies were blotted against both zebrafish embryo and human dermal lymphatic endothelial cell lysates to show whether they would detect just human, zebrafish protein or both (Figure 3.16A). The blot showed that the antibody didn’t bind the human PROX1 and was strongly bound to zebrafish PROX1. While the PROX1 bands were strong, there were two of them with the larger band being the expected 83kDa size of PROX1a, it was thought that the other band could have been PROX1b although that has the weight of 74kDa, so it is unlikely as the second band was in the 43kDa range. The levels of PROX1 protein from zebrafish that have been incubated in different temperatures were also investigated, showing that expression increased greatly when the embryos were incubated at 30°C compared to 27°C, but was reduced when incubated at 32°C

(Figure 3.16C). This indicates that 30°C may increase the lymphatic growth in the embryos but that 32°C could be too hot and detrimental to development. Embryos of less than 1 dpf were also blotted (Figure 3.16C) as the embryos should not express PROX1 at this stage but they will express ACTB, and this shows that the ACTB is not binding to the PROX1 on the membrane and is a suitable loading control. GAPDH was only included in one blot as it was shown to be inconsistent across blots and was therefore not blotted for in subsequent samples, and ACTB was used as a loading control instead.

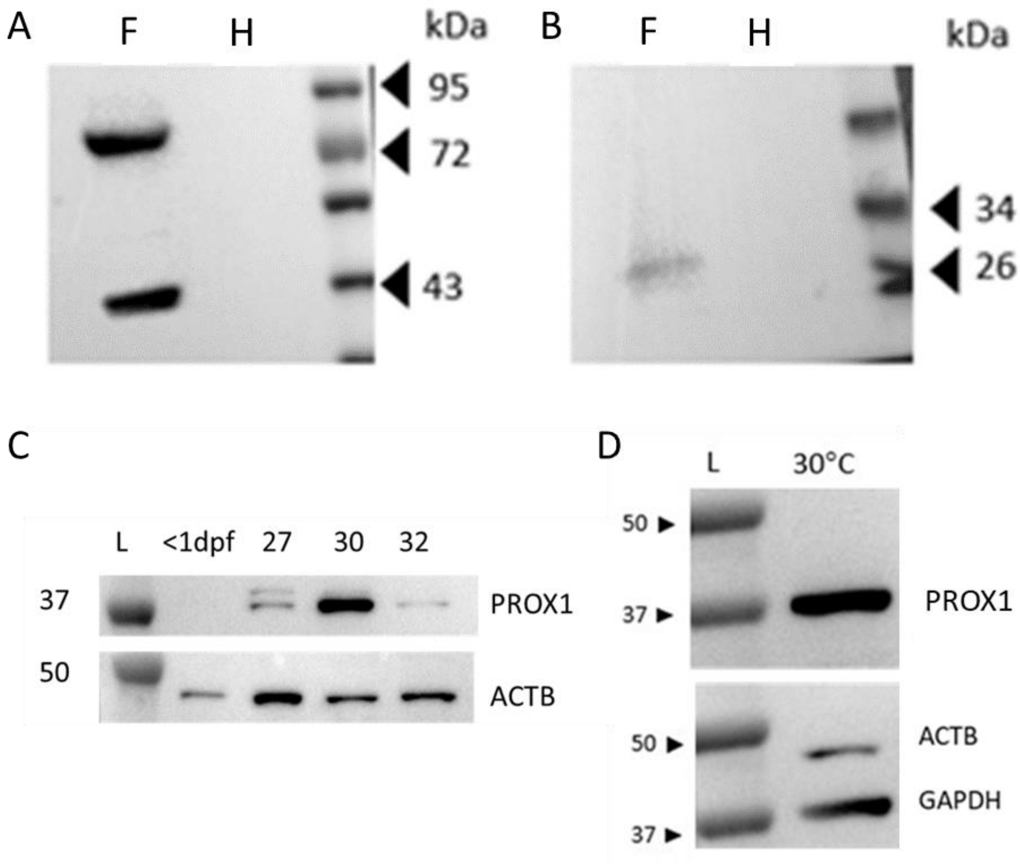

Figure 3.16. *(A+B) Western blot images to check the specificity of the immunofluorescence antibodies for PROX1 (A) and TRPV1 (B). H is human lymphatic endothelial cell lysate and F is fish lysate. (C+D) Western blots for PROX1 using fish lysate. The numbers at the top of the blot refer to the temperature that the embryo was incubated at in °C. A sample of embryos less than 1 dpf were used as PROX1 is not expressed at this stage, whereas ACTB is. N=3, pools of 50 embryos per condition. Human lysate was from cultured primary HDLECs.*

Immunofluorescence

In order to visualise lymphatic development in vivo, 4dpf larvae under the experimental conditions were stained with either an anti-PROX1 antibody, an anti-TRPV1 antibody or a rabbit IgG control antibody. The control antibody should not bind to anything specific and was raised in the same animal as the other antibodies used, in order to identify any cross-reactivity. The white arrows in the panel Figure below (Figure 3.17), denote potential pockets of neural cells of the dorsal root ganglion, as identified recently in a paper by Cheung et al (Cheung et al., 2021). The red arrow in the PROX control condition shows the thoracic duct forming in the developing embryo which has been stained by the PROX1 antibody. The PROX KD image has an orange arrow which labels a potential vessel or vessel precursor. It is worth noting that the KD condition seems to show less developed vessels than the CTRL. There can also be a difference seen between the two TRPV1 images, where the KD embryo had no stained dorsal root ganglia of TRPV1 (Gau et al., 2013), which were however observed in the CTRL TRPV1 stained image. None of these patterns were observed when an IgG control antibody was used.

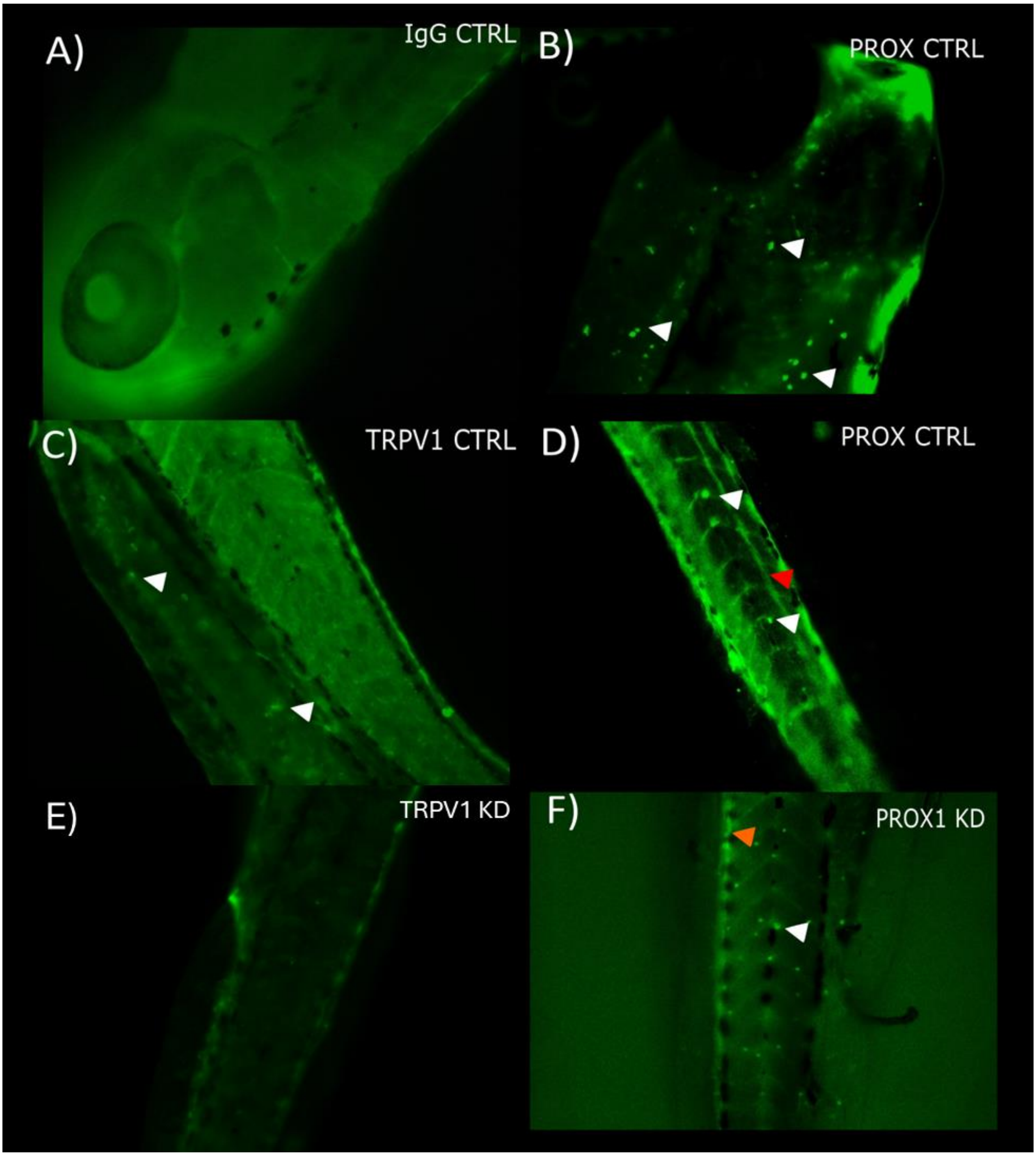

Figure 3.17. *4dpf control embryos raised at 27°C stained for PROX1a and TRPV1, as well as images of the control conditions, "Control" is where no antibody was used. A) IgG Control, B+D) anti-PROX, no knockdown, C) anti-TRPV1 and no knockdown, E) anti-TRPV1 with TRPV1 MO knockdown, F) anti-PROX1 with TRPV1 MO knockdown. The white arrowheads point to potential dorsal root ganglia, orange arrowheads point to a potential vessel and the red arrowheads mark clearly defined vessels. N=5*

3.5 Discussion

Hypothesis 1. TRPV1 knockdown lessened variance in swimming activity of zebrafish exposed to heat stimuli.

The results of this chapter show that the knockdown of TRPV1 using a Morpholino caused the zebrafish larvae to have a (nonsignificant) lower swim distance in higher temperatures, and a significantly more constrained response to heat compared to normal temperature in their behavioural response. Whilst this is reflective of results previously published by Gau and colleagues (Gau et al., 2014), differences in swim behaviour between KD and Scr conditions at normal temperature was less pronounced. It is worth noting that in Gau and colleagues' (2014) paper, the most pronounced swim reduction was obtained by injecting a dosage of MO of 3ng, rather than the 1ng recommendation given by Gene Tools, which is the dosage that was injected in this study. Gau et al. (2014) also performed an experiment at 1ng and showed that it did reduce the swim response in the majority of larvae, but not all - similar to what was observed in this chapter (Figure 3.18). While no significant difference in distance swam was observed here between KD and SCR condition, KD larvae nonetheless had a comparably reduced variance in swim distance, indicating that they sensed heat less well than SCR-injected larvae.

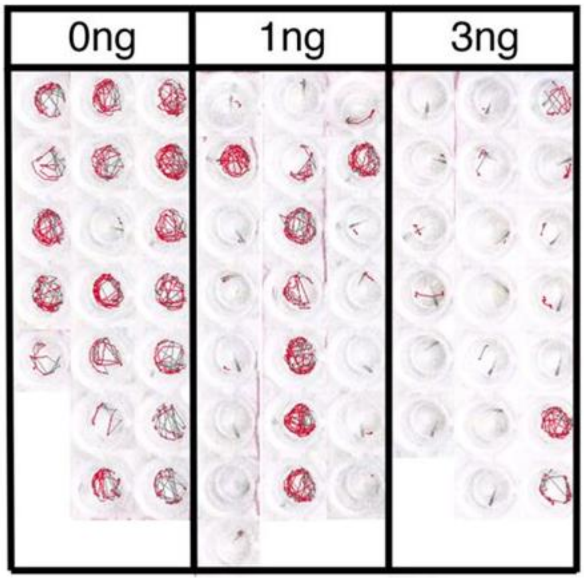

Figure 3.18. *The behavioural analysis from the paper the MO was taken from (Gau et al, 2014) , which showed that 3ng was more effective in knocking down TRPV1 than 1ng.*

Hypothesis 2. TRPV1 knockdown caused a significant change to the zebrafish transcriptome during development, with an emphasis on vascular development.

All of the zebrafish embryos that were sequenced were also exposed to 2-APB in order to activate the TRPV1 channel, in order to show the transcriptional response of the activation and repression of this channel in development. The raw counts of TRPV1 in the RNAseq showed lowest read count in E3 medium control, highest read counts in SCR condition pretreated with 2-APB, and KD condition pretreated with 2-APB having intermediate read counts. This means the injection of the MO reduced (but not eliminated) mature TRPV1 transcripts through the inhibition of splicing, when compared to the SCR condition whilst both were treated with 2-APB.

The Differential gene expression analysis found several genes with log fold change of greater than 2, which is a duplication of expression, especially during the developmental stages of the embryo. Of the genes passing the FDR-adjusted significance threshold, a predicted gene, si:ch211-106k21.5 (ENSDARG00000086052) had the highest fold change. This gene is one that was manually curated but currently has no known function. The gene encodes multiple leucine rich domains, which give the resulting protein a horseshoe structure and implies a protein-protein interaction (Kobe & Kajava, 2001).

A BLAST (Altschul et al., 1990) search of the si:ch211-106k21.5 sequence provided no results in human or mouse, suggesting this sequence is either not conserved between species or not annotated in those species. The significant gene that was most downregulated in the knockdown experimental condition was the EMAP like 5 (EML5) gene. This gene was discovered to be active in the developing rat brain and was shown to be expressed from very early stages of development (O'Connor et al., 2004). The EMAP-like proteins as a whole are responsible for microtubule re-arrangement and regulation during development (Hamill et al., 1998), and therefore it could be speculated that EML5 performs this function in the neuronal development of the brain in zebrafish larvae, too. Enrichment analysis of the differentially expressed genes (including those with unadjusted p-values <0.001) for GO biological functions showed that, as was expected under hypothesis 2, there is an emphasis on both neuronal and vessel development. The resulting list of GO terms also included angiogenesis, which contained four of the differentially expressed genes - SLC2A1a, UNC5b, MYH9a and HSPG2.

All of these genes were overexpressed in the knockdown condition, implying that they are potentially regulated by TRPV1 activation. The gene SLC2A1a is a paralog of the zebrafish homolog of the human GLUT1 gene and had a $\log_2$fold change of 3.34 when TRPV1 was knocked down. This gene is a known glucose transporter (Hruz, 2001) and in zebrafish, has been shown to be expressed during the sprouting stages of vascular development (Quiñonez-Silvero et al., 2020). The expression of SLC2A1a has also been linked to WNT signalling, where the inhibition of WNT during this sprouting phase caused the SLC2A1a expression to also be diminished in the zebrafish (Ulrich et al., 2016). Zebrafish glut1 expression has also been shown to have a correlation with HIF1a, where dexamethasone and prednisolone treatments caused HIF1a activation, in both cases resulting in GLUT1 expression being upregulated (Vettori et al., 2017). This gene has also been shown to be an important prognostic indicator of cancer survival in humans, where over-expression of the gene was found to lead to worse survival rates in a meta-analysis of 26 studies (Wang et al., 2017). It could be speculated that the decrease in survival could be linked to the increased angiogenesis through wnt signalling, causing the solid tumours to grow more aggressively than normal. Similar patterns are seen in diabetic retinopathy, where the overexpression of GLUT1 causes an overload of glucose in the photoreceptor and ganglion cells. Targeted knockdown of SLC2A1a/GLUT1 in the eyes of mice with siRNA caused the symptoms of retinopathy to be relieved, which provides additional evidence for this protein being involved in vessel formation (You et al., 2017). Enrichment analysis also found the PRODH2 ortholog, zgc:92040, to be the most enriched in terms of molecular function. The human version, PRODH2 as well as the proline metabolism pathway has been shown in the past to be related to stress survival and the balancing of intracellular redox homeostasis (Liang et al., 2013).

The enrichment analysis of the ZFIN Disease database returned three conditions relating to the cardiovascular system which remained significant even after FDR correction. These conditions were type I diabetes mellitus, arteriosclerosis and sickle cell anaemia (Figure 3.15). All three of these conditions contained the genes were c3b.1 and c3b.2 (Supplementary Table 3.5), two genes which are tandem duplicates of the b subunit of the human C3 gene. The complement component 3 (C3) protein is one of the most abundant proteins in plasma (Forn-Cuní et al., 2014) and is a main factor in immune response and the complement system, where C3b binds to C3 convertase to cleave C5 into C5a and C5b subunits (Liszewski & Atkinson, 2015). In zebrafish, this gene has been previously shown to be upregulated in response to oxidative stress related to HgCl2 exposure, suggesting a role of these innate immune response genes and subsequent inflammatory response in protecting against Hg and stress (Zhang et al., 2016).

In the RNA-seq experiment, c3b.2 was significant even after FDR correction, and both of the duplicates were upregulated. This implies that the TRPV1 knockdown caused an innate immune system response, which may have been caused by the channel not being present to regulate oxidative stress through the movement of Ca^{2+} ions (Miller & Zhang, 2011). Type 1 diabetes mellitus and sickle cell anaemia both contained the gene APOBa in addition to the c3b duplicates. APOBa, which was also highly enriched in the cellular component for the lipoprotein-related terms and codes for the apolipoprotein Ba protein. Double knockout mutant zebrafish for both APOBa and APOBb displayed numerous defects during development including abnormal liver laterality and hyperangiogenesis. This change in phenotype was due to altered Notch signalling and the vascular phenotypes were rescued by injection of a truncated form of the human APOB protein (Templehof et al., 2021).

The RNA seq results of this experiment show APOBa expression to be increased in our knockdown condition, potentially causing antiangiogenic effects and correlating with the hypothesis that TRPV1 knockdown will decrease vessel development during development. The gene which codes for clotting factor 7 (F7) was also one of the genes in type 1 diabetes mellitus and is one of the essential proteins in the clotting pathway. It forms a complex with the tissue factor (TF) protein, which is expressed on the cell surface of endothelial cells and activates the clotting cascade (Mackman, 2009). This gene was upregulated in the RNA-seq results and overexpression in mouse models caused premature death and thrombosis (Aljamali et al., 2008). Its overexpression in our experiment implies that the TRPV1 knockdown may have caused the endothelial cells to be less structurally stable and require this clotting cascade to occur at a higher-than-normal rate.

Additional investigation into the differentially expressed genes against the ZFIN disease database mostly provided results based on the MYH9 gene (Supplementary Table 3.5), which was upregulated in my experiment. Both “MYH9 related diseases” and “autosomal dominant Alport syndrome” related to both isoforms of the MYH9 gene which encodes for the non-muscle myosin IIA heavy chain. This gene has been shown to be related to deafness, macrothrombocytopenia and nephropathy (Seri et al., 2003). The inclusion of this gene in Alport syndrome is interesting since this syndrome is caused by mutations in the COL4A genes, but mutations in MYH9 are known to mimic many symptoms of Alport syndrome (Fernandez-Prado et al., 2019). Kidney abnormalities are seen in 30-70% of patients with dominant MYH9 mutations, mostly affecting the glomerulus leakiness, causing proteins to appear in urine (Kopp, 2010).

In terms of vessel development, MYH9 was shown to be a key protein in angiogenesis, as it interacts with nucleolin and is responsible for the cellular migration in angiogenesis (Huang et al., 2006). Dysregulation of MYH9 in cell culture was shown to impair angiogenic potential of endothelial cells (Huang et al., 2006). MYH9a was also the gene enriched in the ZFIN phenotype “abnormal glomerular base morphology”, as well as the “regulation of actin cytoskeleton” KEGG pathway, both of which were significantly enriched ($p<0.05$) after FDR correction. The actin cytoskeleton of endothelial cells is integral to barrier function, controlling gap formation (Prasain & Stevens, 2009) and provides further evidence of a link between TRPV1 and healthy vessel development.

The other enriched phenotypes from the ZFIN phenotype database were malformed intersegmental vessels and a collapsed dorsal aorta, both of which remained significant after

FDR correction. Malformed intersegmental vessels were enriched by the genes UNC5b and SLC2A1a. Both of these genes were upregulated in the RNA-seq data and also enriched for angiogenesis; links between SLC2A1a and angiogenesis are described earlier in this discussion. UNC5b is a netrin receptor and has been shown to interact with ROBO4 to maintain vessel integrity through counteracting VEGF signalling and antibody blocking of this interaction increased angiogenesis and reduced vessel integrity (Koch et al., 2011). UNC5b in zebrafish is involved in axon guidance during embryo development, being expressed mostly in the brain, eye and ear (Kaur et al., 2018). The collapsed dorsal aorta ZFIN phenotype was enriched by the gene HSPG2, which is also the gene that was enriched by the ECM-receptor interaction. This gene codes for the perlecan protein. The C terminus of this protein has been shown to have an inhibitory effect on angiogenesis (Mongiat et al., 2003). In addition to this, the HSPG2 protein is known to have a vital role in the notch signalling of endothelial cells and the adhesion junctions between cells (Zhao et al., 2022).

Nitrogen metabolism and -signalling plays an important role in endothelial cell signalling and the development of vessels (Draoui et al., 2017), and this pathway was the most enriched in the KEGG term analysis (Figure 3.14). This pathway however only contained one gene from the RNA-sequencing results, which was the carbonic anhydrase 2 (CA2) gene. The expression of this gene was upregulated in our experiment in **Chapter 2** and was also upregulated in the RNA-Seq results (Table 3.7). This gene is involved in physiological pH homeostasis and would therefore directly correlate to a feedback loop with the acidity sensing properties of TRPV1. In fish, CA2 has been shown to be active in highly oxygenated areas such as the gills (Lin et al., 2008), and it has even been shown to co-localise with TRPV1 in rat ganglion neurons (Tanimoto et al., 2005). In relation to lymphangiogenesis, CA2 is released to the response to vascular endothelial growth factor A (VEGF-A) signalling in both pathological and non-pathological conditions (Annan et al., 2019).

Hypothesis 3. TRPV1 knockdown caused less of the channel to be expressed in developing zebrafish and coincides with lower lymphatic vessel formation, evidenced through PROX1 staining.

The immunofluorescence staining images showed that TRPV1 and PROX1 both appear to localise to the dorsal root ganglion in the lateral line system (Figure 3.17), highlighting their importance in the development of the nervous system in the zebrafish embryo. These results highlight the possibility that there exists a similar co-localisation between CA2 and TRPV1 on the ganglion neurons similar to what was observed in rats (Tanimoto et al., 2005). The dorsal root ganglia (DRG) in vertebrates are responsible for the transmission of somatosensory information to the central nervous system. This includes the detection of external stimuli such as pain, temperature and touch (Honjo et al., 2011). TRPV1 plays a vital role in the detection of these stimuli and so it is unsurprising to observe it being expressed on the DRG. However, there is no evidence of PROX1a being expressed by the DRG, only that it is expressed as a horizontal marker in the neurons of the retina during development (Celotto et al., 2023). It is a known marker of the lateral line which may explain the expression and has been shown to be expressed in a similar pattern to that which is being observed in this experiment (Feijoo et al., 2009). Further investigation would be required to be able to differentiate if this PROX1a expression lies on the DRG or not.

The PROX1 antibody identified sprouting vessel formations, which were missing in the knockdown embryos, strengthening the hypothesis that TRPV1 has a role in healthy vessel formation during development (Figure 3.17, D & F). The knockdown, however, did not reduce the PROX1 expression across the tail. Whilst PROX1a is expressed in a range of endothelial cells during development in zebrafish, PROX1a has been shown in zebrafish to be a lymphatic marker at around 3.5dpf, when the lymphatic endothelial cells form their mature lymphatic vessels. The expression of PROX1a post 3.5dpf can be seen in vessels along the trunk of the zebrafish as well as in the head (van Impel et al., 2014), which is what was also observed in Figures 3.17B & D.

The results of chapter 3 overall did have certain limitations, the main one being the difficulty in visualizing and interpreting the immunofluoresence staining of the embryos. This was mostly due to the background fluoresence of the zebrafish and could have been solved if transgenic fish were able to be used in this study as the fluoresence is much more focused and easier to observe. Another limitation is that a lot of the RNA-seq analysis relies on the knowledge of the genes that were differentially expressed, although a large number of the genes which came out of the analysis were predicted genes or simply open reading frames. Because of this, the RNA-seq analysis can only go as far as our current understanding of zebrafish molecular biology.

3.6 Conclusion

The data collected in this chapter show that TRPV1 receptor activation is important for healthy vascular development. The knockdown of the receptor in zebrafish embryos caused a reduction in vessel formation, and the differential expression of various genes attributed to developmental pathways for both the nervous system and the cardiovascular and lymphatic systems. This was also reflected in the immunofluorescence staining, where the knock down model had less prominent vessels visible through PROX1 staining. This chapter highlights the importance of this channel in endothelial cells in potentially pathological conditions, which could be informative for the generation or repurposing of drugs and treatments for disease phenotypes related to the vascular system such as cancer , diabetes mellitus, and lymphedema. **Chapter 4** of this thesis will further interrogate this pathway by including more experimental conditions and the study of target gene expression.

Chapter 4: Characterisation of the TRPV1-lymph(angio)genesis axis in comparison to an anti-VEGFA treatment

4.1 Abstract

In the previous two chapters, I showed transcriptional changes on a global scale using microarrays (**Chapter 2**) and RNA-seq (**Chapter 3**) relating to the functions of CGRP and TRPV1. In this chapter, I investigated the TRPV1 signalling axis when activated with respect to changes in expression of a smaller set of genes, using the novel LAMP methodology. This chapter builds on **Chapter 3** by including a factorial design for two agonists of TRPV1, heat and (2-APB) in vivo. To assess the significance of TRPV1 modulation on lymphangiogenesis, VEGFA as a major player in vessel morphogenesis was inhibited to enable comparisons. For this, bevacizumab, an anti-VEGFA antibody drug was used, to observe if the loss of VEGFA during development had similar impacts on the zebrafish embryo development as decreased expression of TRPV1. The results showed that the knockdown of TRPV1 caused zebrafish embryos to no longer accelerate development in response to heat stress, combined with a decrease in survival rate at normal temperatures. Injection of bevacizumab caused embryos to develop faster but have a lower survival rate. The LAMP experiments results show that TRPV1 KD both with and without the addition of 2-APB had a significant effect on the expression of a subset of endothelium related genes. The injection of the anti-VEGFA drug bevacizumab also had significant effects on gene expression although the expression patterns were different. Greater understanding of the link between TRPV1 and development has important implications in health and disease, with the potential of becoming a therapeutic target in pathological conditions which cause changes to the endothelial cell cycle, such as neovascularization or cancer.

4.2 Introduction

The main aim of this chapter is to further dissect the impact of TRPV1 signalling on the vascular system of the developing zebrafish embryo. This will expand on the findings from **Chapter 3** by using a factorial design of more experimental conditions and observing target gene expression and phenotypic effects of TRPV1 modulation during embryo development.

In recent years, zebrafish have become an important model for vascular development of vertebrates. This is because they have a closed circulatory system, and the way vessel formation occurs in a similar mechanism to that of humans and other vertebrates. The vascular system in zebrafish has been shown to be present as early as 1 dpf, where circulation is a simple loop system consisting of the dorsal aortas and the caudal vein (Isogai et al., 2001). It is shortly after this stage when the caudal vein becomes a more complex plexus of vessels rather than one singular vessel. At 2 dpf the aortic arch systems develop into more mature vessels with smaller branches beginning to sprout (Isogai et al., 2001). This maturing and sprouting of vessels continue and by day 13 the vascular system of the zebrafish is fully developed (Jung et al., 2017). The importance of the zebrafish as a vascular model was heightened by the discovery of them having a complete lymphatic system (Gore et al., 2012).

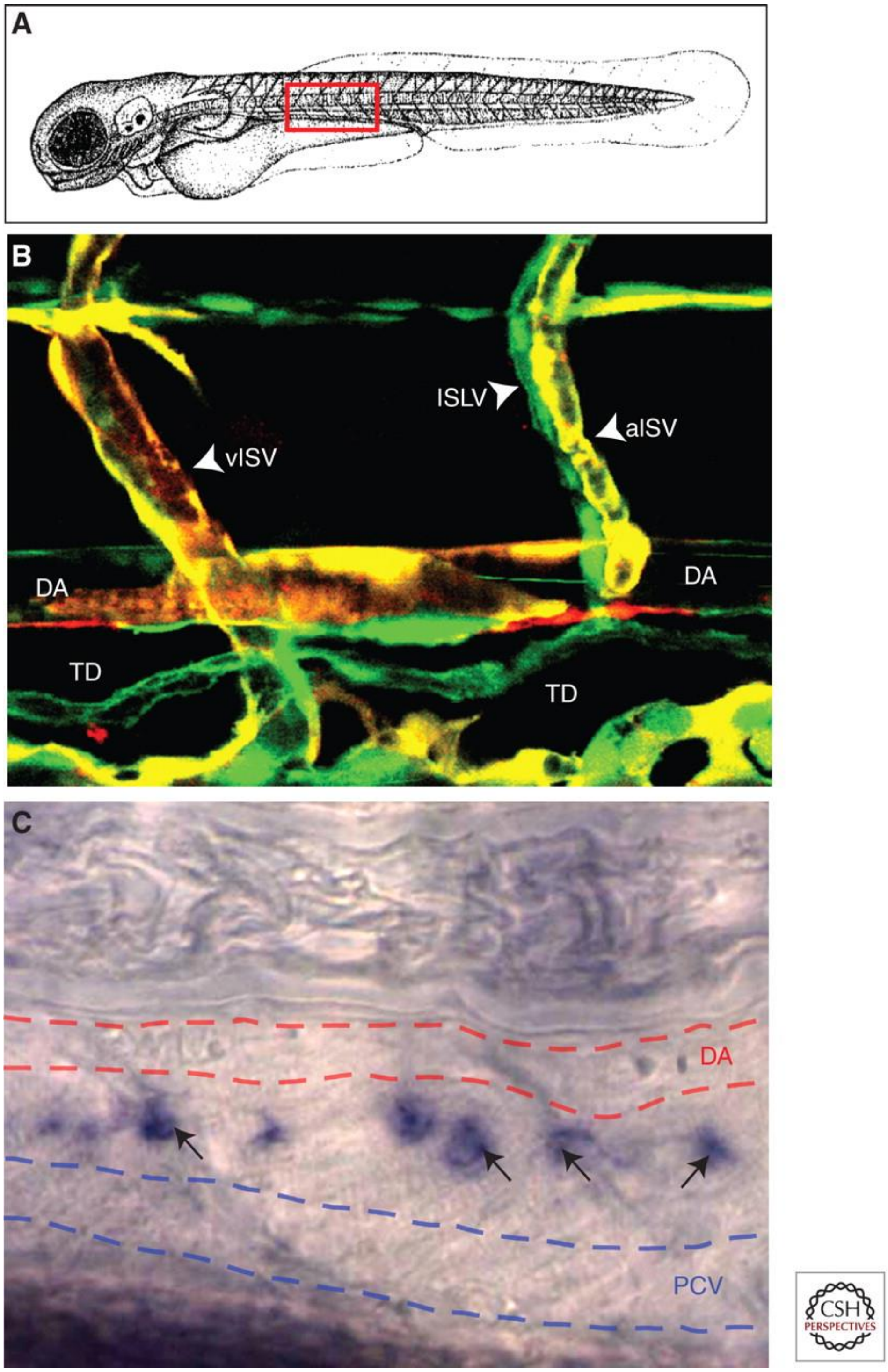

Figure 4.1. *The lymphatic system in the larval zebrafish, including a schematic diagram of a larva (A), confocal (B) and a light microscopy image (C) of the region highlighted by the red box in (A). (B) shows the blood vessels (red/yellow) and the lymphatic vessels (green) of a 3dpf tg(flk:mCherry), tg(fli1a:EGFP) zebrafish embryo.The intersegmental lymphatic vessels (ISLV), arterial intersegmental vessels (aISV), venous intersegmental vessels (vISV), the thoracic duct (TD) have all been labelled along with the posterior cardinal vein (PCV) and the dorsal aorta (DA). (C) shows a 4dpf larva which has in situ hybridization for Prox1, which is highlighted by the black arrows and also displays the DA with red lines and the PCV with blue lines. Image from Gore and colleagues (2012).*

As an important constituent of the lymphatic system, endothelial cells arise during the early stages of zebrafish embryogenesis, with precursors known as a haemangioblast appearing around the ventral mesoderm during gastrulation, and these cells speciate and become angioblasts around the 14 somite stages (Vogeli et al., 2006).

Transient receptor potential (TRP) channels are involved in multiple sensory functions, such as the detection of temperature, pain, vision and various other sensations through the movement of calcium and sodium ions across the cell membrane (Niemeyer, 2005). TRP vanilloid 1 (TRPV1) is a six transmembrane protein belonging to the TRP channel family, which is responsible for the detection of heat, capsaicin, acidity, lipids and a variety of other chemicals (Tominaga & Tominaga, 2005;Trevisani et al., 2004; Carr et al., 2003). It has multiple downstream effects, being responsible for the release of signalling molecules such as CGRP (Meng et al., 2009) and inflammatory markers (Planells-Cases et al., 2005).
Whilst there is little evidence that TRPV1 channels are important in the development of zebrafish, the Ca^{2+} influx caused by the sensitisation of the TRPV1 channel has been linked to cell functions that play important roles in development. These factors include cell migration (Waning et al., 2007) as well as proliferation and apoptosis (Zhai et al., 2020). In endothelial cells, TRPV1 was shown to be activated by anandamide, a molecule known to be involved in various cardiovascular disorders (Hofmann et al., 2014), showing that TRPV1 could indirectly have an effect on the proliferation and network formation of endothelial cells and the vascular system. Another study on *ex vivo* endothelial cells demonstrated the ability of TRPV1 to influence the migration of endothelial cells by having a cell culture grow towards an acidic media, through a signalling cascade mediated by TRPV1 resulting in the induction of lymphangiogenesis (Nakanishi et al., 2016). It was shown in **Chapter 2** that stimulation of human dermal lymphatic endothelial cells with CGRP stimulation of lymphatic endothelial cells, a signalling molecule that is known to be released upon TRPV1 activation (Assas et al., 2014), had a profound effect on their transcriptional response. It is from this data that the

hypothesis was founded that TRPV1 will have an influence on the developing zebrafish and its vasculature. This hypothesis was first tested in **Chapter 3** on the transcriptome level and found to be supported through GO terms related to vascular formation being impacted by TRPV1 knock down, but the importance of the newly discovered TRPV1 - vessel development pathway relative to other, better researched pathways such as the VEGFA pathway, remains yet unknown. VEGFA is essential for the development of blood vessels, being the key signalling molecule for the differentiation of angioblasts into blood endothelial cells, as well as regulating sprouting and barrier functions in mature endothelial cells (Bautch, 2012). Vessel patterning and sprouting is also controlled by VEGFA, in zebrafish, VEGFA is produced by the hypochord which the angioblasts migrate towards to form the dorsal aorta (Hogan et al, 2004). VEGFA has been shown to directly interact with TRP channels in retinal pigment epithelial cells (Strauss et al, 2010), where the increase of IGF-1 through temperature stimulation of TRPV1 increased the release of VEGFA in cell culture. Wan and colleagues suggested VEGFA and TRPV1 both having a role in nerve injury pain, as the two were found to be co-localised in a spare nerve injury induced neuropathic pain model (Wan et al, 2022). These results correlate with the findings of an earlier study where a specific isoform of VEGFA was found to be upregulated in pain in a mouse model (Donaldson et al 2014). In addition, this isoform; VEGFA165a, sensitises neurons through a TRPV1-dependent mechanism. It is therefore of interest to further investigate and compare the effects of both TRPV1 and VEGFA on lymphangiogenesis in the developing zebrafish embryo.

As shown in Chapter 3, TRPV1 can be inhibited through morpholino (MO)-targeted knock down. To inhibit VEGFA, Bevacizumab can be used which is an anti-VEGFA monoclonal antibody drug. Bevacizumab is used for inhibition of vessel formation in the treatment of a variety of vascular cancers (Hurwitz and Saini, 2006; Zhang et al, 2017; Van Cutsem et al, 2012; Nakai and Matsumura, 2022) as well as eye vascular diseases such as glaucoma (Ichhpujani et al., 2007; Moraczewski et al., 2009). Treatment using bevacizumab is known to cause pain to the patient (Moisseiev et al, 2012; Wieder et al, 2021; Enora et al, 2019), providing additional evidence linking VEGFA signalling with pain responses. Bevacuzimab has been studied in vivo in a zebrafish development model, and it was shown that the drug caused significant anti-angiogenesis in zebrafish (Zhang et al, 2018), inhibiting the development of both the retinal blood vessels and subintestinal veins (SIVs) in a dose-dependent manner.

Heat is known to cause increased rates of development in various different ectotherms up to a threshold where it begins to be detrimental to the organism. The temperature size rule predicts that increased temperatures during development lead to faster developmental times but would potentially lead to smaller adult bodies (Sibly & Atkinson, 1994). Sibly and Atkinson (1994) estimated that greater than 80% of ectothermic species follow this rule and it has been proven to be the case for a variety of species, including molluscs, fish and arthropods (Angilletta & Dunham, 2003; Buckley et al., 2022). This is generally accepted as being due to the increase in the metabolic rate of the organism (Clarke & Fraser, 2004), where the enzymes which aid in development reach an optimal working temperature but get denatured if the temperature reaches too high (Ohlberger, 2013). In this experiment, I am interested in the properties of heat to serve as agonist of TRPV1 h since it is a well-known temperature sensor and is expressed during development in both the mouse (Qi et al., 2015) and the zebrafish (Son & Ali, 2022). Studies have shown the importance of TRPV1 as a temperature sensor through the chemical activation of the channel causing hypothermia responses in mouse models, whilst antagonists of the channel gave hyperthermia to the mouse (Saito & Tominaga, 2017). I expect heat treatment to have similar agonistic effects on TRPV1 as 2-APB stimulation.

In order to evaluate the relative importance of TRPV1 and VEGFA inhibition in lymphangiogenesis, treatments will follow a factorial design, combining the factors TRPV1 stimulation with 2-APB or heat, TRPV1 MO knockdown, and bevacizumab injection.

The response variables that I will observe will be the growth rate of the embryo, the survival rate and also gene expression through the use of **q**uantitative reverse transcription (RT) – **l**oopmediated isothermal **amp**lification (qLAMP), in the following called LAMP (figure 4.2). LAMP is a relatively new method that was developed in 2000 (Notomi et al, 2000). The mechanism uses hairpin loop structures and builds upon the same strand of template, in contrast to conventional qPCR methods. The reaction time of LAMP is also considerably shorter, requiring only around 30 minutes per reaction rather than the 45 - 150 minutes that are required by conventional qPCR technologies. LAMP improves on conventional methods of qPCR as it is more robust, requiring six primers per reaction and therefore reducing the risk of amplification of unwanted products. It does have the disadvantage of the product being difficult to use downstream in sanger sequencing for example, due to the tertiary structure that is formed in the reaction (figure 4.2). LAMP is also more expensive than a conventional PCR, requiring extra primers per gene to be designed and purchased. LAMP is becoming more common in research and industry, although the majority of studies are observing only one or two genes (Fallahi et al., 2014; Inaba et al., 2021; Khan et al., 2017). Most recently it was used for COVID-19 testing (Dao Thi et al, 2022). This chapter aims to use LAMP to quantify several genes at once. Furthermore, this chapter develop a novel analysis method that takes into account the unique linear vs. exponential in qPCR amplification dynamics of LAMP, to more accurately predict Ct values. This chapter will also attempt to determine whether a LAMP reaction failed due to the absence of template RNA (true negative), despite the presence of template RNA (false negative), or if there are any false positives (amplification despite target RNA absence). For this purpose, comparisons between LAMP amplification results with those from regular PCR performed on the same samples will be made.

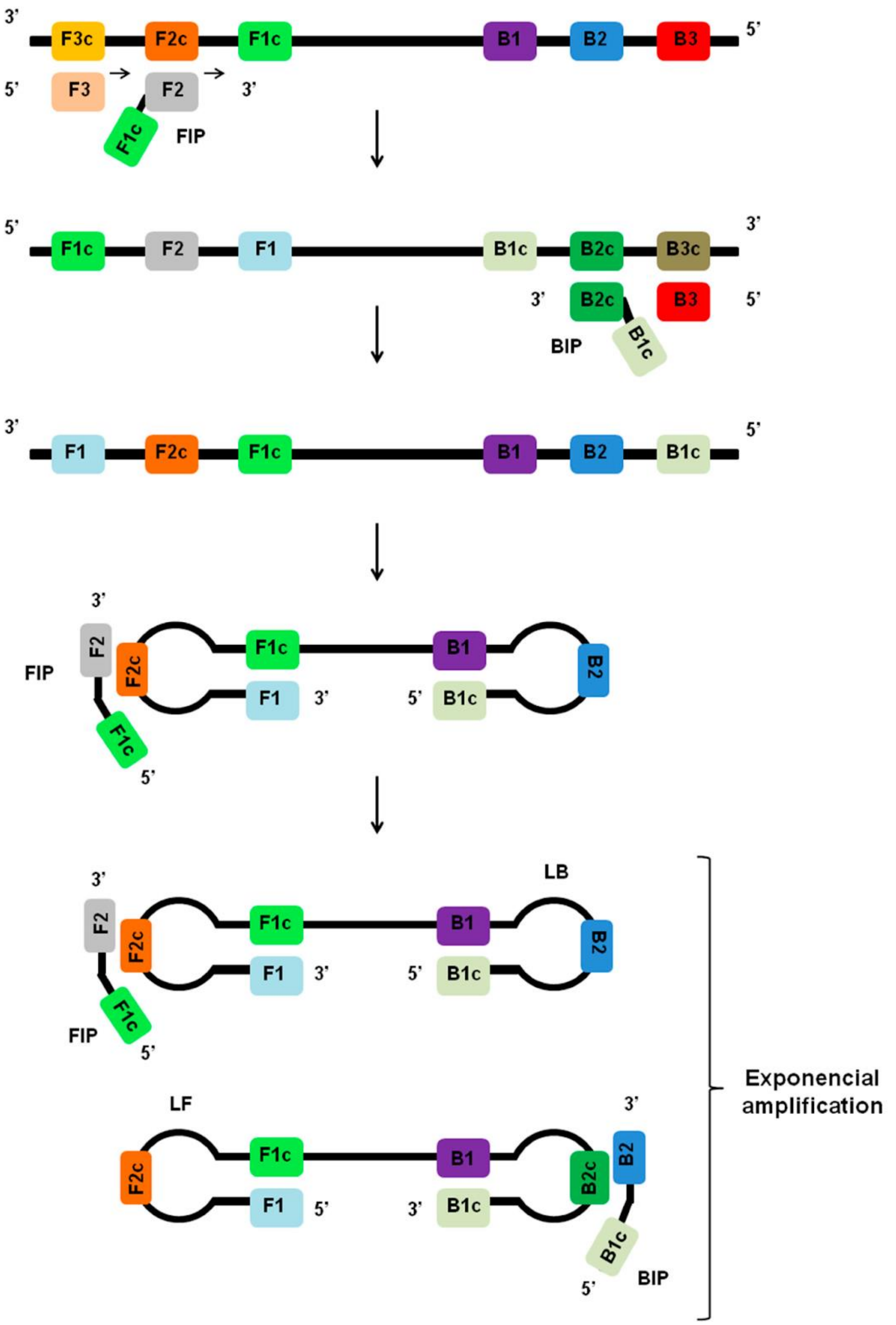

Figure 4.2. *A graphical representation of a typical LAMP reaction. Image taken from Loop-Mediated Isothermal Amplification (LAMP) for the Diagnosis of Zika Virus: A Review (Silva et al., 2020). In the first stages of the reaction, the inner primers, FIP and BIP bind to the template strands and primer is extended by the polymerase to cause the target gene to form a dumbbell loop structure with the self-hybridization regions (F1-F1c & B1-B1c). This structure becomes the starting point for the exponential amplification where the multiple loops are built onto the sample dumbbell structure.*

To detect transcriptional changes, genes that were up- or downregulated in the RNA-seq experiment were selected, respectively, some of which were identified in **Chapter 3**. Eight genes in total were used based on their potential connections to development and the endothelial system and working primers. CALCA codes for CGRP, one of the main signalling molecules that is released upon TRPV1 activation; it also ties this chapter back to **Chapter 2**, in which explored the influence of CGRP on human dermal lymphatic endothelial cells. The CXC chemokine receptor CXCR3 has previously been shown to be expressed in endothelial cells and that its expression was increased in response to inflammation (García-López et al., 2001). This gene is involved in the activation of the immune response, regulating the migration of leukocytes. Finding an altered expression of this gene in our experimental conditions would help link the activation of TRPV1 to these pathological states. F7 was included as its codes for the coagulation factor VII and therefore is expected to be closely regulated within the circulatory system; any alterations to its expression could lead to abnormal clotting or other pathological states in vivo. TAF5L is a subunit of the p300/CBP-associated factor (PCAF) histone acetylase complex, which plays a role in promoter region recognition during transcription. Mutations in the gene have been linked to diabetes mellitus I; an autoimmune disorder (Chistiakov et al., 2005). Similar to CXCR3, finding differential expression of this gene in the experimental conditions outlined here could strengthen the connection between TRPV1 signalling and the immune response with the potential to generate disease-causing states. Lastly, GPRC5b (zebrafish ortholog gprc5bb) was selected because it has been shown to be expressed on the sensory neurons, having a notably high expression in trigeminal ganglia of mice (Manteniotis et al., 2013), as well as in the dorsal root horn in humans, where its expression is reduced in spinal cord injury patients (Chung et al., 2014). The expression of GPRC5b has also been shown to modulate the inflammatory response pathway in glomerular diseases (Zambrano et al., 2019), which were significantly enriched in **Chapter 3**. Because of this evidence, GPRC5b was selected as a marker of neuropathic pain but also may highlight changes to the development of sensory neurons during vessel formation in these experiments. F7 and taf5l were differentially expressed in **Chapter 3.**

In addition to these genes, the lymphatic endothelial cell markers PROX1 and LYVE-1 will also be added to the genes under investigation. This will be done in order to determine if there are any changes to the lymphatic system as the embryo develops.

There are three hypotheses which this chapter will investigate:

1. The stimulation of the TRPV1 channel through heat or 2-APB will have a morphogenetic effect on the vascular development of the zebrafish embryo. I expect that the activation of the TRPV1 channel will cause an increased expression of candidate genes.
2. The knockdown of the TRPV1 channel by MO in the developing zebrafish will have an inhibitory effect on the vascular development. I expect that growth and survival rates will be negatively impacted by the knockdown of TRPV1 and gene expression will indicate a change in vascular (endothelial) markers.
3. The injection of the anti-VEGFA cancer antibody treatment bevacizumab will likewise decrease the vascular development of a developing embryo, uncovering similarities to TRPV1 suppression. Bevacizumab will have a negative effect on the development of the embryo, as shown in previous studies. The gene expression of the developing zebrafish will be similar to that of the TRPV1 knockdown model.

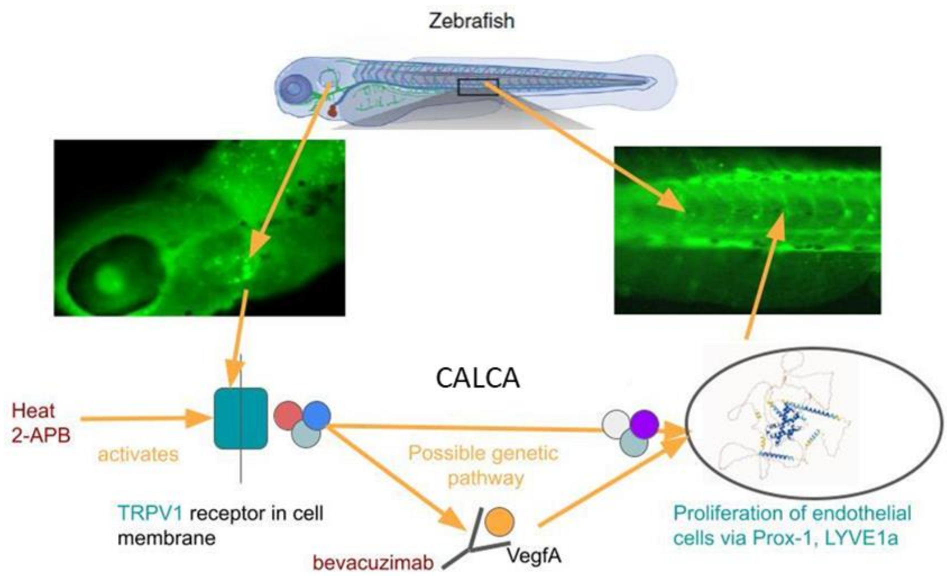

Figure 4.3. *A schematic of the proposed genetic pathway being studied in this chapter. Stressors to this pathway are highlighted in red and the mechanism of activation is outlined in the orange text. The causes of the changes to this pathway in response to the stress are in blue text, being differences to the TRPV1 receptor itself, through knockdown which will lead to potential changes in the proliferation of endothelial cells, observed via changes to PROX1a and LYVE1a expression in the zebrafish.*

4.3 Materials & Methods

4.3.1 Factorial experimental design

In order to investigate the hypotheses outlined above in the introduction, and to be able to apply statistical analysis to the data, a factorial design was created to account for different combinations of variables. The factors that are studied in this chapter are a mix of “treatments" to observe changes in TRPV1 and VEGFA signalling on lymphangiogenesis, and “environmental” modifications used to stimulate activity of TRPV1:

1. Knockdown of TRPV1 using a morpholino - Treatment
2. Injection of bevacizumab - Treatment
3. Immersion in 200nM 2-APB diluted in E3 media - Environment, TRPV1 stimulation.
4. Heat treatment; storage of the embryo at 30°C - Environment, TRPV1 stimulation

Additionally, these experimental conditions were run at two temperatures. Heat treatment is where the embryo has developed at 30°C, and the embryos not exposed to temperature stress were raised at 28°C. The heat treatment of 30°C increased the expression of PROX1 in the western blot (Figure 3.16), without having a detrimental effect which was seen in the 32°C treatment condition. Since heat is known to not only stimulate TRPV1 but also increase the overall metabolic rate of the embryo, heat treatments were analysed separately from normal temperature treatments. Data were analysed in R and plotted with *ggplot2*. This yielded a total number of 9 treatments. The treatments from hereon will be referred to as E3 (none/none), APB (None/APB), and KD (morpholino injection / none), BEV (Bevacizumab injection / none), and HOT (developed at 30°C), and the combinations of them will be denoted with "+" (e.g., BEV + APB). MO was injected into the cell at the one-two cell stage at the same concentration as in **Chapter 3**, 1ng per embryo, and BEV was injected into the yolk sac at the concentration of 2mg/mL with an injection volume of 40nL. 2-APB supplementation was always at the concentration of 200nM throughout all experiments.

Table 4.1. *The experimental conditions that will be performed throughout this chapter. KD refers to knockdown through the TRPV1 morpholino; Bev refers to bevacizumab. These were performed either under hot conditions (30°C) or at normal temperature (28°C)*

Treatment	Environment
None	None
None	2-APB
KD	None
KD	2-APB
Bev	None
Bev	2-APB

4.3.2 Zebrafish husbandry

AB strain zebrafish were purchased from Sheffield University and raised in a closed water system in the university of Hull Aquarium facility with a 14:10 light dark cycle, kept at 28°C. They were fed a mixture of fish flake, artemia and blood worm twice a day. All experiments were performed in accordance with University of Hull ethics form (U144B) and was approved by the faculty of science and engineering's (FoSE) ethics committee.

4.3.3 Survival rates and Development

Single embryos were incubated in individual 0.2mL PCR tubes with 150uL E3 media, kept in a thermocycler set at either 28°C or 30°C with the time set as infinite. Survival rates were documented after 24 hours. The embryos were imaged both prior and post incubation using a Zeiss stereo microscope with the supplied Zen software (Zeiss™). The images taken were staged using ImageJ software (NIH; Rasband, 1997-2018). Staging was performed using the guidelines previously published (Kimmel et al, 1995). Developmental stage was estimated using the metrics; head/neck angle and the relative eye length, two key measurements of developmental age as documented by Kimmel et al (1995). The average development rate was calculated as the arithmetic mean of the age of the embryos before exposure and subtracting that value from the age of the apparent embryo after exposure.

The rate of development of the embryo was calculated as:

(Perceived after age (hpf) - perceived before age (hpf))/24

The relative eye length was recorded in ImageJ by recording the diameter of the eye and then measuring the distance between the tip of the embryos head to the end of its tail and calculating this as units of eye diameter.

4.3.4 Immunofluorescence

Immunofluorescence experiments were performed for the BEV injected embryos using the same protocol as outlined in **Chapter 3**. The embryos were left to develop in either 2-APB or E3 up until 4dpf where they were sacrificed and fixed in paraformaldehyde (PFA) and stained with TRPV targeting antibodies (full list of primary and secondary antibodies in Table 3.2). The stained embryos were imaged on a Zeiss LSM710 confocal microscope or an Olympus IX 71 inverted microscope.

4.3.5 Loop-mediated isothermal AMPlification (LAMP)

RNA extraction was performed using the same Trizol-based protocol that is outlined in **Chapter 3**. Embryos were flash frozen after 24 hours of exposure and pooled into tubes of 20. Each tube of 20 was extracted as one sample for the qLAMP. For the LAMP reactions, the Warmstart master mix with fluorescence dye from New England Biosystems (NEB) were used, following the manufacturer's instructions (product code: #E1700), with the exception of reducing the total reaction volume to 10uL. Primers were designed using NEB's online tool for LAMP primer design (https://lamp.neb.com/) and ordered from IDT (full list available as supplementary Table 4.1). Two housekeeping genes were selected and used - Beta-actin (ACTB) and Elongation factor 1 alpha (EF1a). The reaction itself was performed in a StepOne thermocycler, set at 65°C, and fluorescence was measured every 18 seconds for 100 cycles - for a total incubation time of 30 minutes unless specified. The LAMP reactions were run for 100 cycles, totalling 30 minutes (18 seconds per cycle) were used for all samples and plates initially. One plate that was performed to repeat samples was run for 250 cycles (75 minutes) once it was evident that some of the samples required more time to amplify. This was the case for some samples which actually gave Ct values of around 240, such as CXCR3 which was shown to have late Ct values. One gene that failed to amplify consistently was LYVE-1, even with the increased cycle number. For a LAMP reaction, the mastermix has different concentrations of the required primers in accordance to how much is used in the reaction, for example, FIP and BIP are used in every amplification cycle of the LAMP reaction, they are used in higher concentration (table 4.2). 70ng of RNA was used as input material, as this was previously reported in the literature to be amplified through LAMP reactions (González-González et al., 2020, Karthik et al., 2016).

Table 4.2. *The LAMP primer concentrations used in the LAMP experiment, as recommended by NEB*

PRIMER	10X CONCENTRATION (STOCK)	1X CONCENTRATION (FINAL)
FIP	16 µM	1.6 µM
BIP	16 µM	1.6 µM
F3	2 µM	0.2 µM
B3	2 µM	0.2 µM
LOOP F	4 µM	0.4 µM
LOOP B	4 µM	1.4 µM

4.3.6 Determining the fidelity of qLAMP reaction

To assess the fidelity of the qLAMP reaction, regular PCR on the LAMP product after qLAMP amplification, using the full reaction mix and adding PCRBiosystems taq mix red without adding any additional primers. All PCRs were run using the same conditions (1 min hot start 95℃, 15s denaturing 95℃, 15s annealing 55℃, 2s extension 72℃; 40x cycles), and agarose gels were run using 2% standard agarose concentration and sodium borate buffer. The gels were run for 30 minutes at 120V. NCBI's primer blast web tool was used to determine the sizes of any potential products between the FIP-B3 and BIP-F3 primer combinations that could generate a viable PCR product in the follow-up reaction.

In order to determine the effectiveness of the LAMP and PCR reactions, following best practice, ImageJ software was used to quantify the fluorescence of the bands that are present in the gel. The "analyse gels" function in ImageJ was implemented and the gels were calibrated against the ladder to obtain data on the depth of fluorescence for each lane in the size classes 200+bp, 200-150 bp and 150-100 bp. This allowed for assessing PCR product size classes, excluding primer dimer and various other unwanted products. A gel profile which contained both a smear and a clear band were the samples that were defined as having a true positive result. The smear likely represents the LAMP product, mirroring products with different sizes generated by the LAMP extension. The clear band below the smear would imply the follow-up PCR has generated a product, confirming that at the sample contained mRNA of the gene of interest, and that at least one forward and one reverse primer were effective at amplifying the gene of interest and is labelled “true positive”. A gel which appeared to have no product at all and didn’t amplify in the qLAMP reaction was denoted as a “true negative”. If the LAMP produced a Ct value but the follow up agarose gel has a solid band without a smear is a “false positive”. A LAMP reaction which did not have a Ct value but displayed a smear and a band on the follow up gel, is a “false negative” because the reaction worked but didn’t generate a Ct value.

4.3.7 LAMP analysis with LAMPrey

For the analysis of LAMP, the Ct calculations that are performed by the software supplied with the StepOne machine were found to be insufficient as the procedure is more suited for conventional qPCR rather than LAMP. First, while LAMP reactions do have an exponential phase, the shape of fluorescence curves show that this does not occur at equal time points between different target genes after fluorescence has begun to accumulate. Typically, an auto threshold is selected to subtract noise, selecting the area where the amplification curves are steep, but it does not perform well in qLAMP amplification plots where genes have large differences in Ct value, don’t show uniform amplification, and amplification curve steepness may be influenced by the length of the mRNA fragment amplified. All reactions that failed to amplify were considered true negatives, and Ct values were replaced with the highest value measured for a gene which amplified (Ct = 150). Because of this, a novel R script *LAMPrey* (“the king of LAMP” rey in Spanish = king) was developed which inputs raw data that has been exported from the StepOne machine and calculates the “Ct” cycle number (where each cycle is equal to 18 seconds) for each curve individually, at the point where the reaction is exponential. A calculation is performed that normalises the baseline fluorescence values by subtracting the fluorescence value of each curve at cycle 1 (18 seconds), such that each sample starts at 0 in cycle 5. The script also calculates deltaCt values against a given housekeeping gene, and plots fluorescence curves using the ggplot2 (Wickham, 2016) package. All code is publicly available to download from my github (Bates, 2022) and is also supplied in the Supplementary Material 4.1. An in-depth explanation of the procedure is given in the Results section. A comparison of Ct calling by *LAMPrey* against automated Ct calling of qPCR standards of a NEBNext Quant library kit (#E7630) by the StepOne software. The results of *LAMPrey* against the automated Ct calling were compared using linear modelling to determine the R^2 coefficient.

4.3.8 Statistical Analysis

Differences in developmental rate and relative eye length among treatments were evaluated using multidimensional scaling (MDS) was performed. Performing the Shapiro-Wilk test for normal distribution on the data collected from embryos left to develop at 28°C, it was shown that both dependent variables were not normally distributed (Relative eye length: $w=0.92568$, $p=3.117 \times 10^{-5}$, Development rate: $w=0.73255$, $p=1.32 \times 10^{-12}$). The R package "*BestNormalize*" was subsequently used to find the best way to normalise the non-normally distributed data. This package recommended the method of calculating the *sin* values of both of the non-hot response variables as well as the developmental rate of the hot conditions. This transformation however, whilst making the data closer to being normally distributed, was still non normal following a post-transformation Shapiro-Wilk test. In the embryos that developed at a higher temperature (30°C), the relative eye length data were found to be normally distributed ($w = 0.9824$, $p = 0.183$), while the developmental rate was non-normally distributed ($w = 0.65432$, $p = 1.915 \times 10^{-14}$). The relative eye length of the embryos developing at a normal temperature were recommended to undergo a different transformation method, sqrt(x+1); although this still didn't make the data normally distributed. A full breakdown can be found in **Table 4.3**. Nonparametric PERMANOVAs were therefore performed for both the hot and non-hot groups with 9999 permutations for both developmental rate and the relative eye length. The predictors were tested with interaction terms as that better suited my hypothesis investigating the interactivity of these conditions with TRPV1 channels.

Table 4.3. *The results of the Shapiro-Wilk test for the developmental rate and relative eye length before and after the transformation method suggested by the BestNormalize package.*

Variable	Original	Post transformation	Transformation method
Normal Temperature (28°C)			
Development Rate	1.32×10^{-12}	2.007×10^{-12}	Inverse Sin
Relative eye length	3.117×10^{-5}	0.001707	Sqrt (x+1)
Hot (30°C)			
Development Rate	1.915×10^{-14}	1.737×10^{-14}	Inverse Sin
Relative eye length	0.183	0.9029	Inverse Sin

Since the factorial design had three factors (KD, BEV, and APB), to observe the effects of these predictors on developmental rate, nonparametric PERMANOVAs were performed using the *adonis* function from the "vegan" package with 9999 permutations (Oksanen et al., (2022); Anderson, M.J., 2014). Data from the "hot" experiment were analysed separately from the normal temperature data since it is known that heat has a positive influence on developmental rate (Feugere et al, 2021). PERMANOVA was also used to analyse the effects of the three factors on the LAMP results. To compare the survival rates (a binary outcome variable) between the experimental factors, a logistic regression model was fitted, using base R for the hot and normal temperature conditions separately. To compare the relative strength of the factors BEV, APB + KD and KD on candidate gene expression, the overall variance was partitioned by these predictors and a redundancy analysis performed to investigate the direction of their action (Figure 4.11). For the purpose of observation of the activation or deactivation of gene interaction pathways of the candidate genes, String networks were generated using string.db (Szklarczyk et al., 2015).

4.4 Results

Developmental rate

An MDS plot of the staging results shows the relatedness between the data in both the hot and the normal temperature experiments (Figure 4.4). In the non-hot conditions, there appear to be two separate groups, one consisting mostly of BEV + APB, with a few of the BEV and KD

+ APB samples mixed in, and the rest of the conditions makes another group below this on the graph. The hot experiment graph, on the other hand, seems to have hardly any variation in the samples, and all the grouping ellipses overlap one another to a large extent.

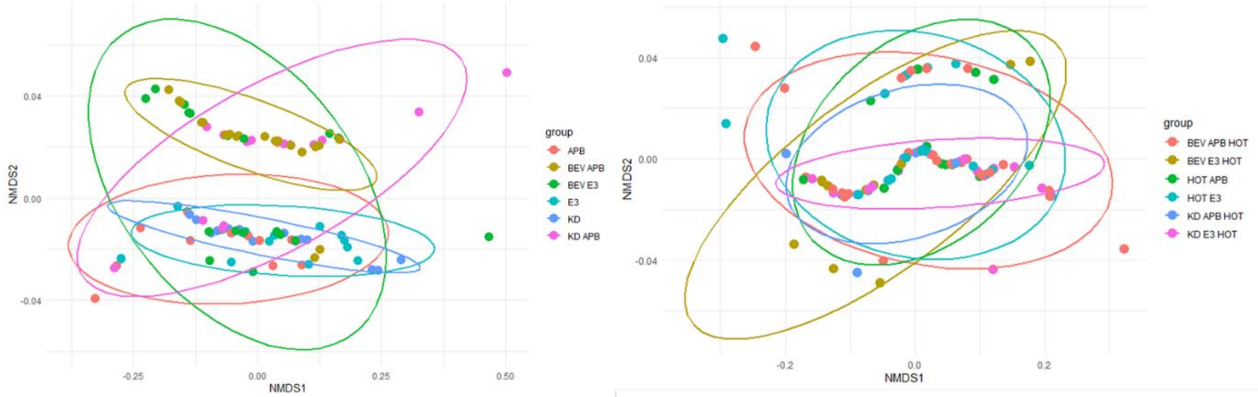

Figure 4.4. *A MDS plot of the embryo stages by condition, where both the developmental rate and the relative eye length were used as factors (NMDS 1 and 2) in the plot. Normal temperature experiment is displayed on the left and the hot experiment is displayed in the graph on the right.*

Figure 4.5 shows a boxplot of the relative eye length and the relative developmental rate in the normal temperature and hot experiments. There is a difference in baseline developmental rate and relative eye length between the normal and hot temperatures of just under 0.2 (approximately 5 hours), where 1 refers to the expected age of 24 hpf (or, 1 day). The baseline for the hot experimental samples increases from 1 to 1.2, which is in line with results from similar studies (Feugere et al, 2021). Interestingly, all but two individuals in the normal temperature experiment for BEV+APB developed at a similar rate to those in the hot experiments: with the actual mean of KD+APB being close to 1.2. BEV and KD + APB had the largest spread of developmental rates in the normal condition, although this was not present upon heat treatment as means from the hot experiment data all lie around 1.2, with the exceptions of APB and E3.

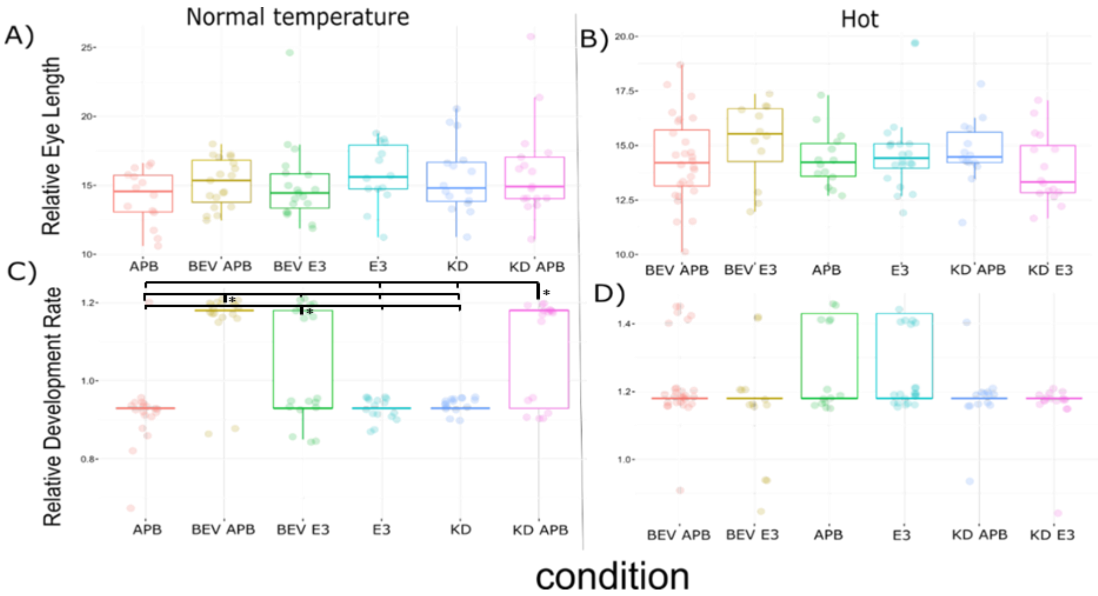

Figure 4.5. *The relative eye length across normal temperature (A) and hot (B) exposed developing zebrafish. relative eye length being the embryo body length in relation to the eye. The average growth rate, determined by average ((hpf after-age before hpf)/24)) across normal temperature (C) and hot (D) exposed developing zebrafish. Significance was calculated using Dunns test with Benjamini-Hochberg correction. N=15*

A PERMANOVA showed that none of the factors in either temperature experiment had a significant effect on the relative eye length of the developing embryo (Table 4.4). In contrast, all of the experimental conditions were highly significant (***) in the normal temperature developmental rate PERMANOVA, showing a significant increase to the relative developmental rate of the developing embryo. The data collected from the heat treatment embryos, however, only had one significant variable and that was the KD condition ($F = 9.65$, $p < 0.002$, Table 4.5). Only one embryo showed developmental acceleration from 1.2 to 1.4 when KD was performed (Figure 4.5).

Table 4.4. *The results of a PERMANOVA for the effect of the predictors APB, Bev, KD, E3 and one interaction term (Bev *APB) on the relative eye length. "*" denotes interaction term between predictor variables.*

Normal Temperature (28°C)					
Predictor	**Df**	**Mean Sqs**	**F. Model**	**R2**	**p**
APB	1	1.55	0.24	0.0024	0.637
BEV	1	2.36	0.36	0.0037	0.557
KD	1	9.97	1.53	0.0156	0.226
E3	1	6.34	0.97	0.0099	0.324
BEV:APB	1	13.21	2.025	0.021	0.167

Hot (30°C)					
Predictor	**Df**	**Mean sqs**	**F.Mode1**	**R2**	**p**
APB	1	0.5	0.16	0.0016	0.693
BEV	1	0.71	0.28	0.0022	0.633
KD	1	1.3	0.42	0.004	0.526
BEV:APB	1	5.78	1.85	0.0181	0.178

Table 4.5*. The results of a PERMANOVA for the effect of the predictors APB, Bev, KD, E3 on the relative developmental rate.*

Normal Temperature (28°C)					
Predictor	**Df**	**Mean Sqs**	**F.ModeI**	**R2**	**p**
APB	1	0.19	18.44	0.1014	0.0002***
BEV	1	0.4	40	0.2202	0.0001 ***
KD	1	0.16	15.95	0.0878	0.0002***
E3	1	0.064	6.32	0.0348	0.0128*
Hot (30°C)					
Predictor	**Df**	**Mean Sqs**	**F.ModeI**	**R2**	**p**
APB	1	0.2	1.45	0.0013	0.222
BEV	1	0.013	0.9	0.0079	0.351
KD	1	0.14	9.65	0.084	0.002**

Survival rates

In a logistic regression analysis of the factors KD, APB and BEV, (Tables 4.6 & 4.7) it was shown that in the normal temperature experiment, the only significant predictor of survival was the KD ($z = -2.138$, $p = 0.033$), where zebrafish embryos which had an injection of the TRPV1 morpholino had an overall lower rate of survival than those who did not (56.25% of embryos in KD compared to 93.75% in the E3 control group). Both BEV and KD were injected, yet the injection of BEV did not have a significant influence on survival. In the hot experiment, KD ($z = -5.077$, $p = 3.8x10^{-7}$), BEV ($z = -2.786$, $p = 0.0053$) and the combination treatment of KD + APB ($z = 3.113$, $p = 0.0019$) were all shown to be significant predictors of survival (Table 4.7).

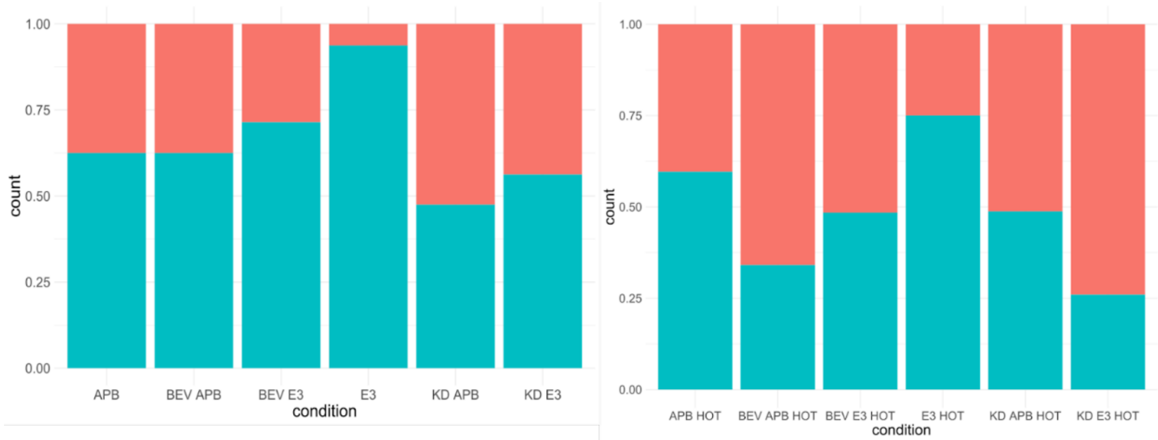

Figure 4.6. *The survival rates of the embryos in each experimental condition, blue is %survived, and red is % died. Count of 1 is 100%. N=20*

Table 4.6. *The results of a logistic regression analysis of the normal temperature experiment survival rate. Significant results have been labelled "*" (<0.05), "**" (<0.01) or "***" (<0.001).*

Normal Temperature (28°C)				
Predictor	**Estimate**	**Std. Error**	**z value**	**Pr(>|z|)**
KD	-2.457	1.149	-2.138	0.03253*
APB	-2.197	1.155	-1.903	0.05706
BEV	-1.792	1.074	-1.668	0.09535
KD:APB	1.846	1.299	1.421	0.15535
APB:BEV	1.792	1.22	1.469	0.1418

Table 4.7. *The results of a logistic regression analysis of the hot temperature experiment survival rate. Significant results have been labelled "*" (<0.05), "**" (<0.01) or "***" (<0.001).*

Hot (30°C)				
Predictor	**Estimate**	**Std. Error**	**z value**	**Pr(>|z|)**
KD	-2.1459	0.4227	-5.077	3.83e-07 ***
APB	-0.7077	0.429	-1.65	0.098956
BEV	-1.1611	0.4167	-2.786	0.005333 **
KD:APB	1.7063	0.548	3.113	0.001850 **
APB:BEV	0.111	0.5451	0.204	0.838612

Immunofluorescence

To follow up from the results from chapter 3, immunofluoresence was performed on zebrafish emrbyos which were injected with bevacuzimab and left to develop in E3 up to 4dpf (n=5). Immunofluorescence staining of TRPV1 in 4dpf zebrafish which had been injected with BEV and allowed to develop at 28°C in E3 media showed more of the dorsal root ganglia (DRG) which had been observed previously in **Chapter 3**. The somatosensory neurons of the DRG are where TRPV1 is likely to be expressed since it is a detector of external stimuli such as high temperature. Staining images of the BEV E3 treatment zebrafish also identified a potentially new expression location of TRPV1, the olfactory epithelium (Figure 4.7; orange arrowheads).

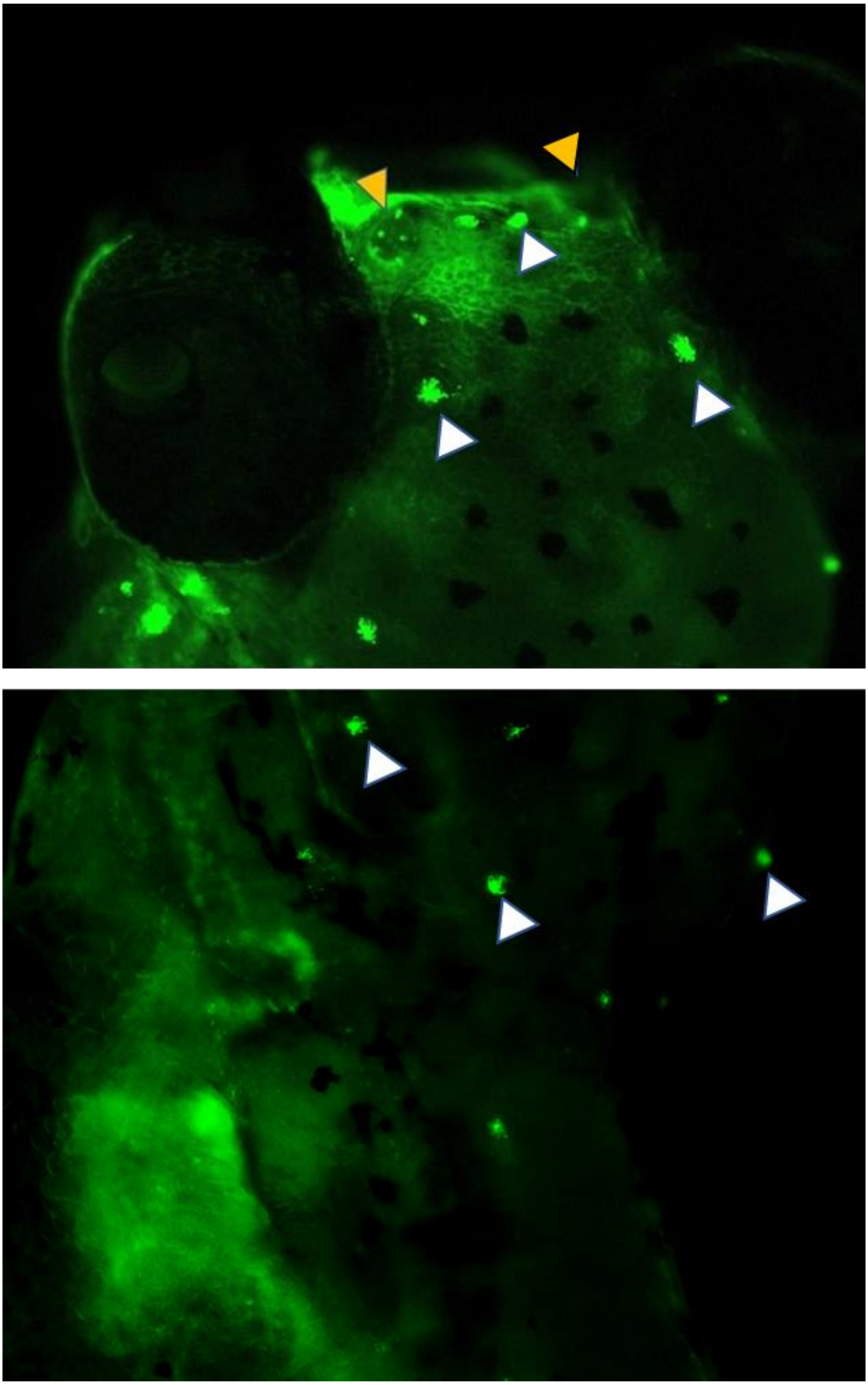

Figure 4.7. *Immunofluorescence staining of TRPV1 in a BEV E3 treated 4dpf zebrafish embryo. The orange arrowheads highlight the olfactory epithelium. The white arrowheads are marking potential neuromasts, either on the dorsal root ganglion (round shaped) or hair cells of the lateral line system (star shaped). N=5*

LAMP analysis of candidate gene expression related to lymphangiogenesis and development of a novel method for LAMP analysis.

qLAMP was performed to test the primers and reagents, with 70 ng starting RNA, all but one of the genes (LYVE-1) were successfully amplified across all conditions. In contrast to standard qPCR, the Ct values were lower, with an exponential increase in fluorescence occurring around the 5th cycle. This could be explained by the differences in the type of reaction, as stated by the authors who first described the method; the target sequence in LAMP is amplified 3-fold every half cycle which is more than the two-fold that would be expected from conventional qPCR (Notomi et al, 2000). An initial run of a LAMP product was ran on an agarose gel, and it can be seen how different it looks to a standard PCR (Figure 4.8), the ELFA1(-) lane also had a product present which was just due to pipette error.

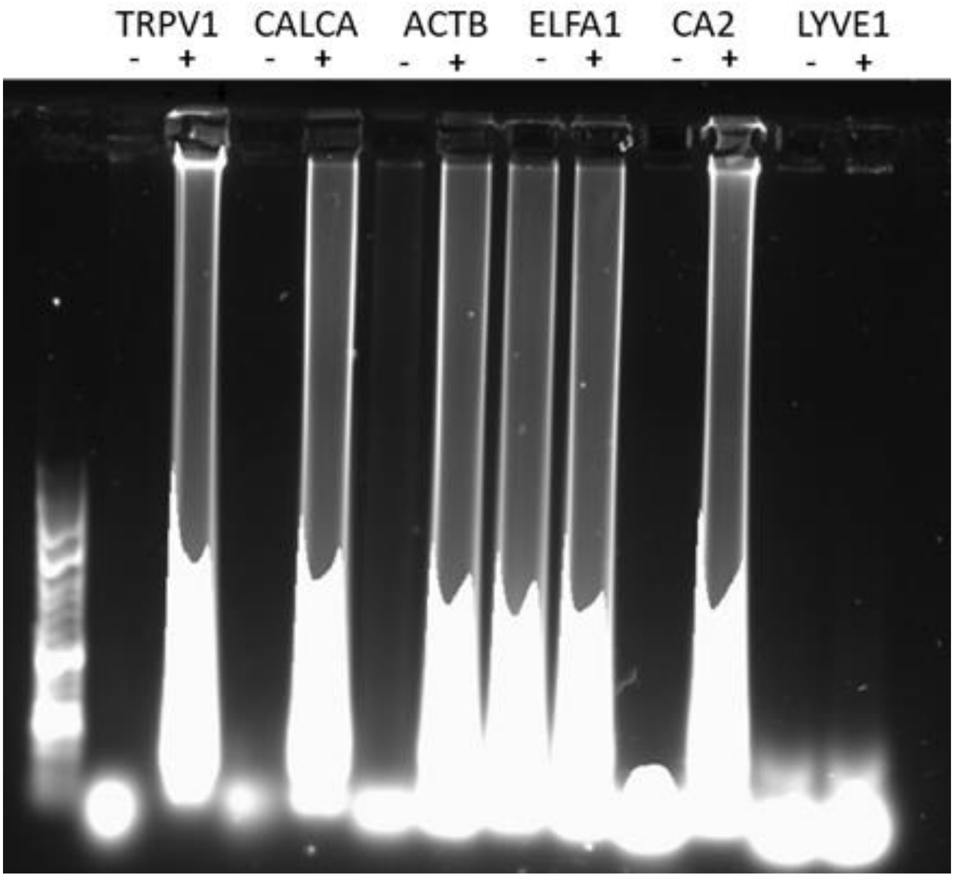

Figure 4.8. *An agarose gel image of the product of a LAMP reaction, showing the first reactions performed using the LAMP primers. The genes are labelled across the top, and + indicates that RNA was added to the reaction and - denotes no template control negative reactions. The ladder used was a 100bp ladder.*

One disadvantage of LAMP are complications to observe the success of the reaction through running the product on a gel. This is due to the product sizes being so large from the continuous formation of a hairpin loop, and the multiple sizes generated from this formation, where some transcripts may finish with 10 loops, others may have 100, forming the smear that can be seen in the gel above. In order to investigate how specific, the primers are, a melt curve analysis would need to be run to observe how many peaks were formed, however this is not possible due to the dumbbell structures formed by the LAMP reaction. The genes that did amplify and are shown in the amplification plot below (Figure 4.9).

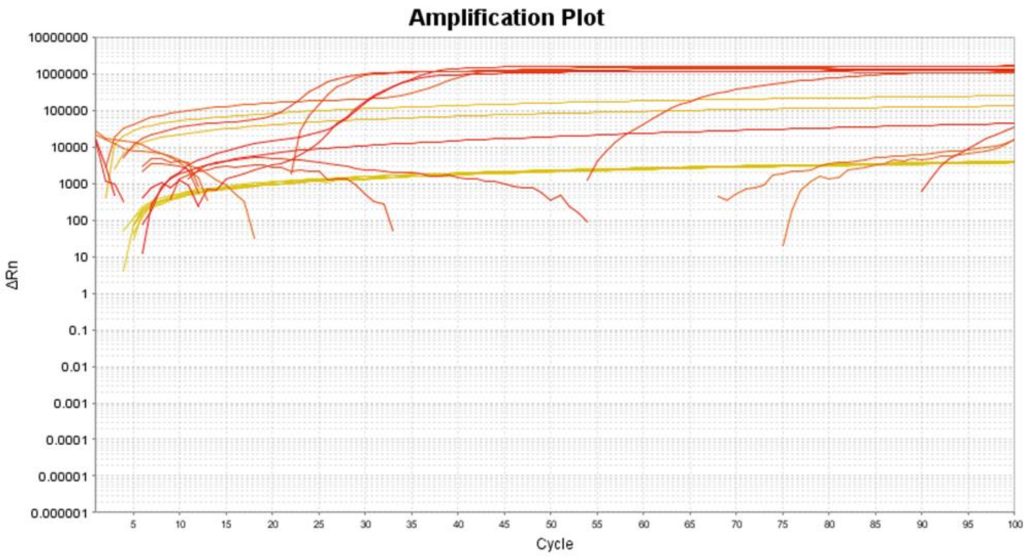

Figure 4.9. *A plot showing the relative absorbance against the cycle number for the LAMP test run.*

It was discovered that the amplification plots that are generated by the StepOne software were not suitable for LAMP due to the software's correction for background noise and fluorescence and auto threshold calculations. For example, some fluorescence curves had two separate amplification phases. Whilst an initial increase in fluorescence was not exponential, that was the one that was passing the auto threshold and therefore causing errors when calculating Ct from the data. The chemistry of LAMP is different to that of SYBR green qPCR mixes as there is no inclusion of ROX as a background fluorescence marker allowing for noise correction. To solve this issue, the raw data was downloaded from the software and the green, fluorescent channel was recorded and plotted in R. Using this data, a Ct value could be calculated for each curve individually using the R *approx()* function, which interpolates an x value when given a specific y value for a line. This method calculates the fold difference between ten given cycles (for LAMP, a cycle was defined as 18 seconds), resulting in a new bell-shaped curve placing the highest values at cycles where the reaction is at its most exponential phase. The resulting graphs from the LAMP experiment are plotted in Figure 4.11, where each graph relates to a gene and a biological replicate and each curve on the graph represents a technical repeat. Cycles remain on the x axis and the newly calculated normalised metric is observed on the y axis. As a proof of concept, this new method was tested using data generated by a library quantification kit (NEBNext Quant library kit (#E7630) by amplifying their standards of known concentration (0.001, 0.01, 0.1, 1, 10, 100 pM) using the supplied mastermix and it was found that the new method of analysis correlated strongly with the ct values that were output by the StepOne software (Figure 4.10), having an $R^2 = 0.9967$ when compared through a linear model. Another benefit of this method is that the analysis can be performed regardless of whether a background dye such as ROX is present in the sample, as noise correction is performed by normalising all curves to their cycle 1 values individually and only the raw data from the specified colour channel is used in the calculation. The raw data from all qLAMP reactions were then converted into Ct values using *LAMPrey*, followed by standard ddCT calculations normalised to the housekeeping gene ACTB.

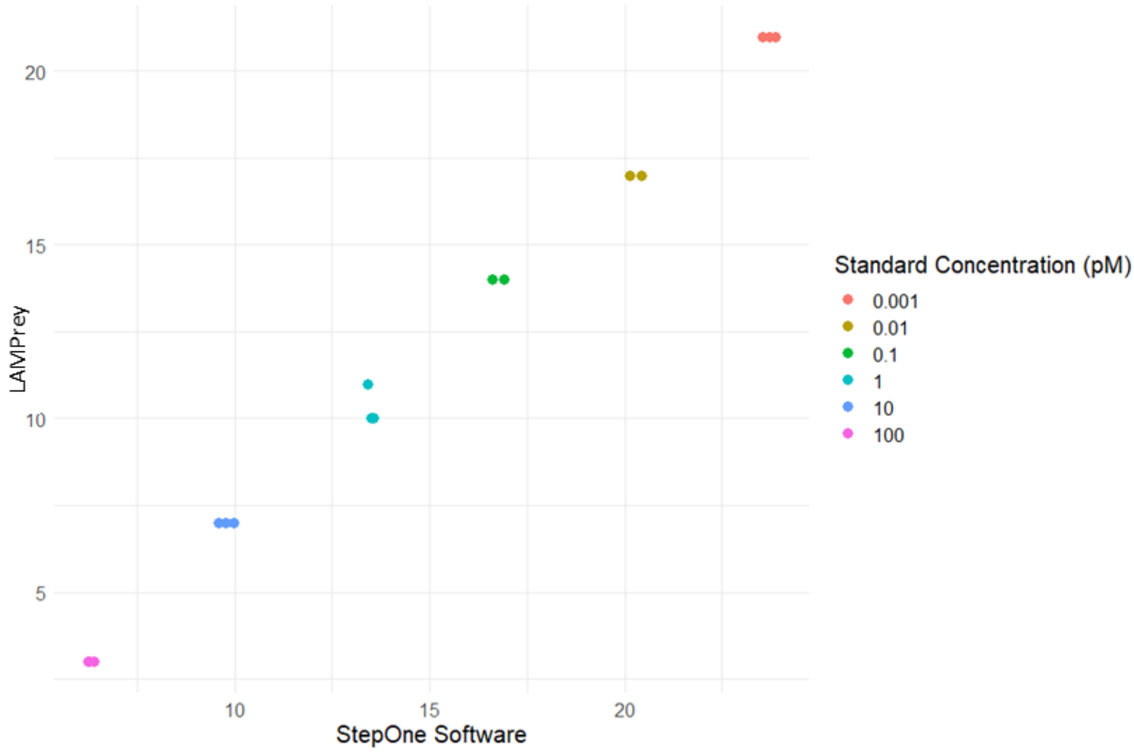

Figure 4.10. *The Ct values calculated for qPCR data of the standards of a NEBNext Quant library kit by the LAMPrey method compared to those calculated by the StepOne software. The concentration of the standard is listed as pM. Linear modelling calculated the correlation coefficient (R^2) between the two methods to be 0.9967, which would mean that the two methods provide identical results*

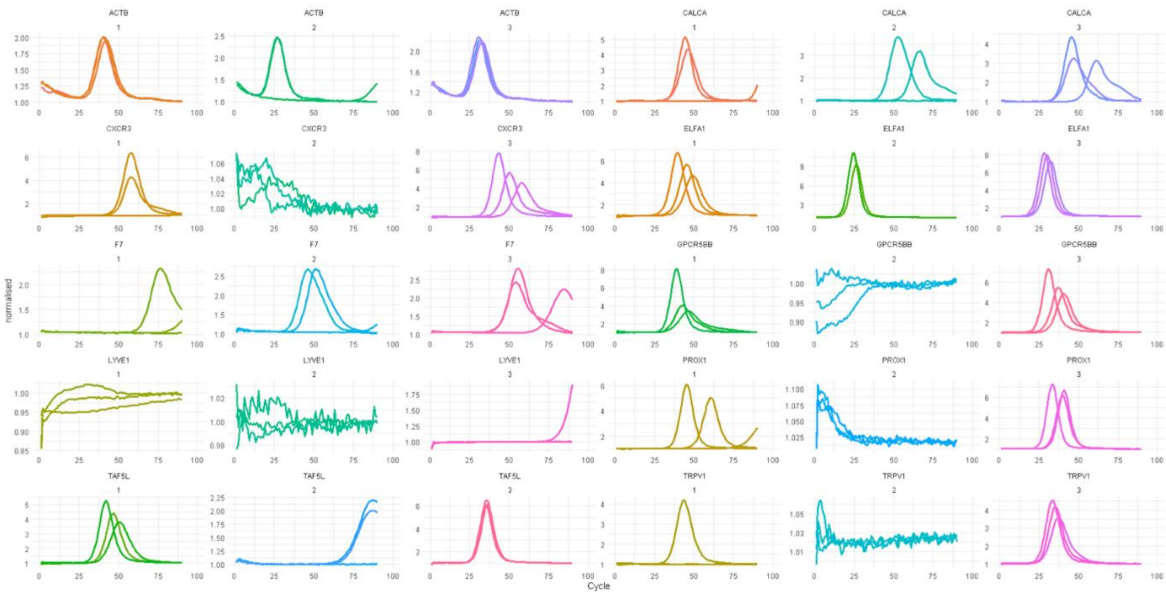

Figure 4.11. *Example amplification curves generated using the LAMPrey method. The peak in the graph is where the reaction is exponential, and this value was taken as the Ct value. Each curve in each plot is one reaction, with the normalised values plotted on the y axis and the "cycle" (18 seconds a cycle) on the x axis. The peak of each curve is the maximum value and shows where the reaction is most efficient and is the new Ct value calculated by LAMPrey. The graphs with no defined curves are those where the LAMP reaction did not*

work and are filtered out based on their low normalised values. N = 9, three biological per each of 3 technical replicates. Each biological replicate was a pool of 20 embryos

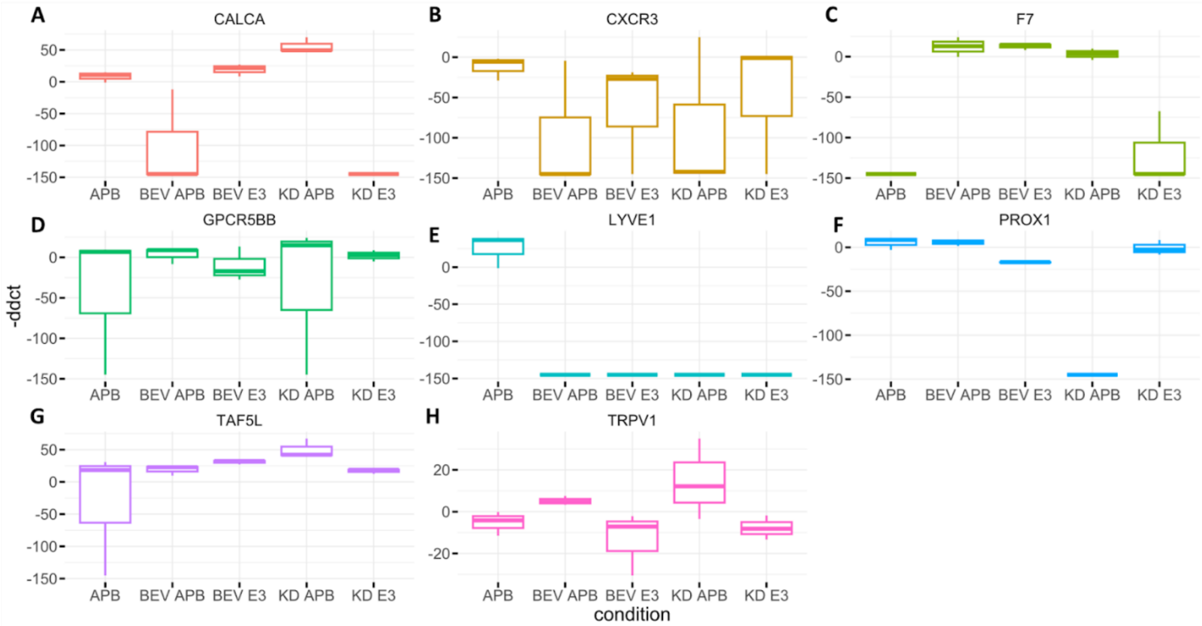

Figure 4.12. *Box plots displaying the -ddct values for candidate gene expression as calculated using the LAMPrey method. -150 is the value used for samples that failed to amplify (e.g., all but one condition of LYVE1). N = 3, each replicate was a pool of 20 embryos*

Performing a PERMANOVA on the results of the LAMP reactions showed that bevacizumab injection had a significant effect on the gene expression of the genes investigated (p.value <0.0001, F = 6.9798). TRPV1 knockdown (KD) also had a significant effect on the gene expression (p.value = 0.0135, F = 2.8505), The effect of TRPV1 knockdown is furthermore amplified in interaction with 2-APB.

Table 4.8. *The Results of a PERMANOVA on the calculated -ddct values from the LAMP reactions.*

LAMP permanova					
	Df	**Sum of Squares**	**F**	**R2**	**Pr**
APB	1	16650	1.0535	0.03085	0.3878
BEV	1	110312	6.9798	0.2044	0.0001 ***
KD	1	45050	2.8505	0.08347	0.0135*
BEV*APB	1	33871	2.1431	0.06276	0.0646
KD*APB	1	144153	9.1211	0.2671	0.0001 ***

The redundancy analysis showed that the knock down of TRPV1 had a similar strong effect on lymphangiogenesis related target gene expression (16% variance explained) than VEGFA inhibition by Bevacizumab (19% variance explained), and that the addition of the agonist 2-APB in combination with TRPV1 knockdown had the strongest effect on targeted gene expression (21% variance explained, Figure 4.13). Redundancy analysis showed that the factors KD and BEV are pointing in the same direction, showing that both factors affect lymphangiogenesis in a similar manner, specifically with respect to TAF5L, TRPV1 and GPRC5B (positively), and with CXCR3 negatively, seen in the positioning of these genes opposite the red arrows. In contrast, APB and KD + TRPV1 affect a different dimension of the gene panel, being positively associated with F7 and negatively with PROX1.

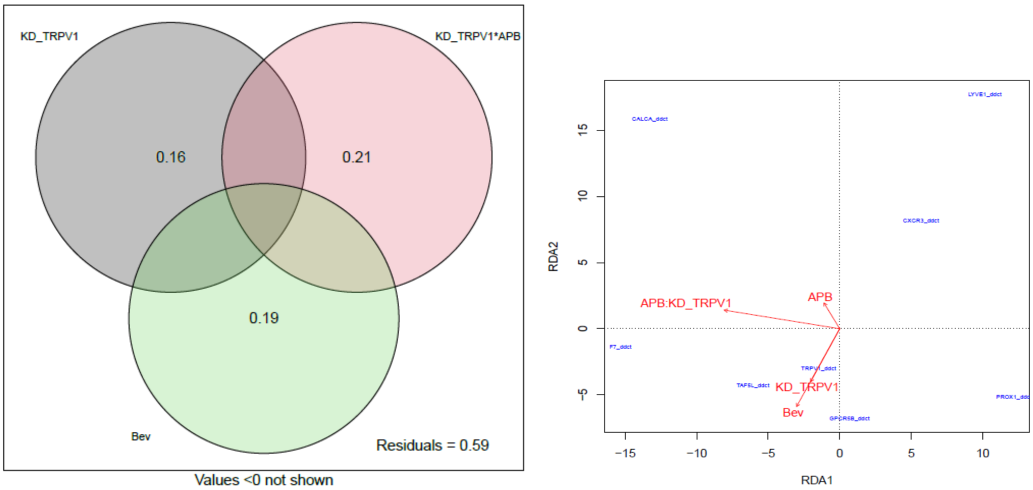

Figure 4.13. A (left) *Venn diagram resulting from the varpart function for variance partitioning between the predictors* ***B (right)*** *Results from redundancy analysis function rda showing influence of predictor variables (red arrows) on expression of different genes (blue names).*

The String network (Figure 4.14) shows the interaction between the genes studied in this chapter, their first interactants which were not studied, and their responses to the experimental treatments. TRPV1 (VR1 in Figure 4.14) had reduced expression in the KD E3 condition although when either the KD or the BEV injected embryos were exposed to APB, its expression was increased. APB by itself had no impact on the expression of TRPV1. The main signalling peptide, which is released upon TRPV1 stimulation, CGRP, had increased expression in both the BEV and KD + APB conditions whilst the expression was decreased in the knockdown and in BEV + APB. A similar pattern can be seen across the conditions with taf5l, which was overexpressed in KD + APB, BEV + APB and BEV, but remained unchanged with KD E3. Interestingly, APB alone was enough to decrease F7, which had increased expression in both the BEV treated conditions and was unchanged in the TRPV1 conditions; showing that the loss of TRPV1 channels removed this response to APB. Overall, the addition of KD in combination with APB caused a similar change in the network than the combination of BEV or BEV + APB, showing that KD and BEV had similar effects. The lowest responses were observed in the E3 control and the 2-ABP on its own.

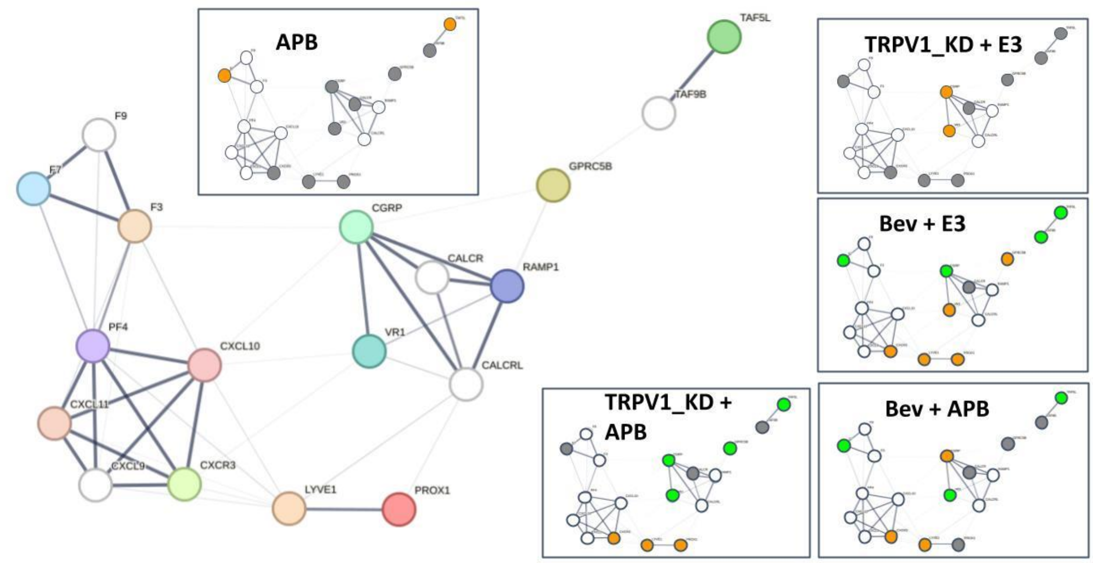

Figure 4.14. *STRING network for relevant genes and their closest interaction partners. Inset figures show those same genes coloured by how they responded to each treatment - increased expression (green) or decreased expression (orange) to treatments compared with E3 control, or whether they did not respond (grey). White circles are interaction partners that were not measured in LAMP. String network generated using string.db.*

Determining the fidelity of qLAMP reaction

Running an array of random samples per gene which appeared to not generate a successful curve in LAMP nor smear on the Agarose gel, in some cases actually did amplify a product when undergoing conventional PCR, as can be seen in the F7 and CXCR3 lanes on the gel

(Figure 4.15), and the lack of a curve generated in the corresponding qLAMP reaction. Reactions which worked in the LAMP were those that also had a smear pattern on the gel after conventional PCR. This smear was likely made up of the different sized handlebar products generated throughout the LAMP reaction. Additionally, LAMP reactions that also show clearly amplified PCR products show that both the mRNA of the gene was present in the sample and that the BIP-F3 and FIP-B3 primers being specific to their respective targets (true positive, see most of the bands for ACTB in Figure 4.16). The size the product was not as to be expected when calcuating the size of the product given the two primer combinations. The difference in the predicted size and the observed size was considered to be due to the tertiary structures that LAMP forms, meaning the products may perform differently that expected in both PCR and agarose-gel electrophoresis. With this information, an ideal post-LAMP gel would be one that had both specifically amplified bands alongside a smear covering a large range of molecular weights. We found that the CXCR3 primers generated neither a smear or a band when amplified by conventional PCR, showing that there was either something wrong with the primers for that gene, or that the gene was not expressed in the samples tested.

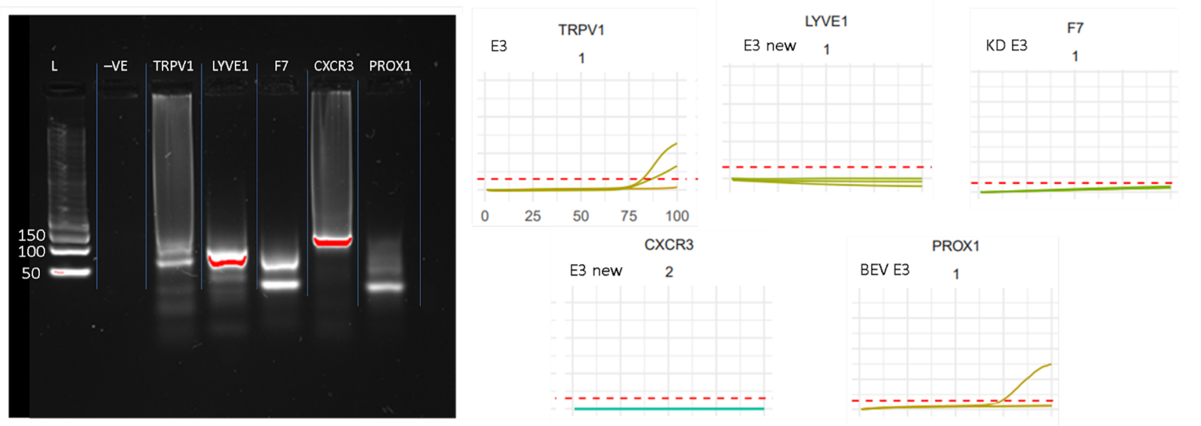

Gene	BIP-F3	FIP-B3
TRPV1	172	169
LYVE1	186	201
PROX1	201	201
F7	205	196
CXCR3	168	175

Figure 4.15. *An agarose gel of the product generated when performing a follow up conventional PCR on the samples, with the result of the qLAMP data displayed on the right. The sizes for the potential stable PCR products generated during this secondary PCR are listed below the images.*

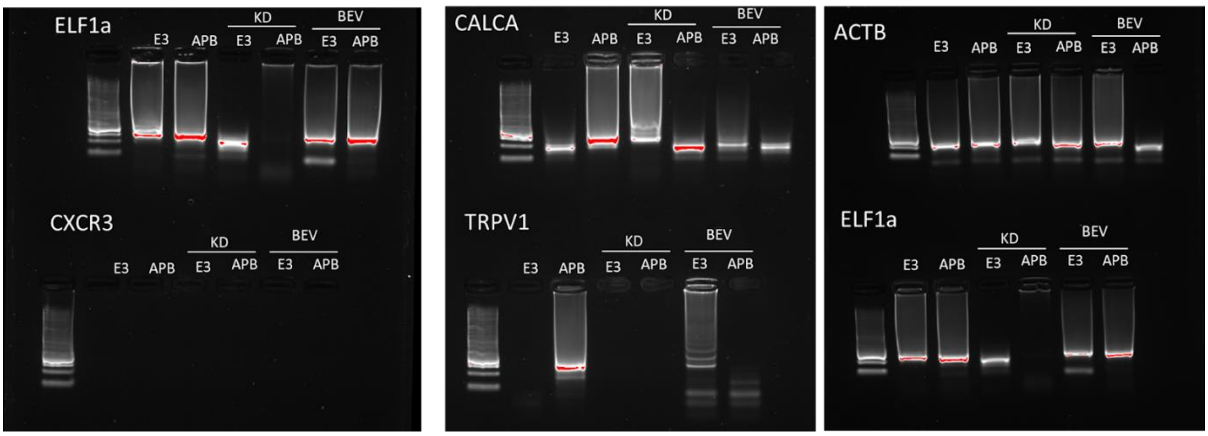

Figure 4.16. *Agarose gels for genes and combinations of treatment conditions after having a secondary, follow up PCR. The Ladder is in the left most lane of every image.*

Analysis of gel bands using ImageJ for presence of smear and PCR bands, compared with LAMP amplification curves, shows an overall success rate of 74% in terms of LAMP reaction accuracy, where 47% of the results were a true positive, generating a Ct value and a gel which contained both a smear and a band (accurate). 27% were true negative where there was no Ct value calculated and there was no result in the post-LAMP gel (accurate). There were (19.9 %) cases in which the gel gave a smear and a band but there was no corresponding LAMP curve, these results were labelled as "false negative". There was the rare case of some genes (6.6 %) where the follow-up PCR agarose gel was blank, but the LAMP reaction had a Ct value combined with a smear these are potential "false positives" (Figure 4.17, Supplementary Table 4.2)

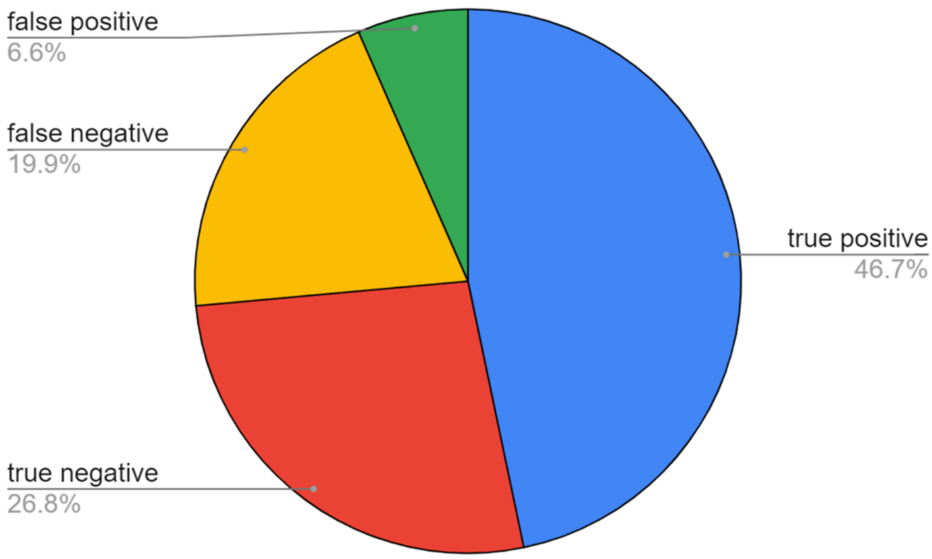

Figure 4.17. *A pie chart showing the results from the PCR follow up analysis of the LAMP reactions. "True positives" had a positive follow up PCR and generated a Ct value in the LAMP experiment. "False positives" had a negative PCR follow up but had a Ct value in LAMP. "False negative" samples had a positive result in the follow up PCR but did not generate a Ct in the original LAMP. "True negatives" had a negative result in both the follow up and the LAMP.*

4.5 Discussion

LAMP fidelity and optimisation of analysis with *LAMPrey*

Observation of the LAMP products on agarose gels showed 74% accuracy between the gel images and the calculations of the LAMP fluorescence values (true positives and true negatives). The other 26%, could be explained through technical errors. In samples labelled here as "false negatives", and accounting for 20% of the samples that were run on agarose gels, some of their six LAMP primers outside those used for follow up PCR could have failed such that the LAMP reaction failed but the two central primers still produced a band on the PCR gel. Besides technical error with the follow-up PCR, the "false positives" in the gel images could be true false positives as in producing a LAMP result despite no target gene mRNA being present. A re-run of these samples would aid in the understanding of how these have occurred, as this is the case for the remaining 6% of the samples. These findings are similar to a study by Österdahl and colleagues (2020), where a comparison between RT-PCR and RT-LAMP detection of SARS-CoV2 in clinical samples showed that RT-LAMP had a positive predictive value of 72% when sequencing known positive samples. Almost a quarter of the results were false positives (Österdahl et al., 2020), although it is stated that retesting of low signal samples increased the sensitivity of the RT-LAMP to 100%. q-RT-LAMP as a diagnostic test can have as little as 63% true positives when using commercially available kits (Artik et al., 2022). However, this q-RT-LAMP sensitivity was calculated using the auto threshold of the qPCR software and did not use a LAMP-customised analysis method such as *LAMPrey*. The *LAMPrey* analysis proved to be an effective method of detecting the expression levels of genes when performing LAMP, taking into consideration their unique properties in accumulating fluorescence during the reaction. It is an improvement on the use of Ct values as these may be unreliable for LAMP and removal of the conventional Ct method with auto threshold, which furthermore has the potential to be not reproducible due to the researcher being able to set their own Ct thresholds manually, which could especially be a problem, if no ROX is used to correct for background noise. Care needs to be taken when processing qPCR data and assigning Ct values, considering that this process requires standardised practices, as mishandling of the data can have significant effects on the final outcome (Burns et al., 2005).The LAMPrey method doesn't use such a threshold and therefore removes this level of researcher interpretation and subjectivity.

Hypothesis 1: The stimulation of the TRPV1 channel through heat or 2-APB may have a morphogenetic effect on the vascular development of the zebrafish embryo.

Temperature is known to play a major role in the development of vertebrates, and it has historically been shown that increased temperatures increase the developmental rate of the organism, up until a point where it has an adverse effect on development and survival rate (Hosseini et al., 2019; Schnurr et al., 2014). However, TRPV1 knockdown in the hot temperature caused a significant slowdown of embryo development rate compared to all other experimental factors and the control, possibly because of an impairment in temperature sensing and related changes in downstream effects of TRPV1, which highlights the importance of this channel during development in a hot environment. There is evidence that 2-APB can activate other TRP channels (Zhao et al., 2021), and there may have been some overlap with the action of other TRP family of channels; It is known that other TRP- channels are involved in developmental processes, such as TRPV3 being a mediator of Ca^{2+} signalling in mouse egg development (Lee et al., 2016), and is also stimulated by 2-APB. This may dampen the effects of the knockdown. TRPV2 can also be activated via 2-APB, and this vanilloid channel is known to be involved in neuronal development (Santoni & Amantini, 2019) and healthy cardiac functions (Iwata et al., 2020). Given these roles of other TRPV channels, during development, their stimulation by 2-APB could potentially be one cause for this increase in development even when experiencing downregulation of TRPV1.

However, the results in this chapter highlight the importance of pathways downstream of TRPV1, suggesting that this channel is essential for development, even when the embryo continues to express the thermosensitive TRPV2 and 3 channels (Zhao et al., 2021).

The survival rates of the hot experiment were lower overall in comparison to the normal temperature (hot, 45% ; normal 52%). The biggest drops in survival were the combined treatment were observed in bevacizumab + 2-APB + heat and knockdown + heat. This could imply that the combined treatments of injection and heat were too stressful to survive in the early days of embryo development. The combination of stressors could cause too large of a calcium influx into the cells of the embryo, which when prolonged can result in apoptotic responses (Harr & Distelhorst, 2010). The decrease in the survival rates in KD + HOT could be due to the TRPV1 channel not being expressed at a high enough level to detect the changes in temperature, potentially causing dysregulation in embryogenesis pathways, since TRPV1 has a protective effect on heat nociception (Rosenberger et al., 2020). The inclusion of 2-APB to knockdown + heat causes an increase to the survival rate and may be explained through 2-APB stimulating other TRP channels which have similar functions to TRPV1 (Zhao et al., 2021). However, since the decrease in survival rate is similar between both TRPV1 knockdown and bevacizumab, it cannot be ruled out that the injection procedure contributed to decreased survival, especially at hot temperature which could promote pathogen growth. The expression of LYVE-1 was increased when the zebrafish embryos were exposed to 2-APB, which is evidence that there is a proportionally higher rate of lymphatic endothelium development upon 2-APB stimulation during development. The data within this chapter show that the TRPV1 agonists heat and APB cause an increase in developmental rate. Neither 2-APB and heat both significantly negatively impacted survival of the developing embryo, even when used in combination. Stimulation using 2-APB caused F7, a gene involved in the clotting cascade to be under expressed, potentially identifying a link between stimulation of TRPV1 with 2-ABP and clotting.

Hypothesis 2: The knockdown of the TRPV1 channel by MO in the developing zebrafish has an inhibitory effect on the vascular development.

The results of this chapter show that the knockdown of TRPV1 had a significant impact on the developmental rate of the zebrafish under both hot and normal temperatures. The development rate increased by 20% when the knockdown embryos were stimulated with APB in the normal temperature experiments. While zebrafish can survive up to 7dpf without a fully functioning cardiovascular system, survival was only investigated for the first 24hpf as the majority of embryo development occurs in this timeframe (Kimmel et al, 1995), meaning it is a key time period in embryogenesis and subsquent fitness and survival. The predictors of survival rate of the developing embryo exposed to normal temperatures were all non-significant apart from TRPV1 knockdown which was significant. This is unlikely to have been caused by the injection procedure, as bevacizumab was also injected but the BEV predictor had a non-significant effect on the survival rate of the embryo. However, injection of BEV occurred in the yolk sac, vs, into the developing embryo in TRPV1 knockdown. It is also worth noting, that bevacizumab is an antibody drug treatment, and is designed to be safe in humans, the MO may be more likely to have off target effects although it is unlikely due to their specificity and their inability to interact electrostatically with proteins (Summerton, 2007). TRPV1 is important in calcium signalling, and a large range of processes in the early stage of development rely on calcium signalling to function correctly (Webb & Miller, 2003). The disruption of these pathways could explain this drop in survival upon knockdown of TRPV1 (Patergnani et al., 2020). The authors of the original experiment where this MO was described did not comment on the survival rates of embryos upon injection, and so these findings cannot be compared to previous studies using this exact MO (Gau et al, 2013). They may also be the possibility that there is residual TRPV1 which may have been present in the chance of an incomplete knock-down from the MO injection.

The LAMP results show that the knockdown of TRPV1 had a significant effect on the expression of a range of endothelial cell related genes, including CALCA (homologous to human CGRP) and LYVE-1. CALCA/CGRP was shown to have a positive effect on the proliferation of endothelial cells in **Chapter 2**, and is a factor known to be released through the activation of TRPV1. The decreased expression of this in the knockdown conditions shows that the knockdown had a potentially detrimental effect on the development of the lymphatic system in the zebrafish embryo. This hypothesis is further backed up with the reduced expression of LYVE-1 which is a lymphatic endothelial cell marker, and this decreased expression - or absence, as the majority of LAMP reactions of treatments did not detect LYVE-1 - caused by the knockdown could be due to there being a lower number of lymphatic endothelial cells present in the embryo. This finding correlates with that of **Chapter 3**, where the KD immunofluorescence staining image did not display vessels when stained with the second marker for lymphatic development used here, PROX1a. This effect of TRPV1 knockdown on the expression of CGRP was normalised through the use of 2-APB, potentially identifying an alternate mechanism of which 2-APB causes CGRP release independent of TRPV1; possibly through the activation of TRPV2, since this channel has also been shown to activate CGRP release (Qin et al., 2008) and is activated by 2-APB. **Chapter 2** highlights the importance of CGRP as an endothelial signalling molecule, and how it can induce proliferation and transcriptional changes to the lymphatic endothelium. The knockdown condition also caused a large reduction in the expression of F7, which was normalised through the addition of 2-APB. In **Chapter 3,** F7 expression was increased in the RNA-Seq of embryos that were knocked down for TRPV1 and incubated in 2-APB. This further elucidates the importance of TRPV1 on F7. The recovery of this reduced expression could be again due to APB binding to different TRPV- channels, although there is no current evidence of a connection between these channels and F7, or with coagulation as a whole. CXCR3 and PROX1 both had similar gene expression patterns where the expression was reduced in the combined treatment of knockdown incubated with 2-APB but had normal expression in TRPV1 knockdown without 2-APB. This could potentially point towards a protective mechanism of TRPV1 against the agonist 2-APB. TRPV1 may alleviate the stress response; something which has been observed before, where TRPV1 activation was sufficient to protect the heart from ischemia injury through upregulation of the PI3K/ Akt signalling pathway (Jiang et al., 2018), as well as having a protective role against non-lethal heat induced nociception, through tachyphylaxis over sustained exposure to stress (Rosenberger et al., 2020) and it is possible that a similar mechanism would be invoked upon 2-APB stimulation. 2-APB is known to activate other TRP channels and this change in expression could be a result of 2-APB binding to the other TRP receptors that are present. Combinations of knockdown combined with 2-APB caused a decrease in PROX1 and CXCR3, both of which were normally expressed in the absence of 2-APB, potentially identifying the pathways which are protected through TRPV1. Expression of CALCA/CGRP in the knockdown embryos had the inverse pattern and was up-regulated in the presence of 2-APB but decreased when the embryos were incubated in standard E3 media. TAF5L was upregulated in every experimental condition and has been reported to be a marker of early Endothelial Precursor Cells (EPCs) during development (Cheng et al., 2013).These results potentially show that in all the experimental treatments there is a slowing of the maturation of endothelial cells, which would correlate with the decreased expression of LYVE-1 and PROX1. VEGFA is a known regulator of the maturation of EPCs (Li et al., 2017), although this is the first recording of TRPV1 having an influence on the maturation of endothelial cells in vivo.

The results in this chapter highlight that the reduction of TRPV1 expression causes a decrease in overall survival and increased expression of the key developmental homeobox gene PROX1 and reduction in the lymphatic marker LYVE-1. The potential lack of TRPV1 receptor during development was enough to cause a decrease in survival and developmental rate under hot conditions. These data show a potentially protective role of TRPV1 under stressed conditions during development.

Hypothesis 3:The injection of the anti-VEGFA cancer antibody treatment bevacizumab will decrease the vascular development of a developing embryo.

Bevacizumab is an anti-angiogenic antibody drug which targets VEGFA and is used in the treatment of highly vascular cancers such as renal (Yang, 2004) and lung (Assoun et al., 2017), and was first described as a treatment for colorectal cancer in 2004 (see Garcia et al., 2020 for a review). It is known to have the same anti-angiogenic effects on a developing zebrafish embryo (Zhang et al., 2018). Surprisingly, in the present experiment, bevacizumab injection was found to have a positive impact on the developmental rate under normal temperature conditions both with and without 2-APB supplementation. Conversely, bevacizumab injection had little to no impact on the development of the zebrafish embryo when combined with a higher incubation temperature. These findings are surprising because of VEGFA's role in proliferation and angiogenesis during development (Matsumoto & Ema, 2014). However, inhibition of VEGFA signalling can cause a compensatory upregulation of the other VEGF signalling pathways (Li, 2018) and this may explain these results. Bevacizumab was found to have no significant impact on survival rate and the only paper which has investigated bevacizumab's antiangiogenic effects in zebrafish did not record the survival rates of the embryos, making it not possible to compare the rates recorded here with that in the literature (Zhang et al., 2018). It is possible that bevacizumab injection would have no effect on survival rate as it has been shown that the developing zebrafish can survive up to 7 dpf without a developed vascular system (Kugler et al., 2021).

The results of the PERMANOVA of candidate gene expression data shows that the injection of bevacizumab resulted in a change to the candidate gene expression of the developing zebrafish embryo. Another interesting finding from the LAMP analysis is that the significance of the BEV condition is lost when 2-APB is included as a factor, implying that 2-APB can reverse the transcriptional changes that are caused through the injection of BEV of these genes in the developing zebrafish embryo. These findings may identify a potential novel link between VEGFA and 2-APB, and further highlight the possibility of APB being important in endothelial cell pathophysiology. Bevacizumab injection had a negative impact on the expression of CALCA and CXCR3, showing some overlap between the genes affected by TRPV1 knockdown. CGRP/CALCA is thought to regulate VEGFA expression in mouse, due to them both having similar patterns of expression during development (Maeda et al., 2017) and CXCR3 also regulates the expression of VEGFA in macrophages in response to tissue repair in porcine models (Li et al., 2020). This decrease in CXCR3 could explain the impairment of wound healing in bevacizumab treated patients (Gordon et al., 2009). These regulatory pathways may explain this decrease in expression upon bevacizumab injection. The increase of F7 is particularly interesting since thrombosis is a known side effect of bevacizumab treatment of cancer, observed in approximately 4% of patients treated for colorectal cancer with bevacizumab (Saif & Mehra, 2006).

The immunofluorescence staining images of 4dpf zebrafish embryos which were injected with bevacizumab at the one cell stage display the recently discovered olfactory epithelium rod cells (Cheung et al, 2021) and is the first evidence of TRPV1 expression on these cell structures during zebrafish embryogenesis. In rat ovaries, antibody inhibition of VEGFA accelerated the development of follicles (McFee et al., 2012) and this increase in developmental rate could explain why these structures were not observed in **Chapter 3's** immunofluorescence images. The function of these cells is still debated, as actin rich projections, they are thought to have either mechano- or chemo- sensory functions (Cheung et al., 2021). There is also speculation that these cells could be important in the immune response, similar to brush cells in mammals (Schneider et al., 2019). In zebrafish, the olfactory system has been shown to be used to detect salinity of water, through the detection of chloride and sodium ions (Herrera et al., 2021). There is a possibility that TRPV1 has a role in this detection as studies on rat TRPV1 has shown that there is an external sodium ion binding site which can stabilise the channel into a closed state (Jara-Oseguera et al., 2016).

Bevacizumab injection into zebrafish embryos overall caused an increase in development without impacting the survival rate of the embryo. The gene expression of candidate genes TAF5L, CALCA and F7 were all increased after injection and the expression of PROX1 and LYVE1 were reduced. This data is evidence for potential overlap between TRPV1 and VEGFA pathways. In addition, variance partitioning showed that TRPV1 KD and BEV influenced candidate gene expression with approximately equal percentages, lending additional importance to TRPV1's importance for (lymph)angiogenesis during development.

4.6 Conclusion

In conclusion, the findings presented in this chapter provide insights into the effects of 2-APB and TRPV1 on zebrafish embryo development. The increased developmental rate induced by 2-APB suggests the involvement of TRPV1 or other 2-APB-sensitive TRPV channels. However, the loss of TRPV1 alone was insufficient to counteract this increase, indicating the potential contribution of other channels in mediating the observed effects. Furthermore, 2-APB was found to decrease the expression of F7, potentially influencing the thrombosis pathway negatively. The knockdown of TRPV1, in combination with different treatments, revealed a potential protective role of this channel during development. Loss of TRPV1 attenuated the heat-induced increase in the developmental rate of the embryos and significantly impacted their survival under heat stress and normal conditions. Combinations of TRPV1 knockdown with 2-APB supplementation resulted in decreased expression of PROX1 and CXCR3, both of which were normally expressed upon knockdown alone. This result shows the possibility that the expression of these genes are protected through a TRPV1 mediated pathway under stress. Conversely, CALCA/CGRP expression in the knockdown embryos exhibited an inverse pattern, being up-regulated in the presence of 2-APB but decreased under standard conditions in E3 media. These findings indicate potential interactions between TRPV1 and CALCA/CGRP in zebrafish development. Interestingly, injection of bevacizumab, an antibody targeting angiogenesis, increased the developmental rate of the embryos and negatively affected the expression of CALCA and CXCR3, indicating some overlap with genes affected by TRPV1 knockdown. Interestingly when analysing the immunofluoresence images, the expression of TRPV1 in the olfactory epithelium was observed in the bevacuzimab injected embryos. These results contribute to our understanding of the complex role of TRPV1 and its interactions with other factors in zebrafish embryonic development, highlighting potential pathways and mechanisms involved. Further research is warranted to elucidate the precise mechanisms underlying these observations and their relevance to human development and disease.

Chapter 5: Discussion

5.1 Reflection on the original aims of this thesis

The overarching aim of this thesis was to investigate the TRPV1-CGRP signalling axis in the context of vessel development, shown through phenotypic and molecular changes. The individual aims of the data chapters were: 1) To investigate the downstream effects of CGRP on HDLEC in vitro in terms of the resulting transcriptional response; 2) To better understand the function of theTRPV1 channel in the development of zebrafish embryos, and to highlight the transcriptional changes that occur under knockdown of the channel; 3) To observe overlaps and differences on a phenotypic and molecular level of VEGFA inhibition and TRPV1 knockdown in the developing zebrafish. For this purpose, combined molecular techniques were used in combination with observations on behaviour and physiological changes. A new method for the analysis of qLAMP data was developed in order to remove researcher bias and more accurately report gene expression changes through LAMP. **Overall, the thesis examined the TRPV1-CGRP signalling axis at various levels, from molecular to phenotypic, and employed innovative approaches to enhance data analysis.**

5.2 Reflection on the knowledge gaps identified in the introduction.

Overall, the literature review revealed several gaps of knowledge related to the TRPV1-CGRP axis both *in vitro* and in vivo. There needed to be a greater understanding of TRPV1 and subsequent downstream activation, via CGRP, affecting the development of lymphatic endothelial cells, which was the topic of focus in **Chapter 2**. **Chapter 2** provided evidence that CGRP elicited a larger transcriptional response in Human Dermal Lymphatic Endothelial Cells (HDLECs), than a known endothelial specific signalling peptide, adrenomedullin (AM). Both of these peptides bind to the same CLR receptor expressed on the surface of endothelial cells, and agonism by CGRP causes the receptor to internalise, whilst AM does not. **Chapter 3** centred on the knowledge gap of better understanding the signalling pathways related to TRPV1 in a developing zebrafish in vivo. This was addressed through the use of an RNA-Seq study of TRPV1 knockdown embryos via morpholino injection. The results of this chapter showed that multiple pathways in development are regulated by TRPV1, including pathways linking to angiogenesis and cardiovascular function, supporting a link between TRPV1 and vessel development. An enrichment analysis of the differentially expressed genes within ZFIN's disease database identified diseases known to have endothelial cell involvement, such as diabetes mellitus and the MYH9 Related Disease (MYH9-RD). Alport syndrome was enriched for MYH9, although this is caused by mutations in COL- genes and MYH9-linked Alport syndrome has since been re-classified (Fernandez-Prado et al., 2019). **Chapter 4** built on the knowledge gained from **Chapter 3** but investigated the TRPV1-CGRP axis relative to VEGFA signalling through a factorial design, using bevacizumab; an anti-VEGFA cancer treatment. This Chapter provided evidence that there is some overlap in signalling pathways, as both knockdown treatments of bevacizumab and TRPV1 morpholino decreased the expression of CALCA/CGRP, although TRPV1 knockdown had more of a detrimental effect on survival of the embryo than VEGFA did.

5.3.1 The relevance of CGRP signalling in endothelial cells.

Chapter 2 Identified differences in expression profiles of HDLECs when agonised with either adrenomedullin or the calcitonin gene related peptide (CGRP). The results showed that there was a large transcriptional response (144 genes) in HDLECs which were exposed to CGRP *in vitro,* identifying many genes which are shared and not shared with AM between the activation of CLR receptors with these two neuropeptides. The two agonists have very similar physiological functions although it became evident through enrichment analysis that CGRP had multiple essential functions relating to endothelial cell biology and cardiovascular development. The main gene which was present across all the endothelial cell functional groups was ADAMTS9, a gene which actively inhibits angiogenesis of micro vessels in cancers via blockade of the mTOR pathway (Du et al, 2012; Koo et al., 2010).

Other genes which were significantly differentially expressed included the carbonic anhydrase, CA2, a physiological pH mediator (Sly & Hu, 1995) and not thought to be expressed by endothelial cells, unless stressed by a cancer microenvironment (Annan et al, 2019), and CXCR4, a chemokine receptor which directly regulates endothelial cell proliferation and migration (Molino et al, 2000); both of which were upregulated upon stimulation with CGRP. **These results show that CGRP could potentially be more important in endothelial cell biology than the endothelial cell specific signalling peptide adrenomedullin.**

5.3.2 The relevance of TRPV1 in development and survival of the developing zebrafish embryo

The data within this thesis has shown that TRPV1 knockdown has a greater impact on zebrafish development than was previously thought, with its knockdown affecting survival and developmental rates to a greater effect than that of bevacizumab; a drug which targets the key player in (lymph)angiogenesis, VEGFA. The knockdown of TRPV1 during development also showed that the embryo no longer developed faster in response to heat stress. Whilst it is known that TRPV1 is a thermosensitive TRP channel, it has not been shown before that the loss of this channel during the developmental stages causes the zebrafish to develop faster no longer as a result of the increased temperature identifying a new direct link between TRPV1 and the regulation of developmental rate, given that 30°C is enough to activate zebrafish TRPV1 (Gau et al, 2013). These zebrafish larvae also had one of the lowest survival rates, with only 25% of embryos surviving up to 24 hpf, which may point to the nociception- protective function of TRPV1 in which there exists a feedback loop to account for temperature stress (Rosenberger et al., 2020) and is something which could have real world implications when investigating species threatened by heat stress under climate change.

Novel patterns of TRPV1 expression during development were also discovered during this work. The TRPV1 receptor is known to exist on the epithelial layer as well as the Dorsal

Root Ganglia (DRG) and the somatosensory system in zebrafish (Gau et al, 2013), but **Chapter 4** provided evidence of TRPV1 also being expressed on the olfactory epithelium's rod cells as well as the hair cells of the lateral line system. The former structures are a relatively recent discovery and were identified by electron microscopy (Cheung et al., 2021). They are thought to serve different functions to that of the olfactory sensory neurons (OSNs), which are known to express a range of TRP- channels, mostly the TRPC receptors (Zufall, 2014). The rod cells in teleost species are believed to enhance the olfactory sensitivity through the movement of water over the olfactory neurons (Reiten et al., 2017) and zebrafish larvae use their olfactory system to detect salinity of their water (Herrera et al., 2021), it is possible that TRPV1 has some involvement in this function, because of its ability to detect and respond to ions in the environment (Ahern et al., 2005). **TRPV1 potentially has multiple important functions in zebrafish, including pathways which protect against thermal stress in development.**

5.3.3 TRPV1 and its involvement in vessel formation

TRPV1 mediates a range of other signalling molecules, which are known to be involved in cell migration (Waning et al., 2007) and proliferation (Zhai et al., 2020); two important functions that are key to embryogenesis. In **Chapter 4**, the expression of lymphatic markers PROX1 and LYVE1 was observed under stress conditions with and without the knockdown of TRPV1 and the drug treatment inhibiting VEGFA. The treatment of both bevacizumab and the TRPV1 morpholino decreased the expression of both LYVE-1 and PROX1, which highlights a potential decrease in lymphatic development. These findings correlated with the immunofluorescence staining images in **Chapter 3**, where the TRPV1 knockdown embryos' vessels were not present when the embryos were stained by PROX1 antibodies. Interestingly, the addition of 2-APB to the E3 media caused a more drastic decrease in PROX1 expression compared to TRPV1 knockdown alone. Despite these obvious changes to the expression of lymphatic markers, the developmental rate of embryos in these treatments remained the same, indicating that it was specifically the lymphatic development that was hindered, rather than organism-wide development. These results potentially point to a specific role of TRPV1 in lymphatic development independent of other TRP channel and 2-APB, with the possibility of a protective mechanism of TRPV1 during lymphangiogenesis. Knockdown of the channel additionally caused CGRP (encoded by the CALCA gene) to be reduced, which as seen in **Chapter 2**, can stimulate and can regulate multiple lymph(angio)genic mechanisms. These results provide further evidence of the importance of TRPV1 in (cardio)vascular development in zebrafish. TAF5L was upregulated across all experimental conditions in **Chapter 4**, this gene is a marker of endothelial precursor cells (EPCs)(Cheng et al., 2013), and its increased expression indicates that the EPCs in the developing embryo may not be maturing. VEGFA is known to have the ability to regulate the maturation of endothelial cells (Li et al., 2017), although this function has never been described for TRPV1. **This is potential evidence of a new role for TRPV1 in a developing cardiovascular system.**

5.3.4 TRPV1 and its role in disease

Both variants of the zebrafish ortholog of the MYH9 gene were upregulated in **Chapter 3** when TRPV1 was knocked down and exposed to 2-APB. These caused enrichment of DEGs for multiple glomerular related changes to the phenotype in the ZFIN Disease database, but also for MYH9 related disease (MYH9-RD) in the ZFIN Disease database. MYH9-RD is an autosomal dominant disorder sufferers of which classically display symptoms of kidney failure (glomerular nephropathy), thrombocytopenia, easy bruising and hearing loss (Kopp et al., 2010; Althaus & Greinacher, 2010). It is known that TRPV1 can have a direct effect on the glomerular filtration, through CGRP and SP signalling (Li & Wang, 2008), where an increased expression of CGRP increased the filtration rate of the glomerulus.The results presented in this thesis are more evidence of this interaction, and show that potentially downstream of this, MYH9 activation could be a contributing factor for this phenotype. **Chapter 4**’s LAMP experiments show that the combination treatment of TRPV1 knockdown and 2-APB increases the release of CGRP during development, which were the same conditions as were used in **Chapter 3**’s RNA-seq experiments which found MYH9 to be upregulated. MYH9-RD currently only have two potential drug treatments; avatrombopag (Arif et al., 2022) and eltrombopag (Zaninetti et al., 2020), both of which are agonists to thrombopoietin receptor to increase platelet production. The results of this thesis could aid in the development of novel drug treatments, or the repurposing of present ones, such as erenumab, the antibody migraine drug, which directly binds to CGRP receptors and prevents it from binding (Edvinsson et al., 2018). **A further investigation into these responses and TRPV1’s involvement may identify even more treatments, since it is possible to target the various conformational changes of the channel, inhibiting the pathway in a structure-dependent manner (Trkulja et al., 2021).**

Type I diabetes mellitus was also significantly enriched in the ZFIN disease enrichment of the RNA-Seq significantly differentially expressed genes. Type I diabetes mellitus is an autoimmune disorder, in which the immune system destroys the beta cells of the pancreas, preventing the patient’s ability to produce insulin (Katsarou et al., 2017). Patients that suffer with type I diabetes mellitus also experience an increased risk of cardiovascular disease (Peng et al., 2020). Of the five genes which were enriched for diabetes, two were the most interesting in terms of their functions in the cardiovascular system. One of these genes, APOBa (which codes for the apolipoprotein Ba protein), was also highly enriched in the cellular component for the lipoprotein-related terms. Double knockout mutant zebrafish for both APOBa and APOBb displayed numerous defects during development including abnormal liver laterality and hyperangiogenesis. This change in phenotype was due to altered Notch signalling and the vascular phenotypes were rescued by injection of a truncated form of the human APOB protein (Templehof et al., 2021). The second gene was F7, coding for clotting factor 7. It forms a complex with the tissue factor (TF) protein, which is expressed on the cell surface of endothelial cells and activates the clotting cascade (Mackman, 2009). This gene was upregulated in the RNA-seq results and overexpression in mouse models caused premature death and thrombosis (Aljamali et al., 2008). **This suggests a potential new role of TRPV1 in the pathobiology of Type I diabetes, which has not been documented previously.**

The enrichment for ZFIN phenotype revealed that malformed intersegmental vessels were enriched by the genes UNC5b and SLC2A1a in **Chapter 3**'s RNA-Seq data. Both of these genes were upregulated in the experiment and also enriched for angiogenesis. UNC5b is a netrin receptor and has been shown to interact with ROBO4 to maintain vessel integrity through counteracting VEGF signalling. Antibody-based blocking of this interaction increased angiogenesis and reduced vessel integrity (Koch et al., 2011). The gene SLC2A1a is an ortholog of the zebrafish homolog of the human GLUT1 gene and had a $\log_2$ Fold change of 3.34 when TRPV1 was knocked down. This gene is a known glucose transporter (Hruz, 2001) and in zebrafish, has been shown to be expressed during the sprouting stages of vascular development (Quiñonez-Silvero et al., 2020). The expression of SLC2A1a has also been linked to WNT signalling, where the inhibition of WNT during this sprouting phase caused the SLC2A1a expression to also be diminished in the zebrafish (Ulrich et al., 2016). **This identifies a potential link between TRPV1, UNC5b and SLC2A1a's downstream roles in neovascularization and vessel integrity.**

5.3.5 VEGFA and TRPV1 interactions in development

Bevacizumab injection into zebrafish embryos overall caused an increase in development without impacting the survival rate of the embryo. This was the opposite of what was expected to be found, since VEGFA plays such a vital role in cardiovascular development (Kliche & Waltenberger, 2001), although zebrafish embryos can live up to 7dpf without a functional cardiovascular system (Kugler et al., 2021) so while this finding was unexpected, it is plausible. There was overlap between the genes whose expressions were affected by either bevacizumab or TRPV1 morpholino. In **Chapter 4,** candidate genes TAF5L, CALCA and F7 were all increased to varying degrees after injection and the expression of PROX1 and LYVE1 were reduced. In addition, variance partitioning showed that TRPV1 KD and BEV influenced candidate gene expression with approximately equal percentages, **lending additional importance to TRPV1's importance for (lymph)angiogenesis during development.**

5.4 Contribution to Science

During the course of this PhD, a range of new discoveries have been made with regards to TRPV1 and its involvement in angiogenesis and the cardiovascular system, becoming the subject of copious review articles on the matter. TRP channels generally have now been evaluated with regards to their roles in promoting vascular growth in cancer, promoting proliferation and the migration of endothelial cells through inflammatory response pathways, and VEGF interactions (Perna et al, 2022). A review discussing the potential of TRPV1 as a molecular target for angiogenesis was also published whilst this PhD was being undertaken. The authors of the review stated that given the evidence around TRPV1's role in vascular function, it is a promising candidate for ischemia drug therapies (Negri et al., 2020). Research into these thermoTRP channels is also gaining more recognition in the field, with the 2021 Nobel Prize being awarded to David Julius and Ardem Patapoutian for their discoveries made relating to TRPV1 and PIEZO channels and their responses to temperature and touch (Cheng, 2021), Julius and his team were the first to identify the TRPV1 channel in 1997 (Caterina et al., 1997). Nevertheless, there is a lot of research still to be undertaken in terms of understanding thermoTRP channels and the roles they could play in (patho)physiology. **The data within this PhD thesis advances this field by highlighting under-researched downstream pathways of TRPV1, as well as by providing the first evidence of TRPV1 actively changing developmental rates of zebrafish in response to external stimuli.**

5.5 Suggested areas of improvement

The areas which could be improved if this research was to be performed again would be to generate more repeats for the LAMP experiments. This would not only alleviate the impact of occasional technical errors but also observe if those samples which did not amplify well, were true negatives or false negatives through the use of extra cycles (or time). However, in this work no more reactions could be performed due to budget limitations. The experiments furthermore would have benefited from continuation of the *in vitro* parallel work on HDLECs alongside the in vivo zebrafish model such that the data from human and zebrafish could be analysed in parallel to further strengthen the findings. For example, such work could involve co-culturing of sensory nerve cells and endothelial cells to observe cross talk between the two and how this is regulated via TRPV1. Another *in vitro* study would involve modifying the experiment of Paradise et al, 2013, where it was shown that HDLECs grow towards an acidic pH through IL-8 signalling mediated by TRPV1, to observe if similar physiological responses via TRPV1 occur when the channel is sensitised with heat or 2-APB prior. The study could have also further benefited from the use of the double transgenic Tg(mrc1a:egfp)y251, Tg(kdrl:mcherry)y171 zebrafish line in order to observe the cardiovascular vessels during development under higher resolution than that which was possible with immunofluorescence staining, but this would have necessitated a GMO Home Office licence.

5.6 Future work

The next steps following on from this research would be to investigate the sustained exposure of these pathways to different stressors such as heat, pH and 2-APB, continuing the research of zebrafish development into adulthood to better understand the phenotypes and compensatory mechanisms which are present upon TRPV1 knockdown. This would help us better understand the importance of this channel in terms of, for example, heat stress. It would also be beneficial to observe these changes across generations, where the zebrafish could be bred and whether environmentally induced alterations to the pathway are epigenetically passed on to their offspring. It would also be beneficial to perform a meta-analysis of the literature and investigation into zebrafish cancer models or disease states to highlight potential TRPV1 involvement in these models. An experiment performing a complete knock-out of TRPV1 in zebrafish using a technique such as CRISPR would aid in our understanding the importance of TRPV1 in vascular development.

5.7. Conclusion

Within the last four years, many new studies have strengthened our understanding that an evolutionarily ancient heat receptor, TRPV1, is able to influence cellular processes and organismal development. When this thesis work was started, these links were implied but not shown yet. The cardiovascular and lymphatic systems are essential to determine fluid homeostasis and metabolic rate. The results presented in this thesis lend further support to the hypothesis that alterations in TRPV1 activity during early organismal development may influence the pattern and process of vessel proliferation. In addition, the involvement of downstream signalling cascades identified here makes the TRPV1-CGRP axis a potential target for therapeutics towards endothelial dysfunctions and neovascularization. **The findings in this thesis contribute to a better understanding of the molecular mechanisms involved in vessel development and pave the way for further research in this field**

References

Althaus, K., & Greinacher, A. (2010). MYH-9 Related Platelet Disorders: Strategies for Management and Diagnosis. Transfusion Medicine and Hemotherapy, 37(5), 260–267.

Adawi, M., Pastukh, N., Saaida, G., Sirchan, R., Watad, A., & Blum, A. (2018). Inhibition of endothelial progenitor cells may explain the high cardiovascular event rate in patients with rheumatoid arthritis. QJM: An International Journal of Medicine, 111(8), 525–529.

Ahern, G. P., Brooks, I. M., Miyares, R. L., & Wang, X. B. (2005). Extracellular cations sensitise and gate capsaicin receptor TRPV1 modulating pain signalling. Journal of Neuroscience, 25(21), 5109–5116.

Aird, W. C. (2012). Endothelial cell heterogeneity. Cold Spring Harbor perspectives in medicine, 2(1), 006429.

Alexiou, D., Karayiannakis, A.J., Syrigos, K.N., Zbar, A., Kremmyda, A., Bramis, I. and Tsigris, C., 2001. Serum levels of E-selectin, ICAM-1 and VCAM-1 in colorectal cancer patients: correlations with clinicopathological features, patient survival and tumour surgery. European Journal of Cancer, 37(18), pp.2392-2397.

Aljamali, M. N., Margaritis, P., Schlachterman, A., Tai, S. J., Roy, E., Bunte, R., Camire, R. M., & High, K. A. (2008). Long-term expression of murine activated factor VII is safe, but elevated levels cause premature mortality. The Journal of Clinical Investigation, 118(5), 1825–1834.

Altschul, S. F., Gish, W., Miller, W., Myers, E. W., & Lipman, D. J. (1990). Basic local alignment search tool. Journal of Molecular Biology, 215(3), 403–410.

Amantini, C., Ballarini, P., Caprodossi, S., Nabissi, M., Morelli, M. B., Lucciarini, R., Cardarelli, M. A., Mammana, G., & Santoni, G. (2009). Triggering of transient receptor potential vanilloid type 1 (TRPV1) by capsaicin induces Fas/CD95-mediated apoptosis of urothelial cancer cells in an ATM-dependent manner. Carcinogenesis, 30(8), 1320–1329.

Anderson, M.J., 2014. Permutational multivariate analysis of variance (PERMANOVA). Wiley statsref: statistics reference online, pp.1-15.

Ando K, Fujita T. Lessons from the adrenomedullin knockout mouse. Regulatory peptides. 2003 Apr 15;112(1-3):185-8.

Ando, J., & Yamamoto, K. (2013). Flow detection and calcium signalling in vascular endothelial cells. Cardiovasc Res, 99(2), 260–268.

Angilletta, J., & Dunham, A. E. (2003). The Temperature-Size Rule in Ectotherms: Simple Evolutionary Explanations May Not Be General. The American Naturalist, 162(3), 332–342.

Annan, D. A., Maishi, N., Soga, T., Dawood, R., Li, C., Kikuchi, H., Hojo, T., Morimoto, M., Kitamura, T., Alam, M. T., Minowa, K., Shinohara, N., Nam, J.-M., Hida, Y., & Hida, K. (2019). Carbonic anhydrase 2 (CAII) supports tumor blood endothelial cell survival under lactic acidosis in the tumor microenvironment. Cell Communication and Signaling, 17(1), 169.

Arif, A. R., Zhao, M., Chen, W., Xue, M., Luo, S., & Wang, Y. (2022). Avatrombopag improves thrombocytopenia in MYH9-related disorder following eltrombopag treatment failure. Platelets, 33(8), 1307–1311.

Artik, Y., Coşğun, A. B., Cesur, N. P., Hızel, N., Uyar, Y., Sur, H., & Ayan, A. (2022). Comparison of COVID-19 laboratory diagnosis by commercial kits: Effectivity of RT-PCR to the RT-LAMP. Journal of Medical Virology, 94(5), 1998–2007.

Assas, B. M., Wakid, M. H., Zakai, H. A., Miyan, J. A., & Pennock, J. L. (2016). Transient receptor potential vanilloid 1 expression and function in splenic dendritic cells: A potential role in immune homeostasis. Immunology, 147(3), 292–304.

Assas, B., Pennock, J., & Miyan, J. (2014). Calcitonin gene-related peptide is a key neurotransmitter in the neuro-immune axis. Frontiers in Neuroscience, 8.

Assoun, S., Brosseau, S., Steinmetz, C., Gounant, V., & Zalcman, G. (2017). Bevacizumab in advanced lung cancer: State of the art. Future Oncology, 13(28), 2515–2535.

Astin, J. W., Haggerty, M. J., Okuda, K. S., Le Guen, L., Misa, J. P., Tromp, A., & Crosier, P. S. (2014). Vegfd can compensate for loss of Vegfc in zebrafish facial lymphatic sprouting. Development, 141(13), 2680–2690.

Azhar, S. H., Lim, H. Y., Tan, B.-K., & Angeli, V. (2020). The Unresolved Pathophysiology of Lymphedema. Frontiers in Physiology, 11.

Basu, S., & Srivastava, P. (2005). Immunological role of neuronal receptor vanilloid receptor 1 expressed on dendritic cells. Proceedings of the National Academy of Sciences, 102(14), 5120–5125.

Bates, Adam (2022). Github repository of LAMPrey Script; Dodged13/LAMPrey. Available at https://github.com/dodged13/LAMPrey/tree/main

Bautch VL. VEGF-directed blood vessel patterning: from cells to organism. Cold Spring Harb Perspect Med. 2012 Sep 1;2(9):a006452.

Beazley-Long, N., Hua, J., Jehle, T., Hulse, R. P., Dersch, R., Lehrling, C., & Churchill, A. J. (2013). VEGF-A165b is an endogenous neuroprotective splice isoform of vascular endothelial growth factor A in vivo and in vitro. The American Journal of Pathology, 183(3), 918–929.

Benjamini, Y., & Hochberg, Y. (1995). Controlling the False Discovery Rate: A Practical and Powerful Approach to Multiple Testing. Journal of the Royal Statistical Society: Series B (Methodological), 57(1), 289–300.

Bilmen, J. G., Wootton, L. L., Godfrey, R. E., Smart, O. S., & Michelangeli, F. (2002). Inhibition of SERCA Ca2+ pumps by 2-aminoethoxydiphenyl borate (2-APB). European Journal of Biochemistry, 269(15), 3678–3687.

Bindea G, Galon J, Mlecnik B. CluePedia Cytoscape plugin: pathway insights using integrated experimental and in silico data. Bioinformatics. 2013 Mar 1;29(5):661-3.

Bindea G, Mlecnik B, Hackl H, Charoentong P, Tosolini M, Kirilovsky A, Fridman WH, Pagès F, Trajanoski Z, Galon J. ClueGO: a Cytoscape plug-in to decipher functionally grouped gene ontology and pathway annotation networks. Bioinformatics. 2009 Apr 15;25(8):1091-3.

Bode, A. M., Cho, Y.-Y., Zheng, D., Zhu, F., Ericson, M. E., Ma, W.-Y., Yao, K., & Dong, Z. (2009). Transient receptor potential type vanilloid 1 suppresses skin carcinogenesis. Cancer Research, 69(3), 905–913.

Brandt, M. R., Beyer, C. E., & Stahl, S. M. (2012). TRPV1 Antagonists and Chronic Pain: Beyond Thermal Perception. Pharmaceuticals, 5(2), Article 2.

Brown, H. K., Schiavone, K., Tazzyman, S., Heymann, D., & Chico, T. J. (2017). Zebrafish xenograft models of cancer and metastasis for drug discovery. Expert Opinion on Drug Discovery, 12(4), 379–389.

Buckley, L. B., Huey, R. B., & Kingsolver, J. G. (2022). Asymmetry of thermal sensitivity and the thermal risk of climate change. Global Ecology and Biogeography, 31(11), 2231–2244.

Burns, M. J., Nixon, G. J., Foy, C. A., & Harris, N. (2005). Standardisation of data from real-time quantitative PCR methods – evaluation of outliers and comparison of calibration curves. BMC Biotechnology, 5(1), 31.

Cardell, L. O., Uddman, R., & Edvinsson, L. (1994). Low plasma concentrations of VIP and elevated levels of other neuropeptides during exacerbations of asthma. European Respiratory Journal, 7(12), 2169–2173.

Carmeliet, P. (2005). VEGF as a key mediator of angiogenesis in cancer. Oncology, 69 Suppl 3, 4–10.

Carr, M. J., Kollarik, M., Meeker, S. N., & Undem, B. J. (2003). A Role for TRPV1 in Bradykinin-Induced Excitation of Vagal Airway Afferent Nerve Terminals. Journal of Pharmacology and Experimental Therapeutics, 304(3), 1275–1279.

Catalano, V., Turdo, A., Di Franco, S., Dieli, F., Todaro, M., & Stassi, G. (2013). Tumor and its microenvironment: A synergistic interplay. In Seminars in cancer biology.

Caterina, M. J., Schumacher, M. A., Tominaga, M., Rosen, T. A., Levine, J. D., & Julius, D. (1997). The capsaicin receptor: A heat-activated ion channel in the pain pathway. Nature, 389(6653), 816.

Celotto, L., Rost, F., Machate, A., Bläsche, J., Dahl, A., Weber, A., Hans, S., & Brand, M. (2023). ScRNAseq unravels the transcriptional network underlying zebrafish retina regeneration (p. 2023.01.26.525679). bioRxiv.

Chaffer, C. L., & Weinberg, R. A. (2011). A perspective on cancer cell metastasis. Science, 331(6024), 1559–1564.

Chen, S., Zhou, Y., Chen, Y., & Gu, J. (2018). fastp: An ultra-fast all-in-one FASTQ preprocessor. Bioinformatics, 34(17), i884–i890.

Chen, Y., Wang, H., Wang, F., Chen, C., Zhang, P., Song, D., Luo, T., Xu, H., & Zeng, X. (2020). Sperm motility modulated by Trpv1 regulates zebrafish fertilization. Theriogenology, 151, 41–51.

Cheng, C.-C., Chang, S.-J., Chueh, Y.-N., Huang, T.-S., Huang, P.-H., Cheng, S.-M., Tsai, T.-N., Chen, J.-W., & Wang, H.-W. (2013). Distinct angiogenesis roles and surface markers of early and late endothelial progenitor cells revealed by functional group analyses. BMC Genomics, 14(1), 182.

Cheng, Y. (2021). TRPV1 and Piezo: The 2021 Nobel Prize in Physiology or Medicine. IUCrJ, 9(Pt 1), 4–5.

Cheung, K. Y., Jesuthasan, S. J., Baxendale, S., van Hateren, N. J., Marzo, M., Hill, C. J., & Whitfield, T. T. (2021). Olfactory Rod Cells: A Rare Cell Type in the Larval Zebrafish Olfactory Epithelium With a Large Actin-Rich Apical Projection. Frontiers in Physiology, 12.

Chinopoulos, C., Starkov, A. A., & Fiskum, G. (2003). Cyclosporin A-insensitive Permeability Transition in Brain Mitochondria: INHIBITION BY 2-AMINOETHOXYDIPHENYL BORATE*. Journal of Biological Chemistry, 278(30), 27382–27389.

Chistiakov, D. A., Chernisheva, A., Savost’anov, K. V., Turakulov, R. I., Kuraeva, T. L., Dedov, I. I., & Nosikov, V. V. (2005). The TAF5L gene on chromosome 1q42 is associated with type 1 diabetes in Russian affected patients. Autoimmunity, 38(4), 283–293.

Chou, M. Y., Hsiao, C. D., Chen, S. C., Chen, I. W., Liu, S. T., & Hwang, P. P. (2008). Effects of hypothermia on gene expression in zebrafish gills: Upregulation in differentiation and function of ionocytes as compensatory responses. Journal of Experimental Biology, 211(19), 3077–3084.

Christopoulos, A., Christopoulos, G., Morfis, M., Udawela, M., Laburthe, M., Couvineau, A., & Sexton, P. M. (2003). Novel receptor partners and function of receptor activity-modifying proteins. Journal of Biological Chemistry, 278(5), 3293–3297.

Chung, H.-J., Kim, J. D., Kim, K. H., & Jeong, N. Y. (2014). G protein-coupled receptor, family C, group 5 (GPRC5B) downregulation in spinal cord neurons is involved in neuropathic pain. Korean Journal of Anesthesiology, 66(3), 230–236.

Clarke, A., & Fraser, K. P. P. (2004). Why does metabolism scale with temperature? Functional Ecology, 18(2), 243–251.

Coelho, M. C., Pinto, R. M., & Murray, A. W. (2019). Heterozygous mutations cause genetic instability in a yeast model of cancer evolution. Nature, 566(7743), 275.

Comunanza, V., & Bussolino, F. (2017). Therapy for cancer: Strategy of combining anti-angiogenic and target therapies. Frontiers in Cell and Developmental Biology, 5, 101.

Congreve M, de Graaf C, Swain NA, Tate CG. Impact of GPCR structures on drug discovery. Cell. 2020 Apr 2;181(1):81-91.

Corey, D. R., & Abrams, J. M. (2001). Morpholino antisense oligonucleotides: Tools for investigating vertebrate development. Genome Biol, 2(5).

Crivellato, E., Nico, B., & Ribatti, D. (2007). Contribution of endothelial cells to organogenesis: A modern reappraisal of an old Aristotelian concept. Journal of Anatomy, 211(4), 415–427. Czikora, Á., Lizanecz, E., Bakó, P., Rutkai, I., Ruzsnavszky, F., Magyar, J., Pórszász, R., Kark, T., Facskó, A., Papp, Z., Édes, I., & Tóth, A. (2012). Structure-activity relationships of vanilloid receptor agonists for arteriolar TRPV1. British Journal of Pharmacology, 165(6), 1801–1812.

Cudennec B, Rousseau M, Lopez E, Fouchereau-Peron M. CGRP stimulates gill carbonic anhydrase activity in molluscs via a common CT/CGRP receptor. Peptides. 2006 Nov 1;27(11):2678-82.

Dao Thi, V. L., Herbst, K., Boerner, K., Meurer, M., Kremer, L. P., Kirrmaier, D., Freistaedter, A., Papagiannidis, D., Galmozzi, C., & Stanifer, M. L. (2020). A colorimetric RT-LAMP assay and LAMP-sequencing for detecting SARS-CoV-2 RNA in clinical samples. Science Translational Medicine, 12(556), eabc7075.

Darash-Yahana M, Pikarsky E, Abramovitch R, Zeira E, Pal B, Karplus R, Beider K, Avniel S, Kasem S, Galun E, Peled A. Role of high expression levels of CXCR4 in tumor growth, vascularization, and metastasis. The FASEB Journal. 2004 Aug;18(11):1240-2.

de Almeida, A. S., Bernardes, L. de B., & Trevisan, G. (2021). TRP channels in cancer pain. European Journal of Pharmacology, 904, 174185. Durham, P. L., & Vause, C. V. (2010). Calcitonin gene-related peptide (CGRP) receptor antagonists in the treatment of migraine. CNS Drugs, 24(7), 539–548.

Deguchi, T., Fujimori, K. E., Kawasaki, T., Ohgushi, H., & Yuba, S. (2009). Molecular cloning and gene expression of the prox1a and prox1b genes in the medaka, Oryzias latipes. Gene Expression Patterns, 9(5), 341–347.

Demunter A, De Wolf-Peeters C, Degreef H, Stas M, van den Oord JJ. Expression of the endothelin-B receptor in pigment cell lesions of the skin. Evidence for its role as tumor progression marker in malignant melanoma. Virchows Arch. 2001;438(5):485-491.

Dhaka, A., Uzzell, V., Dubin, A. E., Mathur, J., Petrus, M., Bandell, M., & Patapoutian, A. (2009). TRPV1 is activated by both acidic and basic pH. Journal of Neuroscience, 29(1), 153–158.

Dobin, A., Davis, C. A., Schlesinger, F., Drenkow, J., Zaleski, C., Jha, S., Batut, P., Chaisson, M., & Gingeras, T. R. (2013). STAR: ultrafast universal RNA-seq aligner. Bioinformatics, 29(1), 15–21.

Draoui, N., de Zeeuw, P., & Carmeliet, P. (2017). Angiogenesis revisited from a metabolic perspective: Role and therapeutic implications of endothelial cell metabolism. Open Biology, 7(12), 170219.

Du W, Wang S, Zhou Q, et al. ADAMTS9 is a functional tumor suppressor through inhibiting AKT/mTOR pathway and associated with poor survival in gastric cancer. Oncogene. 2013;32(28):3319-3328.

Dunworth, W.P., Fritz-Six, K.L. and Caron, K.M., 2008. Adrenomedullin stabilizes the lymphatic endothelial barrier in vitro and in vivo. Peptides, 29(12), pp.2243-2249.

Edvinsson, L., Haanes, K. A., Warfvinge, K., & Krause, D. N. (2018). CGRP as the target of new migraine therapies—Successful translation from bench to clinic. Nature Reviews Neurology, 14(6), 338.

Efron B, Tibshirani R. Empirical Bayes methods and false discovery rates for microarrays. Genetic epidemiology. 2002 Jun;23(1):70-86.

Enora, V., Turpin, A., Lebellec, L., Mouamnia, A., Machuron, F., & Vieillard, M. H. (2019). Does bevacizumab increase joint pain? Preliminary results of the BEVARTHRALGIA study. Annals of Oncology, 30, v731.

Fallahi, S., Seyyed Tabaei, S. J., Pournia, Y., Zebardast, N., & Kazemi, B. (2014). Comparison of loop-mediated isothermal amplification (LAMP) and nested-PCR assay targeting the RE and B1 gene for detection of Toxoplasma gondii in blood samples of children with leukaemia. Diagnostic Microbiology and Infectious Disease, 79(3), 347–354.

Feijoo, C., Cabrera, P., Villablanca, E., Allende, M., & Cotelli, F. (2009). The zebrafish prospero homolog prox1 is required for mechanosensory hair cell differentiation and functionality in the lateral line. BMC Developmental Biology, 9, 58.
Fernandez-Prado, R., Carriazo-Julio, S. M., Torra, R., Ortiz, A., & Perez-Gomez, M. V. (2019). MYH9-related disease: It does exist, may be more frequent than you think and requires specific therapy. Clinical Kidney Journal, 12(4), 488–493.
Fernandez-Prado, R., Carriazo-Julio, S. M., Torra, R., Ortiz, A., & Perez-Gomez, M. V. (2019). MYH9-related disease: It does exist, may be more frequent than you think and requires specific therapy. Clinical Kidney Journal, 12(4), 488–493.
Feugere, L., Scott, V.F., Rodriguez-Barucg, Q., Beltran-Alvarez, P. and Valero, K.C.W., 2021. Thermal stress induces a positive phenotypic and molecular feedback loop in zebrafish embryos. Journal of Thermal Biology, 102, p.103114.
Forn-Cuní, G., Reis, E. S., Dios, S., Posada, D., Lambris, J. D., Figueras, A., & Novoa, B. (2014). The Evolution and Appearance of C3 Duplications in Fish Originate an Exclusive Teleost c3 Gene Form with Anti-Inflammatory Activity. PLoS ONE, 9(6), e99673.
Frétaud, M., Do Khoa, N., Houel, A., Lunazzi, A., Boudinot, P., & Langevin, C. (2020). A new reporter zebrafish line unveils heterogeneity among lymphatic endothelial cells during development. Developmental Dynamics.
Garayoa M, Bodegas E, Cuttitta F, Montuenga LM. Adrenomedullin in mammalian embryogenesis. Microscopy research and technique. 2002 Apr 1;57(1):40-54.
Garcia, J., Hurwitz, H. I., Sandler, A. B., Miles, D., Coleman, R. L., Deurloo, R., & Chinot, O. L. (2020). Bevacizumab (Avastin®) in cancer treatment: A review of 15 years of clinical experience and future outlook. Cancer Treatment Reviews, 86, 102017.
García-López, M. Á., Sánchez-Madrid, F., Rodríguez-Frade, J. M., Mellado, M., Acevedo, A., García, M. I., Albar, J. P., Martínez-A, C., & Marazuela, M. (2001). CXCR3 Chemokine Receptor Distribution in Normal and Inflamed Tissues: Expression on Activated Lymphocytes, Endothelial Cells, and Dendritic Cells. Laboratory Investigation, 81(3), Article 3.
Gau, P., Poon, J., Ufret-Vincenty, C., Snelson, C. D., Gordon, S. E., Raible, D. W., & Dhaka, A. (2013). The zebrafish ortholog of TRPV1 is required for heat-induced locomotion. Journal of Neuroscience, 33(12), 5249–5260.
Gavva, N. R. (2008). Body-temperature maintenance as the predominant function of the vanilloid receptor TRPV1. Trends in Pharmacological Sciences, 29(11), 550–557.
Gavva, N. R., Treanor, J. J., Garami, A., Fang, L., Surapaneni, S., Akrami, A., & Jang, G. R. (2008). Pharmacological blockade of the vanilloid receptor TRPV1 elicits marked hyperthermia in humans. Pain, 136(1–2), 202–210.
Gazzieri, D., Trevisani, M., Springer, J., Harrison, S., Cottrell, G. S., Andre, E., Nicoletti, P., Massi, D., Zecchi, S., Nosi, D., Santucci, M., Gerard, N. P., Lucattelli, M., Lungarella, G., Fischer, A., Grady, E. F., Bunnett, N. W., & Geppetti, P. (2007). Substance P released by TRPV1-expressing neurons produces reactive oxygen species that mediate ethanol-induced gastric injury. Free Radical Biology and Medicine, 43(4), 581–589.
Ge, S. X., Jung, D., & Yao, R. (2020). ShinyGO: A graphical gene-set enrichment tool for animals and plants. Bioinformatics, 36(8), 2628–2629.
Gentleman RC, Carey VJ, Bates DM, Bolstad B, Dettling M, Dudoit S, Ellis B, Gautier L, Ge Y, Gentry J, Hornik K. Bioconductor: open software development for computational biology and bioinformatics. Genome biology. 2004 Sep 1;5(10):R80.
Gibbons, C., Dackor, R., Dunworth, W., Fritz-Six, K., & Caron, K. M. (2007). Receptor Activity-Modifying Proteins: RAMPing up Adrenomedullin Signaling. Molecular Endocrinology, 21(4), 783–796.
Ginestet C. ggplot2: elegant graphics for data analysis. Journal of the Royal Statistical Society: Series A (Statistics in Society). 2011 Jan;174(1):245-6.
Go GW, Mani A. Low-density lipoprotein receptor (LDLR) family orchestrates cholesterol homeostasis. The Yale journal of biology and medicine. 2012 Mar;85(1):19.

Gordon, C. R., Rojavin, Y., Patel, M., Zins, J. E., Grana, G., Kann, B., Simons, R., & Atabek, U. (2009). A Review on Bevacizumab and Surgical Wound Healing: An Important Warning to All Surgeons. Annals of Plastic Surgery, 62(6), 707.

Gore, A. V., Monzo, K., Cha, Y. R., Pan, W., & Weintein, B. M. (2012). Vascular Development in the Zebrafish. Cold Spring Harbor Perspectives in Medicine, 2(5), a006684.

Graham, D. M., Huang, L., Robinson, K. R., & Messerli, M. A. (2013). Epidermal keratinocyte polarity and motility require Ca2+ influx through TRPV1. Journal of Cell Science, 126(20), 4602–4613

Groneberg, D. A., Niimi, A., Dinh, Q. T., Cosio, B., Hew, M., Fischer, A., & Chung, K. F. (2004). Increased expression of transient receptor potential vanilloid-1 in airway nerves of chronic cough. American journal of respiratory and critical care medicine, 170(12), 1276–1280.

Guo J, Lou W, Ji Y, Zhang S. Effect of CCR7, CXCR4 and VEGF-C on the lymph node metastasis of human pancreatic ductal adenocarcinoma. Oncology letters. 2013 May 1;5(5):1572-8.

Hagensen, M. K., Raarup, M. K., Mortensen, M. B., Thim, T., Nyengaard, J. R., Falk, E., & Bentzon, J. F. (2011). Circulating endothelial progenitor cells do not contribute to regeneration of endothelium after murine arterial injury. Cardiovasc Res, 93(2), 223–231.

Hagner S, Stahl U, Grimm T, et al Expression of calcitonin receptor-like receptor in human vascular tumours Journal of Clinical Pathology 2006;59:1104-1107.

Hamill, D. R., Howell, B., Cassimeris, L., & Suprenant, K. A. (1998). Purification of a WD Repeat Protein, EMAP, That Promotes Microtubule Dynamics through an Inhibition of Rescue*. Journal of Biological Chemistry, 273(15), 9285–9291.

Harr, M. W., & Distelhorst, C. W. (2010). Apoptosis and Autophagy: Decoding Calcium Signals that Mediate Life or Death. Cold Spring Harbor Perspectives in Biology, 2(10), a005579.

Hassan MI, Shajee B, Waheed A, Ahmad F, Sly WS. Structure, function and applications of carbonic anhydrase isozymes. Bioorganic & medicinal chemistry. 2013 Mar 15;21(6):1570-82.

Hay, D.L., Garelja, M.L., Poyner, D.R. and Walker, C.S., 2018. Update on the pharmacology of calcitonin/CGRP family of peptides: IUPHAR Review 25. British journal of pharmacology, 175(1), pp.3-17.

Hay, D. L., & Pioszak, A. A. (2016). RAMPs (Receptor-Activity Modifying Proteins): New Insights and Roles. Annual Review of Pharmacology and Toxicology, 56, 469–487. https://doi.org/10.1146/annurev-pharmtox-010715-103120

He, Y., & Wu, N. (2021). Research Progress on Gestational Diabetes Mellitus and Endothelial Dysfunction Markers. Diabetes, Metabolic Syndrome and Obesity: Targets and Therapy, 14, 983–990.

Heaton JO, Lin B, Chang JK, Steinberg ST, Hyman AL, Lippton HO. Pulmonary vasodilation to adrenomedullin: a novel peptide in humans. American Journal of Physiology-Heart and Circulatory Physiology. 1995 Jun 1;268(6):H2211-5.

Herrera, K. J., Panier, T., Guggiana-Nilo, D., & Engert, F. (2021). Larval Zebrafish Use Olfactory Detection of Sodium and Chloride to Avoid Salt Water. Current Biology, 31(4), 782-793.e3.

Himmel, N. J., & Cox, D. N. (2020). Transient receptor potential channels: Current perspectives on evolution, structure, function and nomenclature. Proceedings of the Royal Society B: Biological Sciences, 287(1933).

Hinson, J. P., Kapas, S., & Smith, D. M. (2000). Adrenomedullin, a multifunctional regulatory peptide. Endocrine Reviews, 21(2), 138–167.

Hirata Y, Emori T, Eguchi S, Kanno K, Imai T, Ohta K, Marumo F. Endothelin receptor subtype B mediates synthesis of nitric oxide by cultured bovine endothelial cells. The Journal of clinical investigation. 1993 Apr 1;91(4):1367-73.

Hoffmann, A. A., & Sgrò, C. M. (2011). Climate change and evolutionary adaptation. Nature, 470(7335), Article 7335.

Hofmann, N. A., Barth, S., Waldeck-Weiermair, M., Klec, C., Strunk, D., Malli, R., & Graier, W. F. (2014). TRPV1 mediates cellular uptake of anandamide and thus promotes endothelial cell proliferation and network-formation. Biology Open, 3(12), 1164–1172.

Hogan KA, Bautch VL. Blood vessel patterning at the embryonic midline. Curr Top Dev Biol. 2004;62:55-85.

Honjo, Y., Payne, L., & Eisen, J. S. (2011). Somatosensory mechanisms in zebrafish lacking dorsal root ganglia. Journal of Anatomy, 218(3), 271–276.

Hosaka, K., Rayner, S.E., von der Weid, P.Y., Zhao, J., Imtiaz, M.S. and van Helden, D.F., 2006. Calcitonin gene-related peptide activates different signaling pathways in mesenteric lymphatics of guinea pigs. American Journal of Physiology-Heart and Circulatory Physiology, 290(2), pp.H813-H822.

Hosseini, S., Brenig, B., Tetens, J., & Sharifi, A. R. (2019). Phenotypic plasticity induced using high ambient temperature during embryogenesis in domesticated zebrafish, Danio rerio. Reproduction in Domestic Animals, 54(3), 435–444.

https://imagej.nih.gov/ij/, 1997-2018.

Hu R, Li YJ, Li XH. An overview of non-neural sources of calcitonin gene-related peptide. Current medicinal chemistry. 2016 Mar 1;23(8):763-73.

Hu, H.-Z., Gu, Q., Wang, C., Colton, C. K., Tang, J., Kinoshita-Kawada, M., Lee, L.-Y., Wood, J. D., & Zhu, M. X. (2004). 2-Aminoethoxydiphenyl Borate Is a Common Activator of TRPV1, TRPV2, and TRPV3*. Journal of Biological Chemistry, 279(34), 35741–35748.

Hu, R., Li, Y. J., & Li, X. H. (2016). An overview of non-neural sources of calcitonin gene-related peptide. Current Medicinal Chemistry, 1;23(8):763-73.

Huang, D., Ding, Y., Luo, W. M., Bender, S., Qian, C. N., Kort, E., & Teh, B. T. (2008). Inhibition of MAPK kinase signaling pathways suppressed renal cell carcinoma growth and angiogenesis in vivo. Cancer Research, 68(1), 81–88.

Huang, Y., Shi, H., Zhou, H., Song, X., Yuan, S., & Luo, Y. (2006). The angiogenic function of nucleolin is mediated by vascular endothelial growth factor and nonmuscle myosin. Blood, 107(9), 3564–3571.

Huang, J., Liu, J., & Qiu, L. (2020). Transient receptor potential vanilloid 1 promotes EGFR ubiquitination and modulates EGFR/MAPK signalling in pancreatic cancer cells. Cell Biochemistry and Function, 38(4), 401–408.

Huang, Y., Fliegert, R., Guse, A. H., Lü, W., & Du, J. (2020). A structural overview of the ion channels of the TRPM family. Cell Calcium, 85, 102111.

Huang, R., Wang, F., Yang, Y., Ma, W., Lin, Z., Cheng, N., Long, Y., Deng, S., & Li, Z. (2019). Recurrent activations of transient receptor potential vanilloid-1 and vanilloid-4 promote cellular proliferation and migration in esophageal squamous cell carcinoma cells. FEBS Open Bio, 9(2), 206.

Hulse, R. P., Beazley-Long, N., Hua, J., Kennedy, H., Prager, J., Bevan, H., & Groot, A. G. (2014). Regulation of alternative VEGF-A mRNA splicing is a therapeutic target for analgesia. Neurobiology of Disease, 71, 245–259.

Hulse, R. P., Beazley-Long, N., Hua, J., Kennedy, H., Prager, J., Bevan, H., Qiu, Y., Fernandes, E. S., Gammons, M. V., Ballmer-Hofer, K., Gittenberger de Groot, A. C., Churchill, A. J., Harper, S. J., Brain, S. D., Bates, D. O., & Donaldson, L. F. (2014). Regulation of alternative VEGF-A mRNA splicing is a therapeutic target for analgesia. Neurobiology of Disease, 71, 245–259.

Hurwitz, H., & Saini, S. (2006). Bevacizumab in the treatment of metastatic colorectal cancer: Safety profile and management of adverse events. Seminars in Oncology, 33, S26–S34.

Ichhpujani, P., Ramasubramanian, A., Kaushik, S., & Pandav, S. S. (2007). Bevacizumab in glaucoma: A review. Canadian Journal of Ophthalmology, 42(6), 812–815.

Impel, A., Zhao, Z., Hermkens, D. M., Roukens, M. G., Fischer, J. C., Peterson-Maduro, J., & Schulte-Merker, S. (2014). Divergence of zebrafish and mouse lymphatic cell fate specification pathways. Development, 141(6), 1228–1238.

Inaba, M., Higashimoto, Y., Toyama, Y., Horiguchi, T., Hibino, M., Iwata, M., Imaizumi, K., & Doi, Y. (2021). Diagnostic accuracy of LAMP versus PCR over the course of SARS-CoV-2 infection. International Journal of Infectious Diseases, 107, 195–200.

Isogai, S., Horiguchi, M., & Weinstein, B. M. (2001). The Vascular Anatomy of the Developing Zebrafish: An Atlas of Embryonic and Early Larval Development. Developmental Biology, 230(2), 278–301.

Jara-Oseguera, A., Bae, C., & Swartz, K. J. (2016). An external sodium ion binding site controls allosteric gating in TRPV1 channels. ELife, 5.

Ji, K., Mayernik, L., Moin, K., & Sloane, B. F. (2019). Acidosis and proteolysis in the tumor microenvironment. Cancer and Metastasis Reviews, 1–10.

Jiang, X.-X., Liu, G.-Y., Lei, H., Li, Z.-L., Feng, Q.-P., & Huang, W. (2018). Activation of transient receptor potential vanilloid 1 protects the heart against apoptosis in ischemia/reperfusion injury through upregulating the PI3K/Akt signaling pathway. International Journal of Molecular Medicine, 41(3), 1724–1730.

Jin, T., Wu, H., Wang, Y., & Peng, H. (2016). Capsaicin induces immunogenic cell death in human osteosarcoma cells. Experimental and therapeutic medicine, 12(2), 765–770.

Jordt, S.-E., Tominaga, M., & Julius, D. (2000). Acid potentiation of the capsaicin receptor determined by a key extracellular site. Proceedings of the National Academy of Sciences of the United States of America, 97(14), 8134.

Ju, W., Smith, A. O., Sun, T., Zhao, P., Jiang, Y., Liu, L., Zhang, T., Qi, K., Qiao, J., Xu, K., & Zeng, L. (2018). Validation of Housekeeping Genes as Reference for Reverse-Transcription-qPCR Analysis in Busulfan-Injured Microvascular Endothelial Cells. BioMed Research International, 2018, 4953806.

Jung, H. M., Castranova, D., Swift, M. R., Pham, V. N., Venero Galanternik, M., Isogai, S., Butler, M. G., Mulligan, T. S., & Weinstein, B. M. (2017). Development of the larval lymphatic system in zebrafish. Development (Cambridge, England), 144(11), 2070–2081.

Karpinich, N.O., Kechele, D.O., Espenschied, S.T., Willcockson, H.H., Fedoriw, Y. and Caron, K.M., 2013. Adrenomedullin gene dosage correlates with tumor and lymph node lymphangiogenesis. The FASEB Journal, 27(2), pp.590-600.

Katsarou, A., Gudbjörnsdottir, S., Rawshani, A., Dabelea, D., Bonifacio, E., Anderson, B. J., Jacobsen, L. M., Schatz, D. A., & Lernmark, Å. (2017). Type 1 diabetes mellitus. Nature Reviews Disease Primers, 3(1),

Kato, J., Kitamura, K., & Eto, T. (2006). Plasma adrenomedullin level and development of hypertension. Journal of Human Hypertension, 20(8), Article 8.

Keller, I., & Seehausen, O. (2012). Thermal adaptation and ecological speciation. Molecular Ecology, 21(4), 782–799.

Khan, M., Li, B., Jiang, Y., Weng, Q., & Chen, Q. (2017). Evaluation of Different PCR-Based Assays and LAMP Method for Rapid Detection of Phytophthora infestans by Targeting the Ypt1 Gene. Frontiers in Microbiology, 8.

Khan, S., Olesen, A., & Ashina, M. (2019). CGRP, a target for preventive therapy in migraine and cluster headache: Systematic review of clinical data. Cephalalgia, 39(3), 374–389.

Kim, K. J., Li, B., Winer, J., Armanini, M., Gillett, N., Phillips, H. S., & Ferrara, N. (1993). Inhibition of vascular endothelial growth factor-induced angiogenesis suppresses tumour growth in vivo. Nature, 362(6423), 841.

Kim, M., Sisco, N. J., Hilton, J. K., Montano, C. M., Castro, M. A., Cherry, B. R., Levitus, M., & Van Horn, W. D. (2020). Evidence that the TRPV1 S1-S4 membrane domain contributes to thermosensing. Nature Communications, 11(1), Article 1.

Kim, W., Moon, S.O., Sung, M.J., Kim, S.H., Lee, S., So, J.N. and Park, S.K., 2003. Angiogenic role of adrenomedullin through activation of Akt, mitogen-activated protein kinase, and focal adhesion kinase in endothelial cells. The FASEB journal, 17(13), pp.1937-1939.

Klein KR, Karpinich NO, Espenschied ST, Willcockson HH, Dunworth WP, Hoopes SL, Kushner EJ, Bautch VL, Caron KM. Decoy receptor CXCR7 modulates adrenomedullin-mediated cardiac and lymphatic vascular development. Developmental cell. 2014 Sep 8;30(5):528-40.

Kliche, S., & Waltenberger, J. (2001). VEGF Receptor Signaling and Endothelial Function. IUBMB Life, 52(1), 61–66.

Knudson, A. G. (1971). Mutation and cancer: Statistical study of retinoblastoma. Proceedings of the National Academy of Sciences, 68(4), 820–823.

Kobe, B., & Kajava, A. V. (2001). The leucine-rich repeat as a protein recognition motif. Current Opinion in Structural Biology, 11(6), 725–732.

Koch, A. W., Mathivet, T., Larrivée, B., Tong, R. K., Kowalski, J., Pibouin-Fragner, L., Bouvrée, K., Stawicki, S., Nicholes, K., Rathore, N., Scales, S. J., Luis, E., del Toro, R., Freitas, C., Bréant, C., Michaud, A., Corvol, P., Thomas, J.-L., Wu, Y., … Eichmann, A. (2011). Robo4 Maintains Vessel Integrity and Inhibits Angiogenesis by Interacting with UNC5B. Developmental Cell, 20(1), 33–46.

Koltowska, K., Lagendijk, A. K., Pichol-Thievend, C., Fischer, J. C., Francois, M., Ober, E. A., & Hogan, B. M. (2015). Vegfc regulates bipotential precursor division and Prox1 expression to promote lymphatic identity in zebrafish. Cell Reports, 13(9), 1828–1841.

Koo, B.-H., Coe, D. M., Dixon, L. J., Somerville, R. P. T., Nelson, C. M., Wang, L. W., Young, M. E., Lindner, D. J., & Apte, S. S. (2010). ADAMTS9 is a cell-autonomously acting, anti-angiogenic metalloprotease expressed by microvascular endothelial cells. The American Journal of Pathology, 176(3), 1494–1504.

Kopp, J. B. (2010). Glomerular pathology in autosomal dominant MYH9 spectrum disorders: What are the clues telling us about disease mechanism? Kidney International, 78(2), 130–133.

Korishettar, A. M., Nishijima, Y., & Zhang, D. X. (2019). Endothelin-1 Potentiates Capsaicin-induced Constriction of Human Adipose Arterioles. The FASEB Journal, 33(1_supplement), 827–3.

Kugler, E., Snodgrass, R., Bowley, G., Plant, K., Serbanovic-Canic, J., Hamilton, N., Evans, P. C., Chico, T., & Armitage, P. (2021). The effect of absent blood flow on the zebrafish cerebral and trunk vasculature. Vascular Biology, 3(1), 1–16.

Kumar, A., Williamson, M., Hess, A., DiPette, D. J., & Potts, J. D. (2022). Alpha-Calcitonin Gene Related Peptide: New Therapeutic Strategies for the Treatment and Prevention of Cardiovascular Disease and Migraine. Frontiers in Physiology, 13, 826122.

Kümler, I., Christiansen, O. G., & Nielsen, D. L. (2014). A systematic review of bevacizumab efficacy in breast cancer. Cancer Treatment Reviews, 40(8), 960–973.

Kuwasako K, Kitamura K, Nagata S, Hikosaka T, Takei Y, Kato J. Shared and separate functions of the RAMP-based adrenomedullin receptors. Peptides. 2011 Jul 1;32(7):1540-50.

Lafont, A. -G., Wang, Y. -F., Chen, G. -D., Liao, B. -K., Tseng, Y. -C., Huang, C. -J., & Hwang, P. -P. (2011). Involvement of calcitonin and its receptor in the control of calcium-regulating genes and calcium homeostasis in zebrafish (Danio rerio. J Bone Miner Res, 26, 1072–1083.

Lahav R, Suvà ML, Rimoldi D, Patterson PH, Stamenkovic I. Endothelin receptor B inhibition triggers apoptosis and enhances angiogenesis in melanomas. Cancer research. 2004 Dec 15;64(24):8945-53.

Laursen, W. J., Schneider, E. R., Merriman, D. K., Bagriantsev, S. N., & Gracheva, E. O. (2016). Low-cost functional plasticity of TRPV1 supports heat tolerance in squirrels and camels. Proceedings of the National Academy of Sciences of the United States of America, 113(40), 11342–11347.

Lee, H. C., Yoon, S.-Y., Lykke-Hartmann, K., Fissore, R. A., & Carvacho, I. (2016). TRPV3 channels mediate Ca2+ influx induced by 2-APB in mouse eggs. Cell Calcium, 59(1), 21–31.

Lee, L.-Y., & Gu, Q. (2009). Role of TRPV1 in inflammation-induced airway hypersensitivity. Current Opinion in Pharmacology, 9(3), 243–249.

Lee, W. C., Kopetz, S., Wistuba, I. I., & Zhang, J. (2017). Metastasis of cancer: When and how?

Lewandowski, T., & Szmit, S. (2016). Bevacizumab—Cardiovascular side effects in daily practice. Oncology in Clinical Practice, 12(4), Article 4.

Ley K, Huo Y. VCAM-1 is critical in atherosclerosis. The Journal of clinical investigation. 2001 May 15;107(10):1209-10.

Li, L. X., Xia, Y. T., Sun, X. Y., Li, L. R., Yao, L., Ali, M. I., Gu, W., Zhang, J. P., Liu, J., Huang, S. G., Dai, H. C., & Liu, G. Q. (2020). CXCL-10/CXCR3 in macrophages regulates tissue repair by controlling the expression of Arg1, VEGFa and TNFα. Journal of Biological Regulators and Homeostatic Agents, 34(3), 987–999.

Li, L., Chen, C., Chiang, C., Xiao, T., Chen, Y., Zhao, Y., & Zheng, D. (2021). The Impact of TRPV1 on Cancer Pathogenesis and Therapy: A Systematic Review. International Journal of Biological Sciences, 17(8), 2034–2049. PubMed.

Li, L., Liu, H., Xu, C., Deng, M., Song, M., Yu, X., Xu, S., & Zhao, X. (2017). VEGF promotes endothelial progenitor cell differentiation and vascular repair through connexin 43. Stem Cell Research & Therapy, 8, 237.

Li, X. (2018). Inhibition of VEGF-A upregulates other VEGF family members and VEGF receptors. Investigative Ophthalmology & Visual Science, 59(9), 2630.

Liang Z, Brooks J, Willard M, Liang K, Yoon Y, Kang S, Shim H. CXCR4/CXCL12 axis promotes VEGF-mediated tumor angiogenesis through Akt signaling pathway. Biochemical and biophysical research communications. 2007 Aug 3;359(3):716-22.

Liang, X., Zhang, L., Natarajan, S. K., & Becker, D. F. (2013). Proline Mechanisms of Stress Survival. Antioxidants & Redox Signaling, 19(9), 998–1011.

Liao, M., Cao, E., Julius, D., & Cheng, Y. (2013). Structure of the TRPV1 ion channel determined by electron cryo-microscopy. Nature, 504(7478), Article 7478.

Lin, T.-Y., Liao, B.-K., Horng, J.-L., Yan, J.-J., Hsiao, C.-D., & Hwang, P.-P. (2008). Carbonic anhydrase 2-like a and 15a are involved in acid-base regulation and Na+ uptake in zebrafish H+-ATPase-rich cells. American Journal of Physiology. Cell Physiology, 294(5), C1250-1260.

Liszewski, M. K., & Atkinson, J. P. (2015). Complement regulator CD46: Genetic variants and disease associations. Human Genomics, 9(1), 7.

Liu, T., Wang, G., Tao, H., Yang, Z., Wang, Y., Meng, Z., Cao, R., Xiao, Y., Wang, X., & Zhou, J. (2016). Capsaicin mediates caspases activation and induces apoptosis through P38 and JNK MAPK pathways in human renal carcinoma. BMC Cancer, 16(1), 790.

Lo PH, Lung HL, Cheung AK, et al. Extracellular protease ADAMTS9 suppresses esophageal and nasopharyngeal carcinoma tumor formation by inhibiting angiogenesis. Cancer Res. 2010;70(13):5567-5576.

Loskutoff, D. J., Curriden, S. A., Hu, G., & Deng, G. (1999). Regulation of cell adhesion by PAI-1. APMIS, 107(1–6), 54–61.

Love, M., Anders, S., & Huber, W. (2014). Differential analysis of count data–the DESeq2 package. Genome Biol, 15(550), 10–1186.

Lu X, Mu E, Wei Y, Riethdorf S, Yang Q, Yuan M, Yan J, Hua Y, Tiede BJ, Lu X, Haffty BG. VCAM-1 promotes osteolytic expansion of indolent bone micrometastasis of breast cancer by engaging α4β1-positive osteoclast progenitors. Cancer cell. 2011 Dec 13;20(6):701-14.

Luo D, Zhang YW, Peng WJ, et al. Transient receptor potential vanilloid 1-mediated expression and secretion of endothelial cell-derived calcitonin gene-related peptide. Regul Pept. 2008;150(1-3):66-72.

Mackman, N. (2009). The Role of Tissue Factor and Factor VIIa in Hemostasis. Anesthesia and Analgesia, 108(5), 1447–1452.

Maeda, Y., Miwa, Y., & Sato, I. (2017). Expression of CGRP, Vasculogenesis and Osteogenesis Associated mRNAs in the Developing Mouse Mandible and Tibia. European Journal of Histochemistry : EJH, 61(1), 2750.

Manteniotis, S., Lehmann, R., Flegel, C., Vogel, F., Hofreuter, A., Schreiner, B. S. P., Altmüller, J., Becker, C., Schöbel, N., Hatt, H., & Gisselmann, G. (2013). Comprehensive RNA-Seq Expression Analysis of Sensory Ganglia with a Focus on Ion Channels and GPCRs in Trigeminal Ganglia. PLoS ONE, 8(11), e79523.

Marcu, R., Choi, Y. J., Xue, J., Fortin, C. L., Wang, Y., Nagao, R. J., Xu, J., MacDonald, J. W., Bammler, T. K., Murry, C. E., Muczynski, K., Stevens, K. R., Himmelfarb, J., Schwartz, S. M., & Zheng, Y. (2018). Human Organ-Specific Endothelial Cell Heterogeneity. IScience, 4, 20–35.

Martinez-Alvarez, R. M., Volkoff, H., Cueto, J. M., & Delgado, M. J. (2008). Molecular characterization of calcitonin gene-related peptide (CGRP) related peptides (CGRP, amylin, adrenomedullin and adrenomedullin-2/intermedin) in goldfish (Carassius auratus): Cloning and distribution. Peptides, 29(9), 1534–1543.

Maruyama, T., Kanaji, T., Nakade, S., Kanno, T., & Mikoshiba, K. (1997). 2APB, 2-Aminoethoxydiphenyl Borate, a Membrane-Penetrable Modulator of Ins(1,4,5)P3-Induced Ca2+ Release. The Journal of Biochemistry, 122(3), 498–505.

Matheny HE, Deem TL, Cook-Mills JM. Lymphocyte migration through monolayers of endothelial cell lines involves VCAM-1 signaling via endothelial cell NADPH oxidase. The Journal of Immunology. 2000 Jun 15;164(12):6550-9.

Matsumoto, K., & Ema, M. (2014). Roles of VEGF-A signalling in development, regeneration, and tumours. The Journal of Biochemistry, 156(1), 1–10.

Maurer CA, Friess H, Kretschmann B, Wildi S, Müller C, Graber H, Schilling M, Büchler MW. Over-expression of ICAM-1, VCAM-1 and ELAM-1 might influence tumor progression in colorectal cancer. International journal of cancer. 1998 Feb 20;79(1):76-81.

Mazzuca MQ, Khalil RA. Vascular endothelin receptor type B: structure, function and dysregulation in vascular disease. Biochem Pharmacol. 2012;84(2):147-162.

McCORMACK, D. G., Mak, J. C., Coupe, M. O., & Barnes, P. J. (1989). Calcitonin gene-related peptide vasodilation of human pulmonary vessels. Journal of Applied Physiology, 1;67(3):1265-70.

McFee, R. M., Rozell, T. G., & Cupp, A. S. (2012). The balance of proangiogenic and antiangiogenic VEGFA isoforms regulate follicle development. Cell and Tissue Research, 349(3), 635–647.

McKemy, D. D., Neuhausser, W. M., & Julius, D. (2002). Identification of a cold receptor reveals a general role for TRP channels in thermosensation. Nature, 416(6876), Article 6876.

Meng, J., Ovsepian, S. V., Wang, J., Pickering, M., Sasse, A., Aoki, K. R., Lawrence, G. W., & Dolly, J. O. (2009). Activation of TRPV1 Mediates Calcitonin Gene-Related Peptide Release, Which Excites Trigeminal Sensory Neurons and Is Attenuated by a Retargeted Botulinum Toxin with Anti-Nociceptive Potential. Journal of Neuroscience, 29(15), 4981–4992.

Meyers, J. R. (2018). Zebrafish: Development of a vertebrate model organism. Current Protocols Essential Laboratory Techniques, 16(1), 19.

Mhatre, A. N., Li, Y., Bhatia, N., Wang, K. H., Atkin, G., & Lalwani, A. K. (2007). Generation and Characterization of Mice with Myh9 Deficiency. NeuroMolecular Medicine, 9(3), 205–215.

Michiels, C., Tellier, C., & Feron, O. (2016). Cycling hypoxia: A key feature of the tumor microenvironment. Biochimica et Biophysica Acta (BBA)-Reviews on Cancer, 1866(1), 76–86.

Miller, B. A., & Zhang, W. (2011). TRP channels as mediators of oxidative stress. Advances in Experimental Medicine and Biology, 704, 531–544.

Mitchell, J. E., Campbell, A. P., New, N. E., Sadofsky, L. R., Kastelik, J. A., Mulrennan, S. A., Compton, S. J., & Morice, A. H. (2005). Expression and Characterization of the Intracellular Vanilloid Receptor (trpv1) in Bronchi from Patients with Chronic Cough. Experimental Lung Research, 31(3), 295–306.

Moisseiev, E., Regenbogen, M., Bartfeld, Y., & Barak, A. (2012). Evaluation of pain in intravitreal bevacizumab injections. Current Eye Research, 37(9), 813–817.

Molino, M., Woolkalis, M.J., Prevost, N., Praticó, D., Barnathan, E.S., Taraboletti, G., Haggarty, B.S., Hesselgesser, J., Horuk, R., Hoxie, J.A. and Brass, L.F., 2000. CXCR4 on human endothelial cells can serve as both a mediator of biological responses and as a receptor for HIV-2. Biochimica et Biophysica Acta (BBA)-Molecular Basis of Disease, 1500(2), pp.227-240.

Monteith, G. R., McAndrew, D., Faddy, H. M., & Roberts-Thomson, S. J. (2007). Calcium and cancer: Targeting Ca 2+ transport. Nature Reviews Cancer, 7(7), 519.

Montell, C., & Rubin, G. M. (1989). Molecular characterization of the drosophila trp locus: A putative integral membrane protein required for phototransduction. Neuron, 2(4), 1313–1323.

Moraczewski, A. L., Lee, R. K., Palmberg, P. F., Rosenfeld, P. J., & Feuer, W. J. (2009). Outcomes of treatment of neovascular glaucoma with intravitreal bevacizumab. British Journal of Ophthalmology, 93(5), 589–593.

Morrow, G. B., Whyte, C. S., & Mutch, N. J. (2021). A Serpin With a Finger in Many PAIs: PAI-1's Central Function in Thromboinflammation and Cardiovascular Disease. Frontiers in Cardiovascular Medicine, 8.

Mortezaee K. CXCL12/CXCR4 axis in the microenvironment of solid tumors: A critical mediator of metastasis. Life Sciences. 2020 Mar 7:117534.

Muff, R., Buhlmann, N., Fischer, J. A., & Born, W. (1999). An amylin receptor is revealed following co-transfection of a calcitonin receptor with receptor activity modifying proteins-1 or-3. Endocrinology, 140(6), 2924–2927.

Mulderry, P. K., Ghatei, M. A., Spokes, R. A., Jones, P. M., Pierson, A. M., Hamid, Q. A., Kanse, S., Amara, S. G., Burrin, J. M., & Legon, S. (1988). Differential expression of alpha-CGRP and beta-CGRP by primary sensory neurons and enteric autonomic neurons of the rat. Neuroscience, 25(1), 195–205.

Munjuluri, S., Wilkerson, D. A., Sooch, G., Chen, X., White, F. A., & Obukhov, A. G. (2021). Capsaicin and TRPV1 Channels in the Cardiovascular System: The Role of Inflammation. Cells, 11(1), 18.

Myers, B. R., Bohlen, C. J., & Julius, D. (2008). A Yeast Genetic Screen Reveals a Critical Role for the Pore Helix Domain in TRP Channel Gating. Neuron, 58(3), 362–373.

Najib L, Fouchereau-Peron M. Calcitonin gene-related peptide stimulates carbonic anhydrase activity in trout gill membranes. General and comparative endocrinology. 1994 May 1;94(2):166-70.

Nakai, H., & Matsumura, N. (2022). The roles and limitations of bevacizumab in the treatment of ovarian cancer. International Journal of Clinical Oncology, 1–7.

Nakanishi, M., Morita, Y., Hata, K., & Muragaki, Y. (2016). Acidic microenvironments induce lymphangiogenesis and IL-8 production via TRPV1 activation in human lymphatic endothelial cells. Experimental Cell Research, 345(2), 180–189.

Naujokaitis-Lewis, I., Endicott, S., & Guezen, J. (2021). Treatment of climate change in extinction risk assessments and recovery plans for threatened species. Conservation Science and Practice, 3(8), e450.

Negri, S., Faris, P., Rosti, V., Antognazza, M. R., Lodola, F., & Moccia, F. (2020). Endothelial TRPV1 as an Emerging Molecular Target to Promote Therapeutic Angiogenesis. Cells, 9(6), 1341.

Nicenboim, J., Malkinson, G., Lupo, T., Asaf, L., Sela, Y., Mayseless, O., & Gibbs-Bar, L. (2015). Lymphatic vessels arise from specialized angioblasts within a venous niche. Nature, 522(7554), 56.

Nicoli, S., Tobia, C., Gualandi, L., De Sena, G., & Presta, M. (2008). Calcitonin receptor-like receptor guides arterial differentiation in zebrafish. Blood, 111(10), 4965.

Niemeyer, B. A. (2005). Structure-function analysis of TRPV channels. Naunyn-Schmiedeberg's Archives of Pharmacology, 371(4), 285–294.

Nikitenko LL, Blucher N, Fox SB, Bicknell R, Smith DM, Rees MC. Adrenomedullin and CGRP interact with endogenous calcitonin-receptor-like receptor in endothelial cells and induce its desensitisation by different mechanisms. Journal of cell science. 2006 Mar 1;119(5):910-22.

Nikitenko LL, Leek R, Henderson S, Pillay N, Turley H, Generali D, Gunningham S, Morrin HR, Pellagatti A, Rees MC, Harris AL. The G-protein–coupled receptor CLR is upregulated in an autocrine loop with adrenomedullin in clear cell renal cell carcinoma and associated with poor prognosis. Clinical cancer research. 2013 Oct 15;19(20):5740-8.

Nikitenko, L. L., Blucher, N., Fox, S. B., Bicknell, R., Smith, D. M., & Rees, M. C. (2006). Adrenomedullin and CGRP interact with endogenous calcitonin-receptor-like receptor in endothelial cells and induce its desensitisation by different mechanisms. Journal of Cell Science, 1;119(5):910-22.

Notomi, T., Okayama, H., Masubuchi, H., Yonekawa, T., Watanabe, K., Amino, N., & Hase, T. (2000). Loop-mediated isothermal amplification of DNA. Nucleic acids research, 28(12), e63-e63.

O'Connor, V., Houtman, S. H., De Zeeuw, C. I., Bliss, T. V. P., & French, P. J. (2004). Eml5, a novel WD40 domain protein expressed in rat brain. Gene, 336(1), 127–137.

O'Leary, C., McGahon, M. K., Ashraf, S., McNaughten, J., Friedel, T., Cincolà, P., Barabas, P., Fernandez, J. A., Stitt, A. W., McGeown, J. G., & Curtis, T. M. (2019). Involvement of TRPV1 and TRPV4 Channels in Retinal Angiogenesis. Investigative Ophthalmology & Visual Science, 60(10), 3297–3309.

Ochoa-Callejero L, Pozo-Rodrigálvarez A, Martínez-Murillo R, Martínez A. Lack of adrenomedullin in mouse endothelial cells results in defective angiogenesis, enhanced vascular permeability, less metastasis, and more brain damage. Scientific reports. 2016 Sep 19;6(1):1-2.

Ochoa-Callejero, L., Pozo-Rodrigálvarez, A., Martínez-Murillo, R., & Martínez, A. (2016). Lack of adrenomedullin in mouse endothelial cells results in defective angiogenesis, enhanced vascular permeability, less metastasis, and more brain damage. Scientific Reports, 19;6(1):1-2.

Ohlberger, J. (2013). Climate warming and ectotherm body size – from individual physiology to community ecology. Functional Ecology, 27(4), 991–1001.

Ohuchi, K., Amagai, R., Ikawa, T., Muto, Y., Roh, Y., Endo, J., Maekawa, T., Kambayashi, Y., Asano, Y., & Fujimura, T. (2023). Plasminogen activating inhibitor-1 promotes angiogenesis in cutaneous angiosarcomas. *Experimental Dermatology*, *32*(1), 50–59.

Oksanen et al, Package "vegan." (2022). https://cran.r-project.org/web/packages/vegan/vegan.pdf

Österdahl, M. F., Lee, K. A., Lochlainn, M. N., Wilson, S., Douthwaite, S., Horsfall, R., Sheedy, A., Goldenberg, S. D., Stanley, C. J., Spector, T. D., & Steves, C. J. (2020). Detecting SARS-CoV-2 at point of care: Preliminary data comparing loop-mediated isothermal amplification (LAMP) to polymerase chain reaction (PCR). BMC Infectious Diseases, 20(1), 783.

Ozawa, C. R., Banfi, A., & Glazer, N. L. (2004). Microenvironmental VEGF concentration, not total dose, determines a threshold between normal and aberrant angiogenesis. J Clin Invest, 113(4), 516–527.

Padberg, Y., Schulte-Merker, S., & Impel, A. (2017). The lymphatic vasculature revisited-new developments in the zebrafish. Methods Cell Biol, 138, 221–238.

Palazzo, E., Luongo, L., Novellis, V., Rossi, F., Marabese, I., & Maione, S. (2012). Transient receptor potential vanilloid type 1 and pain development. Current opinion in pharmacology, 12(1), 9–17.

Paradise, R. K., Whitfield, M. J., Lauffenburger, D. A., & Van Vliet, K. J. (2013). Directional cell migration in an extracellular pH gradient: A model study with an engineered cell line and primary microvascular endothelial cells. Experimental Cell Research, 319(4), 487–497.

Parameswaran, N., & Spielman, W. S. (2006). RAMPs: The past, present and future. Trends in biochemical sciences, 31(11), 631–638.

Parekh, S., Ziegenhain, C., Vieth, B., Enard, W., & Hellmann, I. (2016). The impact of amplification on differential expression analyses by RNA-seq. Scientific Reports, 6(1), 25533.

Patergnani, S., Danese, A., Bouhamida, E., Aguiari, G., Previati, M., Pinton, P., & Giorgi, C. (2020). Various Aspects of Calcium Signaling in the Regulation of Apoptosis, Autophagy, Cell Proliferation, and Cancer. International Journal of Molecular Sciences, 21(21), 8323.

Paul W. Hruz, M. M. M. (2001). Structural analysis of the GLUT1 facilitative glucose transporter. Molecular Membrane Biology, 18(3), 183–193.

Pearce, A., Redfern-Nichols, T., Harris, M., Poyner, D. R., Wigglesworth, M., & Ladds, G. (2022). Determining the Effects of Differential Expression of GRKs and β-arrestins on CLR-RAMP Agonist Bias. Frontiers in Physiology, 13.

Peng, J., & Li, Y. J. (2010). The vanilloid receptor TRPV1: Role in cardiovascular and gastrointestinal protection. European Journal of Pharmacology, 10;627(1-3):1-7.

Peng, Y.-H., Lin, Y.-S., Chen, C.-H., Tsai, K.-Y., Hung, Y.-C., Chen, H.-J., Liao, W.-C., & Ho, W.-C. (2020). Type 1 diabetes is associated with an increased risk of venous thromboembolism: A retrospective population-based cohort study. PLoS ONE, 15(1)

Phelps, C. B., Wang, R. R., Choo, S. S., & Gaudet, R. (2010). Differential Regulation of TRPV1, TRPV3, and TRPV4 Sensitivity through a Conserved Binding Site on the Ankyrin Repeat Domain *. Journal of Biological Chemistry, 285(1), 731–740.

Pla, F., Alessandra, & Gkika, D. (2013). Emerging role of TRP channels in cell migration: From tumor vascularization to metastasis. Frontiers in Physiology, 4, 311.

Planells-Cases, R., Garcìa-Sanz, N., Morenilla-Palao, C., & Ferrer-Montiel, A. (2005). Functional aspects and mechanisms of TRPV1 involvement in neurogenic inflammation that leads to thermal hyperalgesia. Pflügers Archiv, 451(1), 151–159.

Pletscher-Frankild, S., Pallejà, A., Tsafou, K., Binder, J. X., & Jensen, L. J. (2015). DISEASES: Text mining and data integration of disease–gene associations. Methods, 74, 83–89.

Potente, M., & Mäkinen, T. (2017). Vascular heterogeneity and specialization in development and disease. Nature Reviews Molecular Cell Biology, 18, 477.

Pouysségur, J., Dayan, F., & Mazure, N. M. (2006). Hypoxia signalling in cancer and approaches to enforce tumour regression. Nature, 441(7092), 437.

Prasain, N., & Stevens, T. (2009). The actin cytoskeleton in endothelial cell phenotypes. Microvascular Research, 77(1), 53–63.

Qi, Y., Qi, Z., Li, Z., Wong, C.-K., So, C., Lo, I.-C., Huang, Y., Yao, X., & Tsang, S.-Y. (2015). Role of TRPV1 in the Differentiation of Mouse Embryonic Stem Cells into Cardiomyocytes. PLOS ONE, 10(7), e0133211.

Qin, N., Neeper, M. P., Liu, Y., Hutchinson, T. L., Lubin, M. L., & Flores, C. M. (2008). TRPV2 is activated by cannabidiol and mediates CGRP release in cultured rat dorsal root ganglion neurons. The Journal of Neuroscience: The Official Journal of the Society for Neuroscience, 28(24), 6231–6238.

Quiñonez-Silvero, C., Hübner, K., & Herzog, W. (2020). Development of the brain vasculature and the blood-brain barrier in zebrafish. Developmental Biology, 457(2), 181–190.

R Core Team (2017). R: A language and environment for statistical computing. R Foundation for Statistical Computing, Vienna, Austria. URL https://www.R-project.org/.

Ramsey, I. S., Delling, M., & Clapham, D. E. (2006). An introduction to TRP channels. Annu. Rev. Physiol, 68, 619–647.

Rasband, W.S., ImageJ, U. S. National Institutes of Health, Bethesda, Maryland, USA,

Regazzetti C, De Donatis GM, Ghorbel HH, et al. Endothelial Cells Promote Pigmentation through Endothelin Receptor B Activation. J Invest Dermatol. 2015;135(12):3096-3104.

Reiten, I., Uslu, F. E., Fore, S., Pelgrims, R., Ringers, C., Diaz Verdugo, C., Hoffman, M., Lal, P., Kawakami, K., Pekkan, K., Yaksi, E., & Jurisch-Yaksi, N. (2017). Motile-Cilia-Mediated Flow Improves Sensitivity and Temporal Resolution of Olfactory Computations. Current Biology: CB, 27(2), 166–174.

Reuter, M. S., Jobling, R., Chaturvedi, R. R., Manshaei, R., Costain, G., Heung, T., Curtis, M., Hosseini, S. M., Liston, E., Lowther, C., Oechslin, E., Sticht, H., Thiruvahindrapuram, B., Mil, S. van, Wald, R. M., Walker, S., Marshall, C. R., Silversides, C. K., Scherer, S. W., … Bassett, A. S. (2019). Haploinsufficiency of vascular endothelial growth factor related signaling genes is associated with tetralogy of Fallot. Genetics in Medicine, 21(4), Article 4.

Ribatti, D., Nico, B., Spinazzi, R., Vacca, A., & Nussdorfer, G. G. (2005). The role of adrenomedullin in angiogenesis. Peptides, 1;26(9):1670-5.

Robinson, M. D., McCarthy, D. J., & Smyth, G. K. (2010). EdgeR: a Bioconductor package for differential expression analysis of digital gene expression data. Bioinformatics, 26(1), 139–140.

Rockson, S. G. (2021). Advances in Lymphedema. Circulation Research, 128(12), 2003–2016.

Roh, J., Chang, C. L., Bhalla, A., Klein, C., & Hsu, S. Y. T. (2004). Intermedin is a calcitonin/calcitonin gene-related peptide family peptide acting through the calcitonin receptor-like receptor/receptor activity-modifying protein receptor complexes. The Journal of Biological Chemistry, 279(8), 7264–7274.

Rosenberger, D. C., Binzen, U., Treede, R.-D., & Greffrath, W. (2020). The capsaicin receptor TRPV1 is the first line defense protecting from acute non damaging heat: A translational approach. Journal of Translational Medicine, 18(1), 28.

Ruan, G.-X., & Kazlauskas, A. (2012). VEGF-A engages at least three tyrosine kinases to activate PI3K/Akt. Cell Cycle, 11(11), 2047–2048.

Russell, F. A., King, R., Smillie, S. J., Kodji, X., & Brain, S. D. (2014). Calcitonin gene-related peptide: Physiology and pathophysiology. Physiol Rev, 94(4), 1099–1142.

Russo, A. F. (2015). Calcitonin gene-related peptide (CGRP): A new target for migraine. Annual Review of Pharmacology and Toxicology, 55, 533–552.

Saif, M. W., & Mehra, R. (2006). Incidence and management of bevacizumab-related toxicities in colorectal cancer. Expert Opinion on Drug Safety, 5(4), 553–566.

Saito S, Tominaga M. Evolutionary tuning of TRPA1 and TRPV1 thermal and chemical sensitivity in vertebrates. Temperature (Austin). 2017 Apr 7;4(2):141-152.

Saito, S., & Shingai, R. (2006). Evolution of thermoTRP ion channel homologs in vertebrates. Physiological Genomics, 27(3), 219–230.

Santoni, G., & Amantini, C. (2019). The Transient Receptor Potential Vanilloid Type-2 (TRPV2) Ion Channels in Neurogenesis and Gliomagenesis: Cross-Talk between Transcription Factors and Signaling Molecules. Cancers, 11(3), 322.

Saraceno, R., Kleyn, C. E., Terenghi, G., & Griffiths, C. E. M. (2006). The role of neuropeptides in psoriasis. British Journal of Dermatology, 155(5), 876–882.

Sardar, P., Kumar, A., Bhandari, A., & Goswami, C. (2012). Conservation of Tubulin-Binding Sequences in TRPV1 throughout Evolution. PLOS ONE, 7(4), e31448.

Saunders, C. I., Kunde, D. A., Crawford, A., & Geraghty, D. P. (2007). Expression of transient receptor potential vanilloid 1 (TRPV1) and 2 (TRPV2) in human peripheral blood. Molecular immunology, 44(6), 1429–1435.

Schneider, C., O'Leary, C. E., & Locksley, R. M. (2019). Regulation of immune responses by tuft cells. Nature Reviews Immunology, 19(9), 584–593.

Schnurr, M. E., Yin, Y., & Scott, G. R. (2014). Temperature during embryonic development has persistent effects on metabolic enzymes in the muscle of zebrafish. Journal of Experimental Biology, 217(8), 1370–1380.

Schrader AJ, Lechner O, Templin M, Dittmar KE, Machtens S, Mengel M, Probst-Kepper M, Franzke A, Wollensak T, Gatzlaff P, Atzpodien J. CXCR4/CXCL12 expression and signalling in kidney cancer. British journal of cancer. 2002 Apr;86(8):1250-6.

Schroeder, A., Mueller, O., Stocker, S., Salowsky, R., Leiber, M., Gassmann, M., Lightfoot, S., Menzel, W., Granzow, M., & Ragg, T. (2006). The RIN: an RNA integrity number for assigning integrity values to RNA measurements. BMC Molecular Biology, 7(1), 3.

Selvaraj, D., Gangadharan, V., Michalski, C. W., Kurejova, M., Stösser, S., Srivastava, K., & Shibuya, M. (2015). A functional role for VEGFR1 expressed in peripheral sensory neurons in cancer pain. Cancer Cell, 27(6), 780–796.

Semo, J., Nicenboim, J., & Yaniv, K. (2016). Development of the lymphatic system: New questions and paradigms. Development, 143(6), 924–935.

Seri, M., Pecci, A., Di Bari, F., Cusano, R., Savino, M., Panza, E., Nigro, A., Noris, P., Gangarossa, S., Rocca, B., Gresele, P., Bizzaro, N., Malatesta, P., Koivisto, P. A., Longo, I., Musso, R., Pecoraro, C., Iolascon, A., Magrini, U., … Savoia, A. (2003). MYH9-Related Disease: May-Hegglin Anomaly, Sebastian Syndrome, Fechtner Syndrome, and Epstein Syndrome Are not Distinct Entities but Represent a Variable Expression of a Single Illness. Medicine, 82(3), 203.

Shannon P, Markiel A, Ozier O, Baliga NS, Wang JT, Ramage D, Amin N, Schwikowski B, Ideker T. Cytoscape: a software environment for integrated models of biomolecular interaction networks. Genome research. 2003 Nov 1;13(11):2498-504.

Shepherd, A. J., Mickle, A. D., Kadunganattil, S., Hu, H., & Mohapatra, D. P. (2018). Parathyroid Hormone-Related Peptide Elicits Peripheral TRPV1-dependent Mechanical Hypersensitivity. Frontiers in Cellular Neuroscience, 12.

Shu HB, Agranoff AB, Nabel EG, Leung KW, Duckett CS, Neish AS, Collins T, Nabel GJ. Differential regulation of vascular cell adhesion molecule 1 gene expression by specific NF-kappa B subunits in endothelial and epithelial cells. Molecular and cellular biology. 1993 Oct 1;13(10):6283-9.

Sibly, R. M., & Atkinson, D. (1994). How rearing temperature affects optimal adult size in ectotherms. Functional Ecology, 486–493.

Silva, S. J. R. da, Pardee, K., & Pena, L. (2020). Loop-Mediated Isothermal Amplification (LAMP) for the Diagnosis of Zika Virus: A Review. Viruses, 12(1), Article 1.

Sly, W.S. and Hu, P.Y., 1995. Human carbonic anhydrases and carbonic anhydrase deficiencies. Annual review of biochemistry, 64(1), pp.375-401.

Smith MC, Luker KE, Garbow JR, Prior JL, Jackson E, Piwnica-Worms D, Luker GD. CXCR4 regulates growth of both primary and metastatic breast cancer. Cancer research. 2004 Dec 1;64(23):8604-12.

Smyth, G. K. (2005). Limma: Linear models for microarray data. In Bioinformatics and computational biology solutions using R and Bioconductor (pp. 397–420). Springer.

Son, H.-W., & Ali, D. W. (2022). Endocannabinoid Receptor Expression in Early Zebrafish Development. Developmental Neuroscience, 44(3), 142–152.
Soufir N, Meziani R, Lacapère JJ, et al. Association between endothelin receptor B nonsynonymous variants and melanoma risk. J Natl Cancer Inst. 2005;97(17):1297-1301.
Spinella F, Rosanò L, Di Castro V, et al. Endothelin-1 and endothelin-3 promote invasive behavior via hypoxia-inducible factor-1alpha in human melanoma cells. Cancer Res. 2007;67(4):1725-1734.
Staessen, J. A., Wang, J., Bianchi, G., & Birkenhäger, W. H. (2003). Essential hypertension. The Lancet, 361(9369), 1629–1641.
Stefansson, S., Petitclerc, E., Wong, M. K., McMahon, G. A., Brooks, P. C., & Lawrence, D. A. (2001). Inhibition of Angiogenesis in Vivo by Plasminogen Activator Inhibitor-1 *. Journal of Biological Chemistry, 276(11), 8135–8141.
Stucky, C. L., Dubin, A. E., Jeske, N. A., Malin, S. A., McKemy, D. D., & Story, G. M. (2009). Roles of transient receptor potential channels in pain. Brain Research Reviews, 60(1), 2–23.
Su, K. H., Lin, S. J., Wei, J., Lee, K. I., Zhao, J. F., Shyue, S. K., & Lee, T. S. (2014). The essential role of transient receptor potential vanilloid 1 in simvastatin-induced activation of endothelial nitric oxide synthase and angiogenesis. Acta Physiologica, 212(3), 191–204.
Su, K.-H., Lee, K.-I., Shyue, S.-K., Chen, H.-Y., Wei, J., & Lee, T.-S. (2014). Implication of transient receptor potential vanilloid type 1 in 14,15-epoxyeicosatrienoic acid-induced angiogenesis. International Journal of Biological Sciences, 10(9), 990–996.
Summerton, J. E. (2007). Morpholino, siRNA, and S-DNA Compared: Impact of Structure and Mechanism of Action on Off-Target Effects and Sequence Specificity. Current Topics in Medicinal Chemistry, 7(7), 651–660.
Summerton, J., & Weller, D. (1997). Morpholino antisense oligomers: Design, preparation, and properties. Antisense & Nucleic Acid Drug Development, 7(3), 187–195.
Sun, B., Vaughan-Jones, R.D. and Kambayashi, J.I., 1999. Two distinct HCO 3−-dependent H+ efflux pathways in human vascular endothelial cells. American Journal of Physiology-Heart and Circulatory Physiology, 277(1), pp.H28-H32.
Sun, M.-Y., Zhang, X., Yu, P.-C., Liu, D., Yang, Y., Cui, W.-W., Yang, X.-N., Lei, Y.-T., Li, X.-H., Wang, W.-H., Cao, P., Wang, H.-S., Zhu, M. X., Li, C.-Z., Wang, R., Fan, Y.-Z., & Yu, Y. (2022). Vanilloid agonist-mediated activation of TRPV1 channels requires coordinated movement of the S1–S4 bundle rather than a quiescent state. Science Bulletin, 67(10), 1062–1076.
Szallasi, A., Cruz, F., & Geppetti, P. (2006). TRPV1: A therapeutic target for novel analgesic drugs? Trends in Molecular Medicine, 12(11), 545–554.
Szklarczyk, D., Franceschini, A., Wyder, S., Forslund, K., Heller, D., Huerta-Cepas, J., Simonovic, M., Roth, A., Santos, A., Tsafou, K. P., Kuhn, M., Bork, P., Jensen, L. J., & von Mering, C. (2015). STRING v10: Protein-protein interaction networks, integrated over the tree of life. Nucleic Acids Research, 43(Database issue), D447-452.
Tammela, T., & Alitalo, K. (2010). Lymphangiogenesis: Molecular mechanisms and future promise. Cell, 140(4), 460–476.
Tanaka, M., & Iwakiri, Y. (2016). The Hepatic Lymphatic Vascular System: Structure, Function, Markers, and Lymphangiogenesis. Cellular and Molecular Gastroenterology and Hepatology, 2(6), 733–749.
Tanimoto, T., Takeda, M., Nasu, M., Kadoi, J., & Matsumoto, S. (2005). Immunohistochemical co-expression of carbonic anhydrase II with Kv1.4 and TRPV1 in rat small-diameter trigeminal ganglion neurons. Brain Research, 1044(2), 262–265.
Tao, S., Witte, M., Bryson-Richardson, R. J., Currie, P. D., Hogan, B. M., & Schulte-Merker, S. (2011). Zebrafish prox1b mutants develop a lymphatic vasculature, and prox1b does not specifically mark lymphatic endothelial cells. PLoS One, 6(12), 28934.

Templehof, H., Moshe, N., Avraham-Davidi, I., & Yaniv, K. (2021). Zebrafish mutants provide insights into Apolipoprotein B functions during embryonic development and pathological conditions. JCI Insight, 6(13).

Tobia, C., De Sena, G., & Presta, M. (2011). Zebrafish embryo, a tool to study tumor angiogenesis. Int J Dev Biol, 55(4–5), 505–509.

Tol, J., Koopman, M., Cats, A., Rodenburg, C. J., Creemers, G. J. M., Schrama, J. G., Erdkamp, F. L. G., Vos, A. H., van Groeningen, C. J., Sinnige, H. A. M., Richel, D. J., Voest, E. E., Dijkstra, J. R., Vink-Börger, M. E., Antonini, N. F., Mol, L., van Krieken, J. H. J. M., Dalesio, O., & Punt, C. J. A. (2009). Chemotherapy, Bevacizumab, and Cetuximab in Metastatic Colorectal Cancer. New England Journal of Medicine, 360(6), 563–572.

Tominaga, M., & Tominaga, T. (2005). Structure and function of TRPV1. Pflügers Archiv, 451(1), 143–150.

Tomoda, Y., Isumi, Y., Katafuchi, T. and Minamino, N., 2001. Regulation of adrenomedullin secretion from cultured cells. Peptides, 22(11), pp.1783-1794.

Totoson, P., Maguin-Gaté, K., Prati, C., Wendling, D., & Demougeot, C. (2014). Mechanisms of endothelial dysfunction in rheumatoid arthritis: Lessons from animal studies. Arthritis Research & Therapy, 16(1), 202.

Trevisani, M., Gazzieri, D., Benvenuti, F., Campi, B., Dinh, Q. T., Groneberg, D. A., Rigoni, M., Emonds-Alt, X., Creminon, C., Fischer, A., Geppetti, P., & Harrison, S. (2004). Ethanol Causes Inflammation in the Airways by a Neurogenic and TRPV1-Dependent Mechanism. Journal of Pharmacology and Experimental Therapeutics, 309(3), 1167–1173.

Trkulja, C. L., Jungholm, O., Davidson, M., Jardemark, K., Marcus, M. M., Hägglund, J., Karlsson, A., Karlsson, R., Bruton, J., Ivarsson, N., Srinivasa, S. P., Cavallin, A., Svensson, P., Jeffries, G. D. M., Christakopoulou, M.-N., Reymer, A., Ashok, A., Willman, G., Papadia, D., … Orwar, O. (2021). Rational antibody design for undruggable targets using kinetically controlled biomolecular probes. Science Advances, 7(16)

Tsuji-Tamura, K., & Ogawa, M. (2018). Morphology regulation in vascular endothelial cells. Inflammation and Regeneration, 38(1), 25.

Tukey, J.W. (1977), Exploratory Data Analysis, Reading, MA: Addison-Wesley.

Ulrich, F., Carretero-Ortega, J., Menéndez, J., Narvaez, C., Sun, B., Lancaster, E., Pershad, V., Trzaska, S., Véliz, E., Kamei, M., Prendergast, A., Kidd, K. R., Shaw, K. M., Castranova, D. A., Pham, V. N., Lo, B. D., Martin, B. L., Raible, D. W., Weinstein, B. M., & Torres-Vázquez, J. (2016). Reck enables cerebrovascular development by promoting canonical Wnt signaling. Development, 143(6), 1055

Urushibata, H., Sasaki, K., Takahashi, E., Hanada, T., Fujimoto, T., Arai, K., & Yamaha, E. (2021). Control of developmental speed in zebrafish embryos using different incubation temperatures. Zebrafish, 18(5), 316-325.

Vallance, P., & Hingorani, A. (1999). Endothelial nitric oxide in humans in health and disease. International Journal of Experimental Pathology, 80(6), 291–303.

Van Cutsem, E., de Haas, S., Kang, Y.-K., Ohtsu, A., Tebbutt, N. C., Xu, J. M., Yong, W. P., Langer, B., Delmar, P., & Scherer, S. J. (2012). Bevacizumab in combination with chemotherapy as first-line therapy in advanced gastric cancer: A biomarker evaluation from the AVAGAST randomized phase III trial. Journal of Clinical Oncology, 30(17), 2119–2127.

van Impel, A., Zhao, Z., Hermkens, D. M. A., Roukens, M. G., Fischer, J. C., Peterson-Maduro, J., Duckers, H., Ober, E. A., Ingham, P. W., & Schulte-Merker, S. (2014). Divergence of zebrafish and mouse lymphatic cell fate specification pathways. Development (Cambridge, England), 141(6), 1228–1238.

Vandesompele, J., De Preter, K., Pattyn, F. et al. Accurate normalization of real-time quantitative RT-PCR data by geometric averaging of multiple internal control genes. Genome Biol 3, research0034.1 (2002).

Vettori, A., Greenald, D., Wilson, G. K., Peron, M., Facchinello, N., Markham, E., Sinnakaruppan, M., Matthews, L. C., McKeating, J. A., Argenton, F., & van Eeden, F. J. M. (2017). Glucocorticoids promote Von Hippel Lindau degradation and Hif-1α stabilization. Proceedings of the National Academy of Sciences of the United States of America, 114(37), 9948–9953.

Vicent, D., Ilany, J., Kondo, T., Naruse, K., Fisher, S. J., Kisanuki, Y. Y., & Kahn, C. R. (2003). The role of endothelial insulin signaling in the regulation of vascular tone and insulin resistance. Journal of Clinical Investigation, 111(9), 1373–1380.

Vigna, S. R., Shahid, R. A., & Liddle, R. A. (2014). Ethanol contributes to neurogenic pancreatitis by activation of TRPV1. The FASEB Journal, 28(2), 891–896.

Vogeli, K. M., Jin, S.-W., Martin, G. R., & Stainier, D. Y. R. (2006). A common progenitor for haematopoietic and endothelial lineages in the zebrafish gastrula. Nature, 443(7109), Article 7109.

Vos, M. H., Neelands, T. R., McDonald, H. A., Choi, W., Kroeger, P. E., Puttfarcken, P. S., & Han, P. (2006). TRPV1b overexpression negatively regulates TRPV1 responsiveness to capsaicin, heat and low pH in HEK293 cells. Journal of Neurochemistry, 99(4), 1088–1102.

Wacker, A., & Gerhardt, H. (2011). Endothelial development taking shape. Current Opinion in Cell Biology, 23(6), 676–685.

Wang, H., Cheng, X., Tian, J., Xiao, Y., Tian, T., Xu, F., Hong, X., & Zhu, M. X. (2020). TRPC channels: Structure, function, regulation and recent advances in small molecular probes. Pharmacology & Therapeutics, 209, 107497.

Wang, J., Ye, C., Chen, C., Xiong, H., Xie, B., Zhou, J., Chen, Y., Zheng, S., & Wang, L. (2017). Glucose transporter GLUT1 expression and clinical outcome in solid tumors: A systematic review and meta-analysis. Oncotarget, 8(10), 16875.

Wang Y, Barbacioru C, Hyland F, Xiao W, Hunkapiller KL, Blake J, Chan F, Gonzalez C, Zhang L, Samaha RR. Large scale real-time PCR validation on gene expression measurements from two commercial long-oligonucleotide microarrays. BMC genomics. 2006 Dec;7(1):59.

Wang, Y. F., Lafont, A. G., Lee, Y. C., & Hwang, P. P. (2016). A novel function of calcitonin gene-related peptide in body fluid Cl- homeostasis. Proc Biol Sci, 283(1832).

Waning, J., Vriens, J., Owsianik, G., Stüwe, L., Mally, S., Fabian, A., Frippiat, C., Nilius, B., & Schwab, A. (2007). A novel function of capsaicin-sensitive TRPV1 channels: Involvement in cell migration. Cell Calcium, 42(1), 17–25.

Warnes, G.R., Bolker, B., Bonebakker, L., Gentleman, R., Liaw, W.H.A., Lumley, T., Maechler, M., Magnusson, A., Moeller, S., Schwartz, M. and Venables, B., 2015. gplots: Various R programming tools for plotting data.

Warren, B. (1979). Tumor blood circulation: Angiogenesis, vascular morphology and blood flow of experimental and human tumors. In The Vascular Morphology of Tumors (pp. 1–47). CRC Press, Inc.

Webb, S. E., & Miller, A. L. (2003). Calcium signalling during embryonic development. Nature Reviews Molecular Cell Biology, 4(7), Article 7.

Weber, L. V., Al-Refae, K., Wölk, G., Bonatz, G., Altmüller, J., Becker, C., Gisselmann, G., & Hatt, H. (2016). Expression and functionality of TRPV1 in breast cancer cells. Breast Cancer : Targets and Therapy, 8, 243–252.

Wickham, H. (2016). ggplot2: Elegant Graphics for Data Analysis. Springer International Publishing.

Wieder, M. S., Szlechter, M., Fischman, N., Inker, S., Rusu, I., & Mbekeani, J. N. (2021). Impact of Anxiety Levels and Sleep Patterns on Perceived Pain During Intravitreal Bevacizumab Injections. Ophthalmic Surgery, Lasers and Imaging Retina, 52(9), 498–504.

Wimalawansa SJ. Amylin, calcitonin gene-related peptide, calcitonin, and adrenomedullin: a peptide superfamily. Critical Reviews™ in Neurobiology. 1997;11(2-3).

Witmer, A. N., Vrensen, G. F. J. M., Van Noorden, C. J. F., & Schlingemann, R. O. (2003). Vascular endothelial growth factors and angiogenesis in eye disease. Progress in Retinal and Eye Research, 22(1), 1–29.

Wong, B. W., Zecchin, A., García-Caballero, M., & Carmeliet, P. (2018). Emerging Concepts in Organ-Specific Lymphatic Vessels and Metabolic Regulation of Lymphatic Development. Developmental Cell, 45(3), 289–301.

Wu, J., Strawn, T. L., Luo, M., Wang, L., Li, R., Ren, M., Xia, J., Zhang, Z., Ma, W., Luo, T., Lawrence, D. A., & Fay, W. P. (2015). Plasminogen Activator Inhibitor-1 Inhibits Angiogenic Signaling by Uncoupling VEGF Receptor-2-αVβ3 Integrin Cross-talk. Arteriosclerosis, Thrombosis, and Vascular Biology, 35(1), 111–120.

Xiao, B., Coste, B., Mathur, J., & Patapoutian, A. (2011). Temperature-dependent STIM1 activation induces Ca2+ influx and modulates gene expression. Nature Chemical Biology, 7(6), 351–358.

Yamamoto, K., & Ando, J. (2018). Emerging Role of Plasma Membranes in Vascular Endothelial Mechanosensing. Circulation Journal, 82(11), 2691–2698.

Yang C, Gagnon C, Hou X, Hardy P. Low density lipoprotein receptor mediates anti-VEGF effect of lymphocyte T-derived microparticles in Lewis lung carcinoma cells. Cancer biology & therapy. 2010 Sep 1;10(5):448-56.

Yang, D., Guo, P., He, T., & Powell, C. A. (2021). Role of endothelial cells in tumor microenvironment. Clinical and Translational Medicine, 11(6), e450.

Yang, J. C. (2004). Bevacizumab for Patients with Metastatic Renal Cancer: An Update. Clinical Cancer Research, 10(18), 6367S-6370S.

Yoshiura K, Nakaoka T, Nishishita T, Sato K, Yamamoto A, Shimada S, Saida T, Kawakami Y, Takahashi TA, Fukuda H, Imajoh-Ohmi S. Carbonic anhydrase II is a tumor vessel endothelium–associated antigen targeted by dendritic cell therapy. Clinical cancer research. 2005 Nov 15;11(22):8201-7.

You, Z.-P., Zhang, Y.-L., Shi, K., Shi, L., Zhang, Y.-Z., Zhou, Y., & Wang, C. (2017). Suppression of diabetic retinopathy with GLUT1 siRNA. Scientific Reports, 7, 7437.

Yusen W, Xia W, Shengjun Y, Shaohui Z, Hongzhen Z. The expression and significance of tumor associated macrophages and CXCR4 in non-small cell lung cancer. J BUON. 2018;23(2):398-402.

Zambrano, S., Möller-Hackbarth, K., Li, X., Rodriguez, P. Q., Charrin, E., Schwarz, A., Nyström, J., Wernerson, A. Ö., Lal, M., & Patrakka, J. (2019). GPRC5b Modulates Inflammatory Response in Glomerular Diseases via NF-κB Pathway. Journal of the American Society of Nephrology: JASN, 30(9), 1573–1586.

Zaninetti, C., Gresele, P., Bertomoro, A., Klersy, C., Candia, E. D., Veneri, D., Barozzi, S., Fierro, T., Alberelli, M. A., Musella, V., Noris, P., Fabris, F., Balduini, C. L., & Pecci, A. (2020). Eltrombopag for the treatment of inherited thrombocytopenias: A phase II clinical trial. Haematologica, 105(3), Article 3.

Zhai, K., Liskova, A., Kubatka, P., & Büsselberg, D. (2020). Calcium Entry through TRPV1: A Potential Target for the Regulation of Proliferation and Apoptosis in Cancerous and Healthy Cells. International Journal of Molecular Sciences, 21(11), 4177.

Zhang, J., Gao, B., Zhang, W., Qian, Z., & Xiang, Y. (2018). Monitoring antiangiogenesis of bevacizumab in zebrafish. Drug Design, Development and Therapy, 12, 2423.

Zhang, M., Rehman, J., & Malik, A. B. (2014). Endothelial progenitor cells and vascular repair. Ain the High Cardiovascular Event Rate in Patients with Rheumatoid Arthritis. Qjm, 21(3), 224.

Zhang, Q.-F., Li, Y.-W., Liu, Z.-H., & Chen, Q.-L. (2016). Exposure to mercuric chloride induces developmental damage, oxidative stress and immunotoxicity in zebrafish embryos-larvae. Aquatic Toxicology, 181, 76–85.

Zhang, W., Shen, Z., Luo, H., Hu, X., Zheng, L., & Zhu, X. (2017). The benefits and side effects of bevacizumab for the treatment of recurrent ovarian cancer. Current Drug Targets, 18(10), 1125–1131.

Zhao, X., Zhang, T., Yan, Y., Liu, F., Li, C., Fan, J., Pan, Y., Li, X., & Wang, Y. (2022). Notch signaling regulates vessel structure and function via Hspg2. Gene, 826, 146439.

Zhao, Y., McVeigh, B. M., & Moiseenkova-Bell, V. Y. (2021). Structural Pharmacology of TRP Channels. Journal of Molecular Biology, 433(17), 166914.

Zheng, J. (2013). Molecular Mechanism of TRP Channels. Comprehensive Physiology, 3(1), 221–242.

Zufall, F. (2014). TRPs in olfaction. Handbook of Experimental Pharmacology, 223, 917–933.

Supplementary Material

Supplementary Table 2.1. *The complete list of the differentially expressed genes from HDLECs stimulated with CGRP, compared to PBS control. "Expr" is the average expression and P.values were adjusted using FDR correction.*

Probe	Gene	logFC	Expr	t	P.Value	adj.P.Val	B
ILMN_2199439	CA2	1.787	8.379	15.192	1.15E-15	2.92E-11	21.490
ILMN_1662795	CA2	1.771	9.391	15.153	1.24E-15	2.92E-11	21.445
ILMN_1801584	CXCR4	1.615	8.603	13.415	3.06E-14	4.83E-10	19.276
ILMN_1751904	EDNRB	1.296	8.890	11.374	1.99E-12	2.36E-08	16.233
ILMN_1714691	HOXD10	1.383	7.602	10.648	9.90E-12	9.37E-08	15.004
ILMN_2320888	CXCR4	1.300	7.443	9.820	6.68E-11	5.27E-07	13.501
ILMN_2307903	VCAM1	-1.017	9.565	-9.640	1.02E-10	6.92E-07	13.159
ILMN_2121408	HBEGF	0.956	10.350	9.374	1.94E-10	1.15E-06	12.644
ILMN_3236825	RAPGEF5	0.987	9.549	9.215	2.85E-10	1.50E-06	12.331
ILMN_1654072	CX3CL1	-1.025	8.386	-8.878	6.55E-10	3.10E-06	11.652
ILMN_2371458	CXCR7	1.022	8.330	8.719	9.71E-10	4.18E-06	11.327
ILMN_1700081	FST	0.913	10.630	8.571	1.41E-09	5.56E-06	11.019
ILMN_2087646	HLX	0.953	9.616	8.378	2.30E-09	8.38E-06	10.611
ILMN_1798360	CXCR7	0.901	9.428	8.249	3.20E-09	1.08E-05	10.337
ILMN_1740426	RASD1	0.879	8.994	8.044	5.43E-09	1.71E-05	9.893
ILMN_1712896	FST	1.039	7.874	7.993	6.20E-09	1.75E-05	9.781
ILMN_1745778	SLC45A4	1.284	7.057	7.987	6.30E-09	1.75E-05	9.768
ILMN_1717877	IVNS1ABP	0.974	8.327	7.923	7.43E-09	1.95E-05	9.628
ILMN_1739428	IFIT2	-1.284	6.561	-7.847	9.07E-09	2.26E-05	9.460
ILMN_2397750	IVNS1ABP	0.987	8.369	7.799	1.03E-08	2.43E-05	9.354
ILMN_1799106	MOSC1	1.012	7.486	7.668	1.45E-08	3.27E-05	9.063
ILMN_1781285	DUSP1	0.793	10.262	7.584	1.81E-08	3.90E-05	8.874
ILMN_2053415	LDLR	0.692	11.627	7.489	2.33E-08	4.79E-05	8.660
ILMN_1658494	C13orf15	0.640	12.521	7.300	3.86E-08	7.60E-05	8.229
ILMN_1781514	PCDH17	1.371	5.427	6.988	8.95E-08	0.000169	7.505
ILMN_1689842	SC4MOL	0.885	9.337	6.910	1.11E-07	0.000189	7.322
ILMN_1714988	HOXD8	0.990	6.905	6.909	1.11E-07	0.000189	7.318
ILMN_1699651	IL6	1.110	6.315	6.907	1.12E-07	0.000189	7.313
ILMN_1688775	METRNL	0.754	8.739	6.829	1.38E-07	0.000226	7.130
ILMN_1759954	PTMA	-0.968	8.986	-6.668	2.15E-07	0.000339	6.748
ILMN_1710297	EDNRB	1.301	5.431	6.636	2.34E-07	0.000358	6.672
ILMN_1674908	HOXB5	0.675	9.687	6.555	2.93E-07	0.000434	6.477
ILMN_1685636	KCNN2	-0.662	9.569	-6.388	4.65E-07	0.000667	6.075
ILMN_1709683	RASSF2	0.766	9.532	6.243	6.96E-07	0.000969	5.723
ILMN_1798496	HOXB8	0.890	7.012	6.048	1.20E-06	0.001623	5.245
ILMN_1801307	TNFSF10	-0.583	10.092	-5.962	1.52E-06	0.002004	5.035
ILMN_1813669	ANKS1A	0.577	10.259	5.875	1.95E-06	0.002492	4.819
ILMN_1779852	LOC387934	-0.631	9.113	-5.863	2.01E-06	0.002509	4.790
ILMN_1735996	NOX4	0.581	10.436	5.843	2.13E-06	0.002584	4.741
ILMN_3248551	C2CD4B	-0.664	10.058	-5.808	2.35E-06	0.002786	4.653
ILMN_2352303	RASSF2	0.741	8.859	5.748	2.79E-06	0.003216	4.504
ILMN_1686862	HLX	0.796	7.191	5.729	2.94E-06	0.003309	4.458

ILMN_1720889	SC4MOL	0.588	10.123	5.702	3.17E-06	0.003488	4.391
ILMN_1768226	ARMCX6	1.125	5.524	5.690	3.28E-06	0.003527	4.361
ILMN_1657395	HMGCR	0.610	9.744	5.639	3.79E-06	0.003987	4.233
ILMN_1692177	TSC22D1	0.604	9.248	5.569	4.61E-06	0.004743	4.060
ILMN_1744949	RHOBTB3	-0.816	8.136	-5.554	4.82E-06	0.004848	4.022
ILMN_1798210	E2F7	-0.645	8.264	-5.514	5.39E-06	0.005312	3.922
ILMN_1697448	TXNIP	-0.619	9.525	-5.475	6.01E-06	0.005804	3.826
ILMN_1782922	PDE4B	0.622	8.694	5.462	6.25E-06	0.005915	3.791
ILMN_1808590	GUCY1A3	-0.826	6.530	-5.446	6.52E-06	0.005953	3.753
ILMN_1655595	SERPINE2	-0.565	9.702	-5.445	6.54E-06	0.005953	3.751
ILMN_2391976	SLC45A4	1.098	6.031	5.433	6.77E-06	0.006044	3.720
ILMN_1764709	MAFB	-0.877	6.250	-5.405	7.33E-06	0.00642	3.650
ILMN_3305938	SGK1	0.503	11.038	5.393	7.59E-06	0.006434	3.619
ILMN_1696302	FABP5	-0.544	10.246	-5.392	7.61E-06	0.006434	3.616
ILMN_1742052	SERPINB9	0.831	6.487	5.327	9.13E-06	0.00758	3.455
ILMN_1684197	GPKOW	0.723	7.438	5.263	1.10E-05	0.008936	3.294
ILMN_1805543	ADAMTS9	1.003	5.932	5.231	1.20E-05	0.009629	3.213
ILMN_1802205	RHOB	-0.486	10.559	-5.211	1.27E-05	0.010026	3.162
ILMN_1680692	NUCKS1	-0.929	6.415	-5.203	1.30E-05	0.010072	3.143
ILMN_1755383	LRRC1	0.778	8.853	5.168	1.43E-05	0.010899	3.056
ILMN_1724493	LYSMD2	0.568	9.187	5.164	1.45E-05	0.010899	3.044
ILMN_1659913	ISG20	0.572	9.288	5.152	1.50E-05	0.011087	3.015
ILMN_1760412	SHISA2	-0.937	5.994	-5.138	1.56E-05	0.011195	2.980
ILMN_1790160	KIT	0.968	5.812	5.138	1.56E-05	0.011195	2.979
ILMN_2094360	NR2F2	-0.585	9.408	-5.109	1.69E-05	0.011863	2.908
ILMN_2376205	LTB	-0.489	10.643	-5.107	1.70E-05	0.011863	2.901
ILMN_2325763	VCAM1	-1.101	5.948	-5.076	1.86E-05	0.012628	2.824
ILMN_1738095	PER2	0.828	6.277	5.075	1.87E-05	0.012628	2.820
ILMN_1782439	CNN3	0.438	12.586	5.050	2.00E-05	0.013326	2.760
ILMN_3241870	FRMD8	0.523	9.993	5.042	2.05E-05	0.013459	2.739
ILMN_2342066	METRNL	0.799	6.439	5.035	2.09E-05	0.013544	2.721
ILMN_1689456	ZBTB20	-0.798	7.197	-5.026	2.14E-05	0.013699	2.699
ILMN_1696048	C13orf33	0.658	7.494	5.007	2.26E-05	0.01428	2.650
ILMN_1713846	PPM1H	-0.861	5.950	-4.934	2.78E-05	0.017292	2.468
ILMN_1741970	JUP	0.667	7.308	4.894	3.11E-05	0.019138	2.366
ILMN_1748751	NLF2	-0.474	10.079	-4.881	3.23E-05	0.0196	2.333
ILMN_2041101	ANXA2P1	-0.449	12.461	-4.864	3.39E-05	0.020292	2.291
ILMN_1790014	METRNL	0.940	6.366	4.856	3.47E-05	0.02037	2.271
ILMN_2414533	ARMCX6	0.507	9.442	4.854	3.49E-05	0.02037	2.265
ILMN_1702487	SGK	0.432	11.632	4.842	3.61E-05	0.020831	2.235
ILMN_1758164	STC1	0.829	6.404	4.809	3.96E-05	0.022588	2.152
ILMN_1689353	APLN	0.493	9.807	4.801	4.04E-05	0.022707	2.133
ILMN_1773470	ST5	-0.760	6.440	-4.795	4.12E-05	0.022707	2.118
ILMN_1685371	SUMF2	0.689	7.363	4.792	4.15E-05	0.022707	2.110
ILMN_1766955	VCAM1	-0.756	6.544	-4.784	4.24E-05	0.022707	2.091
ILMN_1885728	KIAA1147	-0.704	7.148	-4.782	4.27E-05	0.022707	2.085

ILMN_1713163	SMARCA5	-0.647	8.063	-4.762	4.52E-05	0.023779	2.034
ILMN_3236021	LOC100133923	-0.703	8.470	-4.755	4.61E-05	0.023952	2.018
ILMN_1723522	APOLD1	0.863	7.179	4.748	4.70E-05	0.02416	2.000
ILMN_3241834	LOC100134504	-0.510	8.945	-4.739	4.82E-05	0.024545	1.977
ILMN_1738578	FILIP1L	-0.507	9.091	-4.728	4.97E-05	0.024907	1.949
ILMN_1656501	DUSP5	0.513	9.387	4.725	5.01E-05	0.024907	1.942
ILMN_1753111	NAMPT	0.540	9.336	4.722	5.05E-05	0.024907	1.935
ILMN_3251404	NUCKS1	-0.576	10.792	-4.686	5.59E-05	0.027031	1.845
ILMN_3248218	SNORD104	0.786	6.955	4.686	5.60E-05	0.027031	1.844
ILMN_2379734	CTBP1	1.166	5.890	4.667	5.90E-05	0.02798	1.797
ILMN_1668514	PIP5K1C	0.558	9.059	4.667	5.91E-05	0.02798	1.795
ILMN_2134056	SOX7	-0.550	8.537	-4.640	6.37E-05	0.029371	1.729
ILMN_1720771	STX11	0.644	7.376	4.639	6.38E-05	0.029371	1.727
ILMN_1803801	LRRC38	0.755	6.347	4.639	6.39E-05	0.029371	1.726
ILMN_2262275	TRIM13	-0.680	7.222	-4.621	6.73E-05	0.03013	1.680
ILMN_1664398	LOC651621	0.852	6.286	4.620	6.74E-05	0.03013	1.679
ILMN_2059452	SLC12A2	-0.592	8.599	-4.620	6.75E-05	0.03013	1.678
ILMN_1659792	HOXD9	0.722	6.524	4.593	7.27E-05	0.031043	1.611
ILMN_1744381	SERPINE1	-0.412	12.566	-4.592	7.30E-05	0.031043	1.607
ILMN_2309926	ZDHHC14	-0.545	9.253	-4.590	7.33E-05	0.031043	1.604
ILMN_1696027	LOC642333	-0.756	8.078	-4.588	7.39E-05	0.031043	1.597
ILMN_2392080	DCAF6	-0.817	6.176	-4.587	7.39E-05	0.031043	1.597
ILMN_1740900	BMP4	-0.528	10.014	-4.585	7.44E-05	0.031043	1.591
ILMN_1813240	EIF1AX	-0.631	8.019	-4.585	7.45E-05	0.031043	1.590
ILMN_1676629	INSIG2	0.602	8.325	4.583	7.48E-05	0.031043	1.586
ILMN_1720048	CCL2	-0.434	12.492	-4.559	8.01E-05	0.032968	1.525
ILMN_2359287	ITGA6	-0.566	8.511	-4.548	8.26E-05	0.033698	1.498
ILMN_1788955	PDLIM1	0.420	10.978	4.526	8.77E-05	0.035118	1.444
ILMN_1701247	LOC132241	0.595	7.557	4.521	8.91E-05	0.035118	1.430
ILMN_1655710	LOC642989	-0.543	9.967	-4.518	8.98E-05	0.035118	1.424
ILMN_1805192	ITPRIP	0.522	9.576	4.518	8.98E-05	0.035118	1.423
ILMN_3245707	RIMKLB	0.613	7.536	4.503	9.37E-05	0.036359	1.385
ILMN_1679025	LOC641848	-0.706	7.400	-4.498	9.51E-05	0.036588	1.372
ILMN_2110829	LOC441743	-0.686	7.834	-4.493	9.64E-05	0.036771	1.361
ILMN_1785191	TMEM14A	0.646	7.964	4.488	9.77E-05	0.036969	1.349
ILMN_1701789	IFIT3	-0.779	6.235	-4.472	0.000102	0.038173	1.308
ILMN_2330787	FRMD6	-0.513	9.123	-4.471	0.000102	0.038173	1.306
ILMN_1673119	AFF1	1.033	5.325	4.453	0.000108	0.039846	1.261
ILMN_1663080	LFNG	-0.500	8.978	-4.438	0.000113	0.040963	1.222
ILMN_1741021	CH25H	-0.586	7.736	-4.414	0.00012	0.043449	1.163
ILMN_2214790	LAMB1	-0.498	8.827	-4.394	0.000127	0.045452	1.112
ILMN_3201221	LOC341315	-0.595	8.480	-4.392	0.000128	0.045452	1.110
ILMN_1759628	ATP1B3	-0.424	10.490	-4.385	0.00013	0.046054	1.091
ILMN_1685714	INHBB	0.749	6.063	4.379	0.000133	0.04649	1.076
ILMN_1698100	ANXA2P1	-0.452	9.721	-4.374	0.000134	0.046744	1.065
ILMN_2091123	HCG2P7	-0.559	11.109	-4.364	0.000138	0.047711	1.040

ILMN_1797594	NFAT5	-0.786	6.994	-4.358	0.000141	0.048263	1.023
ILMN_1782331	TDG	-0.628	7.666	-4.345	0.000146	0.049112	0.992
ILMN_1772241	SQLE	0.462	9.111	4.345	0.000146	0.049112	0.992
ILMN_1750278	FTHL12	-0.442	11.880	-4.342	0.000147	0.049112	0.984
ILMN_1787750	CD200	0.620	7.140	4.341	0.000148	0.049112	0.981
ILMN_1658989	MEX3B	-0.643	7.137	-4.339	0.000148	0.049112	0.976
ILMN_1695945	MEIS2	-0.586	7.196	-4.330	0.000152	0.049988	0.954

Supplementary Table 2.2. *The complete list of the differentially expressed genes from HDLECs stimulated with Adrenomedullin, compared to PBS control. "Expr" is the average expression and P.values were adjusted using FDR correction.*

Probe	Gene	logFC	Expr	t	P.Value	adj.P.Val	B
ILMN_1662795	CA2	1.160	9.085	9.459	3.79E-10	1.03E-05	8.047
ILMN_1751904	EDNRB	1.084	8.784	9.396	4.37E-10	1.03E-05	7.977
ILMN_2199439	CA2	1.009	7.990	7.569	3.37E-08	0.000531	5.652
ILMN_3236825	RAPGEF5	0.833	9.471	7.305	6.53E-08	0.000773	5.269
ILMN_1745778	SLC45A4	1.029	6.930	6.691	3.16E-07	0.002993	4.327
ILMN_1799106	MOSC1	0.847	7.403	6.057	1.68E-06	0.013225	3.287
ILMN_1695157	CA4	0.903	6.467	5.980	2.06E-06	0.013894	3.157
ILMN_2397750	IVNS1ABP	0.722	8.237	5.786	3.45E-06	0.018881	2.824
ILMN_1740200	LOC728216	1.116	5.625	5.750	3.80E-06	0.018881	2.761
ILMN_1801584	CXCR4	0.734	8.162	5.733	3.99E-06	0.018881	2.730
ILMN_1759954	PTMA	-0.796	9.072	-5.567	6.23E-06	0.026628	2.440
ILMN_1714691	HOXD10	0.774	7.297	5.537	6.75E-06	0.026628	2.387
ILMN_1779852	LOC387934	-0.605	9.125	-5.450	8.53E-06	0.029546	2.233
ILMN_2307903	VCAM1	-0.578	9.785	-5.441	8.74E-06	0.029546	2.217
ILMN_1781514	PCDH17	1.054	5.268	5.414	9.42E-06	0.029621	2.168
ILMN_2053415	LDLR	0.529	11.546	5.371	1.06E-05	0.029621	2.091
ILMN_1703337	LOC441763	-0.957	6.272	-5.336	1.16E-05	0.029621	2.030
ILMN_1658494	C13orf15	0.487	12.444	5.332	1.18E-05	0.029621	2.021
ILMN_1700081	FST	0.638	10.493	5.325	1.20E-05	0.029621	2.010
ILMN_1689842	SC4MOL	0.690	9.239	5.309	1.25E-05	0.029621	1.980
ILMN_1740917	SCNN1B	0.838	6.368	5.237	1.52E-05	0.034234	1.851
ILMN_3289352	LOC642828	-0.641	9.323	-5.148	1.93E-05	0.04156	1.690
ILMN_1673113	F2RL1	-0.564	9.157	-5.092	2.25E-05	0.046322	1.588

Supplementary Table 2.3. *The complete list of the differentially expressed genes from HDLECs stimulated with Intermedin, compared to PBS control. "Expr" is the average expression and P.values were adjusted using FDR correction.*

Probe	Gene	logFC	Expr	t	P.Value	adj.P.Val	B
ILMN_2199439	CA2	1.338	8.020	8.603	1.20E-09	5.69E-05	6.107
ILMN_1662795	CA2	1.184	8.979	7.898	7.42E-09	0.000172	5.272
ILMN_1807291	CYP1A1	1.447	7.069	7.752	1.09E-08	0.000172	5.089
ILMN_1751904	EDNRB	1.024	8.652	7.112	6.07E-08	0.000718	4.243
ILMN_1700081	FST	0.887	10.529	6.888	1.12E-07	0.001059	3.931
ILMN_1714691	HOXD10	1.110	7.354	6.530	3.00E-07	0.00237	3.414
ILMN_2307903	VCAM1	-0.846	9.735	-6.375	4.61E-07	0.00312	3.185
ILMN_1654072	CX3CL1	-0.995	8.501	-6.322	5.36E-07	0.003173	3.104
ILMN_3236825	RAPGEF5	0.805	9.377	5.929	1.61E-06	0.008489	2.501
ILMN_2121408	HBEGF	0.750	10.172	5.808	2.27E-06	0.010742	2.311
ILMN_1781514	PCDH17	1.377	5.292	5.750	2.68E-06	0.011531	2.218
ILMN_2053415	LDLR	0.644	11.539	5.277	1.03E-05	0.040439	1.451
ILMN_1699651	IL6	1.048	6.179	5.215	1.22E-05	0.042946	1.349
ILMN_1712896	FST	0.856	7.697	5.199	1.28E-05	0.042946	1.323
ILMN_1685636	KCNN2	-0.692	9.623	-5.177	1.36E-05	0.042946	1.286

Supplementary Table 2.4. *A breakdown of the Jensen DISEASES enrichment analysis of differentially expressed genes from CGRP stimulation.*

Enrichment FDR	nGenes	Pathway Genes	Fold Enrichment	Disease	Genes
7.73E-06	11	283	9.134676	Hypertension	SLC12A2 NOX4 NAMPT SERPINE1 CCL2 SGK1 BMP4 EDNRB IL6 VCAM1 APLN
0.000166	6	83	16.9887	Fatty liver disease	NAMPT SERPINE1 CCL2 HMGCR LDLR IL6
0.00017	8	200	9.400412	Coronary artery disease	CX3CL1 SERPINE1 CCL2 HMGCR LDLR IL6 VCAM1 APLN
0.000249	8	219	8.584851	Cerebrovascular disease	NOX4 SERPINE1 CCL2 HMGCR CXCR4 EDNRB IL6 VCAM1
0.004461	5	108	10.88011	Hyperglycemia	NOX4 SERPINE1 CCL2 VCAM1 TXNIP
0.005813	3	25	28.20124	Collagen disease	CCL2 IL6 VCAM1
0.005813	3	26	27.11657	Toxic shock syndrome	SUMF2 EDNRB IL6
0.007846	3	30	23.50103	Hypercalcemia	PDLIM1 IL6 STC1
0.009278	2	7	67.1458	Impetigo	SUMF2 EDNRB
0.011567	3	38	18.55345	Constipation	EDNRB KIT STC1
0.011567	3	37	19.05489	Diabetic retinopathy	SERPINE1 IL6 VCAM1
0.013275	3	41	17.19588	Meningitis	CCL2 SUMF2 IL6
0.014419	2	11	42.72915	Intestinal obstruction	EDNRB KIT
0.014419	2	11	42.72915	Juvenile myoclonic epilepsy	TMEM14A LRRC1
0.014419	4	101	9.307339	Obesity	HOXB5 INHBB ADAMTS9 MEX3B
0.015378	5	182	6.456327	Arthritis	NAMPT CCL2 DUSP1 CXCR4 IL6
0.017943	2	13	36.15543	Perinatal necrotizing enterocolitis	HBEGF IL6

0.023127	3	57	12.36896	Vasculitis	CCL2 IL6 VCAM1
0.024495	2	16	29.37629	Listeriosis	SUMF2 IL6
0.029009	3	64	11.01611	Eosinophilia	IL6 KIT VCAM1
0.031475	3	67	10.52285	Gout	NFAT5 SGK1 STC1
0.034924	2	21	22.38193	Congestive heart failure	HLX CH25H
0.034924	2	21	22.38193	Ureteral disease	SERPINE1 CCL2
0.0401	2	23	20.43568	Connective tissue disease	ANKS1A ISG20
0.040316	5	252	4.662903	Type 2 diabetes mellitus	CXCR4 ADAMTS9 ZBTB20 PDE4B C2CD4B
0.0419	3	80	8.812887	Pancreatitis	CA2 CCL2 IL6
0.057965	3	92	7.66338	Cleft palate	BMP4 MEIS2 MAFB
0.057965	2	30	15.66735	Peritonitis	CCL2 IL6
0.063464	2	32	14.68814	Lipid metabolism disorder	HMGCR LDLR
0.069007	2	34	13.82414	Periodontitis	CCL2 IL6
0.072252	2	36	13.05613	Congenital diaphragmatic hernia	HLX NR2F2
0.072252	2	36	13.05613	Exanthem	IL6 KIT
0.080838	5	322	3.649228	Acquired metabolic disease	ANKS1A PCDH17 STC1 ADAMTS9 TRIM13
0.080838	2	39	12.05181	Mastitis	SUMF2 IL6
0.081098	3	117	6.025905	Dementia	CCL2 CXCR4 IL6
0.081098	3	117	6.025905	Lung disease	SERPINE1 CCL2 VCAM1
0.081098	1	3	78.33677	Monoclonal gammopathy of	MAFB

				uncertain significance	
0.081098	2	41	11.46392	Williams-Beuren syndrome	PDLIM1 SMARCA5
0.092817	1	4	58.75258	Adjustment disorder	ANKS1A
0.092817	1	4	58.75258	Hemophagocytic lymphohistiocytosis	STX11
0.092817	1	4	58.75258	Trichotillomania	HOXB8
0.094267	4	233	4.034512	Cardiovascular system disease	ANKS1A HMGCR LDLR AFF1
0.094937	1	5	47.00206	Acrodysostosis	PDE4B
0.094937	1	5	47.00206	Disseminated intravascular coagulation	FRMD6
0.094937	1	5	47.00206	Donohue Syndrome	PDLIM1
0.094937	1	5	47.00206	Lethal congenital contracture syndrome	PIP5K1C
0.094937	2	51	9.216091	Orofacial cleft	FILIP1L MAFB
0.094937	1	5	47.00206	POEMS syndrome	IL6
0.094937	2	50	9.400412	Syndactyly	HOXD9 HOXD8
0.094937	1	5	47.00206	Venous insufficiency	SERPINE1
0.096344	1	6	39.16838	Boutonneuse fever	CD200
0.096344	3	147	4.796129	Diarrhea	SUMF2 IL6 KIT
0.096344	1	6	39.16838	Gastrointestinal stromal tumor	KIT
0.096344	1	6	39.16838	Goldberg-Shprintzen syndrome	EDNRB
0.096344	2	54	8.704086	Hyperinsulinism	SERPINE1 IL6

0.096344	3	144	4.896048	Lymphoid leukemia	SGK1 KIT PDE4B
0.096344	1	6	39.16838	Pervasive developmental disorder	LRRC1
0.096344	1	6	39.16838	Skin melanoma	EIF1AX
0.096344	1	6	39.16838	Spastic hemiplegia	TDG
0.105044	1	7	33.5729	Abdominal aortic aneurysm	CCL2
0.105044	1	7	33.5729	Irritant dermatitis	FABP5
0.105044	2	62	7.580978	Pneumonia	SUMF2 IL6
0.105044	1	7	33.5729	Estrogen-receptor positive breast cancer	TMEM14A
0.107818	1	8	29.37629	Aortic valve stenosis	PDLIM1
0.107818	1	8	29.37629	Chondroma	KIT
0.107818	1	8	29.37629	Gastroschisis	HOXB5
0.107818	2	66	7.121525	Human immunodeficiency virus infectious disease	CCL2 CXCR4
0.107818	1	8	29.37629	Lassa fever	CH25H
0.107818	1	8	29.37629	Multiple myeloma	MAFB
0.107818	1	8	29.37629	Small intestine cancer	SLC12A2
0.110395	4	290	3.241522	Cancer	KIT AFF1 MAFB TXNIP
0.110395	2	72	6.528064	Cleft lip	BMP4 MAFB
0.110395	1	9	26.11226	Fibrosarcoma	MAFB
0.110395	1	9	26.11226	Hepatic vein thrombosis	SLC12A2

0.110395	1	9	26.11226	Interstitial cystitis	HBEGF
0.110395	1	9	26.11226	Macular retinal edema	IL6
0.110395	1	9	26.11226	Ritter's disease	EDNRB
0.111841	1	10	23.50103	Bone cancer	KIT
0.111841	1	10	23.50103	Campylobacteriosis	SUMF2
0.111841	1	10	23.50103	Esotropia	CD200
0.111841	1	10	23.50103	Hirschsprung's disease	EDNRB
0.111841	1	10	23.50103	Smooth muscle tumor	KIT
0.111841	1	10	23.50103	Spondylocostal dysostosis	LFNG
0.111841	2	75	6.266942	Vascular disease	TSC22D1 LDLR
0.112438	1	12	19.58419	Acanthosis nigricans	PDLIM1
0.112438	1	14	16.78645	Appendicitis	IL6
0.112438	1	13	18.07772	Bacterial vaginosis	IL6
0.112438	1	11	21.36457	Bacteriuria	IL6
0.112438	1	14	16.78645	Bullous pemphigoid	ITGA6
0.112438	1	13	18.07772	Congenital bile acid synthesis defect	CA2
0.112438	1	14	16.78645	Cryoglobulinemia	DUSP1
0.112438	1	13	18.07772	Cystitis	IL6
0.112438	1	13	18.07772	Dry eye syndrome	IL6
0.112438	1	14	16.78645	Epidermolysis bullosa	ITGA6

0.112438	1	14	16.78645	Fibrodysplasia ossificans progressiva	BMP4
0.112438	1	12	19.58419	Gingivitis	IL6
0.112438	1	11	21.36457	Hypokalemic periodic paralysis	KCNN2
0.112438	1	12	19.58419	Ileus	IL6
0.112438	2	91	5.165062	Influenza	CCL2 IL6
0.112438	1	14	16.78645	LEOPARD syndrome	JUP
0.112438	1	13	18.07772	Limb ischemia	CXCR4
0.112438	1	13	18.07772	Mitral valve insufficiency	PTMA
0.112438	1	11	21.36457	Mowat-Wilson syndrome	EDNRB
0.112438	1	14	16.78645	Multiple endocrine neoplasia type 2B	EDNRB
0.112438	1	13	18.07772	Myositis	CCL2
0.112438	1	13	18.07772	Neurogenic bladder	PIP5K1C
0.112438	1	11	21.36457	Osteopetrosis	CA2
0.112438	1	13	18.07772	Otosclerosis	BMP4
0.112438	1	13	18.07772	Parasitic helminthiasis infectious disease	IL6
0.112438	1	13	18.07772	Piebaldism	EDNRB
0.112438	1	13	18.07772	Prostatitis	IL6
0.112438	1	13	18.07772	Renal tubular acidosis	CA2
0.112438	1	13	18.07772	Shipyard eye	TRIM13

0.112438	1	14	16.78645	Stomach cancer	ZBTB20
0.112438	1	11	21.36457	Theileriasis	MAFB
0.112438	1	11	21.36457	Uveal melanoma	EIF1AX
0.11525	1	15	15.66735	Leptospirosis	SUMF2
0.11525	1	15	15.66735	Mitral valves prolapse	PDLIM1
0.11525	1	15	15.66735	Plague	SUMF2
0.11525	1	15	15.66735	Shigellosis	SUMF2
0.11525	2	94	5.000219	Thrombocytopenia	IL6 KIT
0.117809	1	16	14.68814	Angiomyolipoma	KIT
0.117809	1	16	14.68814	Lissencephaly	LAMB1
0.117809	1	16	14.68814	Macroglobulinemia	CXCR4
0.117809	1	16	14.68814	Megaloblastic anemia	DUSP5
0.117809	1	16	14.68814	Neurilemmoma	KIT
0.119233	1	17	13.82414	3p- syndrome	CA2
0.119233	1	17	13.82414	Cholangitis	IL6
0.119233	2	100	4.700206	Pain agnosia	IL6 TRIM13
0.119233	1	17	13.82414	Synostosis	BMP4
0.119233	1	17	13.82414	Takayasu's arteritis	IL6
0.119233	1	17	13.82414	Testicular cancer	KIT
0.123184	1	18	13.05613	Ectopic pregnancy	FST
0.123184	1	18	13.05613	Paget's disease of bone	CXCR4

0.123184	1	18	13.05613	Pelvic inflammatory disease	SLC12A2
0.126936	1	19	12.36896	Multiple endocrine neoplasia type 2A	EDNRB
0.126936	1	19	12.36896	Osteomyelitis	SUMF2
0.126936	1	19	12.36896	Withdrawal disorder	TRIM13
0.131435	1	20	11.75052	Renal oncocytoma	KIT
0.131435	1	20	11.75052	Typhoid fever	SUMF2
0.13483	1	21	11.19097	Brain edema	SLC12A2
0.13483	1	21	11.19097	Chediak-Higashi syndrome	STX11
0.13483	1	21	11.19097	Seasonal affective disorder	PER2
0.13609	1	22	10.68229	Agammaglobulinemia	CXCR4
0.13609	2	118	3.983226	Bipolar disorder	SLC45A4 KIT
0.13609	1	22	10.68229	Diphtheria	HBEGF
0.13609	1	22	10.68229	Hypertrichosis	PDLIM1
0.13609	1	22	10.68229	Obstructive sleep apnea	IL6
0.13609	1	22	10.68229	Pulmonary fibrosis	NOX4
0.139267	1	23	10.21784	Leiomyoma	KIT
0.139267	1	23	10.21784	Lyme disease	IL6
0.144067	1	24	9.792096	Mastocytosis	KIT
0.14686	1	25	9.400412	Chronic fatigue syndrome	IL6

0.14686	1	25	9.40041 2	Familial adenomatous polyposis	HBEGF
0.14686	1	25	9.40041 2	Lymphedema	APOLD1
0.14858 4	1	26	9.03885 8	Hyperhomocys teinemia	SERPINE1
0.14858 4	2	128	3.67203 6	Immune system cancer	SGK1 KIT
0.14858 4	1	26	9.03885 8	Microphthalmi a	BMP4
0.14858 4	1	26	9.03885 8	Synovitis	IL6
0.15301 6	1	27	8.70408 6	Hemangioma	CA2
0.15737 2	1	28	8.39322 5	Bronchitis	IL6
0.16688	1	30	7.83367 7	Otitis media	IL6
0.16693 4	1	31	7.58097 8	Arthropathy	IL6
0.16693 4	1	31	7.58097 8	Cholera	SUMF2
0.16693 4	1	31	7.58097 8	Sickle cell anemia	VCAM1
0.16693 4	1	31	7.58097 8	Vaccinia	SLC12A2
0.16693 4	1	31	7.58097 8	Obsessive-compulsive disorder	HOXB8
0.17487 8	1	33	7.12152 5	Clubfoot	HOXD10
0.17487 8	1	33	7.12152 5	Gonadoblastom a	KIT
0.17736 7	1	34	6.91206 8	Acute cystitis	SUMF2
0.17736 7	1	35	6.71458	Brain ischemia	IL6
0.17736 7	1	35	6.71458	Leishmaniasis	IL6
0.17736 7	1	35	6.71458	Leukopenia	IL6

0.177367	1	35	6.71458	Neurofibromatosis	KIT
0.177367	1	35	6.71458	Pulmonary embolism	SERPINE1
0.177367	1	34	6.912068	Pre-eclampsia	INHBB
0.180013	1	36	6.528064	Tooth agenesis	BMP4
0.180013	1	36	6.528064	Uveitis	IL6
0.188177	1	38	6.184482	Post-traumatic stress disorder	HBEGF
0.191661	1	39	6.025905	Common cold	IL6
0.192957	1	40	5.875258	Candidiasis	IL6
0.192957	1	40	5.875258	Gastritis	IL6
0.192957	1	40	5.875258	Skin disease	VCAM1
0.196302	1	41	5.731959	Ptosis	CA2
0.199593	1	42	5.595484	Gastroenteritis	SUMF2

Supplementary 3.1. *Code for the RNAseq alignment followed by DESeq analysis.*

Download reference genome from NCBI:

wget http://ftp.ensembl.org/pub/release-103/fasta/danio_rerio/dna/Danio_rerio.GRCz11.dna_sm.primary_assembly.fa.gz

gunzip Danio_rerio.GRCz11.dna_sm.primary_assembly.fa.gz

wget http://ftp.ensembl.org/pub/release-103/gtf/danio_rerio/Danio_rerio.GRCz11.103.gtf.gz

gunzip Danio_rerio.GRCz11.103.gtf.gz

Generate reference genome in STAR:

STAR --runThreadN 6 --runMode genomeGenerate --genomeDir /home/591608/DanioAssembly --genomeFastaFiles Danio_rerio.GRCz11.dna_sm.primary_assembly.fa --sjdbGTFfile Danio_rerio.GRCz11.103.chr.gtf --sjdbOverhang 100

All reads underwent fastqc to check quality:

cd /home/591608/TempStress/SRP180876

fastqc *.fastq

Perform STAR alignment against reference genome:

for i in $(cat /home/591608/SRP180876.txt);

do STAR --runThreadN 6

--runMode alignReads

--genomeDir /home/591608/DanioAssembly # The location of your reference assembly

--readFilesIn /home/591608/TempStress/SRP180876/$i_1.fastq,/home/591608/TempStress/SRP180876/$i_2.fastq # This combines the paired reads into one output.

--readFilesIn /home/591608/TempStress/SRP180876/$i.fastq #This is for if the reads are not paired. if you copy this code, you can hash/unhash these two lines depending on pairing.

--quantMode TranscriptomeSAM GeneCounts

--outFileNamePrefix TempStressAligned/SRP180876/$i. \

--outSAMtype BAM SortedByCoordinate

--outSAMunmapped None

--outSAMattributes Standard;

Done

R installed required packages and defined directory:

if (!requireNamespace("BiocManager", quietly = TRUE))

install.packages("BiocManager")

```
BiocManager::install("DESeq2")

BiocManager::install("biomaRT")

BiocManager::install("edgeR")

BiocManager::install("limma")

library ("DESeq2")

library("biomaRt")

library("edgeR")

library ("limma")

directory <- "/home/591608/TempStressAligned/SRP180876"
```

Define the sample files you want to load in:

```
sampleFiles <- grep("*ReadsPerGene.out.tab$",list.files(directory),value=TRUE)
```

State their experimental conditions in order:

```
sampleCondition <- c("KD", "KD", "KD","wt", "wt", "wt", "wt","SCR","SCR","SCR")
```

Read the samples in as a DESeq dataset:

```
sampleTable <- data.frame(sampleName = sampleFiles, fileName = sampleFiles, condition = sampleCondition)

sampleTable$condition <- factor(sampleTable$condition)

dds <- DESeqDataSetFromHTSeqCount(sampleTable = sampleTable, directory = directory, design= ~ condition)
```

Tidy up the data and remove low reads:

```
dds2 <- dds[-c(1,2,3,4),]

keep <- rowSums(counts(dds2)) >= 10

dds2 <- dds2[keep,]
```

Perform DESeq analysis:

```
dds3 <- dds2[,c(1:3,7:9)] # select the Scrambled and Knockdown columns

dds3$condition <- relevel(dds3$condition, ref = "SCR")

des <- DESeq(dds3)

results <- results(des)
```

Change ENSEMBL IDs to gene symbols using biomaRT:

```
genes <- rownames(results)

ensembl <- useMart("ensembl", host= "www.ensembl.org", dataset= "drerio_gene_ensembl")

genes_ensembl_org <- getBM(attributes <- c("entrezgene_id", "ensembl_gene_id", "external_gene_name",
"description"), filters = "ensembl_gene_id", values = genes, mart = ensembl, uniqueRows=T)
```

```
pmatch_table <- pmatch(genes, genes_ensembl_org[,2], duplicates.ok=T)

ensembl_table <- as.data.frame(matrix(NA, nrow=length(genes), ncol=8))

ensembl_table[which(!is.na(pmatch_table)),] <- genes_ensembl_org[pmatch_table[(!is.na(pmatch_table))], ];

rownames(ensembl_table) <- genes;

colnames(ensembl_table) <- colnames(genes_ensembl_org);

results2 <- cbind(ensembl_table[,3:4], results);

colnames(results2) <- c("symbol", "description",  colnames(dds2));

rownames(results2) <- rownames(results)
```

Supplementary 3.2. *RNA-Seq Adapter sequences*

>polyG

GGGGGGGGGGGGGGGGGGGGGGGGGGGGGGGGGGGGGGGGGGGGGGGGGG

>1

GATCGGAAGAGCACACGTCTGAACTCCAGTCACATCACGATCTCGTATGCCGTCTTCTGCTTG

>2

GATCGGAAGAGCACACGTCTGAACTCCAGTCACCGATGTATCTCGTATGCCGTCTTCTGCTTG

>3

GATCGGAAGAGCACACGTCTGAACTCCAGTCACTTAGGCATCTCGTATGCCGTCTTCTGCTTG

>4

GATCGGAAGAGCACACGTCTGAACTCCAGTCACTGACCAATCTCGTATGCCGTCTTCTGCTTG

>5

GATCGGAAGAGCACACGTCTGAACTCCAGTCACACAGTGATCTCGTATGCCGTCTTCTGCTTG

>6

GATCGGAAGAGCACACGTCTGAACTCCAGTCACGCCAATATCTCGTATGCCGTCTTCTGCTTG

>7

GATCGGAAGAGCACACGTCTGAACTCCAGTCACCAGATCATCTCGTATGCCGTCTTCTGCTTG

>8

GATCGGAAGAGCACACGTCTGAACTCCAGTCACACTTGAATCTCGTATGCCGTCTTCTGCTTG

>9

GATCGGAAGAGCACACGTCTGAACTCCAGTCACGATCAGATCTCGTATGCCGTCTTCTGCTTG

>10

GATCGGAAGAGCACACGTCTGAACTCCAGTCACTAGCTTATCTCGTATGCCGTCTTCTGCTTG

>11

GATCGGAAGAGCACACGTCTGAACTCCAGTCACGGCTACATCTCGTATGCCGTCTTCTGCTTG

>12

GATCGGAAGAGCACACGTCTGAACTCCAGTCACCTTGTAATCTCGTATGCCGTCTTCTGCTTG

>13

GATCGGAAGAGCACACGTCTGAACTCCAGTCACAGTCAACAATCTCGTATGCCGTCTTCTGCTTG

>14

GATCGGAAGAGCACACGTCTGAACTCCAGTCACAGTTCCGTATCTCGTATGCCGTCTTCTGCTTG

>15

GATCGGAAGAGCACACGTCTGAACTCCAGTCACATGTCAGAATCTCGTATGCCGTCTTCTGCTTG

>16

GATCGGAAGAGCACACGTCTGAACTCCAGTCACCCGTCCCGATCTCGTATGCCGTCTTCTGCTTG

>18

GATCGGAAGAGCACACGTCTGAACTCCAGTCACGTCCGCACATCTCGTATGCCGTCTTCTGCTTG

>19

GATCGGAAGAGCACACGTCTGAACTCCAGTCACGTGAAACGATCTCGTATGCCGTCTTCTGCTTG

>20

GATCGGAAGAGCACACGTCTGAACTCCAGTCACGTGGCCTTATCTCGTATGCCGTCTTCTGCTTG

>21

GATCGGAAGAGCACACGTCTGAACTCCAGTCACGTTTCGGAATCTCGTATGCCGTCTTCTGCTTG

>22

GATCGGAAGAGCACACGTCTGAACTCCAGTCACCGTACGTAATCTCGTATGCCGTCTTCTGCTTG

>23

GATCGGAAGAGCACACGTCTGAACTCCAGTCACGAGTGGATATCTCGTATGCCGTCTTCTGCTTG

>25

GATCGGAAGAGCACACGTCTGAACTCCAGTCACACTGATATATCTCGTATGCCGTCTTCTGCTTG

>27

GATCGGAAGAGCACACGTCTGAACTCCAGTCACATTCCTTTATCTCGTATGCCGTCTTCTGCTT

Supplementary Table 3.1. *Biological Function GO Enrichment Results of the differentially expressed genes from the RNA-seq experiment*

Enrichment FDR	nGenes	Pathway Genes	Fold Enrichment	Pathway	GO	Genes
0.065969	2	10	111.6778	Anterior/posterior axon guidance	GO:0033564	robo2 unc5b
0.137389	1	7	79.76984	Branching involved in blood vessel morphogenesis	GO:0001569	unc5b
0.137389	1	7	79.76984	Proline catabolic proc.	GO:0006562	zgc:92040
0.137389	1	11	50.76263	Neural tube closure	GO:0001843	shroom3
0.137389	1	12	46.53241	Proline metabolic proc.	GO:0006560	zgc:92040
0.137389	1	14	39.88492	Morphogenesis of a branching structure	GO:0001763	unc5b
0.121251	2	42	26.58995	Neg. reg. of cell growth	GO:0030308	robo2 osgn1
0.109714	3	84	19.94246	Epithelial cell development	GO:0002064	slc2a1a myh9a shroom3
0.137389	2	78	14.31766	Complement activation	GO:0006956	c3b.2 c3b.1
0.137389	2	82	13.61924	Reg. of cell growth	GO:0001558	robo2 osgn1
0.116653	4	246	9.079494	Angiogenesis	GO:0001525	slc2a1a unc5b myh9a hspg2
0.137389	2	137	8.151663	Immune effector proc.	GO:0002252	c3b.2 c3b.1
0.118912	4	288	7.755401	Blood vessel morphogenesis	GO:0048514	slc2a1a unc5b myh9a hspg2
0.121251	4	324	6.89369	Blood vessel development	GO:0001568	slc2a1a unc5b myh9a hspg2
0.116653	5	421	6.631697	Tube morphogenesis	GO:0035239	slc2a1a unc5b myh9a hspg2 shroom3
0.137389	4	366	6.102611	Vasculature development	GO:0001944	slc2a1a unc5b myh9a hspg2
0.121251	5	527	5.297807	Tube development	GO:0035295	slc2a1a unc5b myh9a hspg2 shroom3
0.117684	6	697	4.806791	Cell adhesion	GO:0007155	itga3b itgb1b.1 dcbld2 hspg2 cdh26.1 comp
0.117684	6	697	4.806791	Biological adhesion	GO:0022610	itga3b itgb1b.1 dcbld2 hspg2 cdh26.1 comp

Supplementary Table 3.2 *Molecular Function GO Enrichment Results of the differentially expressed genes from the RNA-seq experiment*

Enrichment FDR	nGenes	Pathway Genes	Fold Enrichment	Pathway	GO	Genes
0.074876	1	3	186.1296	Proline dehydrogenase activity	GO:0004657	zgc:92040
0.074876	1	3	186.1296	C-X3-C chemokine binding	GO:0019960	itgb1b.1
0.074876	1	3	186.1296	Glucocorticoid receptor binding	GO:0035259	grip1
0.074876	1	5	111.6778	NAD(P)H oxidase H2O2-forming activity	GO:0016174	fmo5
0.074876	1	6	93.06481	Ferroxidase activity	GO:0004322	cp
0.074876	1	6	93.06481	Oxidoreductase activity, acting on metal ions, oxygen as acceptor	GO:0016724	cp
0.074876	1	6	93.06481	5 -flap endonuclease activity	GO:0017108	FO834823.1
0.074876	1	6	93.06481	Flap endonuclease activity	GO:0048256	FO834823.1
0.074876	1	7	79.76984	Netrin receptor activity	GO:0005042	unc5b
0.074876	1	8	69.79861	N,N-dimethylaniline monooxygenase activity	GO:0004499	fmo5
0.074876	1	8	69.79861	Glucose transmembrane transporter activity	GO:0005355	slc2a1a
0.074876	2	79	14.13643	Protein phosphatase regulator activity	GO:0019888	ppp1r14c ppp4r1
0.074876	2	88	12.69066	Phosphatase regulator activity	GO:0019208	ppp1r14c ppp4r1
0.074876	3	266	6.297619	Serine-type endopeptidase activity	GO:0004252	plg tmprss9 f7
0.074876	3	284	5.898474	Serine-type peptidase activity	GO:0008236	plg tmprss9 f7
0.074876	3	284	5.898474	Serine hydrolase activity	GO:0017171	plg tmprss9 f7
0.074876	4	470	4.752246	Actin binding	GO:0003779	myh9b myh9a shroom3
0.074876	4	503	4.440468	Protein-containing complex binding	GO:0044877	myh9b itgb1b.1 myh9a shroom3
0.074876	5	778	3.588618	Cytoskeletal protein binding	GO:0008092	myh9b EML5 myh9a shroom3

***Supplementary Table 3.3** Cellular Component GO Enrichment Results of the differentially expressed genes from the RNA-seq experiment*

Enrichment FDR	nGenes	Pathway Genes	Fold Enrichment	Pathway	URL	Genes
0.086255	1	3	186.1296	Low-density lipoprotein particle	GO:0034362	apoba
0.086255	1	4	139.5972	Protein phosphatase 4 complex	GO:0030289	ppp4r1
0.086255	1	4	139.5972	Very-low-density lipoprotein particle	GO:0034361	apoba
0.086255	1	5	111.6778	Triglyceride-rich plasma lipoprotein particle	GO:0034385	apoba
0.086255	1	5	111.6778	Chylomicron	GO:0042627	apoba
0.095705	1	9	62.04321	Protein-lipid complex	GO:0032994	apoba
0.095705	1	9	62.04321	Plasma lipoprotein particle	GO:0034358	apoba
0.095705	1	9	62.04321	Lipoprotein particle	GO:1990777	apoba
0.117897	1	13	42.95299	SAGA-type complex	GO:0070461	taf5l
0.137461	1	17	32.84641	Melanosome	GO:0042470	itgb1b.1
0.137461	1	17	32.84641	Pigment granule	GO:0048770	itgb1b.1
0.138149	1	18	31.0216	Ruffle membrane	GO:0032587	itgb1b.1
0.086255	2	41	27.23848	Integrin complex	GO:0008305	itga3b itgb1b.1
0.086255	2	41	27.23848	Protein complex involved in cell adhesion	GO:0098636	itga3b itgb1b.1
0.086255	2	47	23.76123	Basal plasma membrane	GO:0009925	erbb3a slc4a1b
0.086255	2	54	20.68107	Basal part of cell	GO:0045178	erbb3a slc4a1b
0.092956	2	87	12.83653	Myosin complex	GO:0016459	myh9b myh9a
0.117897	2	128	8.724826	Plasma membrane signaling receptor complex	GO:0098802	itga3b itgb1b.1
0.095705	3	277	6.047533	Receptor complex	GO:0043235	erbb3a itga3b itgb1b.1
0.095705	3	299	5.602564	Anchoring junction	GO:0070161	itgb1b.1 hspg2 MAGI3

Supplementary Table 3.4*. KEGG Pathway Enrichment Results of the differentially expressed genes from the RNA-seq experiment*

Enrichment FDR	nGenes	Pathway Genes	Fold Enrichment	Pathway	KEGG	Genes
0.105584	1	21	26.58995	Nitrogen metabolism	dre00910	ca2
0.00054	4	96	23.2662	ECM-receptor interaction	dre04512	itga3b itgb1b.1 hspg2 comp
0.17308	1	40	13.95972	Basal transcription factors	dre03022	taf5l
0.018162	4	290	7.701916	Reg. of actin cytoskeleton	dre04810	myh9b itga3b itgb1b.1 myh9a
0.053769	3	229	7.315138	Tight junction	dre04530	myh9b itgb1b.1 myh9a
0.105584	2	164	6.809621	Vascular smooth muscle contraction	dre04270	myh9b myh9a
0.105584	2	168	6.647487	Phagosome	dre04145	itgb1b.1 comp
0.055698	3	258	6.492894	Focal adhesion	dre04510	itga3b itgb1b.1 comp

Supplementary Table 3.5. *ZFIN Disease Enrichment Results of the differentially expressed genes from the RNA-seq experiment*

Enrichment FDR	nGenes	Pathway Genes	Fold Enrichment	Pathway	Genes
7.70E-05	3	12	153.8418	Metabolic acidosis	myh9b slc4a1b myh9a
7.70E-05	3	13	142.0078	Conjunctivitis	c3b.2 plg c3b.1
0.000349	2	3	410.2449	Autosomal dominant Alport syndrome	myh9b myh9a
0.000387	3	27	68.37415	Factor VIII deficiency	c3b.2 c3b.1 cfp
0.000435	3	32	57.69069	Thrombocytopenia	myh9b f7 myh9a
0.000435	2	5	246.1469	MYH-9 related disease	myh9b myh9a
0.000435	5	210	14.6516	Type 1 diabetes mellitus	c3b.2 cp f7 apoba c3b.1
0.000435	3	32	57.69069	Osteochondrodysplasia	hspg2 flnb comp
0.000663	2	7	175.8192	Age related macular degeneration 9	c3b.2 c3b.1
0.000663	2	7	175.8192	Arteriolosclerosis	c3b.2 c3b.1
0.000663	2	7	175.8192	Complement component 3 deficiency	c3b.2 c3b.1
0.000843	3	50	36.92204	Sickle cell anemia	c3b.2 apoba c3b.1
0.000875	3	52	35.50196	Proteinuria	myh9b f7 myh9a
0.000892	2	9	136.7483	Age related macular degeneration 7	c3b.2 c3b.1
0.000974	2	10	123.0735	Orofacial cleft	myh9b myh9a
0.000974	2	10	123.0735	Boutonneuse fever	c3b.2 c3b.1
0.001267	2	12	102.5612	Tropical spastic paraparesis	c3b.2 c3b.1
0.001267	2	12	102.5612	Clubfoot	grip1 flnb
0.001333	3	68	27.14856	Cerebral infarction	plg f7 apoba
0.001347	2	13	94.6719	Lepromatous leprosy	c3b.2 c3b.1
0.001723	2	15	82.04898	Acute myocardial infarction	c3b.2 c3b.1
0.001877	2	16	76.92092	Fuchs' endothelial dystrophy	c3b.2 c3b.1
0.002551	2	19	64.77551	Atypical hemolytic-uremic syndrome	c3b.2 c3b.1
0.002996	2	21	58.60641	Paroxysmal nocturnal hemoglobinuria	c3b.2 c3b.1
0.003161	2	22	55.94249	Silicosis	c3b.2 c3b.1
0.004942	2	28	43.95481	Anterior uveitis	c3b.2 c3b.1
0.00527	2	30	41.02449	Ocular hypertension	c3b.2 c3b.1
0.00527	3	123	15.00896	Diabetes mellitus	slc2a1a f7 apoba
0.005434	2	31	39.70112	Autosomal recessive polycystic kidney disease	c3b.2 c3b.1
0.007235	3	142	13.00072	Rheumatoid arthritis	c3b.2 plg c3b.1
0.007235	2	37	33.2631	Hirschsprung's disease	slc2a1a itgb1b.1
0.009585	3	161	11.46647	Systemic lupus erythematosus	c3b.2 plg c3b.1
0.009585	2	44	27.97124	Kuhnt-Junius degeneration	c3b.2 c3b.1
0.010343	3	170	10.85942	Coronary artery disease	plg f7 apoba
0.010343	2	47	26.18584	Lupus nephritis	c3b.2 c3b.1
0.012264	4	377	6.529097	Myocardial infarction	itga3b plg f7 itgb1b.1
0.012272	2	54	22.79138	Familial hyperlipidemia	f7 apoba

0.012272	3	189	9.767736	Chronic obstructive pulmonary disease	c3b.2 erbb3a c3b.1
0.012272	2	54	22.79138	Pulmonary sarcoidosis	c3b.2 c3b.1
0.012272	2	55	22.37699	Adult respiratory distress syndrome	c3b.2 c3b.1
0.012946	1	3	205.1224	Multiple epiphyseal dysplasia	comp
0.012946	1	3	205.1224	Dextro-looped transposition of the great arteries 1	hspg2
0.012946	1	3	205.1224	Factor VII deficiency	f7
0.012946	1	3	205.1224	Bone development disease	flnb
0.012946	1	3	205.1224	Spinal disease	flnb
0.012946	1	3	205.1224	Retinal artery occlusion	plg
0.012946	1	3	205.1224	Hemangioma	slc2a1a
0.012946	2	61	20.17598	IgA glomerulonephritis	c3b.2 c3b.1
0.012946	2	60	20.51224	Hyperglycemia	f7 hspg2
0.012946	2	64	19.23023	Pulmonary tuberculosis	c3b.2 c3b.1
0.012946	1	3	205.1224	Familial hypobetalipoproteinemia 1	apoba
0.015095	2	71	17.33429	Sensorineural hearing loss	myh9b myh9a
0.015095	1	4	153.8418	Hereditary elliptocytosis	slc4a1b
0.015095	1	4	153.8418	Prothrombin deficiency	f7
0.015095	2	74	16.63155	Human immunodeficiency virus infectious disease	c3b.2 c3b.1
0.015095	2	72	17.09354	Glomerulonephritis	itga3b itgb1b.1
0.015095	1	4	153.8418	Familial hypobetalipoproteinemia 2	apoba
0.015095	1	4	153.8418	Seckel syndrome	cdk5rap2
0.016156	2	78	15.77865	Macular degeneration	c3b.2 c3b.1
0.016156	2	78	15.77865	Atopic dermatitis	c3b.2 c3b.1
0.017356	1	5	123.0735	Hereditary angioedema	f7
0.017356	1	5	123.0735	Inherited blood coagulation disease	f7
0.017356	1	5	123.0735	Hypobetalipoproteinemia	apoba
0.017877	2	85	14.47923	Kidney disease	f7 myh9a
0.01928	1	6	102.5612	Fraser syndrome	grip1
0.01928	1	6	102.5612	Glucosephosphate dehydrogenase deficiency	slc4a1b
0.01928	1	6	102.5612	Hereditary spherocytosis	slc4a1b
0.01928	1	6	102.5612	Biliary tract cancer	apoba
0.020398	4	528	4.661874	Alzheimer's disease	slc2a1a c3b.2 plg c3b.1
0.020398	2	95	12.9551	Rhinitis	c3b.2 c3b.1
0.020895	4	534	4.609493	Type 2 diabetes mellitus	slc2a1a cp f7 apoba
0.020936	1	7	87.90962	CHARGE syndrome	sema3e
0.020936	1	7	87.90962	Bile duct cancer	apoba
0.021514	2	101	12.18549	Systemic scleroderma	c3b.2 c3b.1
0.022856	2	105	11.72128	Arteriosclerosis	f7 apoba
0.022964	1	8	76.92092	Median neuropathy	erbb3a
0.024322	3	309	5.97444	Asthma	c3b.2 f7 c3b.1
0.024834	1	9	68.37415	Carbohydrate metabolic disorder	slc2a1a
0.024834	1	9	68.37415	Common bile duct neoplasm	apoba
0.025045	2	114	10.79592	Hypothyroidism	slc2a1a f7
0.025562	2	116	10.60978	Epilepsy	cp itga3b

0.02593	1	10	61.53673	Osteopetrosis	ca2
0.02593	1	10	61.53673	Gout	plg
0.02593	1	10	61.53673	Wilson disease	cp
0.028166	1	11	55.94249	Congenital hemolytic anemia	slc4a1b
0.03247	1	13	47.33595	Noonan syndrome	plg
0.03247	1	13	47.33595	Acute pancreatitis	f7
0.034543	1	14	43.95481	Vesicoureteral reflux	robo2
0.035373	1	15	41.02449	Carotid stenosis	plg
0.035373	1	15	41.02449	Familial hypercholesterolemia	apoba
0.035373	1	15	41.02449	Familial combined hyperlipidemia	apoba
0.035373	1	15	41.02449	Familial Mediterranean fever	plg
0.03647	2	151	8.150561	Ovarian cancer	f7 apoba
0.036899	1	16	38.46046	Renal tubular acidosis	slc4a1b
0.038358	1	17	36.19808	Cleft palate	flnb
0.038358	1	17	36.19808	Gallbladder cancer	apoba
0.038913	2	160	7.692092	End stage renal failure	myh9b myh9a
0.039754	1	18	34.18707	Chromosome 22q11.2 deletion syndrome, distal	zgc:92040
0.043567	1	20	30.76837	Bilirubin metabolic disorder	f7
0.043567	2	173	7.114073	Diabetic retinopathy	f7 apoba
0.044455	1	21	29.30321	Microcephaly	cdk5rap2
0.044455	3	433	4.263515	Obesity	slc2a1a f7 apoba
0.050193	1	24	25.64031	Thrombophilia	plg
0.051248	1	25	24.61469	Aortic valve stenosis	apoba
0.051248	1	25	24.61469	Lung small cell carcinoma	itgb1b.1
0.054739	1	27	22.79138	Childhood absence epilepsy	slc2a1a
0.060109	1	30	20.51224	Brain edema	cp
0.063423	1	32	19.23023	Intermediate coronary syndrome	f7
0.064753	1	33	18.6475	Iron deficiency anemia	slc4a1b
0.067946	1	35	17.58192	Malaria	slc4a1b
0.074793	1	39	15.77865	Hydrocephalus	itgb1b.1
0.08147	1	43	14.31087	Beta thalassemia	apoba
0.087211	1	47	13.09292	Myopathy	flnb
0.087211	1	47	13.09292	Vascular dementia	plg
0.093516	1	51	12.06603	Cholestasis	cp
0.099667	1	55	11.1885	Hyperthyroidism	cp
0.109842	1	62	9.92528	Autosomal recessive non-syndromic intellectual disability	ank3a
0.109842	1	62	9.92528	Atherosclerosis	plg
0.111321	1	64	9.615115	Nephroblastoma	slc2a1a
0.111321	1	64	9.615115	Carotid artery disease	hspg2
0.115304	1	67	9.184587	Ductal carcinoma in situ	erbb3a
0.120808	1	71	8.667146	Diabetic neuropathy	f7
0.129343	1	77	7.991784	Heart disease	cp
0.132987	1	80	7.692092	Fatty liver disease	apoba
0.138087	1	84	7.325802	Nephrotic syndrome	apoba
0.156598	1	97	6.343993	Colorectal cancer	f7

0.174418	1	110	5.594249	Transitional cell carcinoma	erbb3a
0.180222	1	115	5.35102	Cardiomyopathy	erbb3a

Supplementary Table 3.6 *ZFIN Phenotype Enrichment Results of the differentially expressed genes from the RNA-seq experiment*

Enrichment FDR	nGenes	Pathway Genes	Fold Enrichment	Pathway	Genes
0.021716	2	54	22.79138	Yolk edematous abnormal	slc2a1a myh9a
0.021716	1	3	205.1224	Axon-midline-choice-point-recognition disrupted abnormal	robo2
0.021716	2	21	58.60641	Dorsal-longitudinal-anastomotic-vessel aplastic abnormal	slc2a1a hspg2
0.021716	2	33	37.29499	Glomerular-filtration disrupted abnormal	myh9a shroom3
0.021716	2	25	49.22939	Dorsal-longitudinal-anastomotic-vessel malformed abnormal	slc2a1a unc5b
0.021716	2	41	30.01792	Intersegmental-vessel malformed abnormal	slc2a1a unc5b
0.021716	1	3	205.1224	Embryonic-medial-fin-morphogenesis decreased-process-quality abnormal	itga3b
0.021716	1	3	205.1224	Epidermal-basal-stratum decreased-process-quality abnormal	itga3b
0.021716	1	3	205.1224	Glomerular-basement-membrane morphology abnormal	myh9a
0.021716	1	3	205.1224	Respiratory-gaseous-exchange-by-respiratory-system process-quality abnormal	ca2
0.021716	1	3	205.1224	Trunk-musculature decreased-amount abnormal	hspg2
0.021716	1	3	205.1224	Hair-cell absent abnormal	ca2
0.021716	1	3	205.1224	Pronephros malformed abnormal	myh9a
0.021716	1	3	205.1224	Trunk-musculature dystrophic abnormal	hspg2
0.021716	1	3	205.1224	Regulation-of-heart-rate disrupted abnormal	myh9a
0.021716	1	3	205.1224	Dorsal-aorta collapsed abnormal	hspg2
0.021716	1	3	205.1224	Trunk-musculature refractivity abnormal	hspg2
0.021716	1	3	205.1224	Glomerular-filtration decreased-process-quality abnormal	myh9a
0.021716	1	3	205.1224	Pronephric-glomerular-basement-membrane increased-thickness abnormal	myh9a
0.021716	1	3	205.1224	Olfactory-receptor-cell process-quality abnormal	robo2
0.021716	1	3	205.1224	Anterior-commissure-morphogenesis process-quality abnormal	robo2
0.021716	1	3	205.1224	Supraoptic-tract process-quality abnormal	robo2
0.021716	1	3	205.1224	Postoptic-commissure decreased-width abnormal	robo2
0.021716	1	3	205.1224	Cranial-nerve-VIII defasciculated abnormal	robo2
0.021716	1	3	205.1224	Cranial-nerve-VIII process-quality abnormal	robo2
0.021716	1	3	205.1224	Cranial-nerve-VIII mislocalised abnormal	robo2
0.022089	5	714	4.309295	Pericardium edematous abnormal	slc2a1a myh9a hspg2 setd5 shroom3
0.022089	2	90	13.67483	Heart morphology abnormal	myh9a setd5
0.022089	1	4	153.8418	Glomerular-visceral-epithelial-cell-development disrupted abnormal	shroom3
0.022089	1	5	123.0735	Sprouting-angiogenesis increased-occurrence abnormal	apoba
0.022089	1	6	102.5612	Blood-plasma decreased-amount abnormal	f7
0.022089	1	6	102.5612	Podocyte disorganized abnormal	myh9a

0.022089	1	4	153.8418	Diencephalic-nucleus displaced-to abnormal	robo2
0.022089	1	6	102.5612	Platelet-aggregation disrupted abnormal	dcbld2
0.022089	1	6	102.5612	Subintestinal-vein aplastic abnormal	hspg2
0.022089	1	6	102.5612	Integument circular abnormal	itga3b
0.022089	1	5	123.0735	Sodium-ion-transport disrupted abnormal	ca2
0.022089	1	5	123.0735	Cardiac-ventricle elongated abnormal	hspg2
0.022089	1	4	153.8418	Midbrain-hindbrain-boundary increased-angle-to abnormal	myh9b
0.022089	1	6	102.5612	Retinal-ganglion-cell physical-object-quality abnormal	robo2
0.022089	1	4	153.8418	Retinal-ganglion-cell occurrence abnormal	robo2
0.022089	1	5	123.0735	Intersegmental-vessel unlumenized abnormal	hspg2
0.022089	1	4	153.8418	Trunk-musculature morphology abnormal	hspg2
0.022089	1	6	102.5612	Fin necrotic abnormal	itga3b
0.022089	1	5	123.0735	Intersegmental-vessel decreased-thickness abnormal	slc2a1a
0.022089	1	6	102.5612	Dorsal-fin has-fewer-parts-of-type abnormal	itga3b
0.022089	1	6	102.5612	Pectoral-fin has-fewer-parts-of-type abnormal	itga3b
0.022089	1	4	153.8418	Median-fin-fold rough abnormal	itga3b
0.022089	1	5	123.0735	Anterior/posterior-axon-guidance process-quality abnormal	robo2
0.022089	1	4	153.8418	Actin-filament-bundle-distribution disrupted abnormal	myh9a
0.022089	1	5	123.0735	Sprouting-angiogenesis delayed abnormal	sema3e
0.024188	1	7	87.90962	Head opaque abnormal	slc2a1a
0.024188	1	8	76.92092	Atrium elongated abnormal	hspg2
0.024188	1	8	76.92092	Retinal-ganglion-cell decreased-process-quality abnormal	robo2
0.024188	1	7	87.90962	Retinal-ganglion-cell decreased-occurrence abnormal	robo2
0.024188	1	8	76.92092	Axonal-fasciculation disrupted abnormal	robo2
0.024188	1	8	76.92092	Trunk kinked abnormal	hspg2
0.024188	1	8	76.92092	Myotome shape abnormal	hspg2
0.024188	1	8	76.92092	Pectoral-fin degenerate abnormal	itga3b
0.024188	1	8	76.92092	Fin degenerate abnormal	itga3b
0.024188	1	8	76.92092	Median-fin-fold degenerate abnormal	itga3b
0.024188	1	8	76.92092	Protein-localization disrupted abnormal	hspg2
0.025935	1	9	68.37415	Skeletal-myofibril-assembly disrupted abnormal	hspg2
0.025935	1	9	68.37415	Parachordal-vessel aplastic abnormal	unc5b
0.025935	1	9	68.37415	Retinal-ganglion-cell displaced-to abnormal	robo2
0.027524	1	10	61.53673	Trunk-musculature disorganized abnormal	hspg2
0.027524	1	10	61.53673	Pronephros decreased-amount abnormal	myh9a
0.027524	1	10	61.53673	Medial-fin-morphogenesis process-quality abnormal	itga3b
0.029388	1	11	55.94249	Anal-fin has-fewer-parts-of-type abnormal	itga3b
0.029388	1	11	55.94249	Midbrain-hindbrain-boundary-morphogenesis disrupted abnormal	myh9b
0.031144	1	12	51.28061	Retinal-ganglion-cell mislocalised abnormal	robo2

0.031144	1	12	51.28061	Caudal-fin has-fewer-parts-of-type abnormal	itga3b
0.033251	1	13	47.33595	Pronephric-glomerulus morphology abnormal	myh9a
0.035296	1	14	43.95481	Skeletal-muscle-tissue-development disrupted abnormal	hspg2
0.037284	1	15	41.02449	Sarcomere-organization disrupted abnormal	hspg2
0.038706	1	16	38.46046	Angiogenesis process-quality abnormal	slc2a1a
0.038706	1	16	38.46046	Extension aplastic abnormal	unc5b
0.040052	1	17	36.19808	Intersegmental-vessel process-quality abnormal	slc2a1a
0.040052	1	17	36.19808	Myotome morphology abnormal	hspg2
0.040332	1	18	34.18707	Subintestinal-vein morphology abnormal	apoba
0.040332	1	18	34.18707	Retinal-ganglion-cell-axon-guidance quality abnormal	robo2
0.040332	1	18	34.18707	Blood-vessel-development disrupted abnormal	unc5b
0.040332	1	18	34.18707	Retinal-ganglion-cell misrouted abnormal	robo2
0.042033	1	19	32.38776	Melanocyte irregular-spatial-pattern abnormal	itga3b
0.04369	1	20	30.76837	Retinal-ganglion-cell-axon-guidance process-quality abnormal	robo2
0.044927	3	433	4.263515	Whole-organism decreased-length abnormal	itga3b myh9a hspg2
0.048972	1	23	26.7551	Whole-organism curved-dorsal abnormal	myh9a
0.05048	1	24	25.64031	Retinal-ganglion-cell-axon-guidance disrupted abnormal	robo2
0.051951	1	25	24.61469	Larval-locomotory-behavior process-quality abnormal	setd5
0.055396	1	27	22.79138	Blood-vessel-morphogenesis disrupted abnormal	unc5b
0.062706	1	31	19.85056	Ventricular-system hydrocephalic abnormal	cp
0.065921	1	33	18.6475	Otolith morphology abnormal	cp
0.074797	1	38	16.19388	Intersegmental-vessel decreased-length abnormal	hspg2
0.075889	1	39	15.77865	Midbrain-hindbrain-boundary morphology abnormal	myh9b
0.078816	1	41	15.00896	Pigmentation disrupted abnormal	myh9a
0.081671	1	43	14.31087	Surface-structure quality abnormal	itga3b
0.089873	1	48	12.82015	Whole-organism edematous abnormal	myh9a
0.090738	1	49	12.55852	Trunk bent abnormal	slc2a1a
0.091582	1	50	12.30735	Post-vent-region curved-dorsal abnormal	hspg2
0.09588	1	53	11.6107	Eye morphology abnormal	myh9a
0.096646	1	54	11.39569	Intersegmental-vessel decreased-amount abnormal	hspg2
0.099087	1	56	10.9887	Post-vent-region kinked abnormal	hspg2
0.099799	1	57	10.79592	Angiogenesis disrupted abnormal	hspg2
0.100494	1	58	10.60978	Intersegmental-vessel morphology abnormal	hspg2
0.107694	1	63	9.767736	Whole-organism decreased-pigmentation abnormal	slc2a1a
0.143029	1	86	7.155434	Determination-of-left/right-symmetry disrupted abnormal	cp
0.143228	1	87	7.073188	Somite morphology abnormal	myh9a
0.156985	1	97	6.343993	Liver decreased-size abnormal	rarga
0.161456	1	101	6.092746	Post-vent-region curved-ventral abnormal	hspg2

0.178769	1	114	5.397959	Whole-organism curved abnormal	cp
0.195387	1	127	4.845412	Nervous-system quality abnormal	robo2

Supplementary Material 4.1. *The LAMPrey code which was used in the analysis of the LAMP reactions, using the raw data exported from the StepOne real time thermocycler.*

```
LAMPrey = function(x,df,y,z,hk,f,c,p) {
  library(ggplot2)
  dat = read.csv(choose.files(), header = T)
  colnames(dat)[1] = "Well"
  as.factor = dat$Well
  UsedWells = dat[dat$Well %in% df$well,]
  LAMPDATA = replicate(length(df$well),data.frame(well= replicate(x,1),Cycle = factor(1:x),GREEN=(replicate(x,1)),normalised=(replicate(x,1)),gene =(replicate(x,1)), CT=(replicate(x,1))),simplify = FALSE)
  LAMPDATA = setNames(LAMPDATA, df$well)
  well_list = df$well
  gene_list = df$gene
  ct = data.frame(CT=1:length(df$well))
  rownames(ct) = df$well
  ct$gene = df$gene
  ct$sample = factor(df$sample)
  ctlist = list()
  dat2 = dat[(dat$Well %in% well_list),]
  dat2$gene = gene_list
  dat2$sample = factor(rep(df$sample, x))
  dat2$threshold = y

  cycle_list = unique(dat2$Cycle)
  for (i in unique(well_list)) {
    for (cy in cycle_list) {
      dat2$normalised[dat2$Well == i & dat2$Cycle == cycle_list[cy]]= dat2$GREEN[dat2$Well == i & dat2$Cycle == cycle_list[cy+5]] / (dat2$GREEN[dat2$Cycle == cycle_list[cy] & dat2$Well == i ])
    } }

  for (t in 1:length(df$well)) {
    LAMPDATA[[t]]$well = replicate(x, well_list[t])
    LAMPDATA[[t]]$gene = replicate(x, gene_list[t])
    LAMPDATA[[t]]$GREEN = UsedWells$GREEN[UsedWells$Well == well_list[t]]
    LAMPDATA[[t]]$normalised = LAMPDATA[[t]]$GREEN - LAMPDATA[[t]]$GREEN[LAMPDATA[[t]]$Cycle==25]
    LAMPDATA[[t]]$CT = approx(LAMPDATA[[t]]$normalised, LAMPDATA[[t]]$Cycle, xout=y)[2]
    ct$CT[[t]] = unique(LAMPDATA[[t]]$CT)
  }

  dat_list = replicate(length(unique(ct$gene)), data.frame(CT=(replicate(9,1)), sample = factor(c(rep(1,3),rep(2,3),rep(3,3)))), simplify = FALSE)
  dat_list2 = replicate(length(unique(ct$gene)), data.frame(meanCT=(replicate(3,1)), sample = factor(c(rep(1,1),rep(2,1),rep(3,1))), deltactActin = rep(3,1),deltactELF1A = rep(3,1)), simplify = FALSE)
  dat_list = setNames(dat_list, unique(ct$gene))
  dat_list2 = setNames(dat_list2, unique(ct$gene))

  for (i in unique(ct$gene)){
    dat_list[[i]]$CT = unlist(ct$CT[ct$gene == i])
    dat_list2[[i]]$meanCT[dat_list2[[hk]]$sample == 1] = mean(dat_list[[i]]$CT[dat_list[[hk]]$sample == 1])
    dat_list2[[i]]$meanCT[dat_list2[[i]]$sample == 2] = mean(dat_list[[i]]$CT[dat_list[[i]]$sample == 2])
```

```
      dat_list2[[i]]$meanCT[dat_list2[[i]]$sample == 3] = mean(dat_list[[i]]$CT[dat_list[[i]]$sample
== 3])
      dat_list2[[i]]$deltact = dat_list2[[i]]$meanCT - dat_list2[[hk]]$meanCT
      ctlist[[i]] = (dat_list2[[i]]$deltact)}

    for (i in df$well) {
      df$max[df$well == i] = max(na.omit(dat2$normalised[dat2$Well == i]))
      df$ct[df$well == i] = dat2$Cycle[dat2$normalised == df$max & dat2$Well == i]
    }

    dat3 = data.frame(Well = df$well)
    dat3$gene = df$gene
    dat3$sample = df$sample
    dat3$ct = df$ct
    dat3$normalised = df$max
    dat3$condition = f
    dat3 = dat3[dat3$ct > c,]
    dat3 = dat3[dat3$normalised > p,]

    for (gene in dat3$gene) {
      dat3$meanct[dat3$gene == gene & dat3$sample == 1] = mean(dat3$ct[dat3$gene == gene &
dat3$sample == 1])
      dat3$meanct[dat3$gene == gene & dat3$sample == 2] = mean(dat3$ct[dat3$gene == gene &
dat3$sample == 2])
      dat3$meanct[dat3$gene == gene & dat3$sample == 3] = mean(dat3$ct[dat3$gene == gene &
dat3$sample == 3])
      dat3$deltact[dat3$gene == gene & dat3$sample == 1] = dat3$meanct[dat3$gene == gene &
dat3$sample == 1] - dat3$meanct[dat3$gene == hk & dat3$sample == 1]
      dat3$deltact[dat3$gene == gene & dat3$sample == 2] = dat3$meanct[dat3$gene == gene &
dat3$sample == 2] - dat3$meanct[dat3$gene == hk & dat3$sample == 2]
      dat3$deltact[dat3$gene == gene & dat3$sample == 3] = dat3$meanct[dat3$gene == gene &
dat3$sample == 3] - dat3$meanct[dat3$gene == hk & dat3$sample == 3]
    }

  dat4 = data.frame(gene = rep(unique(df$gene),3))
  dat4$sample = c(rep(1,10),rep(2,10),rep(3,10))
  dat4$condition = f

  for (i in df$gene) {
       dat4$deltact[dat4$gene == i & dat4$sample == 1] = mean(dat3$deltact[dat3$gene == i &
dat3$sample == 1])
       dat4$deltact[dat4$gene == i & dat4$sample == 2] = mean(dat3$deltact[dat3$gene == i &
dat3$sample == 2])
       dat4$deltact[dat4$gene == i & dat4$sample == 3] = mean(dat3$deltact[dat3$gene == i &
dat3$sample == 3])
    }

    ctlist = data.frame(ctlist)



    if(missing(z)) {
        return(dat2)
    }
    else {
      if (z == "deltact"){
        return(ctlist)
      }}
      if (z == "graph"){
        return(ggplot(data = dat2, aes(x=Cycle, y= normalised)) + geom_line(aes(col = Well), size
=1.25) +
```

```
        theme_minimal() + geom_hline(yintercept = p, linetype = 3, size = 1) +
geom_vline(xintercept = c, linetype = 3, size = 1) + facet_wrap(~gene + sample, scales = "free") +
theme(legend.position = "NONE") + labs(title = f)) }

  if ( z == "new"){
   return(dat3)
  }

  if ( z == "newdelta"){
   return(dat4)
  }

   else {
    print("please select one of the following: 'graph' or 'deltact' or 'new'")
   }

 }
```

Supplementary Table 4.1. *The complete list of LAMP primers which were used throughout Chapter 4*

Gene	Primer name	Sequence
CA2	F3 CA2	CA AAG CTG CTC TGA TTG T
	B3 CA2	AA ATG GCA GGG GTA CAG
	FIP CA2	GC AGA CTA CAG AAA ATC CCC AGG TAT GTT CTA GAT TTT GT GCG
	BIP CA2	AC TGC TGA GAC AGC CAG AGA ACA GAT GCC ATC TGT GC
	LF CA2	GC AAG CGG GAA ACC A
	LB CA2	TT AAA AGC CCG GCA GGG A
ACTB	F3 ACTB	CA GCA CTG TGT TGG CAT AC
	B3 ACTB	CT GAC GGT CAG GTC ATC A
	FP ACTB	GC GGT ATC CAT GAG ACC ACC TGT CCT TAC GGA TGT CCA G
	BIP ACTB	CC ATA CCC AGG AAG GAA GGC TCC ATT GGC AAT GAG CGT C
	LF ACTB	CT CCA TCA TGA AGT GCG A
	LB ACTB	AA GAG AGC CTC GGG GCA A
EFLA	F3 EFLA	GA TCT CTC AGG GTT ACG CC
	B3 EFLA	CC AAG AGG AGG GTA GGT AG
	FIP EFLA	CC AGA ACG ACG GTC GAT CTT CGC TGG ATT GCC ACA CTG
	BIP EFLA	AC CCC AAG GCT CTC AAA TCC GAG AAG CTC TCC ACA CAC TG
	LF EFLA	CC TTG AGC TCA GCA AAC TT
	LB EFLA	G TTG AGA TGG TCC CTG GCA
PROX1a	F3 PROX1a	TC CCG TAA CGT GAT CTG TG

	B3 PROX1a	CC CAG CTG ATC AAG TGG T
	FIP PROX1a	CC GTG CTC TCA ACA TGC ACT CAC TTC CAG GAA TCG CTC C
	BIP PROX1a	AC CCT GTC ACG CCG TCA TTC AGC AAC TTC CGC GAG TT
	LF PROX1a	CC AAC GAT TTT GAG GTT CC
	LB PROX1a	CA AAT TTC TCC ATC TGG ATG TAG T
TRPV1	3 TRPV1	AA AAA CAT GAA ACG ACT CAC
	B3 TRPV1	CT GTC TGA CCT TTG TAG T
	FIP TRPV1	CT TGC CTC AAA TTT AAA AGT GCT TCG ACT CAC AAT ATA GT CCA ATG
	BIP TRPV1	AG AAT GAC ACT ATT GAA CAA CTG CTC GGT GTA AGC AGC TTG
	LF TRPV1	CA GCA GGG CTG TCT TTC
	LB TRPV1	GC TGA GAA AAT GGG AGA TTT G
CALCA	F3 CALCA	CT TGA AGC AAT CTT CTC G
	B3 CALCA	C TAT CTG TTG CAC GCA
	FIP CALCA	TC TAA TGC AGC TCC TGC CAG CCT CGT AGT CGC TAA GTG A
	BIP CALCA	CA TCT GGC AAA TAA TCA GAG CGC TGA GCA TCT TAA GGG AC
	LF CALCA	CG CAC TGG AAT CGT CAC
	LB CALCA	GG CAA CAA GAA AAG CGG A
LYVE1	F3 LYVE1a	GT TCA TCT GTG GCT CCT AC
	B3 LYVE1a	GC CAG AAA CAC AGC AAT CA
	FIP LYVE1a	CG AGG AAC ACT GGA CCA ATG GCT GGA GTT CAT CTG AGG GA
	BIP LYVE1a	TG GTC CAC AGG GCT GAT GCT GAT CAG TAA AGC GGC AGG
	LF LYVE1a	AG GGA GTT TAG ATA ATG GGC T

	LB LYVE1a	AG CAG TGG CTC CAC TGA AG
TAF5L	F3 TAF5L	AA ACC GCT GAG GAG ATG G
	B3 TAF5L	GT GCA GGT GCA GGT AGA
	FP TAF5L	CG TAC TGC TGA GGG TCC GCT GAC AGT TCA GAC GGA GTC
	BIP TAF5L	CC AGG CTA CGC TCC TTC CTG AAG AGC GGG AAC AAG ACG
	LF TAF5L	AC ACC ACA TTG GCA CAA C
	LB TAF5L	CT CTG GTA AAG GAG GCG A
GPRC5B	F3 GPRC5B	TG GCT TGG GCT TTA CCT T
	B3 GPRC5B	CT GTG GGG TGT CGT AGT
	FlP GPRC5B	CT CGG TCA CCA AGG CAA CCG CAT CTC GAT TGT GGC GAA
	BIP GPRC5B	C ACG CTA TCC CGG AAA CAC AAG TTC TGT GCG GTA TCT c
	LF GPRC5B	CT AAT GCC GGC TCA TCC
	LB GPRC5B	GCG TCC GTC CAG TC
CXCR3	F 3 CXCR3	CT TCT GGG CTG TAG AGG
	B 3 CXCR3	TG CAG CAA CAG TGA ACC
	FP CXCR3	CA CAG TAG AAA TTG ATC CTG AAC AGA AGG AGT GGA TCT G GC
	BIP CXCR3	A CAT GCT TTC CTG CAT CAG TCT TTT TAC GGG AGT ACA GG
	LF CXCR3	AG TCA GTT TGC AAA GTG GT
	LB CXCR3	CT GTC CAT CGT CCA TGC
F7	F3 F7	CA CGA GGT GTT GAT CAG GA
	B3 F7	TT CTG TGT GGT GCA GAG G
	FIP F7	TT TCT CCT CCA GAC ACT CGC GGC CAA CTC AGG CTG GTT G

	BIP F7	AG CAC ACA GAG GCC ACG AAT GTC ATG CTC ACA TGG ACT G
	LF F7	CC CCG TCT TCA GCT CC
	LB F7	AG TTC TGG AAG ATC TAC GAT GT
CALCR	3 CALCR	TTTTT CAA TGG AGA GGT CC
	B3 CALCR	TG GTA GTTTTT GCC ATT CA
	FIP CALCR	AG CAT CAG ATT GCG TGA TAG TGT TGA GAA GGC ACT GGA T
	BIP CALCR	AG ATC TGC TTC GTA CAC TGC AGT GTT CTG TGT GTC CGT
	LF CALCR	TT CCA AAC TGA ATA CGG TAC TG
	LB CALCR	TC CTC CAT AAC TGA GGT TCA G

Supplementary Table 4.2. *The results of the smear analysis performed on ImageJ for the follow up PCR reaction. 1 denotes presence and 0 is for the absence of that feature.*

Condition	Gene	Smear	200-150bp	150-100bp	100-50bp	worked in lamp (ct)	Smear	All bands	LAMP	Verdict
APB BEV	CALCA	578.899	2672.477	8478.355	2780.012	150	1	1	0	false negative
APB KD	CALCA	889.728	4243.79	12221.284	5214.912	150	1	1	0	false negative
E3 BEV	ELF1A	10393.355	9096.033	12353.891	28119.657	150	1	1	0	false negative
APB BEV	ELF1A	12838.719	9043.79	13683.477	1582.284	150	1	1	0	false negative
APB	CALCA	26250.326	16926.669	8117.355	678.506	150	1	1	0	false negative
E3 KD	CALCA	37803.317	14899.619	1432.87	377.071	150	1	1	0	false negative
E3 KD	TRPV1	0	0	0	0	42.16974899	0	0	1	false positive
APB	CXCR3	0	0	0	0	66.27237833	0	0	1	false positive
E3	CXCR3	0	0	0	0	150	0	0	0	true negative
E3 KD	CXCR3	0	0	0	0	150	0	0	0	true negative
APB KD	CXCR3	0	0	0	0	150	0	0	0	true negative
E3 BEV	CXCR3	0	0	0	0	150	0	0	0	true negative
APB BEV	CXCR3	0	0	0	0	150	0	0	0	true negative
E3	TRPV1	0	0	0	0	150	0	0	0	true negative
APB KD	TRPV1	0	0	0	0	150	0	0	0	true negative
APB KD	ELF1A	1188.556	69.828	184.95	28085.485	150	1	1	0	true negative
APB BEV	TRPV1	0	128.95	449.899	2409.669	51.11443492	0	1	1	true positive
E3 KD	ELF1A	128.95	3176.255	14806.477	6367.154	61.21746999	1	1	1	true positive
APB BEV	ACTB	288.485	2753.941	4124.92	1967.598	56.33715165	1	1	1	true positive
E3	CALCA	1052.263	3390.426	9278.062	4084.083	53.14229526	1	1	1	true positive
E3	ACTB	4857.284	6117.012	4371.92	1567.941	42.14164137	1	1	1	true positive
E3 BEV	CALCA	5089.234	5884.012	7073.062	2284.134	72.39638982	1	1	1	true positive
APB KD	ACTB	7887.477	9017.891	2922.92	2117.083	9.498775358	1	1	1	true positive
APB	ACTB	9856.527	9067.891	2237.92	1536.527	49.44981503	1	1	1	true positive
E3 KD	ACTB	11054.719	9435.012	602.092	1217.062	30.59691272	1	1	1	true positive
E3 BEV	ACTB	12875.77	10295.477	1348.92	1653.012	34.64047619	1	1	1	true positive
E3 BEV	TRPV1	16737.832	4467.012	571.607	25196.657	85.54292373	1	1	1	true positive

APB	ELF1A	18916.205	15494.154	8968.891	28118.778	66.06108249	1	1	1	true positive
E3	ELF1A	21662.368	19510.397	3062.477	28117.485	45.3246259	1	1	1	true positive
APB	TRPV1	23333.69	14620.598	5800.355	1811.284	50.25735156	1	1	1	true positive